TITLE:
INTEGRATED ASSESSMENT OF CLIMATE CHANGE AND HUMAN ACTIVITIES IMPACTS ON WATER RESOURCES AND QUALITY(Dissertation_全文)

AUTHOR(S):
Duan, Wei Li

CITATION:
Duan, Wei Li. INTEGRATED ASSESSMENT OF CLIMATE CHANGE AND HUMAN ACTIVITIES IMPACTS ON WATER RESOURCES AND QUALITY. 京都大学, 2014, 博士(工学)

ISSUE DATE:
2014-09-24

URL:
https://doi.org/10.14989/doctor.k18565

RIGHT:
許諾条件により本文は2015/09/01に公開; 許諾条件により要旨は2014/10/01に公開

京都大学学術情報リポジトリ
KURENAI 紅
Kyoto University Research Information Repository

INTEGRATED ASSESSMENT OF CLIMATE CHANGE AND HUMAN ACTIVITIES IMPACTS ON WATER RESOURCES AND QUALITY

(気候変動と人間活動による水資源と水質への影響の総合的評価に関する研究)

by

Weili Duan

A dissertation
Submitted in partial fulfillment of the requirements for the Degree of Doctor of Engineering

Department of Civil and Earth Resources Engineering
Kyoto University, Japan

2014

~Sensei, thank you very much~

Acknowledgements

This Ph.D. thesis was supported by a scholarship awarded by the China Scholarship Council (CSC) and two Global COE programs (“Sustainability/Survivability Science for a Resilient Society Adaptable to Extreme Weather Conditions” and “Global Center for Education and Research on Human Security Engineering for Asian Megacities”) of Kyoto University. I gratefully acknowledge the financial support and the opportunity to take part in the interesting and very useful seminars.

I would like to express my sincere gratitude and appreciation to my supervisor, Professor Kaoru Takara for his attention, guidance, and continuous support from the preliminary to concluding level enabled me to develop understanding on the proposed research subject and to find the meaning and give the new points for my proposed research. His support also enabled me to share my research findings in various international and local events which contributed to define a proper direction of my research. With his friendly attention on my economic and life conditions, I could have a comfortable environment and high level equipment for doing my Ph.D. research. Without his supports I could not have opportunities to extend my sights by taking internships in Princeton University, the Center for Agricultural Resources Research of Shijiazhuang and Nanjing Institute of Geography and Limnology, Chinese Academy of Sciences, and Center for Global Environmental Research, National Institute for Environmental Studies, and making presentations on many conferences such as in Malaysia, Kyoto, Hiroshima and Hokkaido.

I also would like to give my great appreciate to Professor Bin He for his encouragement, suggestion, and continuous support for my research. He helped me so much in study and life including prepared materials for applying scholarship when I came here, collected hydrological data, taught the hydrological knowledge, and supported me financially.

I also express my thanks to Professor Yosuke Yamashiki, Professor Masahito Ishihara, Dr. Pingping Luo and Dr. Daniel Nover, for their kind comments, technical assistance, and support. Professor Masahito Ishihara helped me to collect the meteorological data. Dr. Pingping always helped me and we discussed with each other

about my research for many times.

I also would like to give my great appreciate to Professor Eiichi Nakakita, Professor Tomoharu Hori, Professor Yasuto Tachikawa, Professor Sunmin Kim, Professor Kenji Tanaka and Professor Weiqiang Ma for their kind suggestions and comments on my research.

I also would like to give special thanks to Professor Eric F. Wood, Professor Yanjun Shen and Dr. Naota Hanasaki, for their kind help when I studied in their Labs. I want to thank my former teachers, Professor Zeyi Xiao, Professor Guixing Wang in the Sichuan University, and Professor Guohua Chen in the South China University of Technology.

I wish to express my gratitude to Mrs. Sono Inoue for her kind supports of administrative tasks, Mrs. Yoko Yonekawa, Mrs. Nishimura and Mrs. Kaori Saidera for their advance assistance, and Mr. Shigeo Fujiki for his technical assistance. I also would like to make a special reference to Mrs. Yuko Takii and Ms. Saho Matsuda.

I express my thanks to the laboratory members, Dr. Apip, Dr. Pedro, Dr. Remy, Dr. Sahu, Dr. Maja, Mr. Liu Mr. Mizuoka, Mr. Kato, Mr. Sawai, Ms. Kusajima, Ms. EunBi Kang, Ms. YongA Shing, Mr. Azuma and Mr. Sasaki, and Ms. Teramoto, Mr. Hu, Mr. Xue, Mrs. Eliza, Miss Shi, Ms. Khai Lin, Ms. Eva, Mr. Josko, Mr. Vilaysane, Mr. Hendy, Mr. Khang, Mr. Tien, Mr. Loi, Mr. Adnan, Mr. Goto, for being wonderful friends and grateful friendship during my stay at Kyoto, Japan. My deep thanks also give to my friend Miss. Zhang for companying, encouraging and supporting me.

Finally, I would like to thank my family for their life-long love and support. I especially owe much to my parents and elder brothers for offering their invaluable love, encouragement and understanding. Without them, this work could not have been completed.

DPRI, Kyoto University, Uji, September 2014

Abstract

With the rapid increase of world population, the global water shortage is set to be the major crises of the twenty-first century; that is, population dynamics (growth, age distribution, urbanization and migration) create pressures on freshwater resources due to the increased water demands and pollution. Moreover, water resources management faces a new uncertainty- i.e. the potential for longer-term and more persistent climate change nowadays, which, in coming years, may significantly affect the availability of supply and patterns of water demand. Evidence for climate change impacts on the hydro-climatology of Japan is plentiful. The possibility of frequent occurrence of extremely low rainfall, decrease in snowfall, and earlier thaw will tend to increase the vulnerability of water resources. Meanwhile, extreme rainfall and temperature tend to cause hydrological disasters including floods, water quality incidents, and so on. Therefore, the main purpose of this thesis is to evaluate the changes of water quality incidents, extreme precipitation events for whole Japan, and then give more details about precipitation variations in Hokkaido because Hokkaido is typically the most affected by climate change compared to other places in Japan, and finally explore the relationship between aquatic environment, water sources and climate change in the Ishikari River basin.

Water quality improvement and pollution incident risk reduction have become urgent priorities for water resources management. Analysis of water pollution incidents is necessary to describe and assess a country's water quality conditions and to establish governmental priorities pertaining to development of indicators of water quality and implementation of prevention rules. So, from aspects of incident numbers, incident causes, pollutant categories, and pollution effects, a spatiotemporal evaluation of the trend and distribution of water quality incidents was presented for whole Japan from 1996 to 2007, using a combination of Geographic Information System (GIS) and statistical methods. The nationwide trend for Japan and that the total number of water quality incidents fluctuated between 400 and 1600 per year, and the average from 1996-2007, from 1996 to 1999, from 2000 to 2003 and from 2004 to 2007 are 962, 499, 902 and 1487, separately. Natural disasters are threatening water quality and will likely remain important for water pollution.

Increasing trends in precipitation climate extremes in Japan have been found in many researches, but information of changes in precipitation amounts and precipitation climate

extremes over last century Need More Research. So based on 51 weather stations, chapter 3 characterized the precipitation variability in Japan from 1901 to 2012, by calculating the precipitation amounts and precipitation extremes indices and found Variations in R10mm, R20mm, CWD and PRCPTOT indicated a decreasing trend for a whole Japan, with while an increasing trend for R95p, R99p, CDD, RX1day, RX5day, and SDII. The spatial distributions of these indices were obvious. Negative trends dominated for PRCPTOT, R10mm and R20mm, with the exception of the Hokkaido, and stations with statistical significant trends for R95p, R99p and SDII mainly scattered in the southwest area of Japan.

Based on previous chapters, Hokkaido area was chosen to make further study in subsequent chapters. The spatial annual, seasonal, and monthly precipitation trends in Hokkaido were characterized, during 1980-2011, using the Mann-Kendall test and geostatistical interpolation techniques. The possible association with water vapor flux in an attempt to understand the latest precipitation trends in the region examined. Results show precipitation varied substantially in spatial-temporal. The analyses of the water vapor flux in whole layers under 300 hpa possibly explain the spatiotemporal distribution of precipitation trends in Hokkaido.

Combining the Maintenance of Variance-Extension type 3 (MOVE. 3) and the regression model Load Estimator (LOADEST), Chapter 5 is to describe a procedure for estimation of constituent loads in rivers which have only sparse measurements of flow and water quality constituent concentrations to obtain reliable unbiased estimates of seasonal total nitrogen (TN), total phosphorus (TP) and suspended sediment (SS) loads for the Ishikari River and demonstrate the utility of regression methods for estimation of seasonal TN, TP, and SS loads from instantaneous samples. Findings indicate average loads of TN, TP, and SS, by month, were highly variable at the five sites in the Ishikari River basin, from January 1985 to December 2010. April had the largest loads, then the estimated average loads decreased, and increased again. The estimated seasonal loads were also highly variable from 1985 to 2010 in the Ishikari River and its tributaries, with the greatest loads occurring in the spring and the smallest loads occurring in the winter, reflecting fluctuations in discharge as a result of the combined effects of seasonal runoff patterns, the exact timing of which vary from year to year.

Combining the results from the previous two chapters, Chapter 6 developed a SPARROW-based sediment model for surface waters in the Ishikari River basin. This

model was based on stream water-quality monitoring records collected at 31 stations for the period1985 to 2010 and used four source variables including developing lands, forest lands, agricultural lands, and steam channels, three landscape delivery variables including slope, soil permeability, and precipitation, two in-stream loss coefficients including small stream (drainage area $\leq$ 200 km^2) and big stream (drainage area > 200 km^2), and reservoir attenuation. Results indicate the percent of total incremental flux generated for agricultural lands, developing lands, forested lands, and stream channels is 35.11%, 23.42%, 22.91% and 18.56%, respectively. Sediment total yields and incremental yields accumulate in the sub-basin along the middle and lower reaches of the Ishikari River, showing which sub-basin is most susceptible to erosion. Combined with land use, management actions should be designed to reduce sedimentation of agricultural lands and developing lands in the sub-basin along the middle and lower reaches of the Ishikari River.

In the last chapter, outputs (e.g., maximum temperature, minimum temperature, and precipitation) at a global scale from HadCM3 GCM A2a and B2a climatic scenarios were downscaled to local−scale hydrologic variables to compute and evaluate hydrological components for water resources variability and risk of hydrologic extremes in future. In the Upper Ishikari River basin, the downscaling results indicated that the average annual maximum temperature might increase by 1.80°C and 2.01°C, 3.41°C and 3.12°C, and 5.69°C and 3.76°C, the average annual minimum temperature might increase by 1.41°C and 1.49°C, 2.60°C and 2.34°C, and 4.20°C and 2.93°C, and the average annual precipitation possibly decrease by 5.78% and 8.08%, 10.18% and 12.89%, and 17.92% and 11.23% in 2030s (2020-2039), 2060s (2050-2069) and 2090s (2080-2099) for A2a and B2a emission scenarios respectively, compared with the base period 1981-2000. The annual mean streamflow will be likely to increase for the all three future periods for both scenarios except the 2090s under the A2a scenario. Among them, the largest increase is observed in the 2030s for A2a scenario, up to approximately 7.56%. Also, a pronounced increase is exhibited in winter for the all future periods for both scenarios, while a decrease is found in summer except the 2030s for A2a scenario.

Overall this thesis mainly focused on the climate and human impacts on water quality and water resources in Japan. After investigating spatiotemporal trends and causes of the water quality incidents, changes of precipitation extreme events were analyzed in whole Japan, which indicated Hokkaido was a special area under climate change compared to other places. So over the subsequent chapters, the thesis just focused on the climate and

human impacts on water quality and water resources in Hokkaido area. The results obtained in this thesis substantially enhance the knowledge of climate change impacts on the water quality and water resources in Japan, which may provide a means to reduce water quality incidents and mitigate future impacts by adapting water management. Furthermore, the improved methods for water quality modeling in data scarce regions are transferable to other study areas and applicable in future research.

Contents

List of Tables

List of Figures

Chapter 1 Introduction

1.1 Background

The sustainable development of human social economy requires access to water resources. With the rapid increase of world population, the global water shortage is set to be the major crises of the twenty-first century (Pearce 2006, Schade and Pimentel 2010, Vörösmarty et al., 2010); more concretely, population dynamics (growth, age distribution, urbanization and migration) create pressures on freshwater resources due to the increased water demands and pollution (Polizzotto et al., 2008). Climate change is also currently a big problem for increasing the burden of water resources (Arnell 1999, Barnett et al., 2005). According to the World Health Organization (WHO)'s report (2006), around 1.2 billion people (almost one-fifth of the world's population) live in areas of physical scarcity, and 500 million people are approaching this situation; another 1.6 billion people (almost one quarter of the world's population) face economic water shortage.

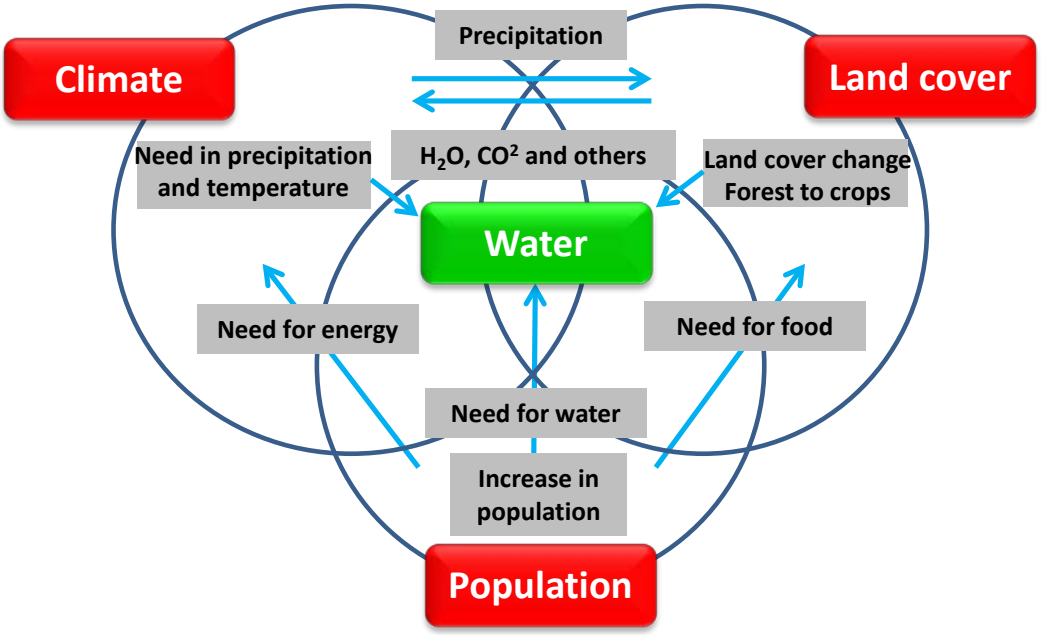

Figure 1.1 Drivers of global change and feedbacks to the global water cycle (Modified from the (Richard Harding and Pavel Kabat, 2007))

Water pollution caused by both human activities and natural activities is a serious problem that increases pressures on freshwater resources. Increasing population will intensify land use, bringing about changes not only in evaporation and runoff but also (probably increasing) changes in greenhouse gas emissions (**Figure 1.1**). Water quality is affected by changes in nutrients, sedimentation, temperature, pH, heavy metals, non-metallic toxins, persistent organics and pesticides, and biological factors, among many other factors (Carr and Neary, 2008). First, increasing population will be a need for increased agricultural productivity, which will naturally lead to increases in polluted irrigation return flows because of the use of fertilizers and pesticides. Second, land-use change caused by population dynamics will greatly influences the aquatic environment. For example, deforestation will increase as more cropland and wood for fuel are needed, accelerating erosion and leaching and increasing water pollution. Thirdly, climate change has a major impact on the world's freshwater resources, water quality, and water management (Bates et al., 2008; Pachauri, 2008). Increases of in surface temperature induced by global warming and changes in the timing and amount of runoff caused by spatial-temporal precipitation variations are likely to produce unfavorable changes in surface-water quality, which will in turn affect human ecosystem health.

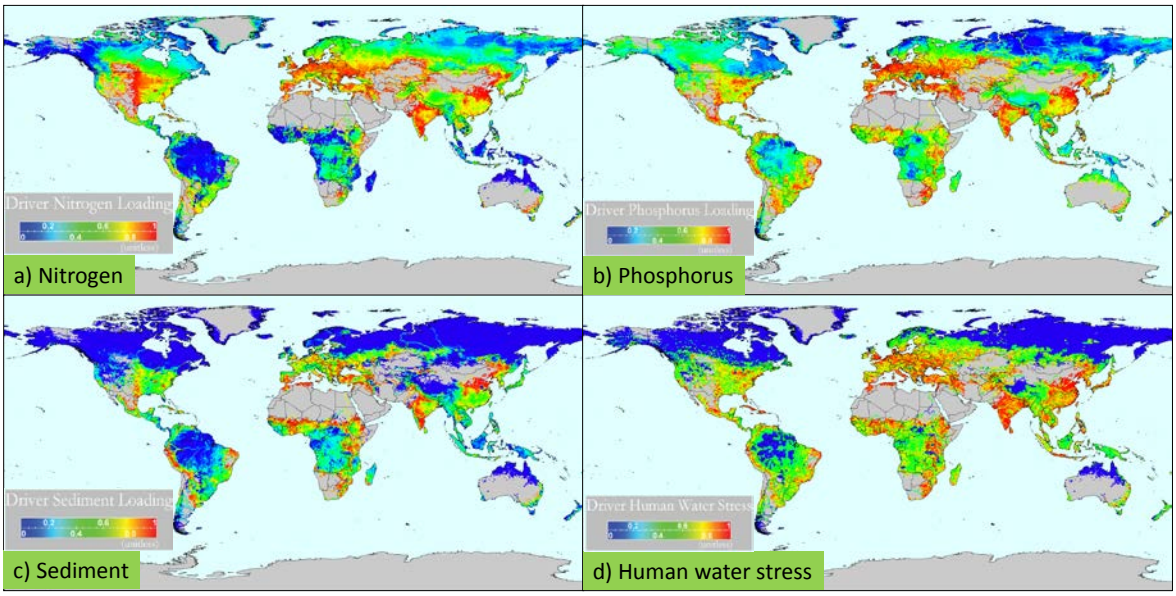

Figure 1.2 Global geography of driver scores for human water security (HWS) threats and biodiversity (BD) threats to river system: a) nitrogen loading, b) phosphorus loading, c) sediment loading, and d) human water stress. Maps display standardised scores, indicating the spatial distribution of relative threats from low (blue) to high (red) (Data source: Vörösmarty et al., 2010)

For example, higher surface-water temperatures will probably accelerate biological productivity, increase the amount of bacteria and fungi in the water, and promote algal blooms in that temperature can control the types of aquatic life that can survive, regulates the amount of dissolved oxygen in the water, and influences the rate of chemical and biological reactions (Kundzewicz et al., 2008). Both increased floods from extreme precipitation along with periodic storm surges intensified by rising sea levels due to climate change, may affect water quality, overloading infrastructure, such as stormwater drainage operations, wastewater systems, treatment facilities, mine tailing impoundments, and landfills, which can increase the risk of contamination (Duan et al., 2013; McCarthy, 2001). Overall, deterioration of water quality caused by climate change and human activity needs to be stopped for a sustainable society. **Figure 1.2** shows that the driver scores for human water security (HWS) threats and biodiversity (BD) threats to river system, suggesting that nutrients such as nitrogen and phosphorus, sediment, and human population are the main factors in HWS threats and BD threats to river system. Here, human water stress was calculated as the ratio of discharge to local human population, thereby capturing the negative consequences for water supplies of both high human population density and naturally-low water availability.

Moreover, water managements face a new uncertainty- i.e. the potential for longer-term and more persistent climate change nowadays, which, in coming years, may significantly affect the availability of supply and patterns of water demand (Vörösmarty et al., 2000). Climate change is a significant and lasting change in the statistical distribution of weather patterns over periods ranging from decades to millions of years, which affects the hydrological cycle and hence the availability of water for its users. First, the distribution of precipitation in space and time is very uneven, leading to tremendous temporal variability in water resources worldwide (Oki and Kanae, 2006). For example, the Atacama Desert in Chile, the driest place on earth, receives imperceptible annual quantities of rainfall each year. On the other hand, Mawsynram, Assam, India receives over 450 inches annually. If all the freshwater on the planet were divided equally among the global population, there would be 5,000 to 6,000 m^3 of water available for everyone, every year (Vörösmarty et al., 2000). Second, the rate of evaporation varies a great deal, depending on temperature and relative humidity, which impacts the amount of water available to replenish groundwater supplies. The combination of shorter duration but more intense rainfall (meaning more runoff and less infiltration) combined with increased evapotranspiration (the sum of

evaporation and plant transpiration from the earth's land surface to atmosphere) and increased irrigation is expected to lead to groundwater depletion (Konikow and Kendy, 2005, Wada et al., 2010).

Another problem caused by climate change is water-related disasters. Water-related disasters arising from floods, droughts, tropical cyclones, landslides and tsunamis are undoubtedly increased over recent decades and appears to continue to rising, and pose major impediments to achieve human security and sustainable socio-economic development (Milly et al., 2002), as recently witnessed with disasters such as Hurricane Katrina in 2005, 2011 Tohoku earthquake and tsunami and Thai Floods 2011. **Figure 1.3** shows the water-related disasters events increased from 1970 to 2013. Floods and storm events increased drastically from 1970 to 2013, but other types of disaster did not increase significantly in this period. The average of floods from 2001 to 2013 doubled over the average from 1986 to 2000 and storms increased more than 1.5 times.

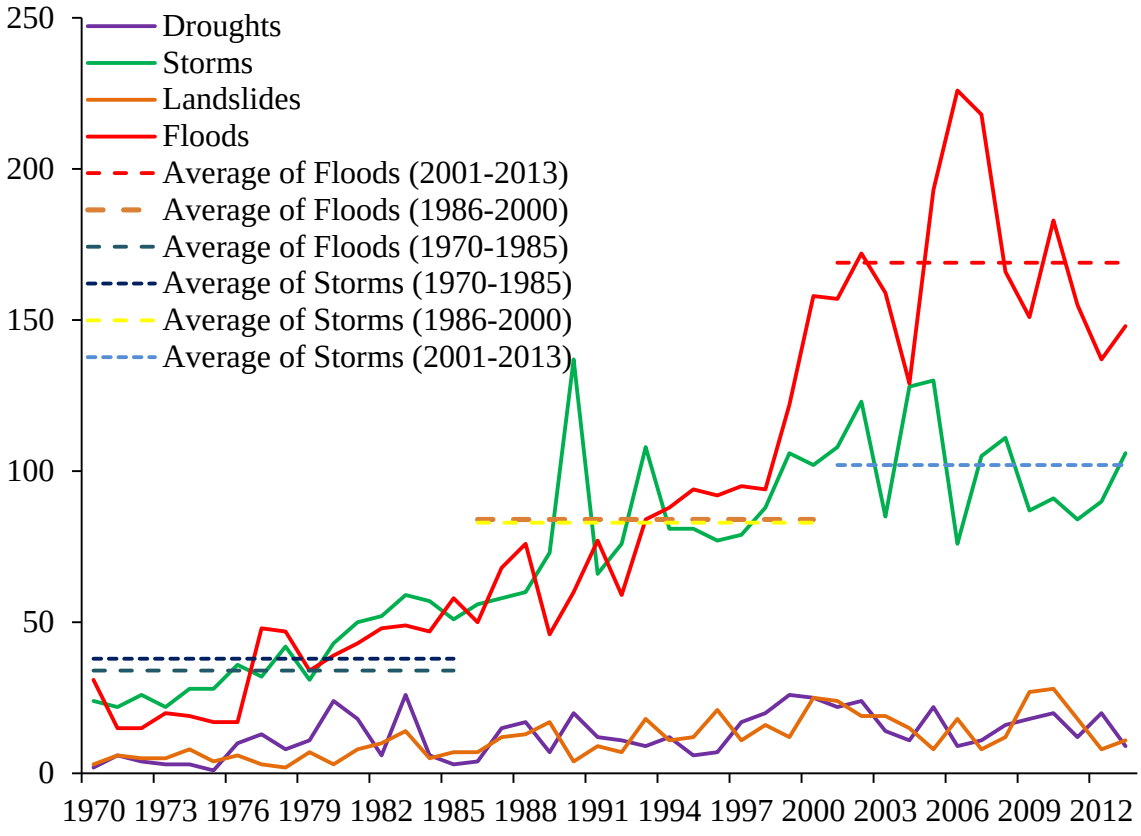

Figure 1.3 Water-related disaster events recorded globally, 1970 to 2013. (Data from the Emergency Event Database of the Centre for Research on the Epidemiology of Disasters. http://www.emdat.be (accessed 25 April 2014)).

Table 1.1 Hydrological disasters from 1970 to 2013.

Continent	Occurrence	Deaths	Injured	Affected	Damage(000 US$)
Africa	2,262	859,176	81,758	452,256,918	26,574,852
Americas	2,819	519,718	2,938,072	236,704,736	948,201,308
Asia	4,567	1,953,106	3,559,008	5,860,665,083	1,195,187,529
Europe	1,523	186,681	85,362	38,520,962	356,116,657
Oceania	536	6,485	9,928	20,609,528	74,048,170
Total	11,707	3,525,166	6,674,128	6,608,757,227	2,600,128,516

Source: Frequencies are authors' estimates based on data from the Emergency Event Database of the Centre for Research on the Epidemiology of Disasters. http://www.emdat.be (accessed 25 April 2014).

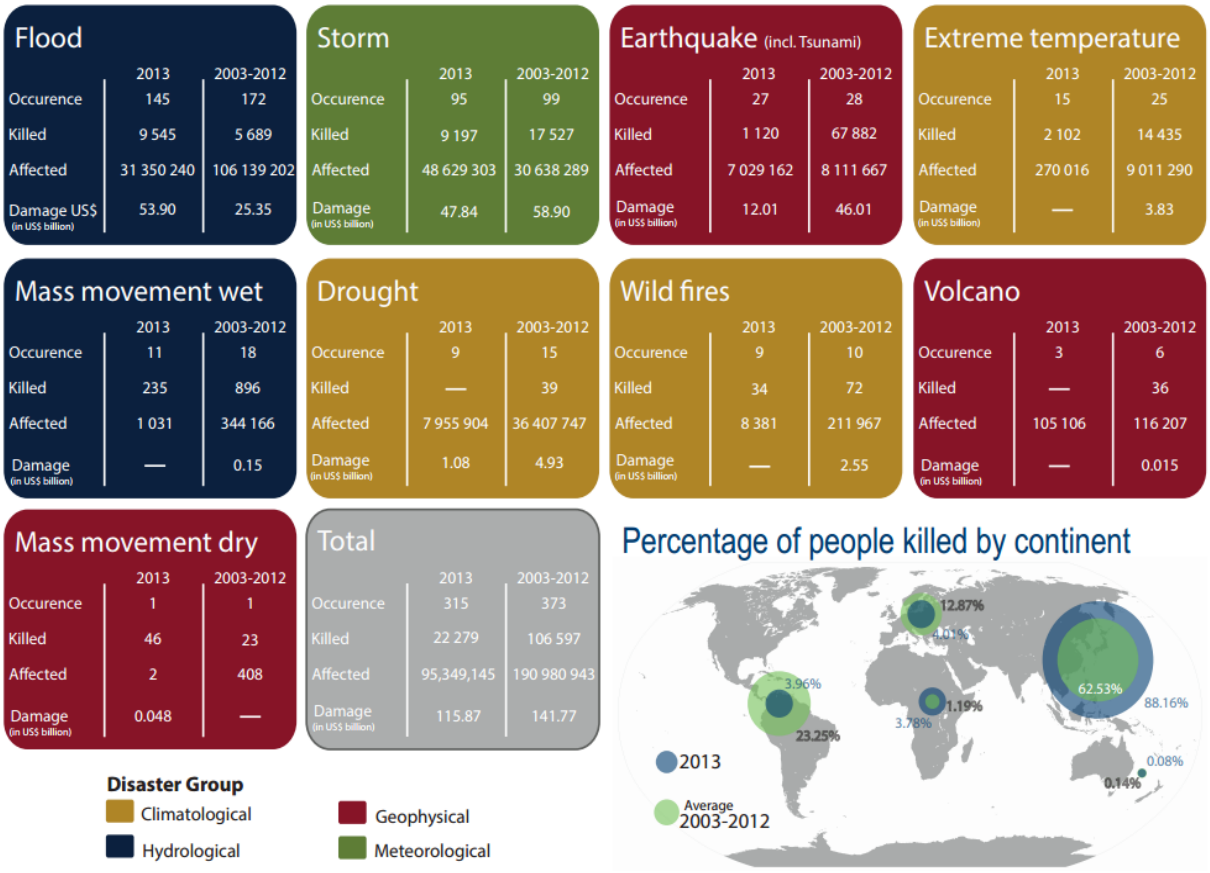

Figure 1.4 Human and economic impact by disaster types (2013 versus average 2003-2012) (Source: The Emergency Event Database of the Centre for Research on the Epidemiology of Disasters. http://www.emdat.be (accessed 25 April 2014))

Extreme weather and climate events interacting with exposed and vulnerable human and natural systems can lead to disasters, often causing a lot of damage to property and casualties. Worldwide, 11,707 reported hydrological disasters caused the death of more than 3,525,166 people, made 6,608,757,227 victims and caused a record amount of US$ 2,600,128,516 of damages, during 1970- 2013 (**Table 1.1**). **Figure 1.3** more clearly shows the human and economic impact by disaster types in 2013 compared to the average of 2003-2012. Obviously, damages caused by extreme weather and climate events occupied a very large part of total disasters. Also, we can see most of disasters happened in Asia. For example, the number of disasters happened in 2013 in Asia was up to approximately 88.16%.

Overall, global change including all the future changes due to anthropogenic activities, has significantly affected water resources availability and quality, extreme events, surface and ground water, marine and continental water, and, consequently, the accomplishment of different water policies related to river basin management, marine environment, water quantity (floods, droughts, water scarcity), water and health (drinking and bathing water) and water pollution (water treatment). Therefore, it is momentous to evaluate water quality, extreme events, and water resources under climate change, and therefore to fully understand the relationship between the hydrological process and the watersheds characters and identify the trend of the vulnerable of the water-related problems. The objective of this thesis is to investigate the water quality incidents and precipitation extremes in Japan, expound the detailed changes of precipitation in Hokkaido, and evaluate the water quality and water resources in the Ishikari River basin under climate change and human activities.

1.2 Problem Statement and Previous Researches

Evidence for climate change impacts on the hydro-climatology of Japan is plentiful (Solomon, 2007). The Japan Meteorological Agency (JMA) show that annual average air temperatures nationwide rose by a rate equivalent to 1.15°C per century between 1898 and 2010, which is considerably higher than the global average temperature rise of 0.74°C over the last century (according to the Intergovernmental Panel on Climate Change's "Climate Change 2007: Synthesis Report Summary for Policymakers"); moreover, although no clear trends have been observed, the annual precipitation in Japan varies largely from year to

year. All these changes in precipitation and temperature have greatly influenced water supply in Japan. For instance, concerning precipitation, years of low rainfall have become frequent since around 1970, and the amount of precipitation was much below average in 1973, 1978, 1984, 1994, and 1996, when water shortages caused damage. It tremendously affected drinking water supply because approximately 78% of it (actual record in the fiscal year 2004) is taken from rivers, lakes, marshes and so forth. The possibility of frequent occurrence of extremely low rainfall, decrease in snowfall, and earlier thaw will tend to increase the vulnerability of water resources. Meanwhile, extreme rainfall and temperature induced lots of hydrological disasters including floods, water quality incidents, and so on. Here, problems about water quality, extreme precipitation events, land-use change and water resources are raised.

Stringent discharge regulation, development of sewerage systems and other relevant efforts in watersheds management have led to significant improvements in Japanese river water quality in recent years (Jun et al., 2004; Luo et al., 2011; Takahasi, 2009). However, water pollution risks remain and controlling environmental pollution remains an active area of research in Japan (Honma and Hu, 2009; Nakano et al., 2008). For example, Ham et al., (2012) investigated the public health risk due to antibiotic concentrations in Tama River; Zushi et al., noted that water of the Tokyo Bay basin contained high levels of perfluorononanoate, perfluorooctanoate, and perfluorooctanesulfonate (Zushi et al., 2008). Other researchers identified heavy metal pollution in metropolitan bay areas (Hosono et al., 2010; Tsujimoto et al., 2006; Yasuhara and Yamazaki, 2005), especially after the great east Japan earthquake (Shibata et al., 2012). The number of accidental spills in watersheds has increased grammatically in recent years (Jun et al., 2004; Wakakura and Iiduka, 1999), resulting in obstruction in water supply, often leading to negative consequences for the environment (Schwarz et al., 2006). However, there are few relevant studies that investigate the spatiotemporal distribution of water quality incidents in recent years in Japan.

Increasing trends in precipitation climate extremes have also been found for Japan because of the impact of climate change on the hydro-climatology (Solomon, 2007). For example, on the basis of 50 stations, Fujibe et al., (2005; 2006) argued that the extreme daily precipitation, extreme four-hourly and hourly precipitation increased in the past century. Miyajima and Fujibe (2011) found that the distribution of top ten-minute precipitation has a moderate north-south gradient, and extreme precipitation shows local

maxima on southern sides of land in western Japan corresponding to orographic enhancement. On the other hand, some authors have analyzed variations in precipitation amounts across Japan at different timescales and territories. For example, using linear regression method, Iwasaki and Sunaga (2009) elucidated the features of weak rainfall between June and September for 31 years. Takeshita (2010) estimated the precipitation variation in Miyazaki prefecture and Suzuki and Hayakawa (2006) explored the characteristics of summertime convective precipitation in Yamaguchi prefecture. Although all these studies detected characteristics of precipitation change, most of them focused on inter-annual or summer variability and little has been done to analyze these features on multiple temporal scales (e.g. spatial, annual, seasonal, and monthly) and information of changes in precipitation amounts and precipitation climate extremes over last century is few.

Efforts at water management in Japan have led to significant improvements in the estimation of water quality. For example, a nationwide data collection network (http://www1.river.go.jp/) called the National Land with Water Information was established to provide real-time water data including water quality, precipitation, and river discharge. These monitoring systems are essential for evaluating and understanding the various hydrologic and biogeochemical processes governing water quality and nutrient cycling in watersheds and their ecological impacts. Because the load estimation process is complicated by retransformation bias (Ferguson, 1986; Webb et al., 1997), data censoring (Gilbert, 1987) , and non-normality (Helsel and Hirsch, 1992; Shumway et al., 2002), biases generally exist in estimated loads from modeling studies (Johnes, 2007). There is therefore an urgent need to improve estimation methods to compliment improving monitoring programs and resolve common shortcomings in estimation methods.

In the Japanese context, high suspended sediment loads is increasingly recognized as an important problem for watershed management (Mizugaki et al., 2008; Somura et al., 2012). For example, the Ishikari River basin has long been plagued by high suspended sediment loads, generally causing high turbidity and bed erosion along the river, including in Sapporo, Hokkaido's economic and government center. The pervasiveness of the problem has generated several sediment management studies in the Ishikari River basin. Asahi et al., (2003) found that it is necessary to consider tributary effects directly and that sediment discharged from tributaries contributes to the output sediment discharged from the river's mouth. However, detailed accounting of sediment sources and transport in the

Ishikari River basin remains poorly understood.

Based on the GCMs output, lots of efforts at evaluation of hydro-climatology of Japan under climate change have been made. For example, Sato et al., (2013) investigated the impact of climate change on river discharge in several major river basins in Japan through a distributed hydrological simulation using the MRI-AGCM and found winter river discharge is projected to increase more than 200% in February, but decrease approximately 50-60% in May in the Tohoku and Hokuriku regions. In the Agano River basin, the monthly mean discharge for the 2070s was projected to increase by approximately 43% in January and 55% in February, but to decrease by approximately 38% in April and 32% in May (Ma et al., 2010). However, there is less done on small river basins in Hokkaido about the hydro-climatology variations under climate change.

1.3 Objectives of the Study

Considering the above problems, the purpose of this study is to evaluate the changes of water quality incidents, extreme precipitation events in whole Japan, give more details about precipitation variations in Hokkaido, and explore the relationship between aquatic environment, water sources and climate change in the Ishikari River area. The specific objectives are itemized as follows:

(1) To evaluate the trend and distribution of water quality incidents in Japan. More specifically, the national and local trends in water quality incidents in Japan using a combination of Geographic Information System (GIS) and statistical methods, including aspects of incident numbers, incident cause, pollutant categories, and pollution effects have been elucidated. Additionally, potential reasons for the fast growth in pollution incidents and changes in pollutant categories were discussed.

(2) To calculate the spatial and temporal variability of the seasonal changes in precipitation amounts, develop indices and indicators for monitoring trends in climate extremes and apply them to the projection of future changes in climate extremes in Japan.

(3) To elucidate trends and causes of precipitation variability at multiple time scales in Hokkaido, Japan, using the Mann-Kendall test (a non-parametric trend test) and geostatistical interpolation techniques. The results may offer insights into precipitation trends and provide tools for forecasting future climate conditions.

(4) To estimate total nitrogen (TN), total phosphorus (TP) and suspended sediment (SS) loads at five sites on the Ishikari River, from January 1985 to December 2010, by combining the Maintenance of Variance-Extension type 3 (MOVE. 3) and the regression model Load Estimator (LOADEST), which explains how short records of daily waterflow and components concentration can be combined to obtain meaningful estimates of seasonal TN, TP and SS loads.

(5) To develop a spatially explicit, regional empirical model of suspended sediment for the Ishikari River basin in Hokkaido, on the basis of the Spatially Referenced Regression on Watershed Attributes (SPARROW) model. The results will improve our understanding of SS dynamics and watershed processes in general, which will benefit both the scientific and the management community in safeguarding water resources.

(6) To investigate the possible impacts of climate change on water resources in the Upper Ishikari River basin, Hokkaido, Japan, on the basis of outputs from the HadCM3 (Hadley Centre Climate Model 3) Global Circulation Model (GCM).

1.4 Framework and Organization of the Dissertation

This dissertation consists of eight chapters. A brief explanation of each chapter is outlined as follows **(Figure 1.5)**:

Chapter 1 presents the background for proposing the research problems and therefore point out the objective of this study that is to evaluate the water resources and quality under climate change and human activities.

Chapter 2 gives a spatiotemporal evaluation of water quality incidents in Japan to provide numerous insights into the total of incident numbers, incident causes, pollutant categories, and pollution affects. Also, this chapter analyzes the cause of trends in incident occurrence, such as social-economic development, human actives and extreme events (e.g., extreme precipitation).

Chapter 3 evaluates the spatial and temporal variability of the seasonal changes in Japan by assessing the Expert Team on Climate Change Detection and Indices (ETCCDI) at 51 weather stations from 1901 to 2012. This chapter focuses on the whole Japan, and results show the Hokkaido area is a special area for precipitation extremes, suggesting further studies are needed in this area.

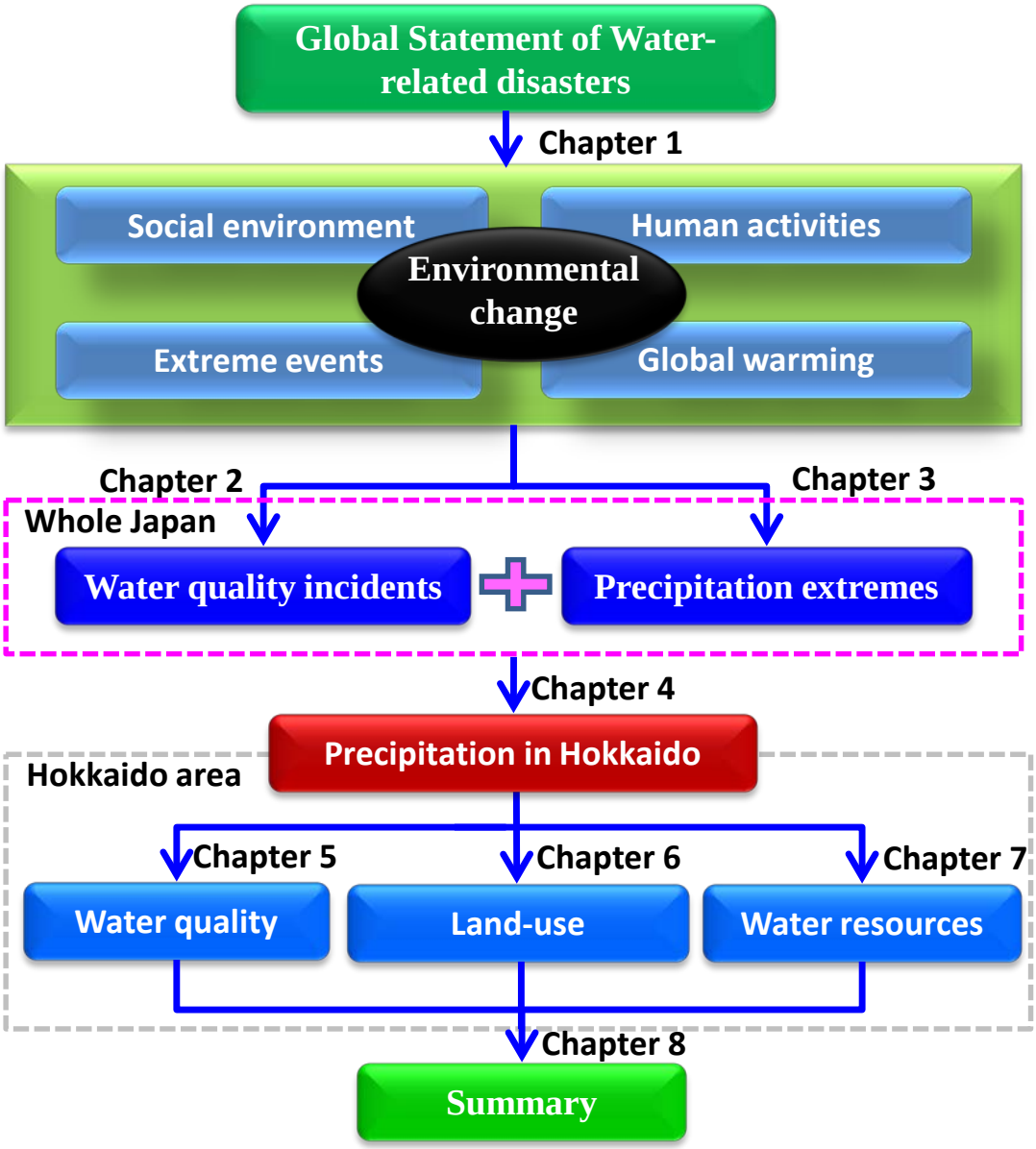

Figure 1.5 Framework of this Ph.D. thesis

Chapter 4 characterizes annual, seasonal and monthly precipitation trends in Hokkaido for the period 1980-2011 using the Mann-Kendall test and geostatistical interpolation techniques and explores possible association with large-scale atmospheric circulation in an attempt to understand the latest precipitation trends in the region. The changes of precipitation can contribute to the following researches.

Chapter 5 develops regression equations by combining the Maintenance of Variance-Extension type 3 (MOVE. 3) and the regression model Load Estimator (LOADEST) to estimate loads of total nitrogen (TN), total phosphorus (TP) and suspended sediment (SS)

at five sites on the Ishikari River from January 1985 through December 2010. The results of this chapter can be used in the next chapter.

Chapter 6 develops a SPARROW-based sediment model for surface waters in the Ishikari River basin, the largest watershed in Hokkaido, which is based on stream water-quality monitoring records collected at 31 stations for the period1982 to 2010 and uses four source variables including developing lands, forest lands, agricultural lands, and steam channels, three landscape delivery variables including slope, soil permeability, and precipitation, two in-stream loss coefficients including small stream (drainage area $\leq$ 200 km^2) and big stream (drainage area > 200 km^2), and reservoir attenuation. Results obtained in this chapter can help resource managers identify priority sources of pollution and mitigate this pollution in order to safeguard water resources and protect aquatic ecosystems.

Chapter 7 uses the Soil and Water Assessment Tool (SWAT) to simulate the possible effects of climate change on water resources for the 2030s, 2060s and 2090s periods in the Upper Ishikari River basin on the basis of projected climate conditions by using GCM outputs of HadCM3 SRES A2a and B2a emissions scenarios with Statistical Downscaling (SDSM) modeling approach.

Chapter 8 is based on the overall research results and findings presented and discussed in the previous chapters, some of the important conclusions and further concerns are referred in this chapter.

1.5 References

Arnell, N.W., 1999. Climate change and global water resources. Global environmental change, 9: S31-S49.

Asahi, K., Kato, K. and Sshimizu, Y., 2003. Estimation of Sediment Discharge Taking into Account Tributaries to the Ishikari River. Journal of natural disaster science, 25(1): 17-22.

Barnett, T.P., Adam, J.C. and Lettenmaier, D.P., 2005. Potential impacts of a warming climate on water availability in snow-dominated regions. Nature, 438(7066): 303-309.

Bates, B., Kundzewicz, Z.W., Wu, S. and Palutikof, J., 2008. Climate change and water.

Intergovernmental Panel on Climate Change (IPCC).

Carr, G.M. and Neary, J.P., 2008. Water quality for ecosystem and human health. UNEP/ Earthprint, 120 pp.

Duan, W. et al., 2013. Spatial and temporal trends in estimates of nutrient and suspended sediment loads in the Ishikari River, Japan, 1985 to 2010. Science of the Total Environment, 461: 499-508.

Ferguson, R.I., 1986. River loads underestimated by rating curves. Water Resources Research, 22(1): 74-76.

Fujibe, F., Yamazaki, N. and Kobayashi, K., 2006. Long-term changes of heavy precipitation and dry weather in Japan (1901-2004). Journal of the Meteorological Society of Japan, 84(6): 1033-1046.

Fujibe, F., Yamazaki, N., Katsuyama, M. and Kobayashi, K., 2005. The increasing trend of intense precipitation in Japan based on four-hourly data for a hundred years. Sola, 1: 41- 44.

Gilbert, R.O., 1987. Statistical methods for environmental pollution monitoring. Wiley, 336 pp.

Ham, Y.S. et al., 2012. Distribution of antibiotic resistance in urban watershed in Japan. Environmental Pollution, 162: 98-103.

Helsel, D.R. and Hirsch, R.M., 1992. Statistical methods in water resources, 49. Elsevier Science, 510 pp.

Honma, S. and Hu, J.L., 2009. Efficient waste and pollution abatements for regions in Japan. International Journal of Sustainable Development & World Ecology, 16(4): 270-285.

Hosono, T., Su, C.C., Okamura, K. and Taniguchi, M., 2010. Historical record of heavy metal pollution deduced by lead isotope ratios in core sediments from the Osaka Bay, Japan. Journal of Geochemical Exploration, 107(1): 1-8.

Iwasaki, H. and Sunaga, Y., 2009. Study of recent variation in weak rainfall over Japan using 31-year AMeDAS dataset. SOLA, 5(0): 157-159.

Johnes, P.J., 2007. Uncertainties in annual riverine phosphorus load estimation: impact of load estimation methodology, sampling frequency, baseflow index and catchment population density. Journal of Hydrology, 332(1): 241-258.

Jun T., Hiroaki T., Yuji O. and Yutaka S., 2004. River Management and Countermeasure T echnologies for Accidental Spills by Ministry of Land, Infrastructure and Transport in

Japan. http://www.pwri.go.jp/eng/activity/pdf/reports/tsumori,_okayasu_and_suzuki041012.pdf, 03-05-2014.

Konikow, L.F. and Kendy, E., 2005. Groundwater depletion: A global problem. Hydrogeology Journal, 13(1): 317-320.

Kundzewicz, Z.W. et al., 2008. The implications of projected climate change for freshwater resources and their management. Hydrological Sciences Journal, 53(1): 3-10.

Luo, P. et al., 2011. Spatiotemporal trend analysis of recent river water quality conditions in Japan. Journal of Environmental Monitoring, 13(10): 2819-2829.

Ma, X. et al., 2010. Hydrological response to future climate change in the Agano River basin, Japan. Hydrological Research Letters, 4: 25-29.

McCarthy, J.J., 2001. Climate change 2001: impacts, adaptation, and vulnerability: contribution of Working Group II to the third assessment report of the Intergovernmental Panel on Climate Change. Cambridge University Press.

Milly, P., Wetherald, R., Dunne, K.A. and Delworth, T.L., 2002. Increasing risk of great floods in a changing climate. Nature, 415(6871): 514-517.

Miyajima, J. and Fujibe, F., 2011. Climatology of extreme precipitation in Japan for different time scales. SOLA, 7: 157-160.

Mizugaki, S. et al., 2008. Estimation of suspended sediment sources using 137Cs and 210Pbex in unmanaged Japanese cypress plantation watersheds in southern Japan. Hydrological Processes, 22(23): 4519-4531.

Nakano, T. et al., 2008. Effect of agriculture on water quality of Lake Biwa tributaries, Japan. Science of the Total Environment, 389(1): 132-148.

Oki, T. and Kanae, S., 2006. Global hydrological cycles and world water resources. Science, 313(5790): 1068-1072.

Pachauri, R.K., 2008. Climate change 2007. Synthesis report. Contribution of Working Groups I, II and III to the fourth assessment report, 851 pp.

Pearce, F., 2006. When the rivers run dry: water, the defining crisis of the twenty-first century. Beacon Press. 324pp.

Polizzotto, M.L., Kocar, B.D., Benner, S.G., Sampson, M. and Fendorf, S., 2008. Near-surface wetland sediments as a source of arsenic release to ground water in Asia. Nature, 454(7203): 505-508.

Richard Harding and Pavel Kabat, 2007. Water and Global Change– the WATCH programme, Richard Harding and Pavel Kabat, 50-51 pp.

Sato, Y., Kojiri, T., Michihiro, Y., Suzuki, Y. and Nakakita, E., 2013. Assessment of climate change impacts on river discharge in Japan using the super‐high‐resolution MRI‐AGCM. Hydrological Processes, 27(23): 3264-3279.

Schade, C. and Pimentel, D., 2010. Population crash: prospects for famine in the twenty-first century. Environment, Development and sustainability, 12(2): 245-262.

Schwarz, G.E. and US, G.S., 2006. The SPARROW surface water-quality model: Theory, application, and user documentation. U.S. Geological Survey, 248 pp.

Shibata, T., Solo-Gabriele, H.M. and Hata, T., 2012. Disaster Waste Characteristics and Radiation Distribution as a Result of the Great East Japan Earthquake. Environmental Science and Technology, 46(7): 3618-3624

Shumway, R.H., Azari, R.S. and Kayhanian, M., 2002. Statistical approaches to estimating mean water quality concentrations with detection limits. Environmental Science & Technology, 36(15): 3345-3353.

Solomon, S., 2007. Climate change 2007-the physical science basis: Working group I contribution to the fourth assessment report of the IPCC, 4. Cambridge University Press, 1056 pp.

Somura, H. et al., 2012. Impact of suspended sediment and nutrient loading from land uses against water quality in the Hii River basin, Japan. Journal of Hydrology.450-451: 25-35

Suzuki, K. and Hayakawa, S., 2006. Convective Precipitation in Yamaguchi Prefecture in Summer. Journal of Agricultural Meteorology, 62(4): 127-132.

Takahasi, Y., 2009. History of Water Management in Japan from the End of World War II. Water Resources Development, 25(4): 547-553.

Takeshita, S., 2010. Influence on precipitation and the distribution in Miyazaki [Japan] Prefecture with climate changes. Bulletin of the Faculty of Agriculture, Miyazaki University (Japanese), 56: 73-78.

Tsujimoto, A., Nomura, R., Yasuhara, M., Yamazaki, H. and Yoshikawa, S., 2006. Impact of eutrophication on shallow marine benthic foraminifers over the last 150 years in Osaka Bay, Japan. Marine Micropaleontology, 60(4): 258-268.

Vörösmarty, C.J. et al., 2010. Global threats to human water security and river biodiversity. Nature, 467(7315): 555-561.

Vörösmarty, C.J., Green, P., Salisbury, J. and Lammers, R.B., 2000. Global water resources: vulnerability from climate change and population growth. Science,

289(5477): 284.

Wada, Y. et al., 2010. Global depletion of groundwater resources. Geophysical Research Letters, 37(20): L20402.

Wakakura, M. and Iiduka, Y., 1999. Trends in chemical hazards in Japan. Journal of Loss Prevention in the Process Industries, 12(1): 79-84.

Webb, B.W. et al., 1997. Load estimation methodologies for British rivers and their relevance to the LOIS RACS (R) programme. Science of the Total Environment, 194: 379-389.

Yasuhara, M. and Yamazaki, H., 2005. The impact of 150 years of anthropogenic pollution on the shallow marine ostracode fauna, Osaka Bay, Japan. Marine Micropaleontology, 55(1): 63-74.

Zushi, Y., Takeda, T. and Masunaga, S., 2008. Existence of nonpoint source of perfluorinated compounds and their loads in the Tsurumi River basin, Japan. Chemosphere, 71(8): 1566-1573.

Chapter 2 Spatiotemporal Evaluation of Water Quality Incidents

2.1 Introduction

Sustainable development of communities requires access to water resources. With rapidly increasing global population, water shortages are set to be the major crises of the 21st century (Pangare, 2006; Polizzotto et al., 2008). Water managers now face additional difficulties as our awareness of the extent of climate change uncertainties increases. Longer-term and more persistent changes in climate may, in coming years, significantly affect water supply and patterns of water demand (Vörösmarty et al., 2000), while being simultaneously exacerbated by increased pollutant loading (Programme, 2009; Schwarzenbach et al., 2010; Törnqvist et al., 2011; Yen et al., 2012).

Therefore, water quality improvement and pollution incident risk reduction have become urgent priorities for water resources management. Analysis of water pollution incidents is necessary to describe and assess a country's water quality conditions and to establish governmental priorities pertaining to development of indicators of water quality and implementation of prevention rules (Hrudey et al., 2006; Ganoulis, 2009; Mao et al., 2011). Recent research has investigated water pollution incidents in many different study systems. For instance, after evaluating a 5-year history (2002-2006) of pollutant incidents in China, Hou et al., (2009) concluded that a lack of a systematic pollution accident notification system reflected a deficiency in pollution management. Wu et al., (2009) classified human errors contributing to 62 drinking water accidents occurring in affluent countries from 1974 to 2001 and then proposed a future research agenda for human error reduction in the water sector. Based on a detailed statistic analysis of hazardous chemical accidents, Duan et al., (2011) reported that majority of hazardous chemical accidents were environmental pollution accidents in China.

Stringent discharge regulation, development of sewerage systems and other relevant efforts in watersheds management have led to significant improvements in Japanese river

** This chapter has been published in **Chemosphere**, 93(6): 946–953. 2013.*

water quality in recent years (Tsumori et al., 2004; Luo et al., 2011; Duan et al., 2013; Takahasi, 2009). However, water pollution risks remain and controlling environmental pollution remains an active area of research in Japan (Honma and Hu, 2009; Nakano et al., 2008). For example, Ham et al., (2012) investigated the public health risk due to antibiotic concentrations in Tama River; Zushi et al., (2008) noted that water of the Tokyo Bay basin contained high levels of perfluorononanoate (PFNA), perfluorooctanoate (PFOA), and perfluorooctanesulfonate (PFOS). Other researchers identified heavy metal pollution in metropolitan bay areas (Hosono et al., 2010; Tsujimoto et al., 2006; Yasuhara and Yamazaki, 2005), especially after the great east Japan earthquake (Shibata et al., 2012). The number of accidental spills in watersheds has increased dramatically in recent years (Tsumori et al., 2004; Wakakura and Iiduka, 1999), resulting in obstruction in water supply, often leading to negative consequences for the environment (Schwarz et al., 2006). However, there are few relevant studies that investigate the spatiotemporal distribution of water quality incidents in Japan.

In this chapter, a spatiotemporal evaluation of the trend and distribution of water quality incidents was presented for whole Japan. More specifically, the national and local trends in water quality incidents were elucidated in Japan using a combination of Geographic Information System (GIS) and statistical methods, which includes aspects of incident numbers, incident cause, pollutant categories, and pollution effects. Additionally, this study discussed potential reasons for the fast growth in pollution incidents and changes in pollutant categories.

2.2 Materials and methods

2.2.1 Regional division and data sources

Japan is an archipelago, consisting of four large islands (Honshu, Hokkaido, Kyushu and Shikoku) and many other small islands (of them, 6,852 islands have more than 100 m of coastline). Japan is also made up of many rivers, and most of them are short and fast flowing. Therefore, river management is very important for the Japanese government and the rivers in Japan are classified into three levels: first-class river systems, second-class river systems and other river systems. So far, there are 109 designated first-class river systems and 2723 designated second-class river systems, and the corresponding channel lengths are 87560 km and 36010 km, respectively. According to the official river

regulations, the Ministry of Land, Infrastructure and Transportation controls big rivers classified as first-class rivers such as the Ishikari River. Governors of urban and rural prefectures control less important second-class rivers. Mayors of municipalities control other small rivers, branches of first and second-class rivers and the upper reaches of the first and second-class rivers. Based on the distribution of the first-class river systems, Japan is divided into nine sub-regions (Hokkaido, Tohoku, Kanto, Hokuriku, Chubu, Kinki, Chugoku, Shikoku and Kyushu), as shown in **Figure 2.1**. Because of the irregular distribution of rivers, management of each sub-region is not strictly aligned with prefectural borders. For example, some rivers managed by Hokuriku run through Tohoku, Kanto and so on (**Figure 2.1**). Of the nine sub-regions, channel length of the first-class river systems in Kanto is the longest (13181.8 km), which occupies 15.05% of the total; while Shikoku is the shortest (5476.2 km), which only occupies 6.25%.

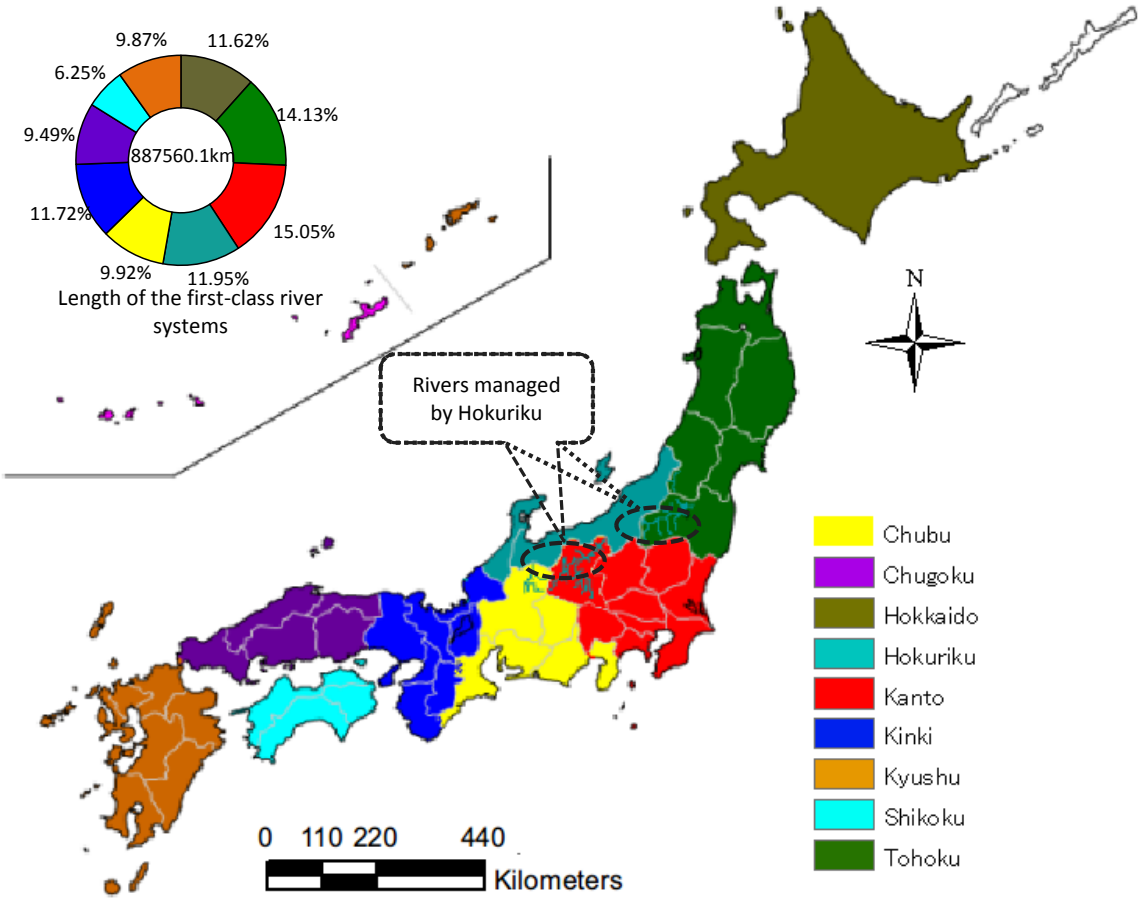

Figure 2.1 Nine regions for river management in Japan (Modified from MLIT)

The water pollution incident data used in this study were obtained from the Japanese River Water Quality Yearbook (1999-2007), which was edited by the Japan River Association (JRA) and supervised by the River Bureau, Ministry of Land, Infrastructure, Transport and Tourism (MLIT). MLIT is generally responsible for river control, water resources, and sewage systems. All of the water quality incidents are recorded initially by nine regions, and then reported to MLIT. Statistical analysis allows us to identify the distribution of incident numbers, pollutant categories, and losses involved in the incidents, and the trend of pollution incidents in Japan.

In addition to incidence data, data about the channel length for the three types of river systems originates from the MLIT (http://www.mlit.go.jp/en/index.html) and JRA (http://www.japanriver.or.jp). The data about water supply establishments comes from the Health Service Bureau, Ministry of Health, Labor and Welfare (MHLW) of Japan (http://www.mhlw.go.jp/english). The data about illegal dumping comes from the Ministry of the Environment of Japan (http://www.env.go.jp/en/).

2.2.2 Methods

Analyses were performed to categorize the frequency and geographic distribution of incidents. Detailed methods are as follows: Step 1: after the extraction process, data (e.g., the number of incidents, and so on) are categorized and transformed into an Excel-format database. Step 2: data are analyzed using descriptive statistics to quantitatively describe the main features of the dataset (Weiss and Hassett, 2012). Here, statistical analyses descriptive statistics and mean analysis are used to discuss the spatial and temporal features of incident trends. For example, the averages from 1996 to 2007, from 1996 to 1999, from 2000 to 2003 and from 2004 to 2007 are calculated to indicate that pollution incidents have increased dramatically in recent years; the fluctuation in different regions is figured according to pollutant category and cause to compare the changes between regions. Step 3, results are presented using the GIS software ArcGIS 10.0 in order to explore national and local trends in water quality incidents in Japan. The shape file of Japan and the Excel-format database processed though previous steps are imported into ArcGIS 10.0. Select the “Properties” option and then click on the “Symbology” tab and select the “Quantities” option on the left hand menu list and finally choose the variable to make out different thematic maps to display the spatial and temporal features in different regions (Details can be seen from http://help.arcgis.com/en/arcgisdesktop/10.0/help/).

2.3 Results

2.3.1 Distribution of the incidents over time

According to the analysis results, the incident numbers increased from 1996 to 2007 (**Figure 2.2** and **Figure 2.3**). **Figure 2.2** shows the nationwide trend for Japan and that the total number of water quality incidents fluctuated between 400 and 1600 /year, and the average from 1996-2007, from 1996 to 1999, from 2000 to 2003 and from 2004 to 2007 are 962, 499, 902 and 1487, separately. The average from 2004 to 2007 reflects a three-fold increase over the average from 2000 to 2003.

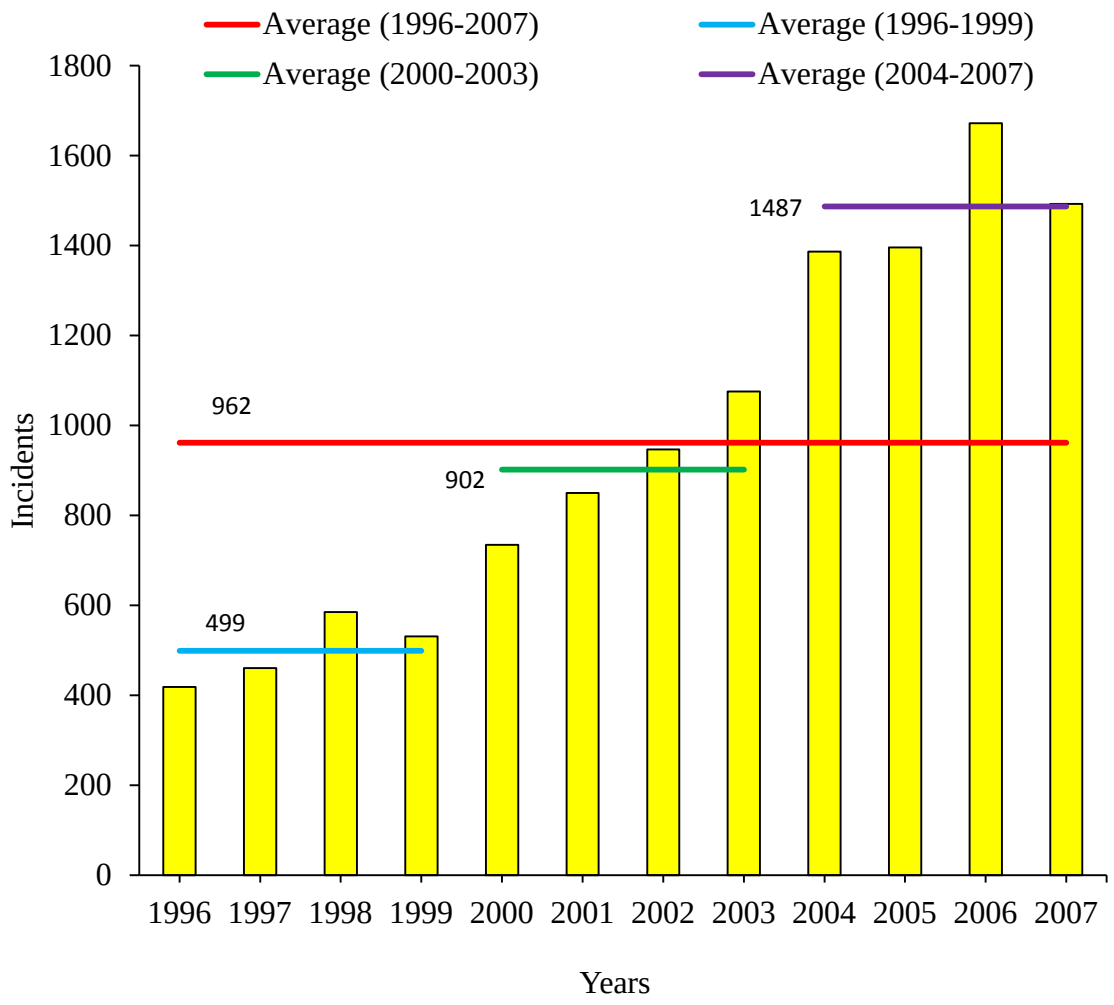

Figure 2.2 Numbers of water pollution incidents in Japan from 1996 to 2007.

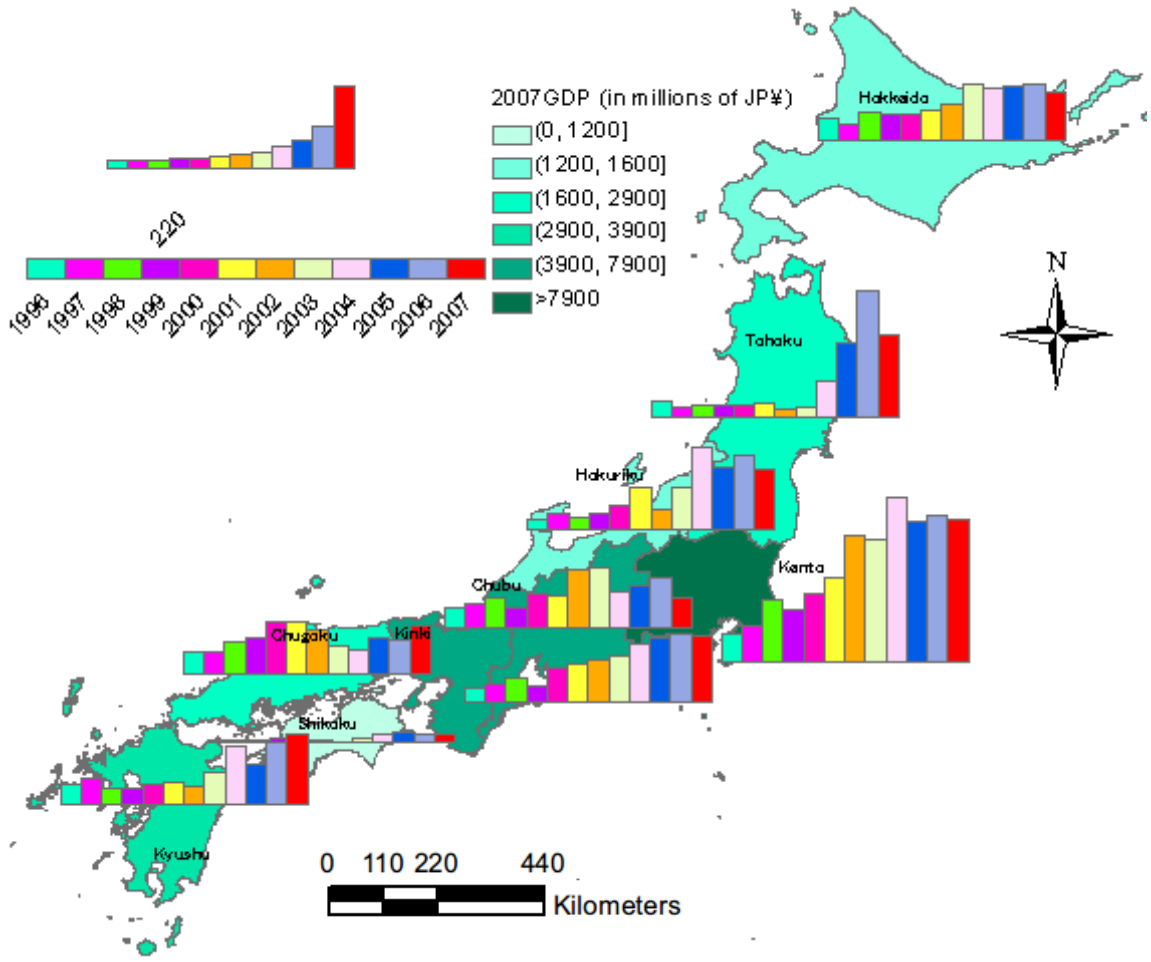

Figure 2.3 Trends of water pollution incidents and GDP (2007) in nine regions.

Figure 2.3 shows the trend of pollution incidents in different regions of Japan. Like the nationwide trend, most of the sub-regions such as Kanto, Hokuriku, Kyushu and Tohoku increased significantly from 1996 to 2007, especially since 2004, while Chugoku and Chubu were relatively stable. In addition, we can see that economically developed regions have more water quality incidents, with Kanto as the most striking example. The reasons for this phenomenon mainly include inequality in development (Akita and Kataoka, 2003), as more enterprises and higher population densities exist in the economically developed regions of Tokyo, Kanto, Osaka, Kinki, Nagoya, and Chubu, which reflect 68.8% of Japan's Gross Domestic Product (GDP) according to the 2007 economic statistics. As a consequence of development, these regions experience greater loads of industrial waste and domestic sewage, generally creating more frequent incidents of pollution and more serious risks water resources infrastructure. Furthermore, as can be seen in Figure 2.1, channel length of the first-class river systems in these places is long

(e.g. Kanto is the longest (13181.8km)), which may increase risk for water quality incidents because of its increasing exposure. In summary, the economically developed regions tend to have more water quality incidents, especially in Kanto.

2.3.2 Results of pollutant category

2.3.2.1 Distribution by pollutant category

Pollutant categories are recorded using five descriptors: “Oil”, “Chemical”, “Spills excepted oil and chemical”, “Other”, and “Natural”. “Other” category includes incidents where the reason was not determined. “Natural” category includes incidents where the category was not directly man-made. For example, water pollution due to fish die-offs in low oxygen water may results from factors such as drought, algal blooms, overpopulation, or a sustained increase in water temperature. **Figure 2.4** shows the national and regional distribution of pollution incidents by pollutant category for total incidents from 1996 to 2007. As can be seen from **Figure 2.4**, oil (76.61%) is the largest proportion of pollutant types in Japan. At the same time, oil is also the major source of each region, and Hokkaido (88.96%) is the largest among them. For “Natural” category, the proportion in Shikoku (0%) is the least; the proportion in Chubu (11.69%) is the largest at 135 incidents. Chubu is the widest part of Honshu and the central part is characterized by high, rugged mountains, which is populated with many sharp, short rivers that are easily impacted by natural hazards. Maybe this is why Chubu had the relatively large portion of "Natural" category.

2.3.2.2 Trend in pollutant category

The trend of water pollution incidents attributed to each category for the period from1996 to 2007 is shown in **Figure 2.5**. During the 12 year period there has been a great deal of change in the category of pollution incidents. First of all, the number of each category shows a growth trend, especially since 2005. Of these, “Oil” and “Other” categories fluctuated dramatically. In addition, the fluctuation in the “Natural” category was largely in Chubu (see **Figure 2.5** (Chubu)), in line with **Figure 2.4**.

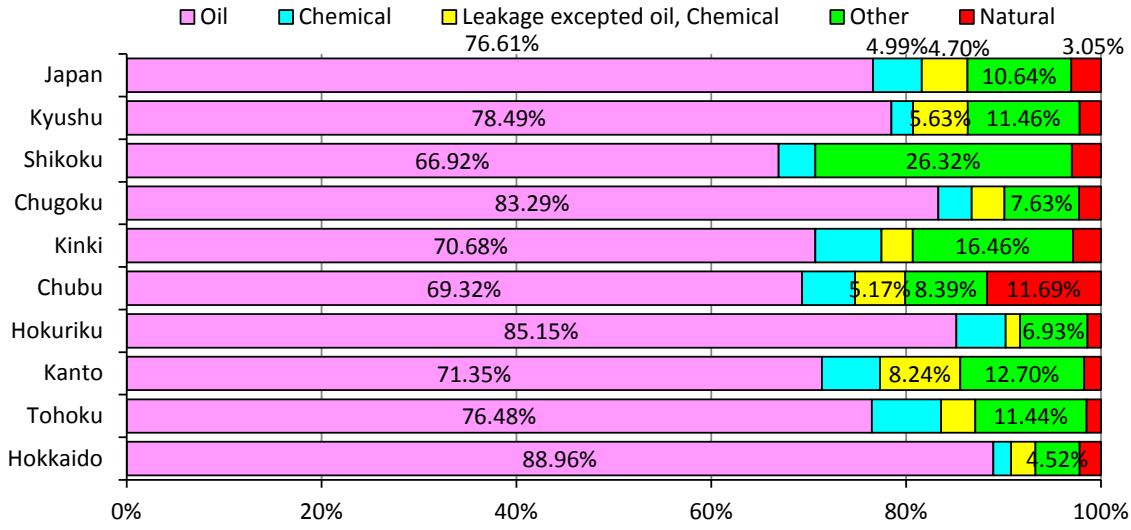

Figure 2.4 Distribution of water pollution incidents by category from 1996 to 2007.

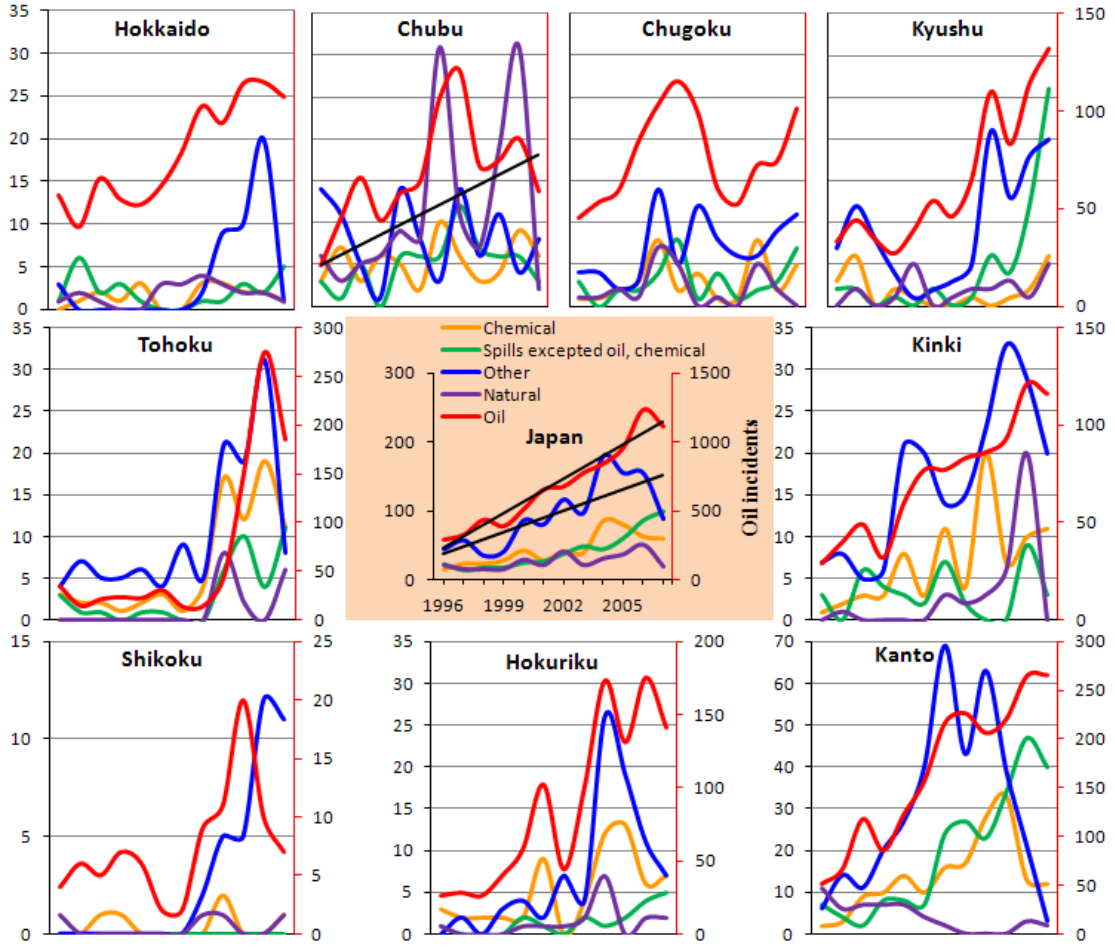

Figure 2.5 Trends in pollutant category from 1996 to 2007. The trend-line in Figure 2.6 (Chubu) shows the trend of pollution incidents caused by "Natural" category; the trend-lines in Figure 2.6 (Japan) show the trend of pollution incidents caused by "Oil" category and "Other" category, respectively.

2.3.3 Results of cause

2.3.3.1 Cause of incidents

To identify the cause of water pollution incidents, pollutant causes are recorded using seven descriptors: Poor working practice, Equipment failure, Accident, Illegal dumping, Other, Unknown, and Natural. “Accident” cause refers to traffic accident. “Other” cause refers to the accident except factory and traffic accident, such as aviation accident, etc. “Unknown” cause includes incidents where the cause was not determined, such as an unexplained oil spill, chemical spill, etc. “Natural” cause includes incidents where the cause was not man-made. Examining the 10581 incidents in Japan reveals that the main cause of incidents was “Unknown” (43%), followed by “Poor working practice” (24%), as shown in **Figure 2.6**. From the regional distribution, meanwhile, we can see that: in Hokuriku, the main cause of incidents was “Poor working practice” (36%), which is greater than “Unknown” (30%); in Tohoku, “Poor working practice” (29%) was equal to “Unknown” (29%); and in Chugoku, the proportion of “Accident” was 18%, which was the largest among all regions.

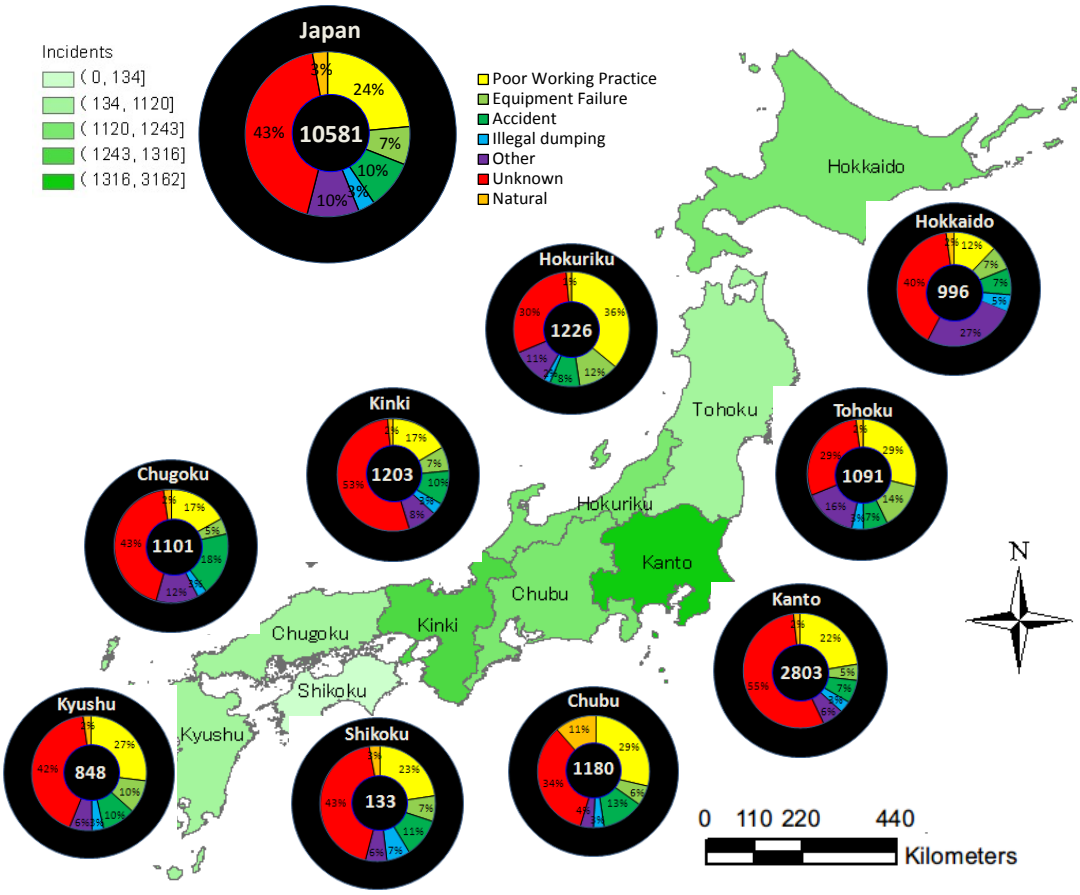

Figure 2.6 Distribution of water pollution incidents by causes from 1996 to 2007.

2.3.3.2 Trend in incident cause

Figure 2.7 shows the trend of incident cause for the period from 1996 to 2007. During the 12 year period, incidents from each cause grew, in particular the "Unknown" cause and "Poor working practice" cause (see **Figure 2.7** (Japan)), which generally reflects the situation in sub-regions (see **Figure 2.7** (Hokkaido) - **Figure 2.7** (Shikoku)). Of course, there are also some special cases. For example, a decreasing trend in incidents from "Other" causes occurred in Chugoku (see **Figure 2.7** (Chugoku)).

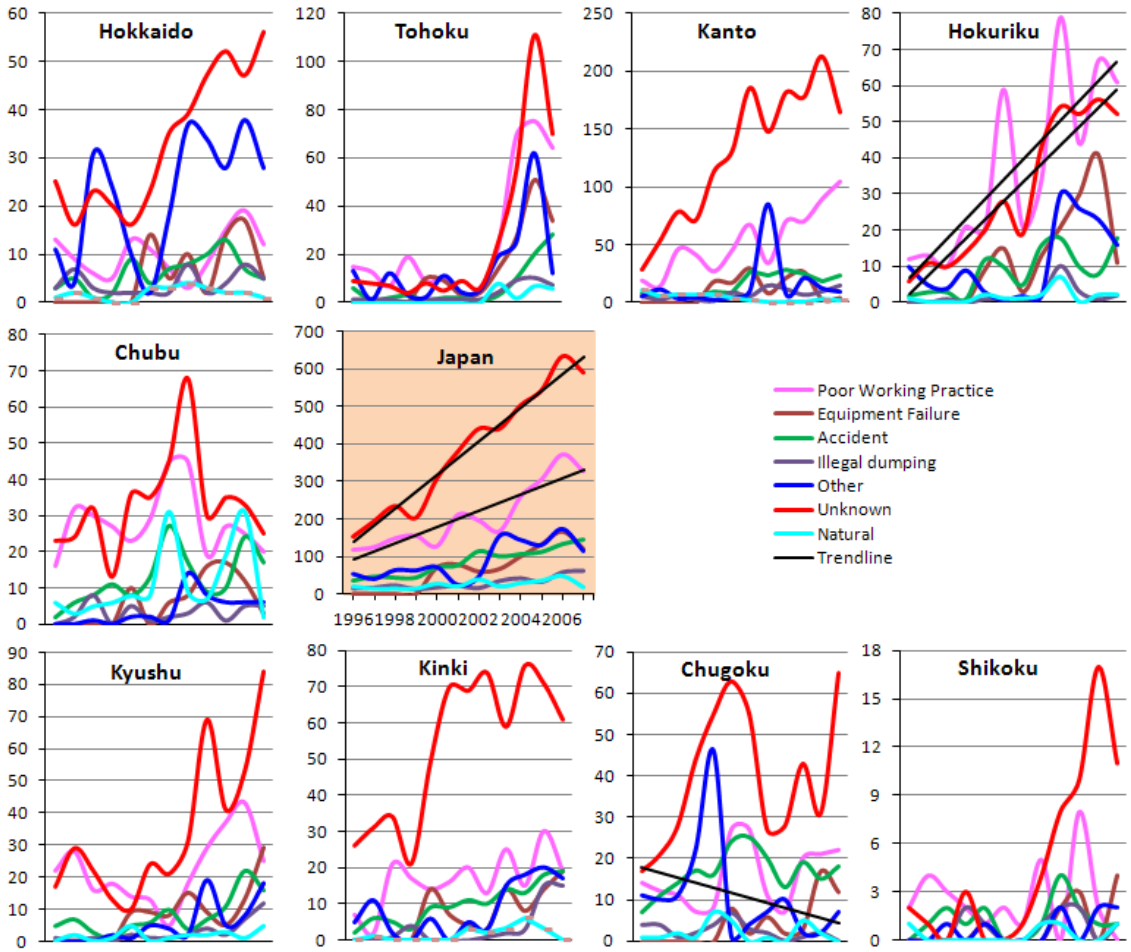

Figure 2.7 Causes of pollution incidents for the period 1996-2007. The trend-line in Figure 2.7 (Hokuriku) shows the trend of pollution incidents caused by "Poor Working Practice" category and "Unknown" category, respectively; the trend-lines in Figure 2.7 (Japan) show the trend of pollution incidents caused by "Unknown" category and "Poor Working Practice" category, respectively; the trend-line in Figure 2.7 (Hokuriku) shows the trend of pollution incidents caused by "Other" category.

2.3.4 Impacts of water pollution

Water pollution incidents can have significant adverse impact on people, communities, and wildlife, and recovery from such incidents may take several years. For example, the Camelford water pollution incident occurred in July 1988 and involved the accidental contamination of the drinking water supply to the town of Camelford, Cornwall, England with 20 tonnes of aluminium sulphate (Mcmillan et al., 1993). Approximately 20,000 people affected with a range of short-and possibly long-term health effects with long-term complication for some victims unclear until now(Exley and Esiri, 2006; Nsiah-Kumi, 2008). Because incidents mainly affect water supply systems such as drinking water, we present the impact of pollution incidents on water supply.

2.3.4.1 Damages to water supply establishments

In Japan, water supply is classified into four kinds of infrastructure (Health Service Bureau, Ministry of Health, Labour and Welfare, 2012). Service water supply includes utilities which supply water by pipe to water enterprises. Waterworks include infrastructure supplying water to populations of 5,001 persons or more. Simplified waterworks include systems supplying populations of 101-5,000 persons. Exclusive waterworks include owned-waterworks systems supplying water to populations of 101 persons or more. **Figure 2.8** shows the changes in four kinds of water supply infrastructure under the impact of water pollution incidents from 1983 to 2008. The most affected type during these years was waterworks, which occupied approximately 60% every year, followed by simplified waterworks. The primary reason for this includes annual water supply by waterworks (for example, it was 15 745 million cubic metres according to the statistic of 2002, which occupied about 94.8%) is more than other kinds of water supply infrastructure, which increases risk for water pollution.

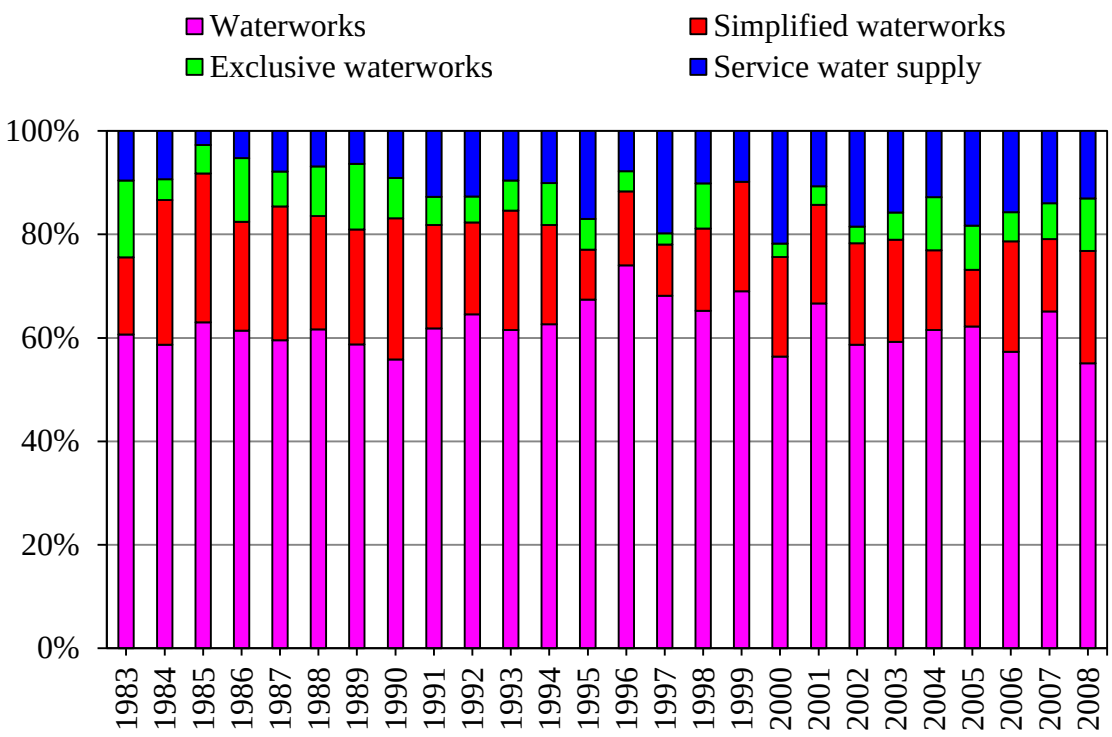

Figure 2.8 Changes in four kinds of water supply establishments under the impact of water pollution incidents from 1983 to 2008. Changes in four kinds of water supply establishments under the impact of water pollution incidents from 1983 to 2008.

2.3.4.2 Water supply by offensive tastes and odors

Figure 2.9 shows the changes in the incidence of water affected by offensive tastes and odors in the water supply from 1983 to 2008. The red broken line shows the population affected by offensive tastes and odors and the green bar graph shows the number of water utilities affected. The number of utilities affected by offensive odors and tastes maintained a relatively high and constant level, while the population decreased dramatically since 1990. The establishment of a legal system for the water supply and the penetration of water supply systems made a significant contribution to the improvement of health and hygienic conditions, which was the reason for the decrease in people since 1990 (Ando, 2008).

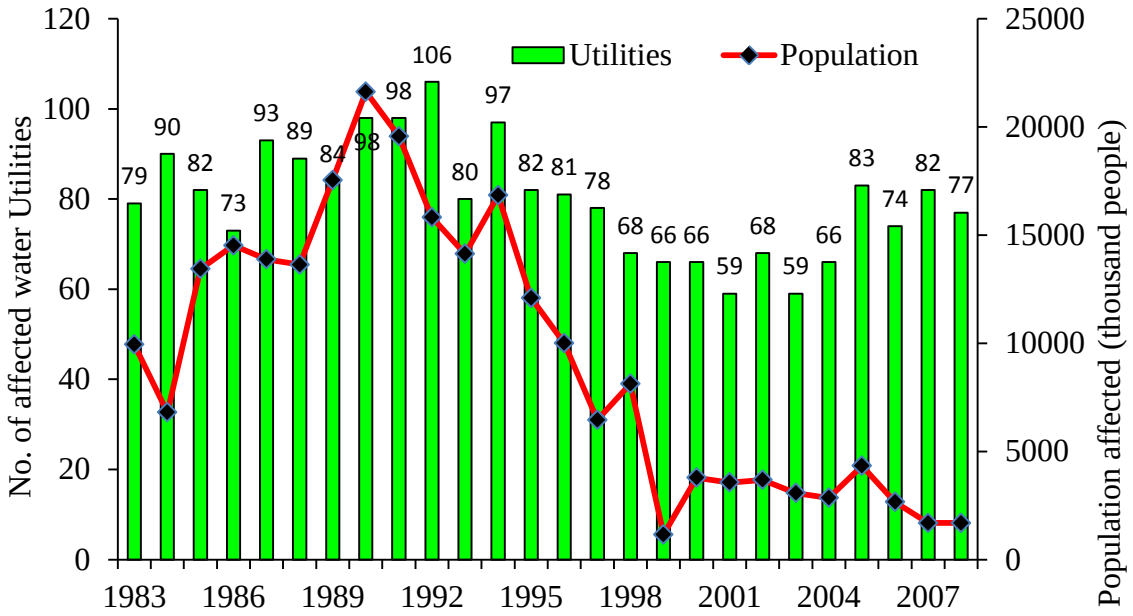

Figure 2.9 Changes in the incidence of offensive tastes and odors in water supply system from 1983 to 2008.

2.4 Discussions

Water pollution is also a big problem in many regions of the world. In recent years, for example, in North Ireland, there were almost 1,200 water pollution accidents annually (Northern Ireland Environment Agency, 2011); in China, there were almost 1,700 water pollution accidents annually and up to 40 percent of rivers were seriously polluted (Economy, 2013). In Japan, the above results show that water pollution incidents almost tripled to about 1487 in the last 10 years with agreement in trends in almost all of 9 regions examined. About 4 incidents happened per day in the first-class river systems. This trend will likely lead to harmful effects on both the economy and society, and certainly work against efforts at improvement of water quality for water supply. We provide our analysis of source categories and incident causes in the hopes that results will inform water managers and promote proactive water policy development.

Oil spills are the incident leading to the greatest risk to water quality both in Japan and worldwide (Wang et al., 2003). The reasons for this phenomenon are mainly related to oil consumption; Japan is the third largest oil consumer worldwide after the United States and China. Although the proportion of oil consumption decreased somewhat with the

widespread availability of energy saving technologies and fuel conversion, oil still represents about half of energy supply (see **Table 2.1**) (Petroleum Association of Japan, 2009). Release of a liquid petroleum hydrocarbon into the environment because of human activity is an inevitable consequence of oil consumption. The main sources of oil spills to Japanese rivers are from individual cars and boats, lawn mowers, underground pipelines, refineries, and airplanes (Yudakuken, 2012). After oil, chemical and other substances spill also contributed to growing incidence of water pollution.

With respect to incident cause, the reasons for oil, chemical and other substance spills were mainly “Unknown”, “Poor working practice”, “Equipment failure” and “Illegal dumping”. Among them, poor working practice was most likely to cause accidents (Bentley and Haslam, 2001) in many industries (Diane et al., 1999; Mearns et al., 2003). In recent years, increasing use of non-regular workers (such as dispatched workers, fixed-term contract workers and part-time workers), who generally lack systematic safety education, is increasing among employed people and was approximately 17.55 million in 2010, accounting for 30% of the total labor force (Ministry of Health, 2011). Illegal dumping is another major issue contributing to water quality incidents in Japan (Ichinose and Yamamoto, 2011; Miyazaki and Une, 2005). Although the number of cases decreased since 2001, the frequency of illegal dumping did not show a corresponding decline (as shown in **Figure 2.10**). Illegal dumping can have a huge negative impact on water quality, leading to release of toxic gasses created from chemical reactions of the waste materials, some poisonous. Finally, although “Natural” cause increased at a modest pace, natural disasters are also threatening water quality. For example, the Great East Japan Earthquake struck sewerage systems in the Tohoku area leading to the failure of many waste water treatment plants, resulting in reduced water quality. Furthermore, nuclear leakage following the Great Tohoku Earthquake continues to contribute to water pollution.

In summary, as oil demand increases, the trend in oil spills caused by “Poor working practice”, “Illegal dumping” and other causes is likely to increase and negatively impact water quality. “Natural” causes will likely remain important for water pollution. The government should reduce risk by strengthening education related to safe production for workers. In addition, adequate enforcement of laws and regulations concerning water pollution is necessary to protect the environment. Finally, more research on the interaction between water pollution and climate change is important as water pollution impacts and incidents my become more serious and frequent in altered climate conditions.

Table 2.1 Primary Energy Supply Trends (%)

Year	Oil	Coal	Natural gas	Nuclear power	Hydropower, geothermal	New energy
1973	77.4	15.5	1.5	0.6	4.1	0.9
1980	66.1	17.0	6.1	4.7	5.3	1.0
1985	56.3	19.4	9.4	8.9	4.8	1.2
1990	57.1	16.7	10.2	9.3	4.1	2.6
1995	54.8	16.5	10.9	11.9	3.4	2.5
2000	50.8	18.1	13.0	12.2	3.3	2.6
2005	49.0	20.3	13.8	11.2	2.9	2.8
2007	47.0	21.3	16.3	9.7	2.8	2.9

(Data source: Petroleum Industry in Japan 2009)

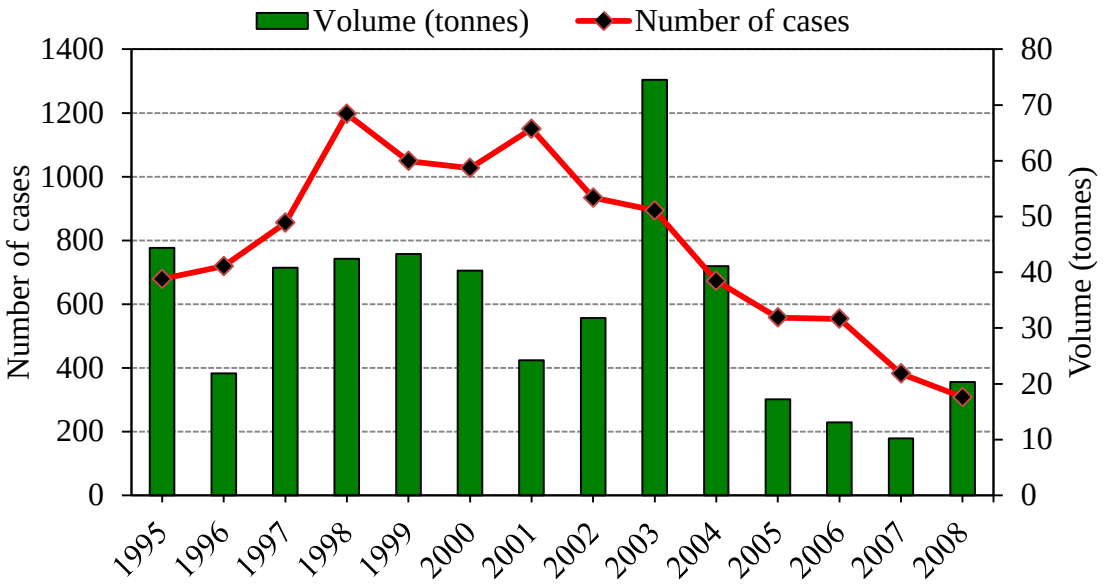

Figure 2.10 Trend in illegal dumping from 1995 to 2008. (Data source: Ministry of the environment of Japan, 2009)

2.5 Conclusions

This spatiotemporal evaluation of water quality incidents in Japan provides numerous insights into the total of incident numbers, incident causes, pollutant categories, and pollution affects. Additionally, this analysis suggests explanations about the cause of trends in incident occurrence. The potential reasons for the fast growth in pollution incidents and

changes in pollutant categories have also been expounded. Fast growth of water quality incidents was the most prominent recent trend observed. Water pollution incidents in the first-class river systems almost tripled to about 1487 in the latest 10 years, and 5 out of nine regions were also in this way. According to the analysis of pollutant category, oil is the most frequent pollutant type in Japan (76.61%) and also the major source of water pollution for each region. The number of each category shows growth trends, especially since 2005. “Oil” and “Other” categories varied dramatically. In addition, the fluctuation of “Natural” category was largely due to variability in Chubu. Of the total 10581 incidents from 1996 to 2007, the main cause of incidents was “Unknown” (43%), followed by “Poor working practice” (24%), and then by “Accident” (10%) and “Other” (10%). In Hokuriku, however, the main cause of incidents was “Poor working practice” (36%), which is greater than “Unknown” (30%). The trend of “Unknown” and “Poor working practice” causes also increased. Among four kinds of water supply infrastructure affected by pollution incidents, waterworks (approximately 60%) was the largest, followed by simplified waterworks. The population affected by offensive odors and tastes peaked in 1990 and has been decreasing since 1990.

2.6 References

Akita, T. and Kataoka, M., 2003. Regional income inequality in the post war Japan, Available: http://www.jyu.fi/ersa2003/cdrom/papers/480.pdf, pp. 27-30.

Amisah, S. and Cowx, I.G., 2000. Response of the fish populations of the River Don in South Yorkshire to water quality and habitat improvements. Environmental Pollution, 108(2): 191-199.

Bentley, T.A. and Haslam, R.A., 2001. A comparison of safety practices used by managers of high and low accident rate postal delivery offices. Safety Science, 37(1): 19-37.

Diane, E., A. G. F. GIBB and Roger A. H., 1999. The quality of accident and health data in the construction industry: interviews with senior managers. Construction Management and Economics, 17(2): 197-204.

Duan, W., Chen, G., Ye, Q. and Chen, Q., 2011. The situation of hazardous chemical accidents in China between 2000 and 2006. Journal of Hazardous Materials, 186(2-3): 1489-1494.

Duan, W., Takara, K., He, B., Luo, P., Nover, D., Yamashiki, Y., Spatial and temporal trends in estimates of nutrient and suspended sediment loads in the Ishikari River, Japan, 1985 to 2010. Science of the Total Environment. DOI: 10.1016/j.scitotenv.2013.05.022.

Economy, E., 2013. China's Water Pollution Crisis. Available: http://thediplomat.com/2013/01/22/forget-air-pollution-chinas-has-a-water-problem/.

Exley, C. and Esiri, M.M., 2006. Severe cerebral congophilic angiopathy coincident with increased brain aluminium in a resident of Camelford, Cornwall, UK. Journal of Neurology, Neurosurgery and Psychiatry, 77(7): 877-879.

Ganoulis, J., 2009. Risk analysis of water pollution, Wiley-VCH, 327 pp.

Ham, Y.S. et al., 2012. Distribution of antibiotic resistance in urban watershed in Japan. Environmental Pollution, 162: 98-103.

Health Service Bureau, Ministry of Health, Labour and Welfare. 2012-3-21(in Japanese). Available: http://www.mhlw.go.jp/seisakunitsuite/bunya/kenkou_iryou/kenkou/.

Honma, S. and Hu, J.L., 2009. Efficient waste and pollution abatements for regions in Japan. International Journal of Sustainable Development and World Ecology, 16(4): 270-285.

Hosono, T., Su, C.C., Okamura, K. and Taniguchi, M., 2010. Historical record of heavy metal pollution deduced by lead isotope ratios in core sediments from the Osaka Bay, Japan. Journal of Geochemical Exploration, 107(1): 1-8.

Hou, Y. and Zhang, T., 2009. Evaluation of major polluting accidents in China--Results and perspectives. Journal of Hazardous Materials, 168(2-3): 670-673.

Hrudey, S.E., Hrudey, E.J. and Pollard, S.J.T., 2006. Risk management for assuring safe drinking water. Environment International, 32(8): 948-957.

Ichinose, D. and Yamamoto, M., 2011. On the relationship between the provision of waste management service and illegal dumping. Resource and Energy Economics, 33(1): 79-93.

Tsumori, J., Tanaka, H., Okayasu, Y., Suzuki, Y., 2004. River Management and Counterm easure Technologies for Accidental Spills by Ministry of Land, Infrastructure and Tra nsport in Japan (Japanese). Available: https://www.pwri.go.jp/eng/activity/pdf/reports /tsumori,_okayasu_and_suzuki041012.pdf.

Luo, P. et al., 2011. Spatiotemporal trend analysis of recent river water quality conditions in Japan. Journal of Environmental Monitoring, 13(10): 2819-2829.

Mao, J., Wang, Y.L., Zhang, Y.Q. and Ying, L., 2011. Analysis and Countermeasures of Drinking Water Contamination Incidents in Shanghai in 2009-2010. Journal of Environment and Health, 28(3): 245-247.

McMillan, T.M. et al., 1993. Camelford Water Poisoning Accident; Serial Neuropsychological Assessments and Further Observations on Bone Aluminium. Human and Experimental Toxicology, 12(1): 37-42.

Mearns, K., Whitaker, S.M. and Flin, R., 2003. Safety climate, safety management practice and safety performance in offshore environments. Safety Science, 41(8): 641-680.

Ministry of Health, Labour and Welfare. Such as dispatched workers, fixed-term contract workers and part-time workers 2011. Available: http://www.mhlw.go.jp/english/org/pamphlet/dl/pamphlet-about_mhlw.pdf.

Ministry of the Environment of Japan. Report of illegal dumping, 2009 (in Japanese). Available: http://www.env.go.jp/press/file_view.php?serial=15096&hou_id=12126.

Miyazaki, M. and Une, H., 2005. Infectious waste management in Japan: A revised regulation and a management process in medical institutions. Waste Management, 25(6): 616-621.

Nakano, T. et al., 2008. Effect of agriculture on water quality of Lake Biwa tributaries, Japan. Science of the Total Environment, 389(1): 132-148.

Nsiah-Kumi, P.A., 2008. Communicating effectively with vulnerable populations during water contamination events. Journal of water and health, 6(1): 63-76.

Pangare, G., 2006. The source of the problem. Nature, 441(7089): 28-28.

Petroleum Association of Japan. Petroleum Industry in Japan 2009. Available: http://www.paj.gr.jp/english/.

Polizzotto, M.L., Kocar, B.D., Benner, S.G., Sampson, M. and Fendorf, S., 2008. Near-surface wetland sediments as a source of arsenic release to ground water in Asia. Nature, 454(7203): 505-508.

Programme, W. W. A, 2009. The United Nations world water development report 3: water in a changing world. UNESCO Publishing, Paris, France and Earthscan London, UK.

Schwarz, G. E. and G. S. US, 2006. The SPARROW surface water-quality model: Theory, application, and user documentation, US Geological Survey.

Schwarzenbach, R.P., Egli, T., Hofstetter, T.B., Von Gunten, U. and Wehrli, B., 2010. Global water pollution and human health. Annual Review of Environment and Resources, 35: 109-136.

Shibata, T., Solo-Gabriele, H.M. and Hata, T., 2012. Disaster Waste Characteristics and Radiation Distribution as a Result of the Great East Japan Earthquake. Environmental Science and Technology, 46: 3618-3624.

Ando S. History and Development of Drinking Water Quality Management in Japan, 2008 (in Japanese). Available: http://www.jwrc-net.or.jp/aswin/projects-activities/rd_files/jp-kr_cooperation/2008_soul100th_es.pdf.

Takahasi, Y., 2009. History of Water Management in Japan from the End of World War II. Water Resources Development, 25(4): 547-553.

Törnqvist, R., Jarsjö, J. and Karimov, B., 2011. Health risks from large-scale water pollution: Trends in Central Asia. Environment International, 37(2): 435-442.

Tsujimoto, A., Nomura, R., Yasuhara, M., Yamazaki, H. and Yoshikawa, S., 2006. Impact of eutrophication on shallow marine benthic foraminifers over the last 150 years in Osaka Bay, Japan. Marine Micropaleontology, 60(4): 258-268.

Vörösmarty, C.J., Green, P., Salisbury, J. and Lammers, R.B., 2000. Global water resources: vulnerability from climate change and population growth. Science, 289(5477): 284.

Wakakura, M. and Iiduka, Y., 1999. Trends in chemical hazards in Japan. Journal Of Loss Prevention In The Process Industries, 12(1): 79-84.

Wang, H., Wang, C., Wu, W., Mo, Z. and Wang, Z., 2003. Persistent organic pollutants in water and surface sediments of Taihu Lake, China and risk assessment. Chemosphere, 50(4): 557-562.

Weiss, N.A. and Hassett, M.J., 2012. Introductory statistics. Pearson Education.

Wu, S. et al., 2009. A role for human reliability analysis (HRA) in preventing drinking water incidents and securing safe drinking water. Water Research, 43(13): 3227-3238.

Yasuhara, M. and Yamazaki, H., 2005. The impact of 150 years of anthropogenic pollution on the shallow marine ostracode fauna, Osaka Bay, Japan. Marine Micropaleontology, 55(1): 63-74.

Yen, C.H., Chen, K.F., Sheu, Y.T., Lin, C.C. and Horng, J.J., 2012. Pollution Source Investigation and Water Quality Management in the Carp Lake Watershed, Taiwan. Clean–Soil, Air, Water, 40(1): 24-33.

Yudakuken. Cases of oil spill, 2012-3-19 (in Japanese). Available: http://www.yudakuken.com/jikorei.html.

Zushi, Y., Takeda, T., Masunaga, S., 2008. Existence of nonpoint source of perfluorinated compounds and their loads in the Tsurumi River basin, Japan. Chemosphere. 71(8): 1566-1573.

Chapter 3 Assessment of Precipitation Amounts and Climate Extremes

3.1 Introduction

Changes in extreme weather and climate extreme events have significant negative impacts on natural environment and human society and are among the most serious challenges to society in coping with a changing climate (Thomas et al., 2008). For example, precipitation extreme events are more frequent than they used to be, which do serious damages on the social and natural systems including flooding and soil erosion (Sugiyama et al., 2010). Considering heavy precipitation events and floods, moreover, adaptation bears a particular urgency, as many water resource structures (such as dams, bridges, storm drains, or sewer systems) are planned for lifetimes exceeding 50 years (Rajczak et al., 2013). Therefore, it is momentous to understand the changes in the past and thereby predict what will happen in the future and finally to improve the ability to manage the risks associated with precipitation extreme events.

Many efforts have been made to assess and predict changes in spatial and temporal patterns of precipitation amounts and extreme events in different scales around the world using observational climatic data and climate scenario data, and show that precipitation extremes will become more frequent, more widespread and/or more intense during the 21st century (Alexander et al., 2006; Coumou and Rahmstorf 2012; Dai 2011; Stocker et al., 2013). For example, based on daily precipitation dataset of 740 stations from 1950 to 2000, Zhai et al., (2005) argued that extreme precipitation significantly increased in western China, in the mid–lower reaches of the Yangtze River, and in parts of the southwest and south China coastal area. Using a 1951-2003 gridded daily rainfall dataset, Krishnamurthy et al., (2009) indicated that statistically significant increasing trends in extremes of rainfall are identified over many parts of India. Kuo et al., (2011) found that the common trends of extreme precipitation at most stations are upward in southern Taiwan.

Meanwhile, some studies have explored the linkages between global Sea Surface

** Part of this chapter is submitted into **Climate Dynamics**, 2014.*

Temperatures (SSTs) and precipitation extremes, indicating changes of SSTs plays a leading role in the precipitation anomalies (Fontaine and Janicot 1996; Nobre and Srukla 1996). For example, Bader and Latif (2003) found that the warming of the Indian Ocean in the last decades is of paramount importance in driving the observed decadal drying trend over the West Sahel. Xie et al., (2010) argued that tropical precipitation changes are positively correlated with spatial deviations of SSTs warming from the tropical mean.

Increasing trends in precipitation climate extremes have also been found for Japan because of the impact of climate change on the hydro-climatology (Solomon 2007). For example, on the basis of 50 stations, Fujibe (2006; 2005) argued that the extreme daily precipitation, extreme four-hourly and hourly precipitation increased in the past century. Miyajima and Fujibe (2011) found that the distribution of top ten-minute precipitation has a moderate north-south gradient, and extreme precipitation shows local maxima on southern sides of land in western Japan corresponding to orographic enhancement. On the other hand, some authors have analyzed variations in precipitation amounts across Japan at different timescales and territories. For example, using linear regression method, Iwasaki and Sunaga (2009) elucidated the features of weak rainfall between June and September for 31 years. Takeshita (2010) estimated the precipitation variation in Miyazaki prefecture and Suzuki and Hayakawa (2006) explored the characteristics of summertime convective precipitation in Yamaguchi prefecture. All of these studies detected characteristics of precipitation, but information of changes in precipitation amounts and precipitation climate extremes over last century is few.

Besides the precipitation amounts, much of these researches are based on the use of so-called “extremes indices”, which are more generally defined for daily temperature and precipitation characteristics such as the hottest or coldest day of the year, heavy precipitation events, and dry spells (Zhang et al., 2011). Moreover, a total of 27 indices were considered to be core indices in describing and assessing climate extremes by the Expert Team on Climate Change Detection and Indices (ETCCDI) (Sillmann et al., 2013).

Therefore, the objectives of this study are to calculate the spatial and temporal variability of the seasonal changes in precipitation amounts, and to develop indices and indicators for monitoring trends in climate extremes and to apply them to the projection of future changes in climate extremes. The study is organized as follows: The datasets, data quality control and methodology are briefly described in the next section. The trend results of precipitation amounts and precipitation extreme indices are presented in Section 3.3,

followed by discussions (Section 3.4) and conclusions (Section 3.5).

3.2 Data and methods

3.2.1 Datasets and quality control

Daily precipitation observed at 51 weather stations in Japan are used to construct interannual and seasonal time series of precipitation amount and 10 extreme precipitation indices from 1901 to 2012 (**Figure 3.1** and **Table 3.1**). All these stations are belong to the Automated Meteorological Data Acquisition System (AMeDAS), which is a high-resolution surface observation network developed by the Japan Meteorological Agency (JMA) used for gathering regional weather data such as sunlight, temperature, precipitation, and wind velocity and direction and verifying forecast performance (Kawamoto et al. 2011). Because the AMeDAS data we obtained is until 2008, so the data from 2009 to 2012 at these stations are used from Japan Meteorological Agency (JMA). All of the daily data were rearranged into monthly, seasonal and annual data using FORTRAN program. According to the climate conditions of Japan, the seasons are considered as: winter = December, January, February; spring = March, April, May; summer = June, July, August; autumn = September, October, November.

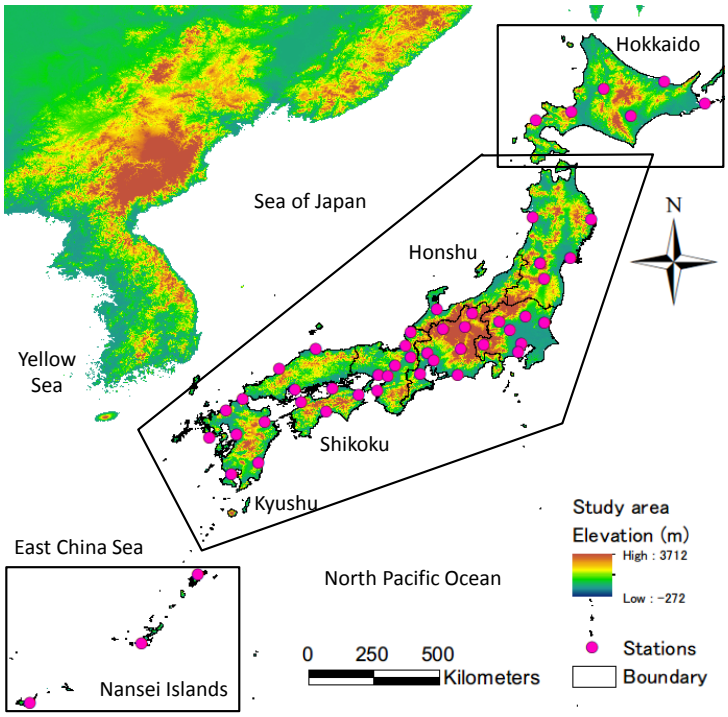

Figure 3.1 Study area and weather stations.

Table 3.1 Weather stations

Station ID	Station number	Station name	Longitude	Latitude	Station ID	Station number	Station name	Longitude	Latitude
J_D1	47409	Abashiri	144.2783	44.01667	J_D27	47629	Mito	140.4667	36.38
J_D2	47582	Akita	140.0983	39.71667	J_D28	47585	Miyako	141.965	39.64667
J_D3	47617	Alpine	137.2533	36.155	J_D29	47830	Miyazaki	131.4133	31.93833
J_D4	47407	Asahikawa	142.3683	43.77167	J_D30	47610	Nagano	138.1917	36.66167
J_D5	47742	Border	133.235	35.54333	J_D31	47817	Nagasaki	129.8667	32.73333
J_D6	47616	Fukui	136.2217	36.055	J_D32	47636	Nagoya	136.965	35.16667
J_D7	47807	Fukuoka	130.375	33.58167	J_D33	47936	Naha	127.685	26.20667
J_D8	47595	Fukushima	140.47	37.75833	J_D34	47909	Naze	129.495	28.37833
J_D9	47606	Fushiki	137.055	36.79167	J_D35	47420	Nemuro	145.585	43.33
J_D10	47632	Gifu	136.7617	35.4	J_D36	47417	Obihiro	143.2117	42.92
J_D11	47755	Hamada	132.07	34.89667	J_D37	47815	Oita	131.6183	33.235
J_D12	47654	Hamamatsu	137.7183	34.70833	J_D38	47772	Osaka	135.5183	34.68167
J_D13	47761	Hikone	136.2433	35.275	J_D39	47412	Sapporo	141.3283	43.05833
J_D14	47637	Iida	137.8217	35.52333	J_D40	47762	Shimonoseki	130.925	33.94833
J_D15	47918	Ishigaki Island	124.1633	24.33667	J_D41	47421	Suttsu	140.2233	42.795
J_D16	47592	Ishinomaki	141.2983	38.42667	J_D42	47890	Tadotsu	133.7517	34.275
J_D17	47827	Kagoshima	130.5467	31.55333	J_D43	47895	Tokushima	134.5733	34.06667
J_D18	47770	Kobe	135.2117	34.69667	J_D44	47662	Tokyo	139.76	35.69
J_D19	47893	Kochi	133.5483	33.56667	J_D45	47651	Tsu	136.52	34.73333
J_D20	47638	Kofu	138.5533	35.66667	J_D46	47631	Tsuruga	136.0617	35.65333
J_D21	47626	Kumagai	139.38	36.15	J_D47	47615	Utsunomiya	139.8683	36.54833
J_D22	47819	Kumamoto	130.7067	32.81333	J_D48	47777	Wakayama	135.1633	34.22833
J_D23	47759	Kyoto	135.7317	35.015	J_D49	47766	Kure	132.55	34.24
J_D24	47624	Maebashi	139.06	36.405	J_D50	47588	Yamagata	140.345	38.255
J_D25	47618	Matsumoto	137.97	36.245	J_D51	47670	Yokohama	139.6517	35.43833
J_D26	47887	Matsuyama	132.7767	33.84333					

Table 3.2 List of stations with more than three missing records

Station ID	Station number	Station name	Periods of unrealistic climatic records	Number of months
J_D6	47616	Fukui	Feb. -Dec., 1938(except May, Jul. and Oct.); Jul. -Aug., 1945	11
J_D20	47638	Kofu	Jun. –Jul., 1945	2
J_D45	47651	Tsu	Jul., 1989	1
J_D12	47654	Hamamatsu	Jun., 1945	1
J_D51	47670	Yokohama	Aug. –Dec., 1923	5
J_D49	47766	Kure	Apr., 1945; Jun., 1945 –Sep., 1946	17
J_D18	47770	Kobe	Mar., 1945	1
J_D33	47936	Naha	Jan. –Jul., 1923; Oct., 1943: Sep., 1944; Feb., 1945 –Dec., 1950; Feb. –Mar., 1951	83

In order to avoid that erroneous outliers can impact seriously on trends, data quality control is an important and necessary step before the analysis of precipitation extremes variation. In this study, data quality control was carried out using the computer program RClimDex (Zhang and Yang 2004), which is a widely used approach because it can identify potentially unrealistic climatic records, including negative values of daily maximum-minus-minimum temperatures outliers (typically exceeding 4 standard deviations difference from the mean), and negative values of daily precipitation (Alexander et al., 2006; Zongxing et al., 2012). **Table 3.2** shows where more than three missing or unrealistic climatic records were found in a month after data quality control. Among these stations, Naha station had the longest period of missing or unrealistic climatic records with up to 83 months, nearly 7 years and all these months were cleared out when we calculated the extremes indices. Except for these stations, the daily precipitation coverage was nearly perfect with missing records less than three from 1901 to 2012, totally 40908 days.

After data quality control, homogeneity assessment is another important step to find whether the precipitation variations are caused only by variations in climate. Usually, most long-term climatological time series have been affected by a number of non-climatic factors such as instruments, observing practices, station locations, formulae used to calculate means, and station environment, that make these data unrepresentative of the actual climate variation occurring over time (Aguilar et al., 2003). It is important, therefore, to remove the inhomogeneities or at least determine the possible error they may

cause. Many researchers have put a great deal of effort into developing ways to identify non-climatic inhomogeneities and then adjust the data to compensate for the biases these inhomogeneities produce (Guttman 1998; Vincent et al., 2005). Here, the RHTest software, developed at the Climate Research Branch of Meteorological Service of Canada, was employed to determine if there were artificial changes at the station (such as station moves) that significantly impacted the observations (Aguilar et al., 2009). This program is based on a two-phase regression model with a linear trend for the entire time series, which can identify multiple step changes at documented (by station history information) or undocumented change points in a time series (Wang 2003; Wang 2008). Results of homogeneity checks show that precipitation data at all stations are good.

3.2.2 Selected extreme precipitation indices

Except for precipitation amounts, we used 10 indices (**Table 3.3**) developed and recommended by the ETCCDI (available at http://www.climdex.org/indices.html) to analyze extremes and detect precipitation variations. All these selected indices (**Table 3.3**) fall roughly into four categories (Sillmann et al., 2013; Zhang et al., 2011):

(1) Absolute indices, which describe, for instance, the annual maximum 1 day or 5 day precipitation rates;

(2) Threshold indices, which count the number of days when a fixed precipitation threshold is exceeded, for instance, frost days or tropical nights;

(3) Duration indices, which describe the length of wet and dry spells such as consecutive wet days (CWD) and consecutive dry days (CDD);

(4) Percentile-based threshold indices, which describe the exceedance rates above or below a threshold which is defined as the 95th or 99th percentile derived from the 1961-1990 base period (R95p and R99p).

Table 3.3 Definitions of 10 precipitation indices used in this study

ID	Indicator name	Definitions	Units
RX1day	Max 1-day precipitation amount	Monthly maximum 1-day precipitation	mm
RX5day	Max 5-day precipitation amount	Monthly maximum consecutive 5-day precipitation	mm
SDII	Simple daily intensity index	Annual total precipitation divided by the number of wet days (defined as RR>=1.0mm) in the year	mm/day
R10mm	Number of heavy precipitation days	Annual count of days when RR>=10mm	day
R20mm	Number of very heavy precipitation days	Annual count of days when RR>=20mm	day
CDD	Consecutive dry days	Maximum number of consecutive days with RR<1mm	day
CWD	Consecutive wet days	Maximum number of consecutive days with RR>=1mm	day
R95p	Very wet days precipitation	Annual total PRCP when RR>95th percentile of precipitation on wet days in the 1961-1990 period	mm
R99p	Extremely wet days precipitation	Annual total PRCP when RR>99th percentile of precipitation on wet days in the 1961-1990 period	mm
PRCPTOT	Annual total wet-day precipitation	Annual total PRCP in wet days (RR>=1mm)	mm

Abbreviations are as follows: RR, daily precipitation. A wet day is defined when RR≧1 mm, and a dry day when RR<1 mm.

3.2.3 Area averaging and trend calculation

After data control, all the seasonal precipitation amounts and extreme indices and the anomalies of these indices were calculated. The select base period for the anomalies was 1981-2010. A positive anomaly value indicates that the precipitation indices was greater than the average precipitation indices from 1980- 2010, while a negative anomaly indicates that the observed precipitation indices was less than the average precipitation indices from 1980- 2010.

Trend analysis was completed using the Kendall's tau test (Press 2007) for monotonic trends to determine if statistically significant trends exist in seasonal precipitation amounts as well as in measures of precipitation extremes, through time. Kendall's tau test is a non-parametric hypothesis test for statistical dependence based on the tau coefficient to

measure the association between two measured quantities (Helsel and Hirsch 1992); that is, Kendall's Tau is interpreted as a simple function of the probability that as x increases, y will increase. Here, the x is time series. Kendall's tau values between −1.0 and 0.0 imply a negative correlation, values between 0.0 and 1.0 imply a positive correlation and values 0.0 imply complete independence of the data set. Tau values are considered statistically significant at $p \leq 0.05$.

Regional analysis is momentous in a changing climate in that it can describe, compare, and explore climate changes between different regions and hence it has been used in many researches (Giorgi and Francisco 2000). So regionally averaged anomaly series for each index were calculated through the following equation:

$$x_{r,t} = \sum_{i=1}^{n_t}(x_{i,t} - \overline{x_i})/n_t \quad (3.1)$$

where $x_{r,t}$ is the regionally averaged index at year t; $x_{i,t}$ is the index for station i at year t; $\overline{x_i}$ is the 1901–2012 index mean at station i; n_t is the number of stations with data in year t. To avoid the average series being dominated by those stations with high value, we standardized $(x_{i,t} - \overline{x_i})$ by dividing by the station standard deviation. Also, it can generally provide more information about the magnitude of the anomalies because influences of dispersion have been removed. Finally spatial distribution maps were generated by applying ordinary kriging, an interpolation technique based on cross-validation of statistical results (Río et al., 2011).

3.3 Results

3.3.1 Annual precipitation amounts and trends

The widely variable nature of Japan precipitation has been evident over roughly the past 112 years. **Figure 3.2 (a)** shows the national precipitation departures in Japan, 1901–2012, based on the average from 1981 to 2010, suggesting what was experienced over the past 112 year. These intervals have included: (1) 8 years with deficits exceeding 200 mm, while 22 years had surpluses exceeding 200 mm; (2) There were relatively two wettest year periods (1901-1923 and 1948-1959) and two driest year periods (1924-1947 and 1960-2012); (3) The wettest consecutive 12 years (1948-1959) of any 12 years interval; (4) 1923

was the wettest year on record, while 1994 was the driest year on record.

Figure 3.2 (b) illustrates the time series of regionally averaged rainfall amounts in Japan, suggesting precipitation had fluctuated from year to year over the period 1901–2012. The value of Kendall's tau was -0.087, which indicates that a substantial decrease in mean annual precipitation has been observed in the past years. More concretely, the solid linear trend line shows that annual precipitation has decreased by 72.4 mm over the past 112 years. Precipitation in 1923 (approximately 1925.89 mm) and 1994 (approximately 1142.44 mm) represent the highest amount and least amount respectively, which are in line with the wettest year and driest year shown in Figure 3.2(a). In comparison with Figure 3.2(a) and Figure 3.2(b), the fluctuation of precipitation became more frequent and intense, especially from 1960s.

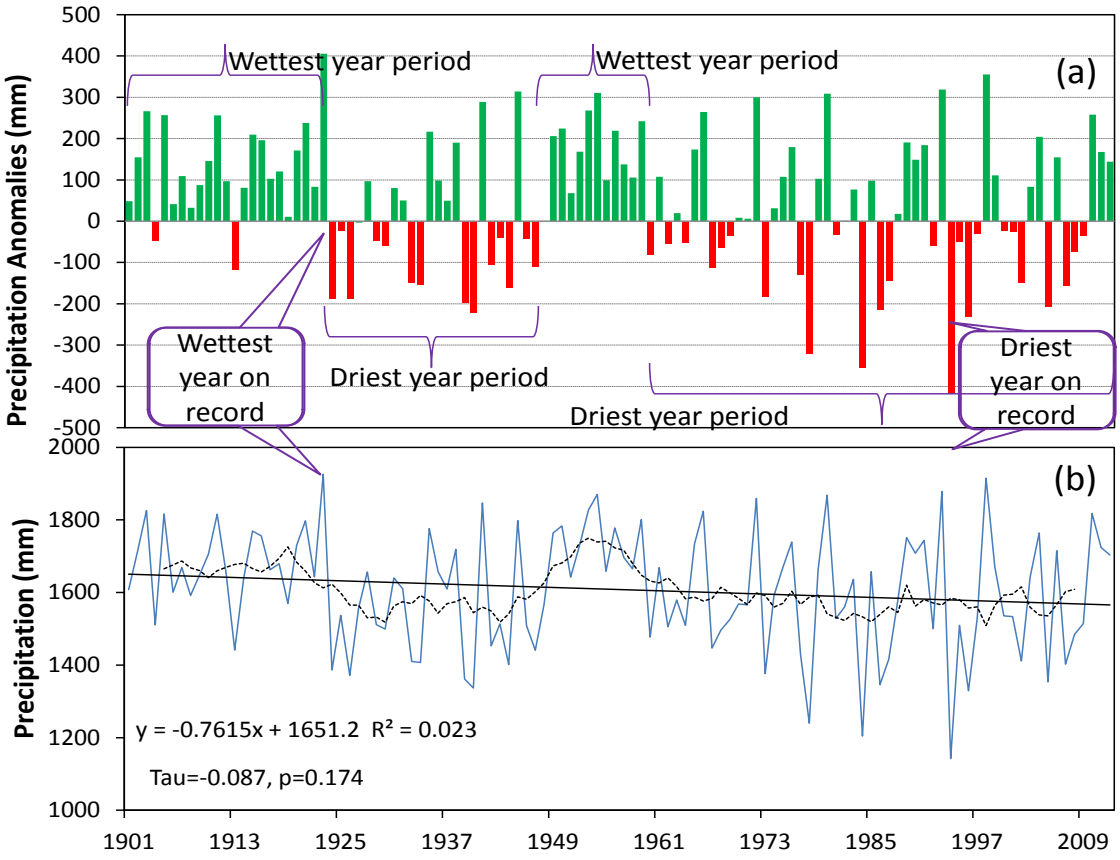

Figure 3.2 (a) National precipitation departures in Japan, 1901–2012, based on the average from 1981 to 2010; (b) Changes of regionally averaged rainfall amounts (mm) with line trend (straight line) and 9-year running mean (dotted curve) in Japan.

Table 3.4 Annual trends and percentage of stations with positive or negative trends for regional indices of precipitation extremes in Japan during 1901–2012

ID	Regional trends	Range	Showing positive trend	Showing significant positive trend	Showing negative trend	Showing significant negative trend
RX1day	0.114	-0.134-0.229	37	2	14	1
RX5day	0.115	-0.107-0.17	38	5	13	0
SDII	**0.140**	-0.136-0.244	43	9	8	1
R10mm	**-0.129**	-0.208-0.169	7	1	44	13
R20mm	-0.023	-0.176-	16	1	35	1
CDD	**0.237**	-0.0377-0.223	47	23	4	0
CWD	**-0.178**	-0.236-0.249	11	2	40	22
R95p	0.083	-0.0856-	38	3	13	0
R99p	**0.150**	-0.142-	40	6	11	1
PRCPTOT	-0.081	-0.161-0.133	7	1	44	4
Annual precipitation	-0.087	-0.169-0.117	6	0	45	4
Spring-precipitation	-0.009	-0.124-0.0759	23	0	29	0
Summer-precipitation	-0.005	-0.188-0.128	27	1	34	1
Autumn-precipitation	-0.116	-0.169-0.0795	5	0	46	11
Winter-precipitation	-0.115	-0.222-0.175	2	1	49	4

As shown in **Figure 3.3**, the annual mean precipitation, which ranges from 836 to 2990 mm across Japan, was much less in the Hokkaido compared to the other regions and much higher in southwest compared to the northeast. **Figure 3.3** also shows annual

precipitation decreasing at 45 stations (approximately 88% of the total number of stations), which were distributed widely across Japan, suggesting precipitation decreased overall from 1901 to 2012. Stations with significance at 95% confidence are mainly distributed in southeast of Japan.

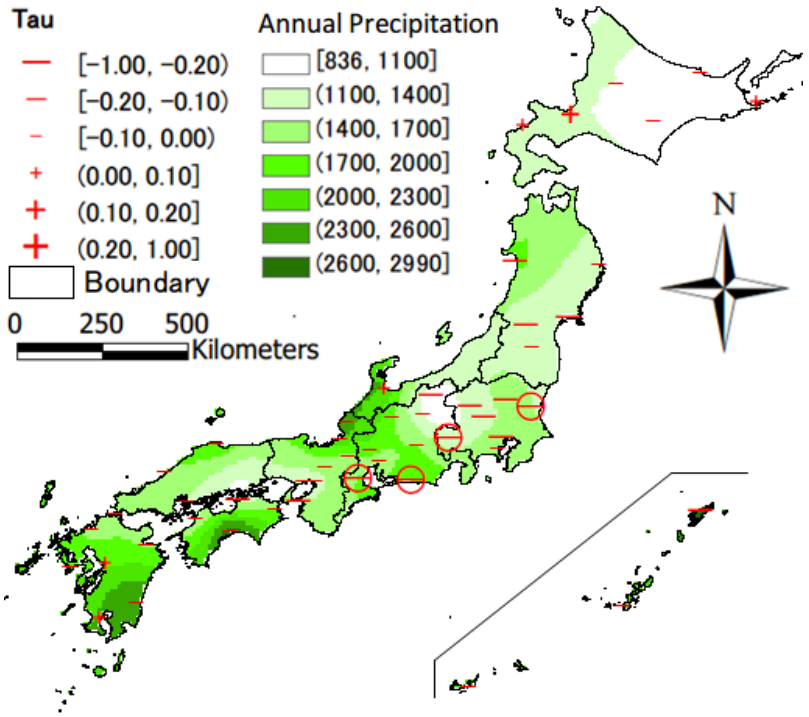

Figure 3.3 Annual mean precipitation (mm), trends (Kendall's tau) for 51 stations and changes of regionally averaged rainfall amounts (mm) in Japan from 1901 to 2012. Positive trends are shown as pluses, negative trends as minuses. Trends that are significant at the 95% level are circled.

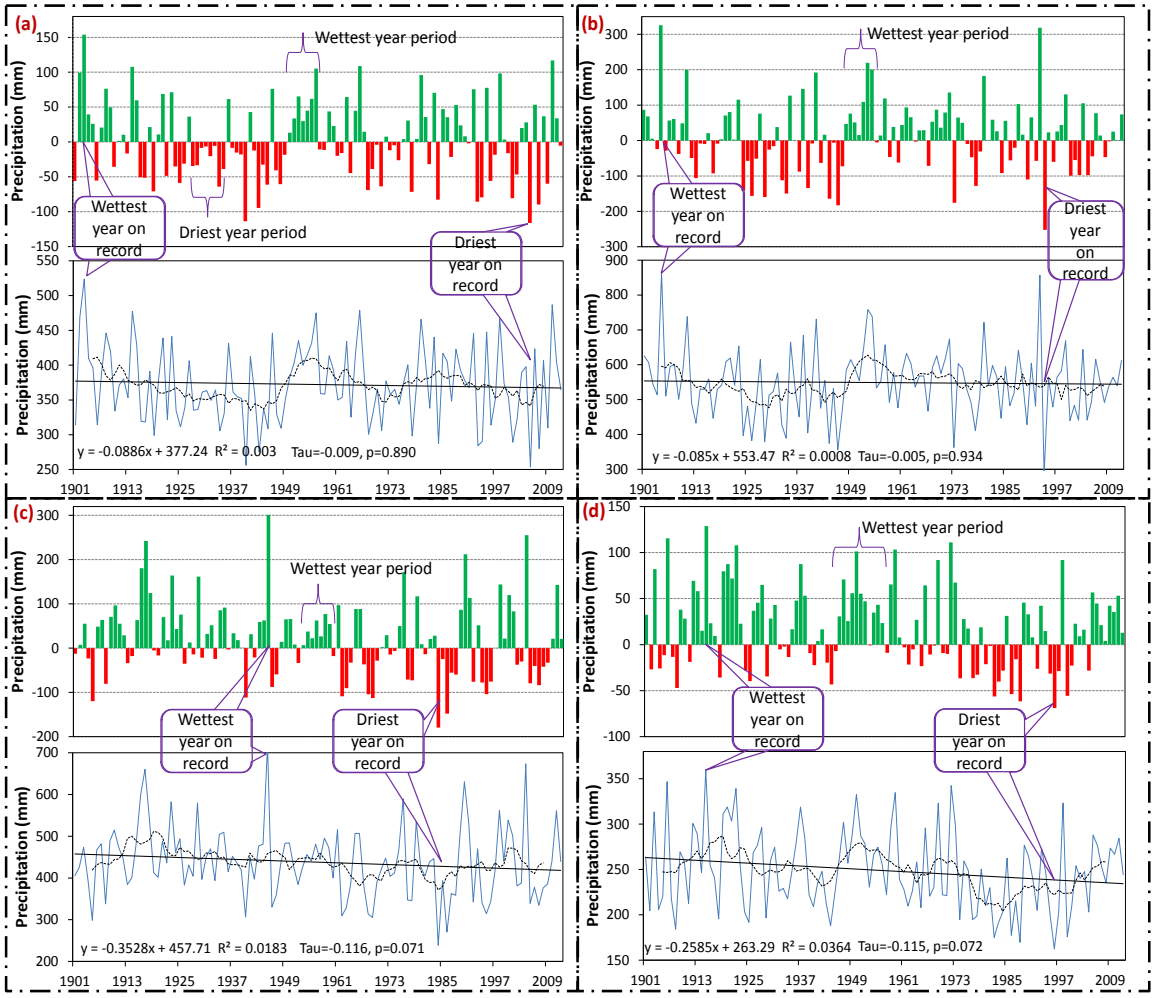

Figure 3.4 As in Figure 3.2 but for four seasons: (a) Spring; (b) Summer; (c) Autumn: (d) Winter.

3.3.2 Seasonal precipitation amounts and trends

Same as the results of annual data, precipitation amounts tended to decrease during all four seasons in more than 57% of the stations (**Table 3.4**); winter had the largest number of negative stations (49, approximately 96%), followed by autumn (46, approximately 90%), summer (34, approximately 67%) and spring (29, approximately 57%). Among these, autumn had 11 stations (approximately 22%, 11 positive and 0 negative) with significance at 95% confidence, while the number decreased to 5 (4 positive and 1 negative) in winter, 2 (1 positive and 1 negative) in summer, and 0 in spring.

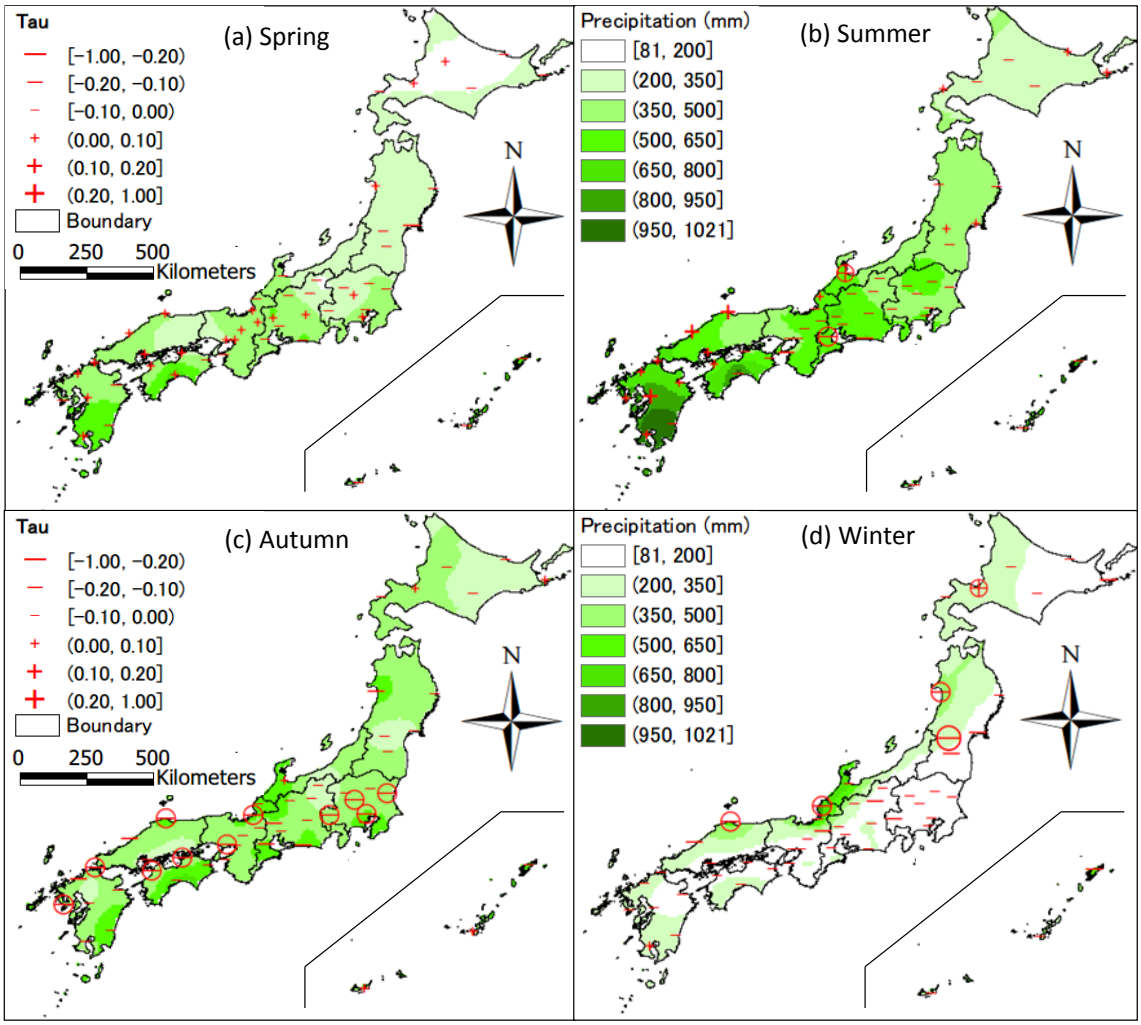

Figure 3.5 As in Figure 3.3 but for four seasons: (a) Spring; (b) Summer; (c) Autumn; (d) Winter.

Like annual trend, more than century-long time series of seasonal precipitation showed a slight (and insignificant) decreasing trend (**Figure 3.4**). Autumn total precipitation had the largest decrease (Tau =-0.116, p=0.071), mainly due to the negative anomalies since the early 1960s (**Figure 3.4 (c)**); winter had the second largest decrease (Tau =-0.115, p=0.072), primarily due to the negative anomalies since the early 1970s (**Figure 3.4 (d)**); decreases in spring (Tau =-0.009, p=0.890, **Figure 3.4(a)**) and summer (Tau =-0.005, p=0.934, **Figure 3.4(b)**) can be negligible. Therefore, total precipitation decreased during autumn and winter is the main cause of reduced annual total precipitation (**Figure 3.2**). Wettest year period and high positive and negative anomalies in different seasons are also identified in **Figure 3.4**. Summer had the highest positive and negative anomalies (326 mm in 1905 and -252 mm in 1994), followed by autumn (301 mm in 1945

and -179 mm in 1984), spring (154 mm in 1903 and -116 mm in 2005) and winter (129 mm in 1915 and -69 mm in 1996). Relatively wettest year periods were 1950-1956 in spring, 1948-1954 in summer, 1953-1959 in autumn, and 1946-1952 in winter, which are in line with the result of annual wettest year period.

Figure 3.5 clearly illustrates seasonal differences in precipitation distribution. Precipitation was mainly concentrated in summer (ranging from 286 mm to 1021 mm) and autumn (ranging from 218 mm to 719 mm). In addition, the southwest part of Japan had higher precipitation than the northeast part in spring, summer and autumn, and the northwest had higher precipitation than the southeast in winter, suggesting uneven spatial distributions across Japan. Spatial distribution of trends based on 51 stations are also indicated in Figure 3.5. Precipitation increased in the northwest area in both spring and summer, while decreasing in the southeast area. In Winter, a few stations with significant negtive trends were mostly scattered in the north fringe; by contrast, in the autumn, a few stations with significant negative trends were mostly scattered in the southeast. These seasonal variations are also in line with the results of Kimoto et al., (2005) and Fujibe et al., (2005).

3.3.3 Changes of annual precipitation extremes

Some of precipitation extreme indices such as R10mm, R20mm, CWD, PRCPTOT exhibited a decreasing trend in the past 112 years at most of stations (**Table 3.4**). Among these, R10mm and PRCPTOT had the largest number of stations with negative trends (44 stations; approximately 86%), followed by CWD (40 stations; approximately 78%) and R20mm(35 stations; approximately 69%); mean while, up to 22 stations showed negtive trents (approximately 43%) at the 95% confidence level for CWD, while the numbers decreased to 14 stations for R10mm, and 4 stations for PRCPTOT. On the other hand, an increasing trend at most of stations were found for some other precipitation extreme indices such as R95p, R99p, CDD, RX1day, RX5day, and SDII (**Table 3.4**). Among these, almost all stations showed positive trends for CDD (47 stations), followed by SDII (43 stations; approxmately 84%), R99p (40 stations; approxmately 78%), R95p (38 stations; approxmately 75%), RX5day (38 stations; approxmately 75%), and RX1day (37 stations; approxmately 73%); mean while, up to 23 stations showed positive trents (approximately 43%) at the 95% confidence level for CDD, while the number decreased to 9 stations for SDII, and 6 stations for R99p.

For the regionally averaged trend, variations in R10mm, R20mm, CWD and PRCPTOT also indicated a decreasing trend in the past 112 years (**Table 3.4**), while an increasing trend for R95p, R99p, CDD, RX1day, RX5day, and SDII. Moreover, four indices (CDD, CWD, R10mm, R99p and SDII) had statistically sigficant trends.

Like the precipitation amounts, generally, the southwest of Japan had higher value of precipitation extreme indices compared to the northeast part (**Figure 3.6**). For example, SDII was ranging from 13 mm day^{-1} to 18 mm day^{-1} in the southwest, while 7 mm day^{-1} to 13 mm day^{-1} in the northeast part; R20mm was ranging from 19 days to 42 days in the southwest, while 8 days to 19 days in the northeast part. More concretly, the values of extreme indices were ratilvely lower in Hokkaido compared to the other regions in Japan.

Figure 3.6 also shows that spatial differences in precipitation extremes trends were obvious for different indices. Negative trends dominated for PRCPTOT, R10mm and R20mm, with the exception of the Hokkaido, and stations with statistical significant trends were mainly distributed on the southeast area of Japan. In contrast, there was generally increased in very wet day precipitation (R95p), extremely wet day precipitation (R99p) and average wet day precipitation (SDII), and stations with statistical significant trends mainly scattered in the southwest area of Japan. Moreover, although the precipitation amounts decreased in the past 112 years (**Figure 3.2** and **Figure 3.3**), the max 1-day precipitation amount and max 5-day precipitation amount increased (**Figure 3.7(a)** and **(b)**).

For consecutive dry days (CDD), as shown in Figure 3.7(c), most stations with positive trends were observed and up to 23 stations (approximately 43%) had statistical significant increases, suggesting the number of consecutive dry days increased over the past years. In contrast, the number of consecutive wet days decreased over the past 112 years, largely indicating that most stations with negative trends were scattered over Japan, with the exception of Hokkaido area (**Figure 3.7(d)**).

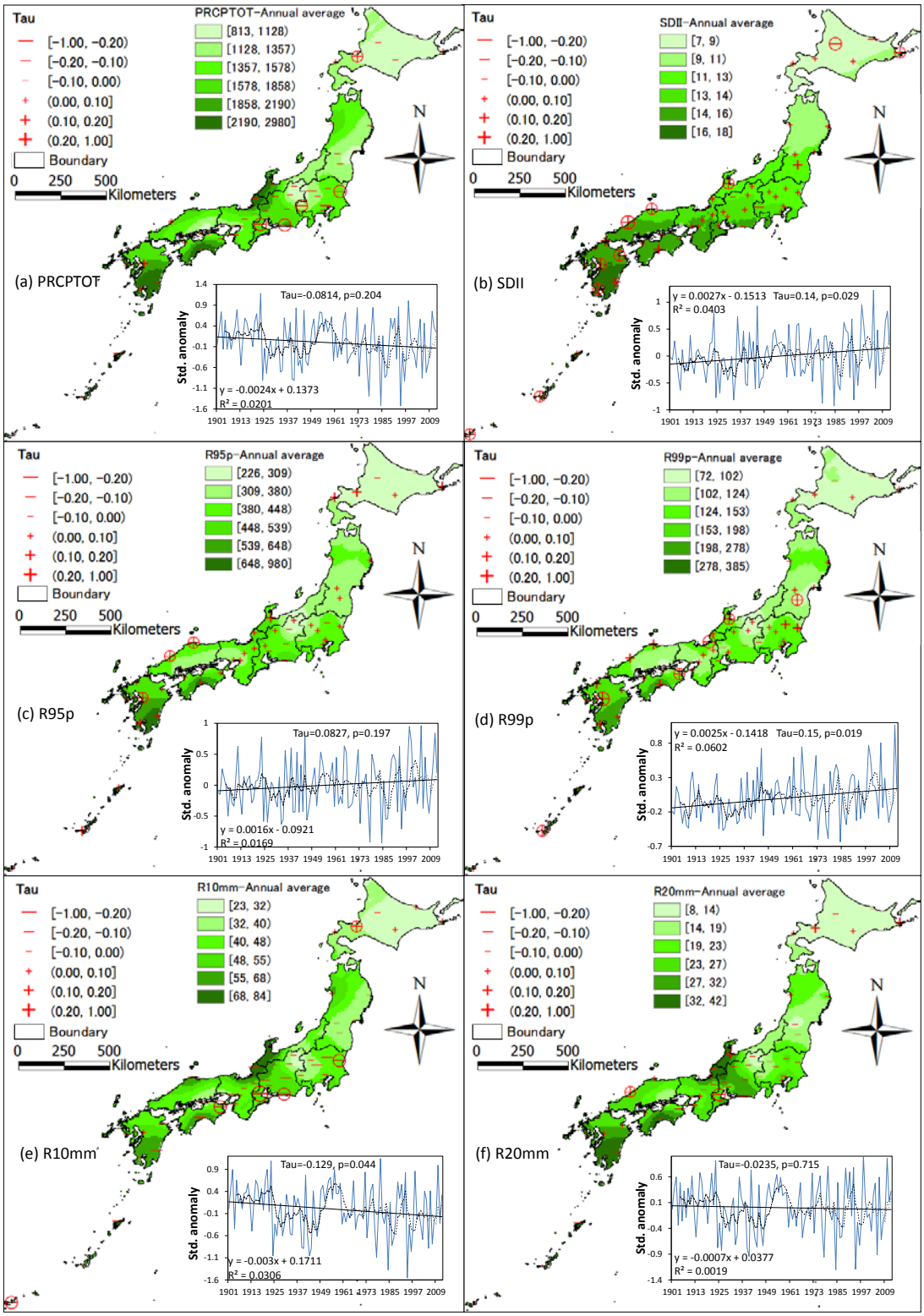

Figure 3.6 Spatial patterns of trends (Kendall's tau), spatial distribution of annual mean, and regional averaged standardized series for precipitation extremes indices. Positive trends are shown as pluses, negative trends as minuses. Trends that are significant at the 95% level are circled. Insets show the regionally averaged standardized anomalies relative to 1981-2010.

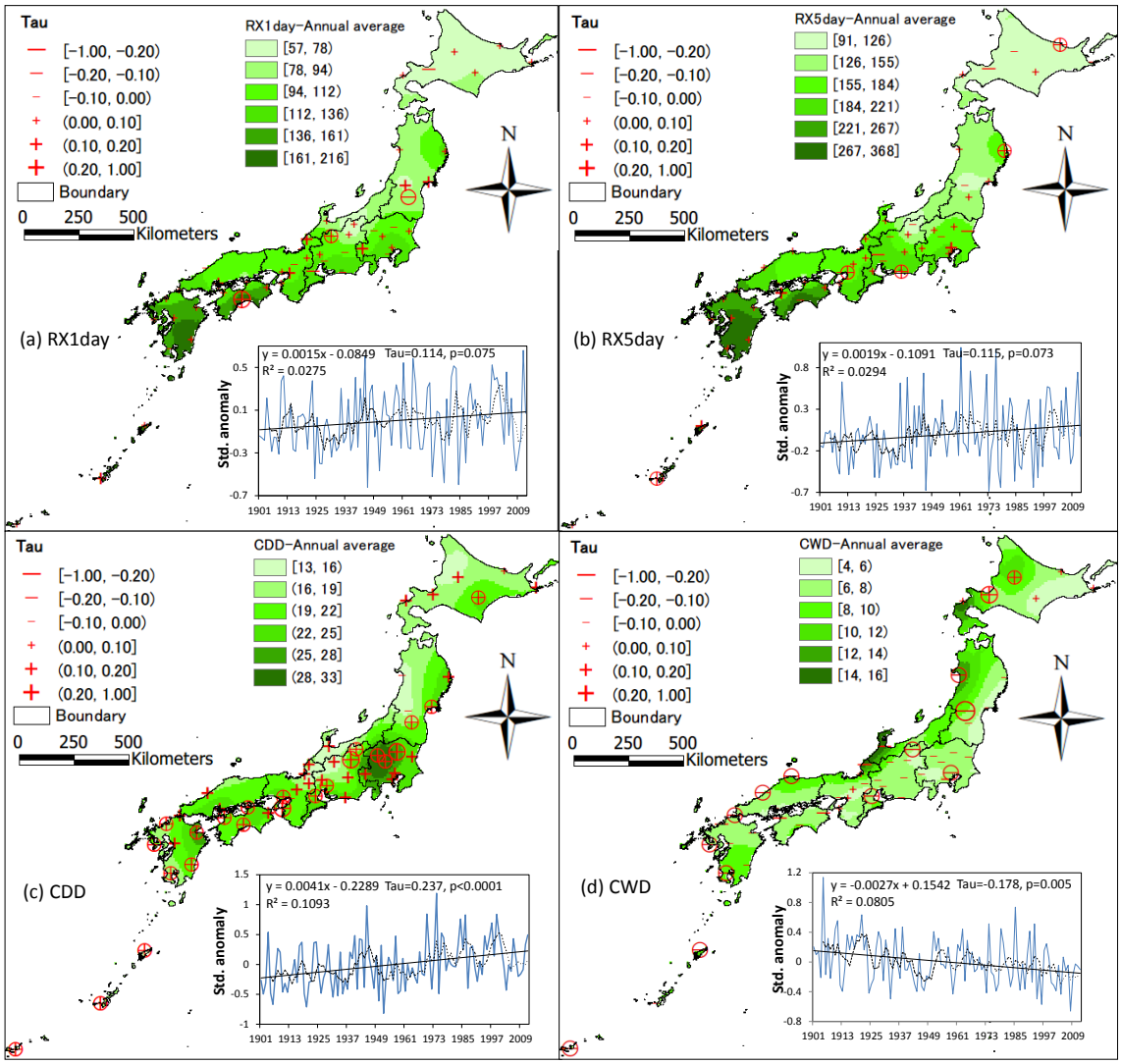

Figure 3.7 As in Figure 3.6 but for precipitation spell indices.

3.4 Discussions

Evidence for climate change impacts on the hydro-climatology of Japan is plentiful, one of which is the variation of precipitation (Solomon 2007). Decreasing trends of annual precipitation amount have been found, approximately 72.4 mm over the past 112 years (**Figure 3.2** and **Figure 3.3**), which are line with the results of Kimoto et al. (2005) and Fujibe et al. (2005). It has been an important issue for supplying the demand of water resources, although annual precipitation in Japan is about 1,700 mm, roughly two times as much as the world average of about 800 mm. From 1960s, in addition, the fluctuation of precipitation became more frequent and intense, indicating the difference in precipitation between high (wet year) and low (dry year) rainfall years increased, which will exacerbate

the management of water resources.

On a seasonal time scale, decreasing trends in precipitation amounts were also seen in all four seasons (**Figure 3.4** and **Figure 3.5**), may further leading to water shortage in different seasons. In Japan, because of East Asian summer monsoon (Qian et al., 2002), maximum precipitation falls in the early summer, and the minimum occurs in winter-except on the Sea of Japan coast. Also, August to October is the peak typhoon season in Japan, which usually brings lots of precipitation. However, variation of the East Asian Summer Monsoon has been found by Chen et al., (2004) and Wang (2002). More concretely, Nakamura et al., (2002) reported that the strength of the East Asian winter monsoon (i.e., Siberian high) was weakening in the late 1980's and the cyclonic activity in early winter was stronger when the winter monsoon activity was weaker; Bertacchi et al., (2001) noted that the main characteristic of the winter season in Japan is the presence of the winter monsoon that comes from the north and brings cold air and precipitation, mainly to the northern part of the country, at the beginning of the season. All these variations may explain decreases in precipitation amounts in four seasons in whole Japan, especially in summer and autumn.

Another interesting finding is most of precipitation extreme indices increased over the past 112 years in spite of the decreases in annual and seasonal precipitation amounts (**Figure 3.6** and **Figure 3.7**). According to the definition of precipitation extreme indices, the decreasing trends in R10mm, R20mm, CWD, PRCPTOT represent the annual and seasonal precipitation really reduced. On the other hand, the increases in R95p, R99p, RX1day, RX5day, and SDII indicate that the extreme short-term precipitation became more frequent and much bigger over the last century. These results are in accordance with some previous researches. Based on four stations, Manton et al., (2001) showed that rain days decreased and the extreme rainfall indices increased from 1961 to 1998. Fujibe (2013) also found that both annual maximum and 95^{th} percentile precipitations of the maximum value of precipitation in a 10-min interval have positive trends that are significant at the 1% level in the latter three decades (1981-2010). Because of the high-relief topography and complex geological conditions in Japan, these changes in precipitation intensity and duration significantly cause water-related natural disasters increasing (Duan et al., 2013; Saito et al., 2010).

3.5 Conclusions

Based on 51 weather stations, this study characterized the precipitation variability in Japan from 1901 to 2012, by calculating the precipitation amounts and precipitation extremes indices. Major conclusions can be summarized as follows: (1) Precipitation amounts exhibited a substantial decrease at both the annual and seasonal scales, with 49 stations (approximately 96% of the total number of stations) showing negative trends on a seasonal basis in winter, followed by autumn (46, approximately 90%), annual basis (45, approximately 88%), summer (34, approximately 67%) and spring (29, approximately 57%). The fluctuation of precipitation became more frequent and intense at both the annual and seasonal scales in the latest decades. (2) Precipitation varied substantially in spatial-temporal. Precipitation was mainly concentrated in summer (ranging from 286 mm to 1021 mm) and autumn (ranging from 218 mm to 719 mm), while precipitation amounts were less in winter and spring. The southwest had higher precipitation than the southeast in spring, summer, autumn and interannually, with precipitation concentrated in the southeast in winter. (3) Variations in R10mm, R20mm, CWD and PRCPTOT indicated a decreasing trend for a whole Japan, with while an increasing trend for R95p, R99p, CDD, RX1day, RX5day, and SDII. The spatial differences of these indices were obvious. Negative trends dominated for PRCPTOT, R10mm and R20mm, with the exception of the Hokkaido, and stations with statistical significant trends for R95p, R99p and SDII mainly scattered in the southwest area of Japan.

3.6 References

Aguilar, E. et al., 2009. Changes in temperature and precipitation extremes in western central Africa, Guinea Conakry, and Zimbabwe, 1955−2006. Journal of Geophysical Research: Atmospheres (1984-2012), 114(D2): doi: 10.1029/2008JD011010.

Aguilar, E., Auer, I., Brunet, M., Peterson, T.C. and Wieringa, J., 2003. Guidance on metadata and homogenization. WMO TD, 1186: 53.

Alexander, L.V. et al., 2006. Global observed changes in daily climate extremes of temperature and precipitation. Journal of Geophysical Research: Atmospheres (1984 – 2012), 111(D5): doi:10.1029/2005JD006290.

Bertacchi Uvo, C. et al., 2001. Statistical atmospheric downscaling for rainfall estimation

in Kyushu Island, Japan. Hydrology and Earth System Sciences, 5(2): 259-271.

Chen, T., Wang, S., Wan-Ru Huang, S. and Yen, M., 2004. Variation of the East Asian summer monsoon rainfall. Journal of Climate, 17(4): 744-762.

Coumou, D. and Rahmstorf, S., 2012. A decade of weather extremes. Nature Climate Change, 2(7): 491-496.

Dai, A., 2011. Drought under global warming: a review. Wiley Interdisciplinary Reviews: Climate Change, 2(1): 45-65.

Duan, W. et al., 2013. Spatiotemporal evaluation of water quality incidents in Japan between 1996 and 2007. Chemosphere, 93(6): 946-953.

Fujibe, F., 2013. Clausius‐Clapeyron‐like relationship in multidecadal changes of extreme short‐term precipitation and temperature in Japan. Atmospheric Science Letters, 14(3): 127-132.

Fujibe, F., Yamazaki, N. and Kobayashi, K., 2006. Long-term changes of heavy precipitation and dry weather in Japan (1901-2004). Journal of the Meteorological Society of Japan, 84(6): 1033-1046.

Fujibe, F., Yamazaki, N., Katsuyama, M. and Kobayashi, K., 2005. The increasing trend of intense precipitation in Japan based on four-hourly data for a hundred years. SOLA, 1: 41- 44.

Giorgi, F. and Francisco, R., 2000. Evaluating uncertainties in the prediction of regional climate change. Geophysical Research Letters, 27(9): 1295-1298.

Guttman, N.B., 1998. Homogeneity, data adjustments and Climatic Normals. National Cli matic Data Center. Asheville, United State. Available: http://www.stat.washington.edu /peter/7IMSC/Normals.pdf.

Helsel, D.R. and Hirsch, R.M., 1992. Statistical methods in water resources, 49. Elsevier, 510 pp.

Iwasaki, H. and Sunaga, Y., 2009. Study of recent variation in weak rainfall over Japan using 31-year AMeDAS dataset. SOLA, 5(0): 157-159.

Kawamoto, N., Oki, R. and Shimizu, S., 2011. Comparison between TRMM/PR and AMeDAS ground rain gauge network in terms of annual rainfall. IEEE, pp. 2590-2593.

Kimoto, M., Yasutomi, N., Yokoyama, C. and Emori, S., 2005. Projected changes in precipitation characteristics around Japan under the global warming. SOLA, 1(0): 85-88.

Krishnamurthy, C.K.B., Lall, U. and Kwon, H.H., 2009. Changing frequency and intensity of rainfall extremes over India from 1951 to 2003. Journal of Climate, 22(18): 4737-4746.

Kuo, Y., Chu, H., Pan, T. and Yu, H., 2011. Investigating common trends of annual maximum rainfalls during heavy rainfall events in southern Taiwan. Journal of Hydrology, 409(3): 749-758.

Manton, M.J. et al., 2001. Trends in extreme daily rainfall and temperature in Southeast Asia and the South Pacific: 1961 – 1998. International Journal of Climatology, 21(3): 269-284.

Miyajima, J. and Fujibe, F., 2011. Climatology of extreme precipitation in Japan for different time scales. SOLA, 7: 157-160.

Nakamura, H., Izumi, T. and Sampe, T., 2002. Interannual and decadal modulations recently observed in the Pacific storm track activity and East Asian winter monsoon. Journal of Climate, 15(14): 1855-1874.

Press, W.H., 2007. Numerical recipes 3rd edition: The art of scientific computing. Cambridge university press, 1235 pp.

Qian, W., Kang, H. and Lee, D., 2002. Distribution of seasonal rainfall in the East Asian monsoon region. Theoretical and Applied Climatology, 73(3-4): 151-168.

Rajczak, J., Pall, P. and Schär, C., 2013. Projections of extreme precipitation events in regional climate simulations for Europe and the Alpine Region. Journal of Geophysical Research: Atmospheres, 118(9): 3610-3626.

Río, S., Herrero, L., Fraile, R. and Penas, A., 2011. Spatial distribution of recent rainfall trends in Spain (1961 – 2006). International Journal of Climatology, 31(5): 656-667.

Saito, H., Nakayama, D. and Matsuyama, H., 2010. Relationship between the initiation of a shallow landslide and rainfall intensity- duration thresholds in Japan. Geomorphology, 118(1): 167-175.

Sillmann, J., Kharin, V.V., Zhang, X., Zwiers, F.W. and Bronaugh, D., 2013. Climate extremes indices in the CMIP5 multimodel ensemble: Part 1. Model evaluation in the present climate. Journal of Geophysical Research: Atmospheres, 118: 1716-1733.

Smith, T.M., Reynolds, R.W., Peterson, T.C. and Lawrimore, J., 2008. Improvements to NOAA's historical merged land-ocean surface temperature analysis (1880-2006). Journal of Climate, 21(10): 2283-2296.

Solomon, S., 2007. Climate change 2007: the physical science basis: contribution of

Working Group I to the Fourth Assessment Report of the Intergovernmental Panel on Climate Change. Cambridge University Press, 1056 pp.

Stocker, T.F., Qin, D. and Platner, G.K., 2013. Climate Change 2013: The Physical Science Basis. Working Group I Contribution to the Fifth Assessment Report of the Intergovernmental Panel on Climate Change. Summary for Policymakers (IPCC, 2013).

Sugiyama, M., Shiogama, H. and Emori, S., 2010. Precipitation extreme changes exceeding moisture content increases in MIROC and IPCC climate models. Proceedings of the National Academy of Sciences, 107(2): 571-575.

Suzuki, K. and Hayakawa, S., 2006. Convective Precipitation in Yamaguchi Prefecture in Summer. Journal of Agricultural Meteorology, 62(4): 127-132.

Takeshita, S., 2010. Influence on precipitation and the distribution in Miyazaki [Japan] Prefecture with climate changes. Bulletin of the Faculty of Agriculture, Miyazaki University (Japanese), 56: 73-78.

Vincent, L.A. et al., 2005. Observed trends in indices of daily temperature extremes in South America 1960-2000. Journal of Climate, 18(23): 5011-5023.

Wang, B., 2002. Rainy season of the Asian–Pacific summer monsoon. Journal of Climate, 15(4): 386-398.

Wang, X.L., 2003. Comments on “Detection of undocumented change points: A revision of the two-phase regression model”. Journal of Climate, 16(20): 3383-3385.

Wang, X.L., 2008. Accounting for autocorrelation in detecting mean shifts in climate data series using the penalized maximal t or F test. Journal of Applied Meteorology and Climatology, 47(9): 2423-2444.

Zhai, P., Zhang, X., Wan, H. and Pan, X., 2005. Trends in total precipitation and frequency of daily precipitation extremes over China. Journal of Climate, 18(7): 1096-1108.

Zhang, X. et al., 2011. Indices for monitoring changes in extremes based on daily temperature and precipitation data. Wiley Interdisciplinary Reviews: Climate Change, 2(6): 851-870.

Zhang, X. and Yang, F., 2004. RClimDex (1.0) user manual. Climate Research Branch Environment Canada, Downsview, 23 pp.

Zongxing, L. et al., 2012. Changes of daily climate extremes in southwestern China during 1961-2008. Global and Planetary Change, 80: 255-272.

Chapter 4 Spatiotemporal Variability of Precipitation in Hokkaido

4.1 Introduction

Spatio-temporal variability in precipitation distributions is an important attribute of the hydro-climatological systems that underpin human societies (Brown and Funk, 2008; Coumou D and Rahmstorf S, 2012; Hendrix and Salehyan, 2012). For example, interannual precipitation variation in equatorial East Africa has severe impacts on human habitation and food security (Wolff et al., 2011). Drastic reductions in precipitation can have severe impacts on regional ecosystems and human settlements and can lead to societal decay (e.g. the Mayan civilization) (Medina-Elizalde and Rohling, 2012) as well as decreasing biodiversity (e.g. Amazonia in 2005) (Marengo et al., 2008). It is therefore important to understand changes to patterns of precipitation distribution and the causes of these changes. Many studies have focused on precipitation change at large (e.g. global) spatial scales. Some researchers have identified increasing trends in precipitation extremes worldwide (Coumou and Rahmstorf S, 2012; Lenderink and Van, 2008), while others have recorded increasing frequency of draughts under global warming (Burns et al., 2010; Dai, 2011; Kerr, 2007). Some studies have also looked at precipitation variability at local or regional scales in recent decades. Río et al., (2011) reported a decreasing trend in Spanish precipitation in February and June and after exploring changes in total versus extreme precipitation and dry periods through the end of the twenty-first century, Hertig et al., (2012) reported widespread increases in precipitation during summer and autumn along with reductions in winter, total and extreme precipitation over the entire Mediterranean region. Several authors (Bray et al., 2011; Pal and Al-Tabbaa, 2011; Reiser and Kutiel, 2011) have analyzed the behavior of precipitation under extreme events, including reports of increasing precipitation rates near the tropical cyclone centre (Knutson et al., 2010; Walsh et al., 2011), sensitivity of precipitation to variations in El Niño (Feng et al., 2011; Taschetto and England, 2009), etc.

** This chapter is submitted into **Journal of Hydrology,** 2014.*

Large-scale atmospheric circulation, which is becoming more erratic under global warming, has a major impact on precipitation variability (Muñoz-Díaz and Rodrigo, 2006). Change in atmospheric moisture is one of the results of a warming climate. Folland et al., (2002) reported that total atmospheric water vapor has increased by several percent per decade over many regions of the Northern Hemisphere since the early 1970s, resulting in precipitation variability; Zhang et al., (2009a; 2009b) demonstrated that precipitation variations likely reflect changes in atmospheric moisture or water vapor flux.

Evidence for climate change impacts on the hydro-climatology of Japan is plentiful (Solomon, 2007). Since 1898, the annual temperature in Japan had been rising at a rate of about 1.1°C per century, and high-temperature years have been particularly frequent after the 1990s; moreover, although no clear trends have been observed, the annual precipitation in Japan varies largely from year to year. Accordingly, many authors have analyzed variations in precipitation across Japan at different timescales. For example, Iwasaki and Sunaga (2009) applied linear regression analysis to elucidate the features of weak precipitation between June and September for 31 years. Utsumi et al., (2008) used a gauge-based analysis of daily precipitation over Japan from 1981 to 2000 on a 0.01° grid to show that Japan receives nearly 2000 mm/year of precipitation on average, approximately 10% higher than commonly thought. Other studies have focused on different territories of Japan. For instance, Yue and Hashino (2003) indicated that different climatic regions experienced different hydrological changes in Japan. Takeshita (2010) estimated the precipitation variation in Miyazaki prefecture and Suzuki and Hayakawa (2006) explored the characteristics of summertime convective precipitation in Yamaguchi prefecture. Although all of these studies detected characteristics of precipitation change, most of the research focused on inter-annual or summer variability and little has been done to analyze these features on multiple temporal scales (e.g. spatial, annual, seasonal, and monthly) in recent decades. It is important to analyze regional changes in precipitation trends using the latest data to improve understanding of the variability of precipitation in Japan.

The objective of this study is therefore to elucidate trends and causes of precipitation variability at multiple time scales in recent decades in Hokkaido, Japan. Considering the availability and integrity of data, daily precipitation data from 1980 to 2011 at 169 stations were chose to investigate the precipitation variations in Hokkaido using Mann-Kendall test (a non-parametric trend test) and geostatistical interpolation techniques. Meanwhile, correlations between water vapor flux and precipitation was explored based on reanalysis

data. We discuss the study area, data and methodology followed by results including spatial annual, seasonal, and monthly precipitation data and trends obtained in section 4.3 followed by discussion and conclusions. The results of this study offer insights into precipitation trends and provide tools for forecasting future climate conditions.

4.2 Materials and methods

4.2.1 Study area

Hokkaido, the northernmost major island of Japan (41°21′–45°33′N, 139°20′–148°53′E; **Figure 4.1**) and the largest of Japan's 47 prefectures (area=78,423 km^2), is bounded by the Sea of Japan to the west, the Pacific Ocean to the south and east, and the Sea of Okhotsk to the north. Hokkaido is known for relatively cool summers and cold winters. The average August temperature ranges from 17 to 22°C, while the average January temperature ranges from -12 to -4°C, in both cases depending on elevation and distance from the ocean, though temperatures on the western side of the island tend to be a little warmer than on the eastern. Unlike the other major islands of Japan, Hokkaido is normally not affected by the June–July rainy season and the relative lack of humidity and typically warm (rather than hot) summer weather makes its climate an attraction for tourists from other parts of Japan. In winter, the generally high quality of powder snow and numerous mountains in Hokkaidō make it one of Japan's most popular regions for snow sports. Total precipitation varies from 1,600 mm on the mountains of the Sea of Japan coast to around 800 mm (the lowest in Japan) on the Sea of Okhotsk coast and interior lowlands and up to around 1,100 mm on the Pacific side.

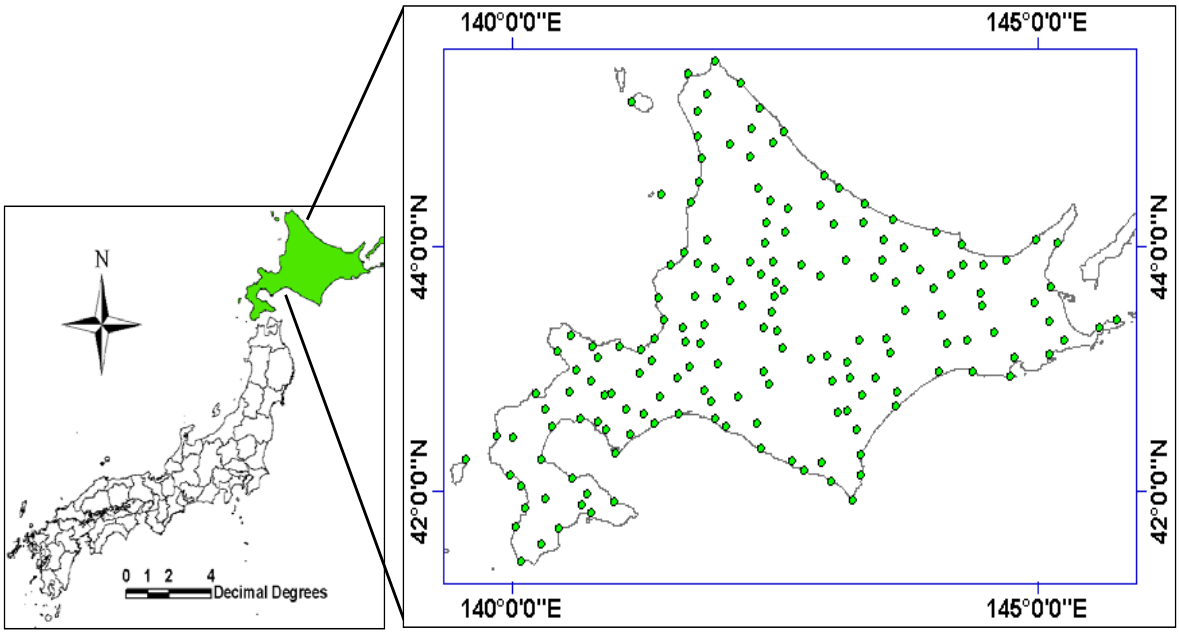

Figure 4.1 Rain gauge station distributions used in this study.

4.2.2 Data

The Automated Meteorological Data Acquisition System (AMeDAS), a high-resolution surface observation network developed by the Japan Meteorological Agency (JMA) used for gathering regional weather data and verifying forecast performance, has reached about 1300 stations since 1974 separated on average, by about 17 km (Kawamoto et al., 2011). The data, including hours of sunlight, temperature, precipitation, and wind velocity and direction, are observed automatically and transmitted to the AMeDAS Center in real time through telephone lines. There are about 220 AMeDAS stations in Hokkaido. Our analyses use daily precipitation data collected over 32 years from 1980 to 2011 to reflect the latest trends. We chose AMeDAS stations with less than 1% missing or uncertain values relative to the total dataset for each year (**Figure 4.1**). All of the daily data were rearranged into monthly, seasonal and annual data using MATLAB. The seasons were considered as: winter = December, January, February; spring = March, April, May; summer = June, July, August; autumn = September, October, November.

Monthly means of air temperature (°C), horizontal wind speed (m s^{-1}), specific humidity (g kg^{-1}), and vertical velocity (hPa s^{-1}) from 1980 to 2011 were extracted from the reanalysis dataset which was established by the National Centers for Environmental Prediction – National Center for Atmospheric Research (NCEP–NCAR) (Kalnay et al.,

1996; Kistler et al., 2001) and consists of monthly averages from 1948 to present at the spatial resolution of 2.5° latitude by 2.5° longitude and 17 vertical pressure levels (specific humidity is concentrated in eight pressure levels ranging from 1,000 to 300 hPa). The extracted data was used to represent atmospheric circulation in this study.

4.2.3 Methods

4.2.3.1 Trend analysis

Mann-Kendall test is a non-parametric rank-based statistical test (Kendall, 1975; Mann, 1945), which has been used to analyze trends in hydro-meteorological time series such as streamflow, precipitation, temperature, and water quality (Türkeş, 1996; Yue et al., 2002). For independent and randomly ordered on a time series $X_i\{X_i, i = 1, 2, \dots, n\}$, the null hypothesis H_0 in Mann-Kendall test assumes that there is no trend and this is tested against the alternative hypothesis H_1, which assumes that there is a trend. The Mann-Kendall S Statistic is computed as follows:

$$S = \sum_{i=1}^{n-1} \sum_{j=i+1}^{n} sign(T_j - T_i) \tag{4.1}$$

$$sign(T_j - T_i) = \begin{cases} 1 & if\ T_j - T_i > 0 \\ 0 & if\ T_j - T_i = 0 \\ -1 & if\ T_j - T_i < 0 \end{cases} \tag{4.2}$$

where T_j and T_i are the precipitation variability at multiple time scales j and i, $j > i$, respectively.

When $n \geq 10$, the statistic S is approximately normally distributed with the mean and variance as follows:

$$E(S) = 0 \tag{4.3}$$

The variance (σ^2) for the S – statistic is defined by:

$$\sigma^2 = \frac{n(n-1)(2n+5) - \sum t_i(i)(i-1)(2i+5)}{18} \tag{4.4}$$

where t_i denotes the number of ties to extent i. The summation term in the numerator is used only if the data series contains tied values. The standard test statistic Z_S is calculated as follows:

$$Z_S = \begin{cases} \frac{S-1}{\sigma} & for\ S > 0 \\ 0 & for\ S = 0 \\ \frac{S+1}{\sigma} & for\ S < 0 \end{cases} \tag{4.5}$$

The test statistic Z_S is used a measure of significance of trend (see Yue *et al.*, 2002 for detail). This test statistic is used to test the null hypothesis (H_0). That is, if $|Z_S|$ is great than $Z_{\alpha/2}$, where α is the chosen significance level (e.g., 5% with $Z_{0.025} = 1.96$) then the null hypothesis is invalid implying that the trend is significant.

Precipitation maps were generated using geostatistical interpolation techniques. In this paper, ordinary kriging, an interpolation technique based on cross-validation of statistical results (Río et al., 2011) was employed to perform spatial prediction. The spherical semivariogram model (best fit for all directions) was selected as the best function to plot the empirical variogram. All of these were carried out using ArcGis software.

4.2.3.2 Atmospheric circulation analysis

To better understand the atmospheric circulation patterns behind the spatial and temporal variations in precipitation, water vapor flux and related transport characteristics were explored using NCAR/NCEP reanalysis data (Xu et al., 2004). In this study, we calculated changes in water vapor flux and other features annually and seasonally for the periods 1980-1995 and 1996-2011 respectively. According to the European Centre for Medium-Range Weather Forecasts (ECMWF) analyses (Cullather et al., 1998) and others (Zhang et al., 2008; Zhang et al., 2011), atmospheric moisture is considered negligible above 300 hPa and so only layers under 300 hPa (z≤8) were used to calculate the water vapor flux. The zonal moisture transport flux (Q_u), meridional moisture transport flux (Q_v) and whole layer moisture budget (Q_T) at regional boundaries were calculated based on the following equations (Miao et al., 2005; Zhang et al., 2011; Zhang et al., 2009)

$$Q_v(x,y,t) = \frac{1}{g}\int_p^{p_s} q(x,y,p,t) * v(x,y,p,t)dp \tag{4.6}$$

$$Q_W = \sum_{\varphi_1}^{\varphi_2} Q_u(\lambda_1, y, t) \tag{4.7}$$

$$Q_E = \sum_{\varphi_1}^{\varphi_2} Q_u(\lambda_2, y, t) \tag{4.8}$$

$$Q_S = \sum_{\lambda_1}^{\lambda_2} Q_v(x, \varphi_1, t) \tag{4.9}$$

$$Q_N = \sum_{\lambda_1}^{\lambda_2} Q_v(x, \varphi_2, t) \tag{4.10}$$

$$Q_T = Q_W - Q_E + Q_S - Q_N \tag{4.11}$$

where u and v are the zonal and meridional components of the wind field, respectively, q is the specific humidity, p_s is surface pressure (z=1), p is 300 hPa (z=8), g is acceleration due to gravity, Q_W, Q_E, Q_S, Q_N are the West, East, South and North regional boundaries, respectively, and φ_1, φ_2, λ_1, λ_2 are the latitude and longitude according to the regional boundaries (Miao et al., 2005).

4.2.3.3 Correlation analysis

After calculating water vapor flux, the correlation analysis between precipitation changes and water vapor flux was performed using Kendall's tau method, which is a measure of correlation and therefore measures the strength of the relationship between the two variables. Kendall's tau, like Spearman's rank correlation, is carried out on the ranks of the data. In the case of no ties in the x and y variables, Kendall's rank correlation coefficient, tau, may be expressed as $\tau = S/D$ where

$$S = \sum_{i<j}(sign(x[j] - x[i]) * sign(y[j] - y[i])) \tag{4.12}$$

$$D = n(n-1)/2 \tag{4.13}$$

where S is called the score and D is the denominator, representing the maximum possible value of S. The p-value of tau under the null hypothesis of no association is computed by in the case of no ties using an exact algorithm given by (Best and Gipps, 1974). So, in this

study, the Kendall's τ was calculated to examine the relationships between precipitation characteristics and water vapor flux in order to explore the impact of large-scale circulation patterns on trends in annual and seasonal precipitation.

4.3 Results

4.3.1 Annual precipitation amounts and trends

Table 4.1 shows results of the Mann-Kendall test for 169 stations in Hokkaido. The trends of the Mann-Kendall test are reported at the 90% and 95% confidence level and explained in terms of positive and negative implications. **Figure 4.5** and **4.7** show spatial distribution of seasonal and monthly precipitation and trends for 169 stations in Hokkaido, 1980–2011, respectively. These changes are in line with the result of (Iwasaki and Sunaga, 2009), both of whom showed mean precipitation increases over long time periods across Japan.

Figure 4.2(a) shows the changes of regionally averaged rainfall amounts in Hokkaido, revealing precipitation had fluctuated from year to year during the period 1980-2011. The linear trend line indicates that a substantial increase in mean annual precipitation has been observed over the past 32 years. Precipitation in 1981 (approximately 1423.22 mm) and 1984 (approximately 1423.22 mm) represent the highest amount and least amount respectively, which are according with the wettest year and driest year shown in **Figure 4.2 (b)**. **Figure 4.2 (b)** also indicates that there was less precipitation in consecutive 7 years (1982-1988).

As shown in **Figure 4.3**, the annual mean precipitation is much higher in the southwest compared to the northeast. Morino station (42.632°N, 141.245°E) had the highest mean annual precipitation (2213.53 mm) of all 169 stations, while Tokoro station (44.115°N, 144.037°E) had the lowest (694.75 mm). **Figure 4.3** also shows increasing annual precipitation at 147 stations (approximately 87% of the total number of stations) in Hokkaido. Out of 169 stations, trends are significant for 50 stations (approximately 30%, 47 positive and 3 negative) at the 90% confidence level and for 34 stations (approximately 20%, 31 positive and 3 negative) at the 95% confidence level (**Table 4.1**). These stations are distributed widely across Hokkaido (**Figure 4.3**), suggesting annual precipitation increased overall from 1980 to 2011. Sakaino station (43.707°N, 143.643°E; Z=3.55) and Okushiri station (42.248°N, 139.557°E; Z=-2.45) represent the largest positive and

negative trends respectively. Sakaino station, located in an area of lower average precipitation in northeast Hokkaido, saw an increase in precipitation from 500 mm to 900 mm from 1980 to 2011 with a peak in 2006 (approximately 1100 mm, **Figure 4.4**).

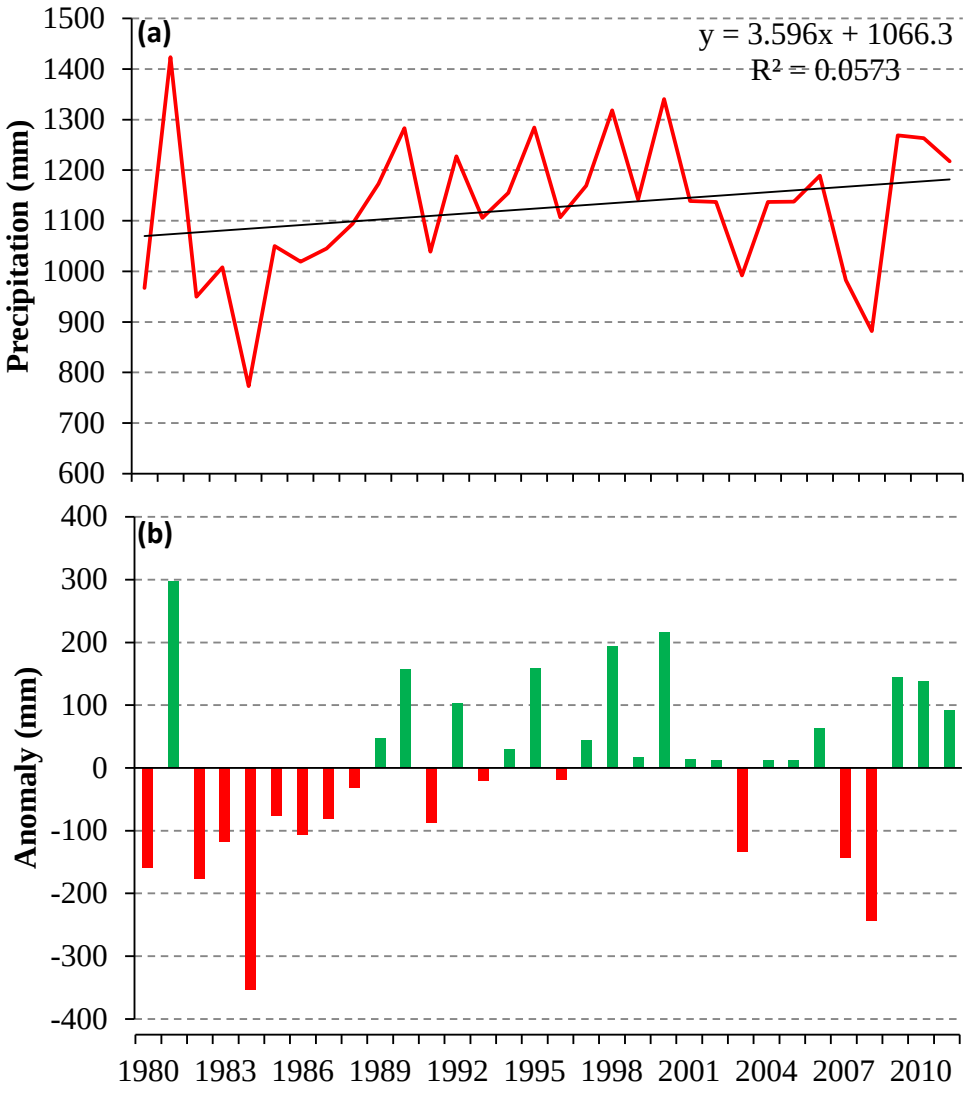

Figure 4.2 (a) Time series of regionally averaged precipitation amounts(mm) with line trend (straight line) in Hokkaido; (b)Time series of yearly precipitation anomalies in Hokkaido, 1980- 2011, based on the average from 1980 to 2011.

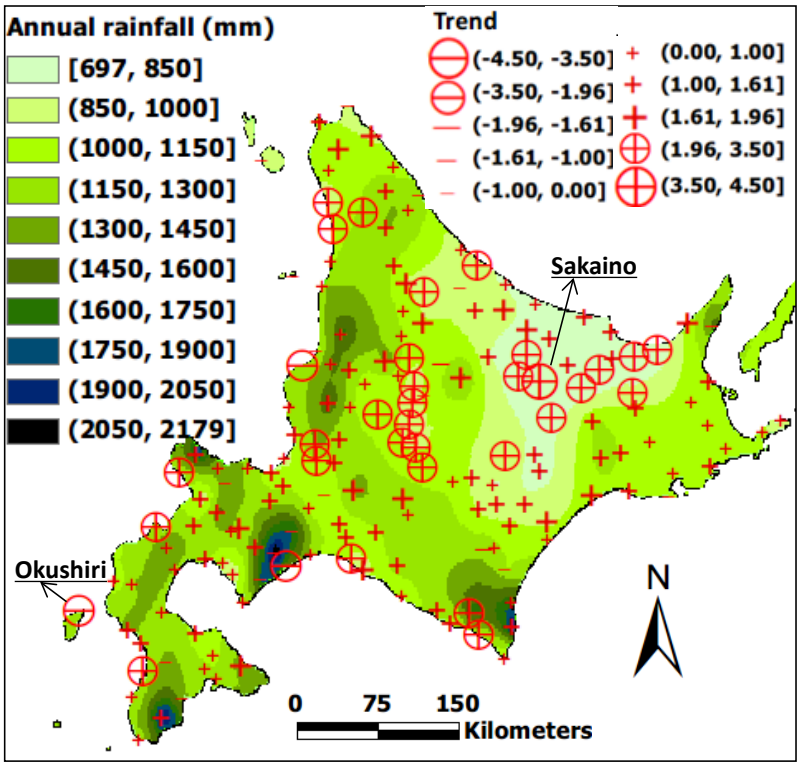

Figure 4.3 Annual rainfall amounts and trends for 169 stations in Hokkaido from 1980 to 2011. Positive trends are shown as pluses, negative trends as minuses. Trends that are significant at the 95% level are circled.

4.3.2 Seasonal precipitation amounts and trends

As in the case of annual data, precipitation amounts tended to increase during all four seasons in more than 60% of the stations (**Table 4.1** and **Figure 4.6**); spring had the largest number of positive stations (143, approximately 85%), followed by summer (139, approximately 82%), autumn (116, approximately 69%) and winter (103, approximately 61%). Among these, summer had 58 stations (approximately 34%, 58 positive and 0 negative) with significance at 90% confidence, while the number decreased to 45 (26 positive and 19 negative) in winter, 24 (23 positive and 1 negative) in spring, and 8 (5 positive and 3 negative) in autumn. The solid linear trend line of Figure 4.5 indicates that summer had the highest increase, followed by spring, autumn and winter. The increased precipitation of them was about 70.83 mm, 57.23 mm, 27.37 mm, and 15.37 mm, respectively. Also, the biggest anomaly was observed in summer, 1981, up to 245.58 mm, causing the highest precipitation amount appeared this year (**Figure 4.2**). These seasonal variations are also in line with the results of Kimoto et al., (2005) and Fujibe et al., (2005).

Table 4.1 Results of Mann-Kendall test for 169 stations, Hokkaido

Variable	Positive	Negative	Significant 95%		Significant 90%	
			Positive	Negative	Positive	Negative
Annual	147	22	31	3	47	3
Winter	103	66	17	14	26	19
Spring	143	26	13	1	23	1
Summer	139	30	38	0	58	0
Autumn	116	53	0	1	5	3
January	68	101	4	20	4	24
February	101	68	7	9	22	14
March	75	94	6	5	8	7
April	69	100	0	0	0	3
May	168	1	29	0	64	0
June	114	55	1	0	3	0
July	165	4	55	0	77	0
August	89	80	0	7	1	11
September	138	31	2	2	8	2
October	53	116	0	3	1	9
November	115	54	3	3	6	6
December	122	47	9	5	28	10

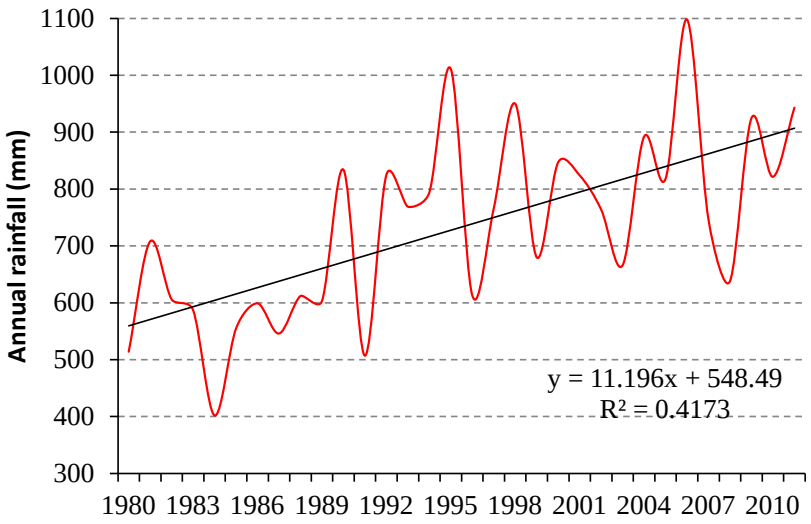

Figure 4.4 Annual changes of precipitation amounts at Sakaino station. The black line is the linear trend line.

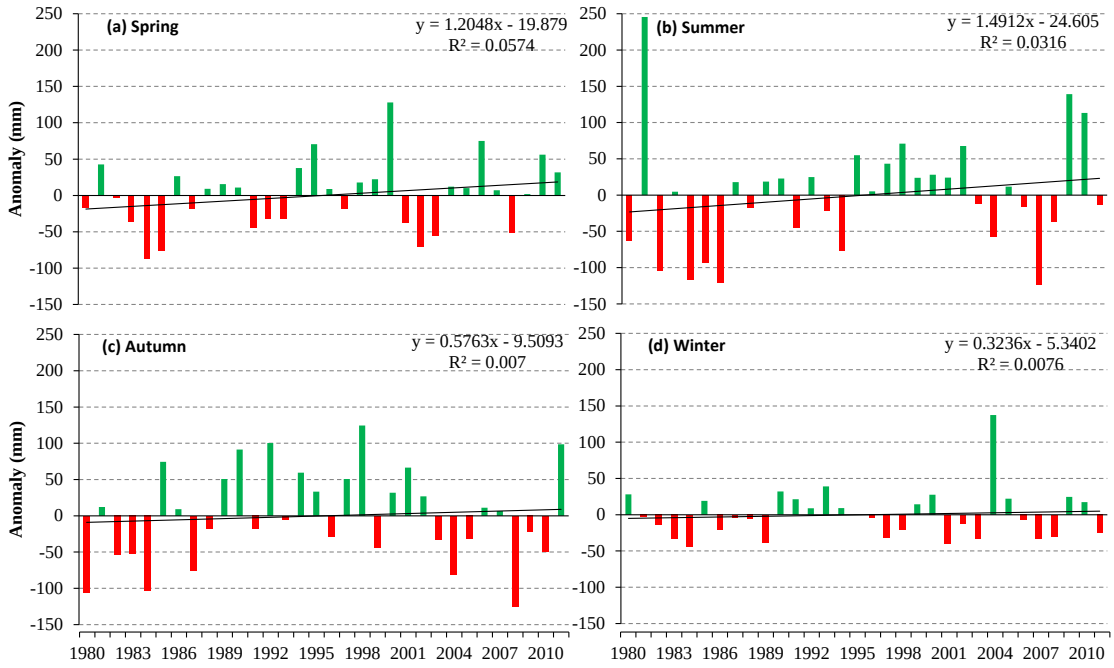

Figure 4.5 Time series of seasonal precipitation anomalies (a) spring, (b) summer, (c) autumn, and (d) winter in Hokkaido, 1980- 2011, based on the average from 1980 to 2011. The black line is the linear trend line.

Figure 4.6 shows that precipitation decreased in the western area in winter, while increasing in the eastern area. Results from the winter reveal that there were more stations with significant negative trends in the western fringe. Similar distributions were found in autumn, but values of the trends (mostly less than 1.96) were less than in winter; there were only three stations with negative trends in the eastern area. In spring, a few stations with negative trends were mostly scattered in the northwest; by contrast, in the summer, a few stations with negative trends were mostly scattered in the southeast, especially in the southeastern fringe. Moreover, stations with significant positive trends mainly occurred in the central area in summer.

Figure 4.6 clearly illustrates seasonal differences in precipitation distribution over Hokkaido. Precipitation was mainly concentrated in summer (ranging from 233 mm to 751 mm) and autumn (ranging from 218 mm to 724 mm), while precipitation was reduced in winter and spring. Uneven spatial distributions are also shown in **Figure 4.6**. The northwest had higher precipitation than the southeast in winter and autumn, suggesting that most of the stations with negtive trends were located in areas with higher precipitation, whereas stations with positive trends tended to be clustered in areas with lower precipitation; precipitation was concentrated in the southeast in both spring and summer.

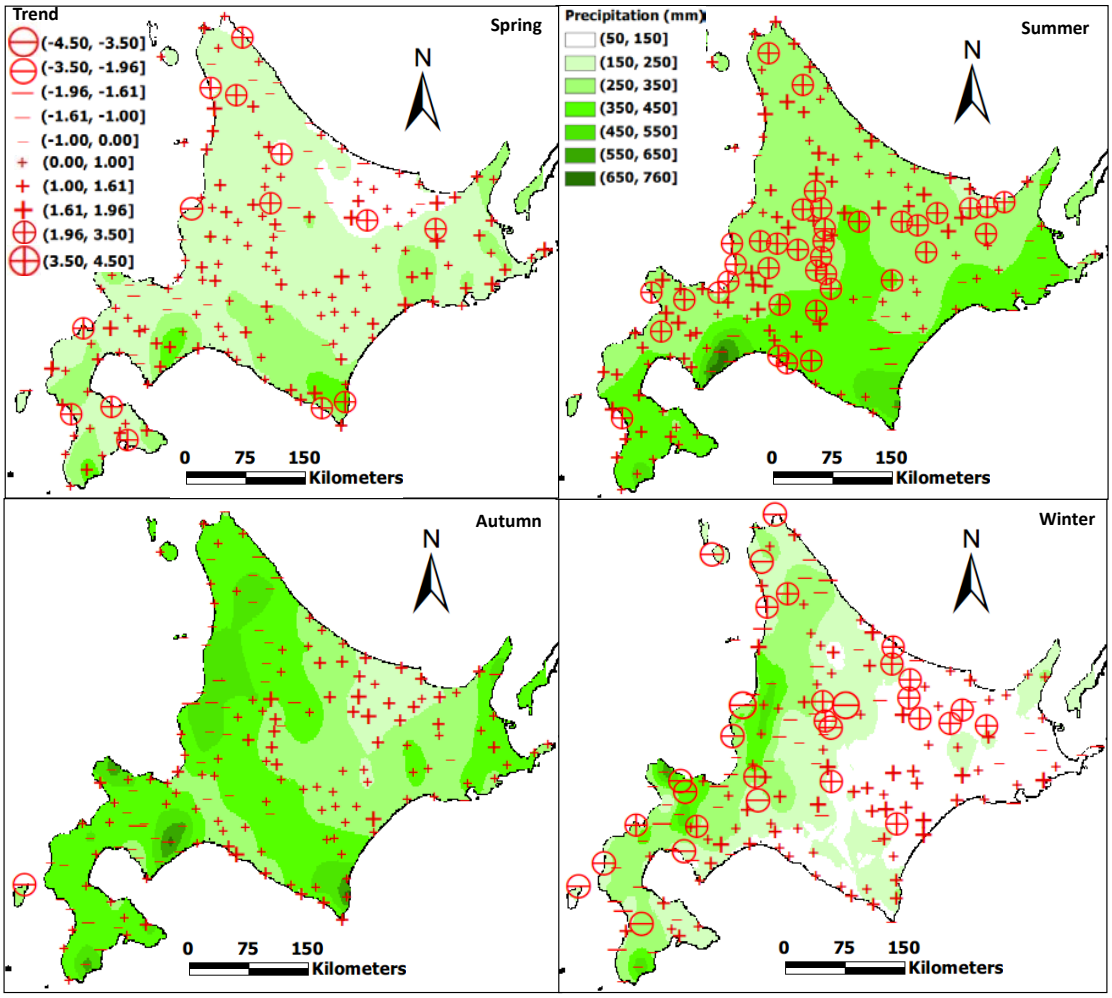

Figure 4.6 Spatial distribution of rainfall amounts (mm) and trends (the value of *Z*) at seasonal scale in Hokkaido (1980–2011). Positive trends are shown as pluses, negative trends as minuses. Trends that are significant at the 95% level are circled.

4.3.3 Monthly precipitation amounts and trends

On a monthly timescale, increases in precipitation were mainly seen in February, May, June, July, September, November and December at more than 100 stations (**Table 4.1**). Among these, almost all stations showed positive trends in May (168 stations) and July (165 stations); meanwhile, 77 stations showed positive trends (approximately 46%, 77 positive and 0 negative) at the 90% confidence level in July, while the numbers decreased to 64 stations (approximately 38%, 64 positive and 0 negative) in May. More than 100 stations showed negative trends in January, April and October. Among these, October had the largest number of stations with negative trends (116 stations; approximately 69%);

January had the largest number of stations with negative trends at the 95% (20 stations) and 90% (24 stations) confidence levels; April was the only month that showed no increases or decreases at 95% confidence in all 169 stations. Increases in precipitation for June-August have also been reported by Yamada et al., (2012), who identified declines in line-shaped rainbands (LRBs) between 1990-2003 and 2004-2010. More than 100 stations revealed negative trends in January, April and October. Decreases in precipitation for January were reported by Nomoto (2003).

Figure 4.7 shows that spatial differences in precipitation trends were obvious in different months. Spatial distribuations of precipitation trends suggest that precipitation decreased in most regions in January, March, April and October, but increased in other months, especially in May and July with almost 100% in all stations. Among these, stations with negative trends were distributed across Hokkaido in January and March, mainly observed in the northwest in February, April, October, November and December, and mostly observed in the southeast in June and August. Positive trends dominated in September, with the exception of the southwest corner of Hokkaido.

Figure 4.7 also shows that January (ranging from 31 mm to 162 mm), February (ranging from 16 mm to 154 mm), March (ranging from 21 mm to 136 mm) and December (ranging from 35 mm to 179 mm) had less precipitation, while other months had more, especially July (ranging from 75 mm to 243 mm), August (ranging from 95 mm to 340 mm) and September (ranging from 101 mm to 317 mm). There was more precipitation in northwestern Hokkaido in January, February, October, November and December, which was similar to autumn and winter; moreover, like spring and summer, the southeastern area had higher precipitation than the northwestern area in winter and autumn in April, May, June, July, August and September. During February, August, October, November and December, most stations with negative trends were observed in areas with higher precipitation.

4.3.4 Effect of water vapor transport on precipitation

Precipitation variation is directly related to the characteristics of water vapor transport and budget because atmospheric water vapor transport can provide water vapor for precipitation so that the variability of water vapor flux much affects the variability of local precipitation (Zhang et al., 2014). In this study, the seasonal variability of water vapor flux (**Figure 4.8**) and its correlations with precipitation (**Figure 4.10**) were explored to

investigate effects of water vapor flux on precipitation.

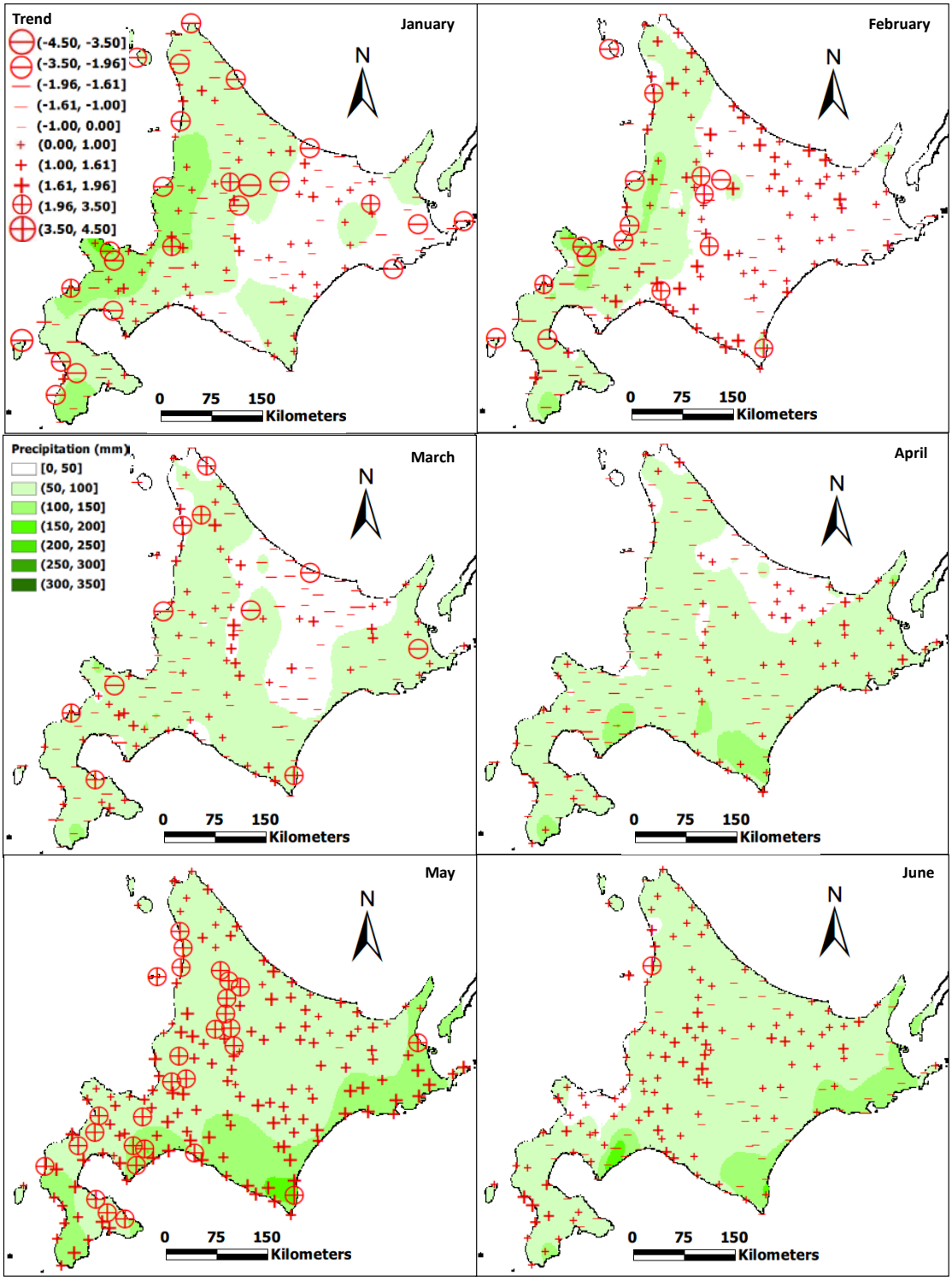

Figure 4.7 Spatial distribution of rainfall amounts (mm) and trends (the value of *Z*) at monthly scale in Hokkaido (1980–2011). Positive trends are shown as pluses, negative trends as minuses. Trends that are significant at the 95% level are circled.

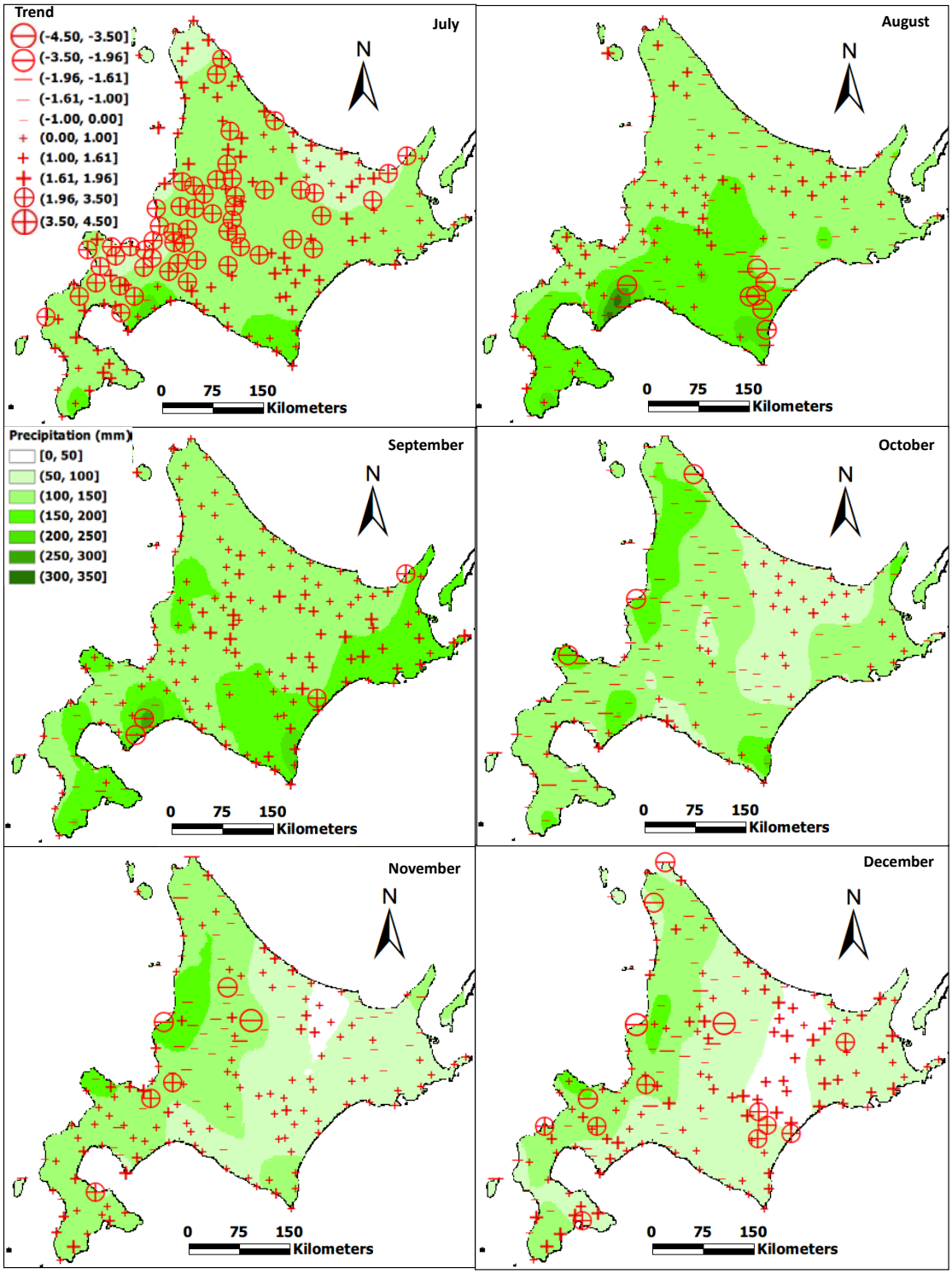

Figure 4.7 (Continued)

Considering Hokkaido is located between 148°53' and 139° 20' E longitude and 41° 21' and 45° 33' N latitude and the resolution of reanalysis data is 2.5° latitude by 2.5° longitude, **Figure 4.8** shows the latitude-time cross-section of whole layer vertically integrated atmospheric water vapor flux (kg m^{-1} s^{-1}) averaged over 137.5°-150°E in 1000-

300 hPa. From **Figure 4.8**, we can see the water vapor flux decreased gradually from the south to the north in all seasons, which may explain the annual and seasonal mean precipitation in Hokkaido (**Figure 4.3** and **Figure 4.6**) is much higher in the south area compared to the north area. Among them, summer (**Figure 4.8(c)**) had the highest water vapor flux between 40°and 50°N, followed by autumn (**Figure 4.8(d)**), winter ((**Figure 4.8(e)**) and spring (**Figure 4.8 (b)**), which may explain precipitation was mainly concentrated in summer and autumn, while precipitation was reduced in winter and spring (**Figure 4.6**).

In terms of time, water vapor flux exhibited an increasing trend for both annual and seasonal scales between 40°and 50°N during the period 1980-2011. Between 40°and 50°N, for example, the contour of 1200 kg m^{-1} s^{-1} rose gradually from the south to the north in **Figure 4.8(a)**, the contour of 600 kg m^{-1} s^{-1} extended to 50°N in 2010 in **Figure 4.8(c)** and since 2004, the contour of 500 kg m^{-1} s^{-1} frequently appeared in **Figure 4.8 (d)**. More concretely, the mean water vapor flux between 137.5° and 150°E longitude and 40°and 50°N latitude was shown in **Figure 4.9,** more clearly suggesting a substantial increase has been observed for both annual and seasonal scales over the past 32 years. All these trends are likely to cause the increases of precipitation, basically reflecting the changes in **Figure 4.2** and **Figure 4.5**. **Figure 4.9** also indicates that summer had the highest water vapor flux in Hokkaido from 1980 to 2011, followed by autumn, winter and spring, which are in line with the **Figure 4.8**.

For further understand spatial relationship between water vapor flux and precipitation, **Figure 4.10** gives the correlation patterns between precipitation in Hokkaido and water vapor flux (kg/m·s) in whole lays under 300 hpa in annual, spring, summer autumn, and winter from 1980 to 2011 by calculating the Kendall's tau. Among them, the water vapor flux had a positive correlation with precipitation in Hokkaido in spring (**Figure 4.10(b)**), summer (**Figure 4.10(c)**) and winter (**Figure 4.10(e)**) over the past 32 years, which may explain precipitation amounts tended to increase during these seasons in more than 60% of the stations (**Table 4.1** and **Figure 4.6**). However, a negative correlation with precipitation in Hokkaido was observed in autumn, especially in the North of Hokkaido, which does not fit well with the changes of precipitation distribution (**Figure 4.6(c)**).

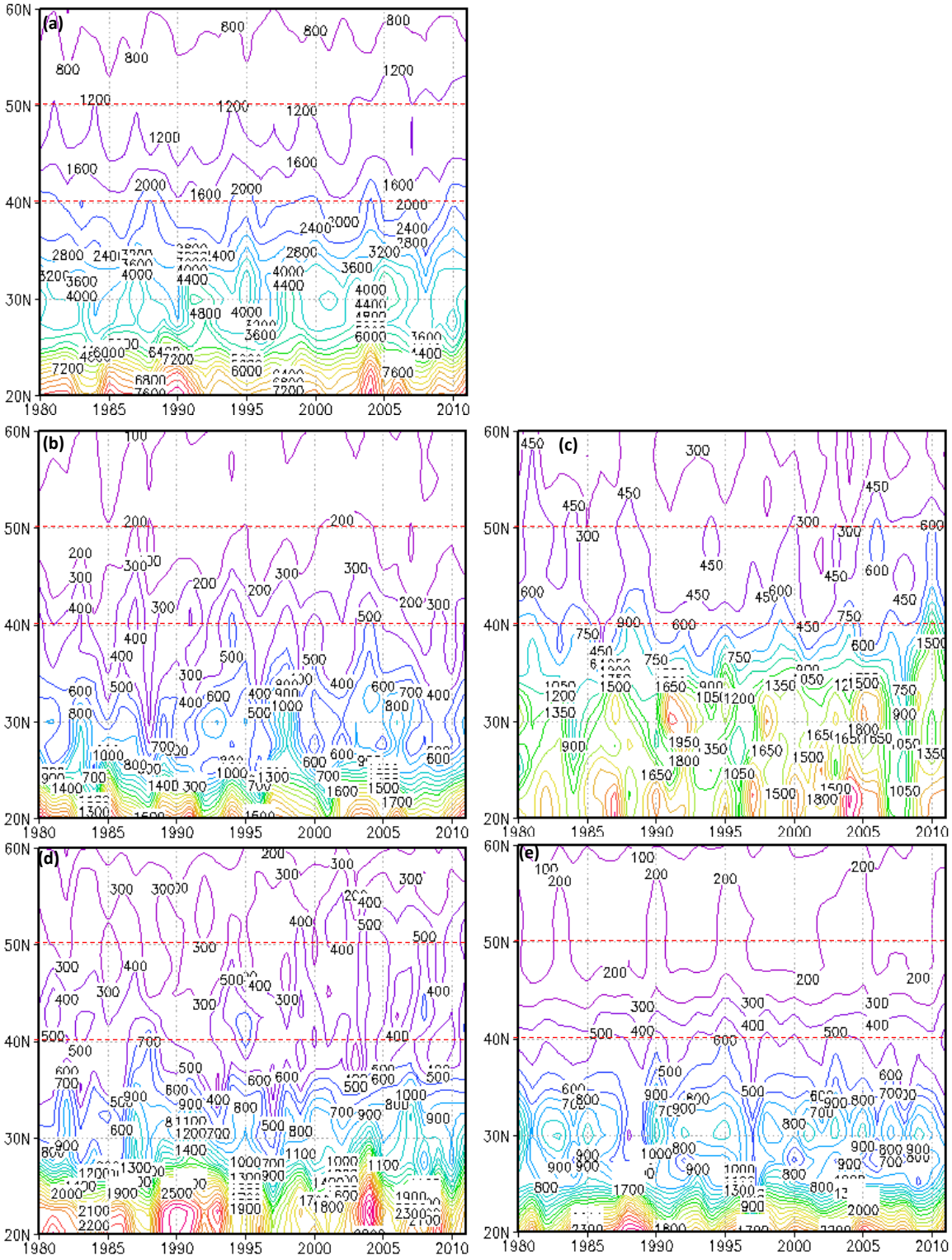

Figure 4.8 The latitude-time cross-section of water vapor flux (kg/m·s) in whole lays under 300 hpa in annual (a), spring (b), summer (c), autumn (d), and winter (e) averaged over 137.5E-150E. Red dotted line shows the area which the Hokkaido is located on similar latitudes to.

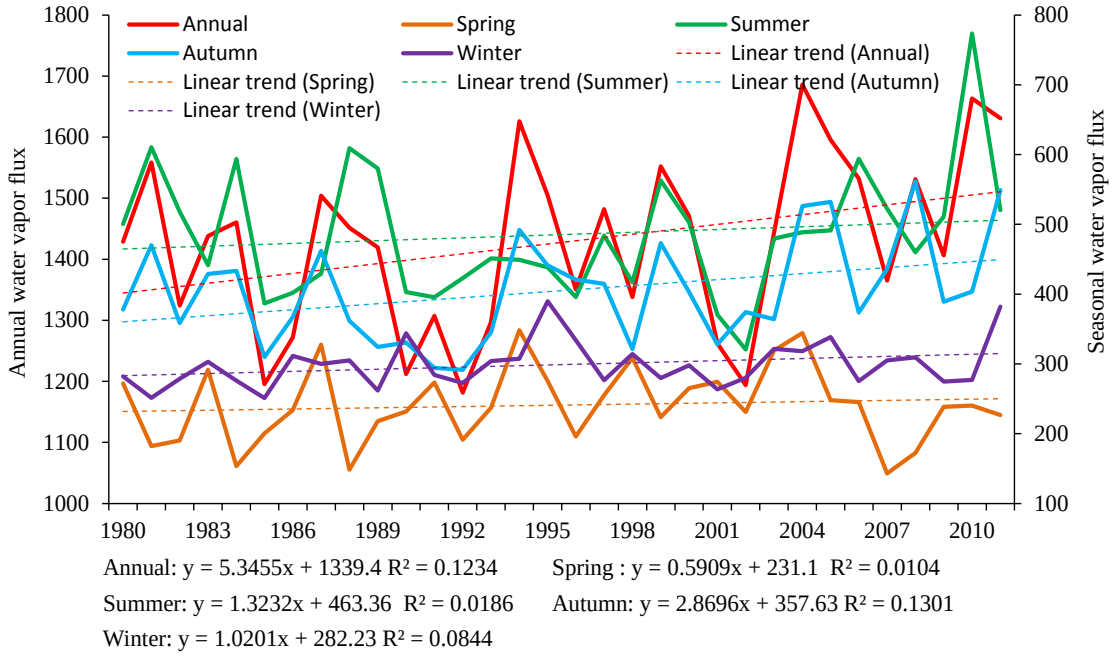

Figure 4.9 Changes of mean water vapor flux (kg/m·s) between 137.5° and 150°E longitude and 40°and 50°N latitude in whole lays under 300 hPa in annual, spring, summer, autumn, and winter from 1980 to 2011.

4.4 Discussion

As the above result shows, precipitation variations exhibited different changes in different timescales and these changes were in close association with the water vapor transport and budget in Hokkaido in recent decades. These findings also generate several interesting question despite clearly indicating significant trends in precipitation in Hokkaido. First, why was precipitation less in winter and more in summer? Winter is the coldest season of the year in Hokkaido and precipitation generally falls as snow. Nakamura et al., (2002) reported that the strength of the East Asian winter monsoon (i.e., Siberian high) was weakening in the late 1980's and the cyclonic activity in early winter was stronger when the winter monsoon activity was weaker; Bertacchi et al., (2001) noted that the main characteristic of the winter season in Japan is the presence of the winter monsoon that comes from the north and brings cold air and precipitation, mainly to the northern part of the country, at the beginning of the season. The average temperature is the highest and East Asian monsoon is the most active in summer in Hokkaido (Yamada et al., 2012), resulting in higher summer precipitation.

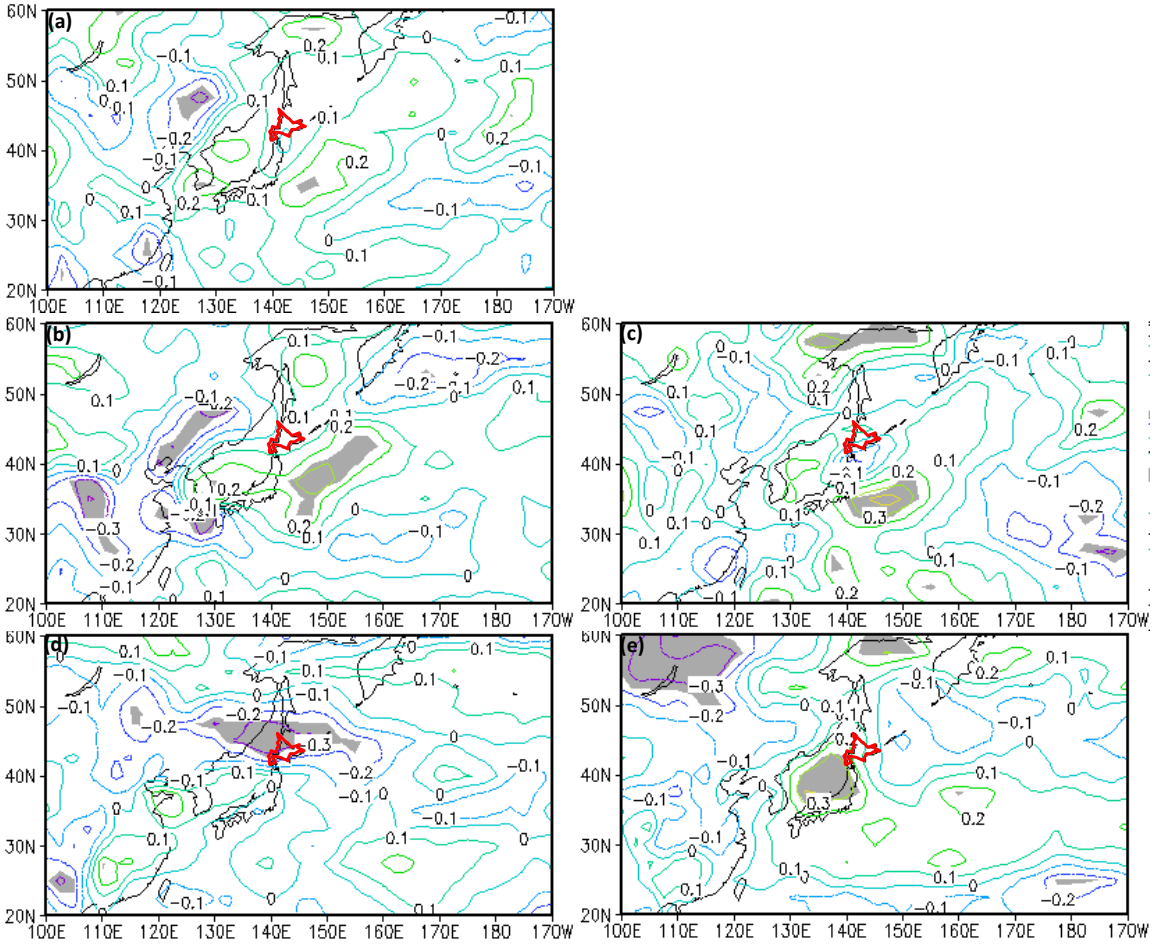

Figure 4.10 Correlations between precipitation in Hokkaido and water vapor flux (kg/m·s) in whole lays under 300 hPa in annual (a), spring (b), summer (c), autumn (d), and winter (e) from 1980 to 2011. The contour interval is 0.1; shading denotes regions where the trend is significant at the 95% confidence level.

Another question is why the downtrend in winter and autumn was clearer at stations on the Japan Sea side where precipitation was higher (**Figure 4.6**). As mentioned in Section 4.3.4, precipitation distribution in winter and autumn can roughly be explained by large-scale atmospheric circulation. Asian monsoon plays an important role in large-scale climate variability over much of the globe (Wang, 2002; Yuan et al., 2004), (You et al., 2011). Weakening of the Asian winter monsoon has been observed in many recent studies (Nakamura et al., 2002; Panagiotopoulos et al., 2005), which may explain the downtrend in winter and autumn. Jhun and Lee (2004) indicated that variability in the intensity of the East Asian winter monsoon is influenced by both the Siberian high and the Aleutian low. Consequently, the winter-time precipitation pattern in Hokkaido is thought to be affected not only by Siberian high strength but also by the Aleutian low. Further studies about the

synergistic influence of Asian land surface air temperatures, sea surface temperature (SST) anomalies, and Tropical Pacific SST anomalies associated with the El Niño-Southern Oscillation (ENSO) are necessary to elaborate the changes of precipitation on the fringe of Hokkaido.

Thirdly, will water vapor flux variations bring more rain in Hokkaido? Water vapor flux is related to the sea level pressure, temperature, wind and geopotential height. For example, because a warmer atmosphere holds more water vapor (Cline, 1991), temperature increases are likely to impact water vapor flux and therefore contribute to precipitation variability. Yue and Hashino (2003) found that surface temperature increased from 1900 to 1906 in Japan and will be likely to increase in the future. Assessment Report of the Intergovernmental Panel on Climate Change (IPCC, 2007), Kurihara et al., (2005) pointed out that changes of surface temperatures in and around Hokkaido were predicted to be larger than those in other regions of Japan, and indicated that anticyclonic circulation in the south of Japan will likely intensify and induce a strong water vapor flux along the rim of the anticyclonic anomaly in the future, which would increase the likelihood of heavy precipitation. Westerly moisture flux associated with the prominent pattern of surface pressure anomalies between the main island of Japan and the Sea of Okhotsk also influence the precipitation in Japan (Yamada et al., 2012).

Finally, in Japan, water-related disasters such as flooding and sediment pulses, and damage caused by heavy precipitation are projected to increase. As shown in **Figure 4.5(b)**, high precipitation was observed in summer, 1981, which induced a big flood, causing severe damage in the basins of the Ishikari River. River discharge and water quality is affected by precipitation amounts in the Ishikari River basin, Hokkaido (Duan et al., 2013; Duan et al., 2012). Future research will need to explore the extent to which precipitation trends will drive changes in environmental health and water resources in Hokkaido.

4.5 Conclusions

This study characterized the causes of precipitation variability in Hokkaido, Japan, during 1980-2011, using the Mann-Kendall test. We also examined possible association with water vapor flux in an attempt to understand the latest precipitation trends in the region. Major conclusions can be summarized as follows:

(1) Precipitation tended to increase across Hokkaido during 1980-2011 at both the annual and seasonal scales, with 147 stations (approximately 87% of the total number of stations) showing positive trends on an annual basis, followed by spring (143, approximately 85%), summer (139, approximately 82%), autumn (116, approximately 69%) and winter (103, approximately 61%).

(2) Precipitation varied substantially in spatial-temporal. Precipitation was mainly concentrated in summer and ranged from 233 mm to 751 mm and autumn with a range of 218 mm to 724 mm, while precipitation amounts were less in winter and spring. Higher precipitation occurrence in the warm seasons is consistent with observed monthly distributions. The northwest had higher precipitation than the southeast in winter, autumn and interannually, with precipitation concentrated in the southeast in both spring and summer. These results are generally in line with monthly distributions.

(3) Most stations with negative trends are located in areas with higher precipitation, such as the west in winter and autumn (the Japan Sea side in **Figure 4.6**), the southeastern fringe in summer, and scattered across the areas with lower precipitation in spring. Most stations with negtive trends were observed in areas with higher precipitation amounts during February, August, October, November and December (**Figure 4.7**). This suggests that larger increases in precipitation occurred in areas with lower precipitation overall.

(4) The changes of the water vapor transport and budget in whole layers under 300hpa between the period 1980-2011 posibly explain the spatiotemporal distribution of precipitation trends in Hokkaido. Water vapor flux decreased gradually from the south to the north in all seasons, possibly explaining the annual and seasonal mean precipitation. Seasonal distributions of water vapor flux may reflect precipitation was mainly concentrated in summer and autumn, while precipitation was reduced in winter and spring.

4.6 References

Bertacchi Uvo, C. et al., 2001. Statistical atmospheric downscaling for rainfall estimation in Kyushu Island, Japan. Hydrology and Earth System Sciences, 5(2): 259-271.

Best, D.J. and Gipps, P.G., 1974. Algorithm AS 71: The upper tail probabilities of Kendall's Tau. Applied Statistics, 98-100.

Bray, M., Han, D., Xuan, Y., Bates, P. and Williams, M., 2011. Rainfall uncertainty for extreme events in NWP downscaling model. Hydrological Processes, 25(9): 1397-

1406.

Brown, M.E. and Funk, C.C., 2008. Food security under climate change. Science, 319(5863): 580-581.

Burns, A., Gleadow, R., Cliff, J., Zacarias, A. and Cavagnaro, T., 2010. Cassava: The drought, war and famine crop in a changing world. Sustainability, 2(11): 3572-3607.

Cline, W.R., 1991. Scientific basis for the greenhouse effect. The Economic Journal, 101(407): 904-919.

Coumou D and Rahmstorf S, 2012. A decade of weather extremes. Nature Climate Change, 2(7): 491-496.

Cullather, R.I., Bromwich, D.H. and Van Woert, M.L., 1998. Spatial and Temporal Variability of Antarctic Precipitation from Atmospheric Methods. Journal of Climate, 11(3): 334-367.

Dai, A., 2011. Drought under global warming: a review. Wiley Interdisciplinary Reviews: Climate Change, 2(1): 45-65.

Duan, W.L., He, B., Takara, K., Luo, P.P. and Yamashiki, Y., 2012. Estimating the Sources and Transport of Nitrogen Pollution in the Ishikari River Basin, Japan. Advanced Materials Research, 518: 3007-3010.

Duan, W.L., He, B., Takara, K., Luo, P.P. and Yamashiki, Y., 2013. Spatial and temporal trends in estimates of nutrient and suspended sediment loads in the Ishikari River, Japan, 1985 to 2010. Science of the Total Environment, 461: 499-508.

Feng, J., Chen, W., Tam, C.Y. and Zhou, W., 2011. Different impacts of El Niño and El Niño Modoki on China rainfall in the decaying phases. International Journal of Climatology, 31(14): 2091-2101.

Folland, C.K., Karl, T.R. and Jim Salinger, M., 2002. Observed climate variability and change. Weather, 57(8): 269-278.

Fujibe, F., Yamazaki, N., Katsuyama, M. and Kobayashi, K., 2005. The increasing trend of intense precipitation in Japan based on four-hourly data for a hundred years. SOLA, 1(0): 41-44.

Hendrix, C.S. and Salehyan, I., 2012. Climate change, rainfall, and social conflict in Africa. Journal of Peace Research, 49(1): 35-50.

Hertig, E. et al., 2012. Changes of total versus extreme precipitation and dry periods until the end of the twenty-first century: statistical assessments for the Mediterranean area. Theoretical and Applied Climatology, 108: 1-20.

Iwasaki, H. and Sunaga, Y., 2009. Study of recent variation in weak rainfall over Japan using 31-year AMeDAS dataset. SOLA, 5(0): 157-159.

Jhun, J.G. and Lee, E.J., 2004. A new East Asian winter monsoon index and associated characteristics of the winter monsoon. Journal of Climate, 17(4): 711-726.

Kalnay, E. et al., 1996. The NCEP/NCAR 40-year reanalysis project. Bulletin of the American Meteorological Society ,77: 437–471.

Kawamoto, N., Oki, R. and Shimizu, S., 2011. Comparison between TRMM/PR and AMeDAS ground rain gauge network in terms of annual rainfall. IEEE, pp. 2590-2593.

Kendall, M.G., 1975. Rank Correlation Methods: Charles Griffin. London, 272 pp.

Kerr, R.A., 2007. Global warming is changing the world. Science, 316(5822): 188-190.

Kimoto, M., Yasutomi, N., Yokoyama, C. and Emori, S., 2005. Projected changes in precipitation characteristics around Japan under the global warming. SOLA, 1(0): 85-88.

Kistler, R. et al., 2001. The NCEP-NCAR 50-year reanalysis: Monthly means CD-ROM and documentation. Bulletin-American Meteorological Society, 82(2): 247-268.

Knutson, T.R. et al., 2010. Tropical cyclones and climate change. Nature Geoscience, 3(3): 157-163.

Kurihara, K. et al., 2005. Projection of climatic change over Japan due to global warming by high-resolution regional climate model in MRI. SOLA, 1(0): 97-100.

Lenderink, G. and Van Meijgaard, E., 2008. Increase in hourly precipitation extremes beyond expectations from temperature changes. Nature Geoscience, 1(8): 511-514.

Mann, H.B., 1945. Nonparametric tests against trend. Econometrica, 13: 245-259.

Marengo, J.A., Nobre, C.A., Tomasella, J., Cardoso, M.F. and Oyama, M.D., 2008. Hydro-climatic and ecological behaviour of the drought of Amazonia in 2005. Philosophical Transactions of the Royal Society B: Biological Sciences, 363(1498): 1773-1778.

Medina-Elizalde, M. and Rohling, E.J., 2012. Collapse of Classic Maya Civilization Related to Modest Reduction in Precipitation. Science, 335(6071): 956-959.

Miao, Q.J., Xu, X.D. and Zhang, S.Y., 2005. Whole layer water vapor budget of Yangtze River valley and moisture flux components transform in the key areas of the plateau. Acta Meteorological Sinica, 63: 93-99.

Muñoz-Díaz, D. and Rodrigo, F.S., 2006. Seasonal rainfall variations in Spain (1912–2000) and their links to atmospheric circulation. Atmospheric Research, 81(1): 94-

110.

Nakamura, H., Izumi, T. and Sampe, T., 2002. Interannual and decadal modulations recently observed in the Pacific storm track activity and East Asian winter monsoon. Journal of Climate, 15(14): 1855-1874.

Nomoto, S., 2003. Decreases in the number of foggy days in Thailand and Japan, and possible causes. Journal of International Economic Studies, 17: 13-28.

Pal, I. and Al-Tabbaa, A., 2011. Monsoon rainfall extreme indices and tendencies from 1954–2003 in Kerala, India. Climatic Change, 106(3): 407-419.

Panagiotopoulos, F., Shahgedanova, M., Hannachi, A. and Stephenson, D.B., 2005. Observed trends and teleconnections of the Siberian high: A recently declining center of action. Journal of Climate, 18(9): 1411-1422.

Reiser, H. and Kutiel, H., 2011. Rainfall uncertainty in the Mediterranean: time series, uncertainty, and extreme events. Theoretical and Applied Climatology, 104(3): 357-375.

Río, S., Herrero, L., Fraile, R. and Penas, A., 2011. Spatial distribution of recent rainfall trends in Spain (1961-2006). International Journal of Climatology, 31(5): 656-667.

Solomon, S., 2007. Climate change 2007: the physical science basis: contribution of Working Group I to the Fourth Assessment Report of the Intergovernmental Panel on Climate Change. Cambridge University Press.

Suzuki, K. and Hayakawa, S., 2006. Convective Precipitation in Yamaguchi Prefecture in Summer. Journal of Agricultural Meteorology, 62(4): 127-132.

Takeshita, S., 2010. Influence on precipitation and the distribution in Miyazaki [Japan] Prefecture with climate changes. Bulletin of the Faculty of Agriculture, Miyazaki University (Japanese), 56: 73-78.

Taschetto, A.S. and England, M.H., 2009. El Nino Modoki impacts on Australian rainfall. Journal of Climate, 22(11): 3167-3174.

Türkeş, M., 1996. Spatial and temporal analysis of annual rainfall variations in Turkey. International Journal of Climatology, 16(9): 1057-1076.

Utsumi, N. et al., 2008. Importance of wind-induced undercatch adjustment in a gauge-based analysis of daily precipitation over Japan. Hydrological Research Letters, 2(0): 47-51.

Walsh, K.J.E., McInnes, K.L. and McBride, J.L., 2011. Climate change impacts on tropical cyclones and extreme sea levels in the South Pacific–a regional assessment. Global

and Planetary Change, 80-81: 149-164.

Wang, B., 2002. Rainy Season of the Asian-Pacific Summer Monsoon*. Journal of Climate, 15(4): 386-398.

Wolff, C. et al., 2011. Reduced Interannual Rainfall Variability in East Africa During the Last Ice Age. Science, 333(6043): 743-747.

Xu, X., Chen, L., Wang, X., Miao, Q. and Tao, S., 2004. Moisture transport source/sink structure of the Meiyu rain belt along the Yangtze River valley. Chinese Science Bulletin, 49(2): 181-188.

Yamada, T.J., Sasaki, J. and Matsuoka, N., 2012. Climatology of line‐shaped rainbands over northern Japan in boreal summer between 1990 and 2010. Atmospheric Science Letters, 13(2): 133-138.

You, Q. et al., 2011. Changes in daily climate extremes in China and their connection to the large scale atmospheric circulation during 1961–2003. Climate dynamics, 36(11): 2399-2417.

Yuan, D. et al., 2004. Timing, duration, and transitions of the last interglacial Asian monsoon. Science, 304(5670): 575-578.

Yue, S. and Hashino, M., 2003. Long term trends of annual and monthly precipitation in Japan. Journal of the American Water Resources Association, 39(3): 587-596.

Yue, S., Pilon, P. and Cavadias, G., 2002. Power of the Mann–Kendall and Spearman's rho tests for detecting monotonic trends in hydrological series. Journal of Hydrology, 259(1): 254-271.

Zhang, Q. et al., 2008. Spatial and temporal variability of precipitation maxima during 1960–2005 in the Yangtze River basin and possible association with large-scale circulation. Journal of Hydrology, 353(3): 215-227.

Zhang, Q., Xu, C., Gemmer, M., Chen, Y.D. and Liu, C., 2009. Changing properties of precipitation concentration in the Pearl River basin, China. Stochastic Environmental Research and Risk Assessment, 23(3): 377-385.

Zhang, Q., Xu, C.Y., Chen, X. and Zhang, Z., 2011. Statistical behaviours of precipitation regimes in China and their links with atmospheric circulation 1960–2005. International Journal of Climatology, 31(11): 1665-1678.

Zhang, Z., Zhang, Q., Xu, C., Liu, C. and Jiang, T., 2009. Atmospheric moisture budget and floods in the Yangtze River basin, China. Theoretical and Applied Climatology, 95(3): 331-340.

Chapter 5 Estimation of Nutrient and Suspended Sediment Loads in the Ishikari River

5.1 Introduction

Surface water quality is increasingly recognized for its importance in controlling the health of aquatic ecosystems and impacting drinking water resources and human health. Nutrients (primarily nitrogen and phosphorus) are essential for plant and animal life, but in high concentrations can cause a number of ecological problems including algal blooms, decreased dissolved oxygen (DO) concentrations, and increased fish mortality (Carpenter et al., 1998; Li et al., 2011; Smith, 1982; Sprague and Lorenz, 2009). Suspended sediment (SS, soil and other particulate matter) is ubiquitous in aquatic ecosystems and contributes to bottom material composition, water-column turbidity, and chemical constituent transport. Excessive amounts of sediment can degrade water quality and harm aquatic ecosystems through physical, biological, and chemical processes (Terrio, 2007). In addition, extreme events such as floods can cause massive accumulations of sediment (Turner et al., 2006), significantly compromise phosphorus retention (Novak et al., 2007), and alter nitrate distribution (Bu et al., 2011) of wetland systems. For example, Turner et al., (2006) estimated that more than 131×10^6 metric tons (MT) of inorganic sediments accumulated in coastal wetlands when Hurricanes Katrina and Rita crossed the Louisiana coast in 2005, plus another 281×10^6 MT when accumulation was prorated for open water area; Letcher et al., (1999) observed that 86% of the annual total phosphorous load was transported into the Australian South Pine catchment in a few days; Chen et al., (2012) demonstrated that extreme storms in 2010 caused a four-fold increase in dissolved

** This chapter has been published in **Science of the Total Environment**, 461: 499-508, 2013*

inorganic N fluxes (DIN), with a greater fraction of ammonium (up to 30% of DIN) compared with moderate storms and background flow conditions (less than 15%), which might have been connected to harmful algal blooms in the adjacent estuary and Xiamen Bay. Therefore, understanding the temporal dynamics of nutrients and SS concentrations and loads in streams and rivers is important in order to effectively manage and protect water resources (Gruber and Galloway, 2008; Sprague and Lorenz, 2009).

Nutrient and SS concentrations and loads are generally estimated using models on the basis of infrequent monitoring data (Armour et al., 2009; Kulasova et al., 2012; Li et al., 2011; Li et al., 2009; Ma et al., 2011). Stream-discharge data, usually obtained from sparse monitoring stations, provide a basis for estimation of critically important water quality constituents because concentrations and loads of constituents commonly vary naturally with stream-flow. Such estimates are critical for many planning and design activities including water-supply analysis (Medellín-Azuara et al., 2007; Rajagopalan et al., 2009), calibration of surface- and ground-water models (Lautz and Siegel, 2006; Mas-Pla et al., 2012; Zhang et al., 2011), and water-quality assessments (Chen et al., 2012; Erturk et al., 2010; Ferrer et al., 2012). Although reliable estimates of constituent loads require sufficient sampling (Hoque et al., 2012), it is often difficult to obtain water-quality records representing constituents concentrations in rapidly changing streamflow over long time periods (years to decades). Consequently, uncertainty in constituent load estimation tends to be quite high (Christensen et al., 2000; Reckhow, 1994). Unfortunately, few estimates of nutrient loads reported in the literature present associated uncertainties (Kulasova et al., 2012). Observational uncertainties are critically important in defining and contributing to parametric uncertainty and errors in the conceptual models underpinning diffuse pollution research and management (Brouwer and De Blois, 2008). Many countries have therefore developed monitoring programs and protocols which enable a reliable quantification of nitrogen (N), phosphorus (P), and SS loadings and concentrations in the aquatic environment (e.g. the National Monitoring and Assessment Program (NOVA) in Denmark (Conley et al., 2002; Kronvang et al., 2005), the Harmonized Monitoring Scheme (HMS)

in Britain (Hurley et al., 1996; Morvan et al., 2008), and the National Water-Quality Assessment (NAWQA) in the United States (Gilliom et al., 1995; Rosen and Lapham, 2008). Meanwhile, load estimation methods and models have improved substantially (Shrestha et al., 2008).

Efforts at water management in Japan have led to significant improvements in the estimation of water quality. For example, a nationwide data collection network (http://www1.river.go.jp/) called the National Land with Water Information was established to provide real-time water data including water quality, precipitation, and river discharge. These monitoring systems are essential for evaluating and understanding the various hydrologic and biogeochemical processes governing water quality and nutrient cycling in watersheds and their ecological impacts. Because the load estimation process is complicated by retransformation bias* (Ferguson, 1986; Webb et al., 1997), data censoring (Gilbert, 1987) , and non-normality (Helsel and Hirsch, 1992; Shumway et al., 2002), biases generally exist in estimated loads from modeling studies (Johnes, 2007). There is therefore an urgent need to improve estimation methods to compliment improving monitoring programs and resolve common shortcomings in estimation methods.

In this study, the Maintenance of Variance-Extension type 3 (MOVE. 3) and the regression model Load Estimator (LOADEST) were applied to estimate total nitrogen (TN), total phosphorus (TP) and SS loads at five sites on the Ishikari River, Japan, from Jan. 1985 to Dec. 2010. We describe a procedure for estimation of constituent loads in rivers which have only sparse measurements of flow and water quality constituent concentrations. The primary goal of this study is to obtain reliable unbiased estimates of seasonal TN, TP, and SS loads for the Ishikari River and demonstrate the utility of regression methods for estimation of seasonal TN, TP, and SS loads from instantaneous samples.

* When a water-quality constituent is transformed (that is, into logarithmic units) as part of the building of a regression equation, the constituent must be retransformed to obtain an estimate in the original units. Estimates of constituent concentration that are unbiased in the transformed scale will be biased upon retransformation to the original scale ((Ferguson, 1986; Webb et al., 1997).

5.2 Materials and methods

5.2.1 Study area and data collection

The Ishikari River basin is located in central Hokkaido Island within the range of 43° N and 44° N, with total drainage area of 14,330 km^2 (see **Figure 5.1**). The Ishikari River originates from Mt. Ishikaridake (elev. 1967 m) in the Taisetsu Mountains of central Hokkaido, and flows southward into the broad Ishikari Plain and finally into the Sea of Japan. The length of the Ishikari River mainstream is 268 km and ranks third longest in Japan. Major tributaries of the river include the Chūbetsu, Uryū, Sorachi, and Toyohira. The highest elevation in the Ishikari Plain is less than 50 m and the plain is bordered by a mountain range with peaks exceeding 1,000 m in elevation. At the Sapporo weather station (elev. 17 m), monthly air temperature in the warmest month (August) is 22.0 °C, and the coldest month (January) is -4.1 °C. Snow cover in Sapporo lasts for approximately four months from December to March. Average annual snowfall is 630cm, and the year's deepest snow depth averages 101cm (1970-2000) (Usutani and Nakatsugawa, 2006).

Five monitoring sites were chosen for analysis in this study (see **Figure 5.1**, **Table 5.1**). Sites Yinou-oohashi, Yiwamizawa-oohashi, and Yishikarikakou-bashi are located in the upper, middle and lower reaches of the mainstream, respectively, while sites Akane-bashi and Umaoyi-bashi are located in the Uryū and Yūbari Tributaries, respectively. Samples of water quality (TN, TP, and SS) concentration and river discharge were collected at each site from 1985 to 2010 by the National Land with Water Information (http://www1.river.go.jp/) monitoring network. In general, water quality concentration and river discharge were measured and collected once a month or two months at each site. Monthly samples were collected at sites Akane-bashi, Yinouo-ohashi, and Umaoyi-bashi, with a total number of 312 for each testing parameter at each site; 274 samples were collected for each testing parameter at SitesYiwamizawa-oohashi and Yishikarikakou-bashi.

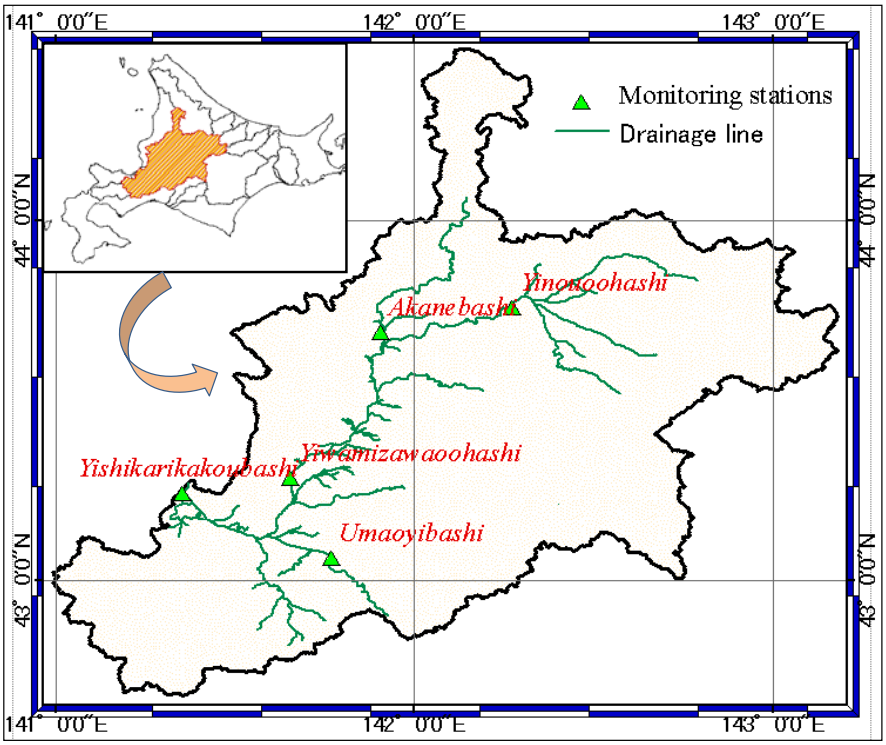

Figure 5.1 Study area, and monitoring stations for the Ishikari River

Table 5.1 Studied stations information for loads estimation

Station ID	Station name	Latitude(N)	Longitude(W)
401031281104020	Yinouoohashi	43°45'55"	142°16'34"
401031281101080	Akanebashi	43°40'54"	141°54'0"
401031281101040	Yiwamizawaoohashi	43°13'23"	141°39'41"
401031281101360	Umaoyibashi	43°3'42"	141°46'4"
401031281101060	Yishikarikakoubashi	43°13'44"	141°21'7"

5.2.2 Streamflow extension

Although the Water Information (http://www1.river.go.jp/) monitoring network covers all of Japan, there are some streamflow gaging stations with short periods of record or missing flow values that reflect gaps in long-term hydrologic conditions. Streamflow record extension methods such as the Maintenance of Variance-Extension type 1 (MOVE.1) (Hirsch, 1982) and the Maintenance of Variance-Extension type 3 (MOVE.3)

(Vogel and Stedinger, 1985) are employed to estimate missing flow values or to extend the record at a short-record station on the basis of daily streamflow values recorded at nearby, hydrologically similar index stations. Both of them can be described as follows:

$$Y_i = mX_i + b + e_i \tag{5.1}$$

where Y_i is the logarithm of the discharge for the ith day at the short-record site; X_i is the logarithm of the discharge for the ith day at the long-record site; m is the regression-line slope; b is the regression-line intercept; e_i is the difference between the regression-line estimate and the measured Y value for the ith measurement.

The estimated discharge values are finally obtained as 10^{Y_i}. MOVE.1 is a parametric method that calculates the slope (m) as the product of the sign of the correlation coefficient (r) and the ratio of the standard deviations of the Y values (S_y) to the standard deviation of the concurrent X values (S_x). The intercept (b) is calculated so that the line with slope m passes through a point with XY coordinates that equal the mean of the X and Y populations, respectively. Vogel and Stedinger (1985) indicated that MOVE.1 estimates produce populations of Y values based on statistics of the X and Y samples during the concurrent period of record, and this may not fully utilize information available in the total population of X values from the long-term record station. Therefore, MOVE.3 method was developed by Vogel and Stedinger (1985) to capture statistics from the full length of the available record. It uses estimates of the mean and standard deviation for the concurrent period from both stations but also incorporates the mean and standard deviation for the nonconcurrent period from the index station. For this study, MOVE.3 is therefore used to extend or augment the daily discharge series over the period 1985-2010.

5.2.3 Loads estimation

Stream-water SS or chemical constituent load ($\emptyset$) can be calculated using constituent concentration (C) and discharge (Q) integrated over time(t):

$$\emptyset = \int C(t)Q(t)dt \tag{5.2}$$

A continuous record of concentration and discharge is required to estimate loads using the integral in equation 5.2. Although discharge can be easily measured at a sufficiently high frequency, however, the expense of collecting and analyzing samples for water quality constituents means it is often difficult to obtain continuous data. Equation 5.2 can therefore be written as:

$$L_T = \Delta t \sum_{i=1}^{n} L_i \tag{5.3}$$

where L_T is an estimate of total load, L_i is an estimate of instantaneous load, n is the number of discrete points in time, and Δt is the time interval represented by the instantaneous load.

In addition, the FORTRAN Load Estimator (LOADEST) uses time-series streamflow data and constituent concentrations to calibrate a regression model that describes constituent loads in terms of various functions of streamflow and time, enabling a direct calculation of equation 5.3 (Runkel et al., 2004). LOADEST performs calibration procedures and makes load estimates with four statistical estimation methods: Adjusted Maximum Likelihood Estimation (AMLE), Maximum Likelihood Estimation (MLE), Linear Attribution Method (LAM), and Least Absolute Deviation (LAD). AMLE and MLE are suitable when the model calibration errors (residuals) are normally distributed; AMLE is the more appropriate method of the two when the calibration data set contains censored data (i.e. when data are reported as less than or greater than some threshold). LAM and LAD are useful when the residuals are not normally distributed. Because the input data in this study included censored data, and because the model calibration residuals were normally distributed within acceptable limits, the AMLE estimation method was selected in each site. The output regression model equations take the following general form (Runkel et al., 2004):

$$\mathrm{Ln}(L_i) = a + b\ln Q + c\ln Q^2 + d * sin(2\pi dtime) + e * cos(2\pi dtime) + f dtime + g dtime^2 + \varepsilon \quad (5.4)$$

where L_i is the calculated load for sample i; Q is stream discharge; $dtime$ is time, in decimal years from the beginning of the calibration period; ε is error; and $a, b, c, d, e, f, and\ g$ are the fitted parameters in the multiple regression model. Some of the regression equations in this study did not include all of the above terms, depending on the lowest Akaike Information Criterion (AIC) values (Sakamoto et al., 1986).

$$AIC = 2k - 2\ln(L) \quad (5.5)$$

where k is the number of parameters in the statistical model, and L is the maximized value of the likelihood function for the estimated model.

Combining the equations above, monthly and seasonal average TN, TP and SS loads were calculated. The seasons were considered as follows: winter (December, January, February); spring (March, April, May); summer (June, July, August); autumn (September, October, November).

5.3 Results

5.3.1 Streamflow extension

The stations with short periods of record or missing flow values were extended by filling in missing values using the MOVE.3 method from nearby gauges. The long-term index station was chosen according to several criteria, including that it be unregulated, have a portion of its period of record coincident with that at the short-term station, and have a substantially longer period of record than the short term station (Nielsen, 1999). Another criterion is the Pearson's correlation ρ between the logarithms of the daily streamflows at the short and long-term stations. Usually, $\rho > 0.8$ means there is a strong positive association between changes of daily streamflows at the short and long-term stations

(Vogel and Stedinger, 1985). The long-term station exhibiting the largest correlation with each short-term station was chosen as the index station for that particular short-term station. **Table 5.2** shows the Pearson's correlation coefficient (ρ), ranging from 0.79 (Umaoyi-bashi) to 0.96 (Yiwamizawa-oohashi) with an average value of 0.88 for the five stations, suggesting strong relationships between index stations and studied stations on average. **Figure 5.2** illustrates the correlation of concurrent daily mean discharge between study stations and nearby index stations, with the best performance at station Yiwamizawa-oohashi.

The MOVE.3 method was used to extend daily flow records at each study station after determining an index station. To evaluate the accuracy of the MOVE.3 method, two statistics, the root mean square error (RMSE) (a method indicting the magnitude of the population of residual errors) of the estimating equations for each index station, and the Nash Sutcliffe efficiency (NSE) (Legates and McCabe Jr, 1999) for the final values were calculated (**Table 5.2**). RMSE of the estimating equations ranged from 0.08 (Yiwamizawa-oohashi) to 0.38 (Umaoyi-bashi) and NSE coefficients for the final models ranged from 0.21 (Umaoyi-bashi) to 0.78 (Yiwamizawa-oohashi) with a mean value of 0.51. Umaoyi-bashi has the largest RMSE and the smallest NSE, indicating relatively poor model performance at this site. As expected, the results of NSE are proportional to the values of Pearson's correlation ρ.

Table 5.2 Pearson's correlation coefficient ρ for correlation between logarithms of flows at study stations and nearby index stations, RMSE of the estimating equations for each index station, and NSE of the model performance in waterflow simulation

Site	Yinou-oohashi	Akane-bashi	Yiwamizawa-oohashi	Umaoyi-bashi	Yishikarikakou-bashi
ρ	0.88	0.90	0.96	0.79	0.84
EMSE	0.13	0.19	0.08	0.38	0.16
NSE	0.54	0.55	0.78	0.21	0.45

5.3.2 Regression evaluation

Coefficients of determination (R^2) for the best-fit regression models for loads of TN, TP, and SS for the five studied sites (**Table 5.1**) ranged from 71.86 % to 90.94 % (site Akane-bashi was the highest). Meanwhile, according to the calibrated data at each site, different models were selected on the basis of the lowest AIC and then coefficients were calculated using the AMLE (**Table 5.3**). For example, for TN estimation at site Akane-bashi, the lowest of AIC was 0.729 and the coefficients $a, b, c, d, e, f, and\ g$ were 7.6937, 1.0148, -0.0659, 0.2336, -0.0402, and -0.0166; while at site Umaoyi-bashi, the lowest of AIC was 0.928 and the coefficients employed were a (6.3542), b (0.9862), and c (0.0212).

5.3.3 Estimated loads

Although the model provided daily load estimates, these are not discussed in detail in this study because of their limited utility for analyses of long time periods. Average monthly and seasonal loads are more suitable for data synthesis as they minimize day-to-day variation (which can be misleading and cause invalid interpretation). Most of the discussion in the following sections therefore refers to monthly, seasonal, and annual load estimates.

Figure 5.3 shows time-series graphs comparing monthly average TN, TP and SS loads at all five sites. Seasonal fluctuations in loads can clearly be seen for the period 1985 to 2010, even though the dates of peak discharge were not the same every year. Overall, estimated loads at Yishikarikakou-bashi were larger than at the other sites, with TN, TP, and SS loads ranging from 8519.00 to 200189.00 kg/day (Apr. 1999), 395.87 to 52299.00 kg/ day (Apr. 1999), and 92111.00 to 92500000.00 kg/day (Sep.2001), respectively. Estimated loads at Akane-bashi and Umaoyi-bashi were comparable; loads at these sites were the lowest in the five sites. Meanwhile, decreasing trends can be seen in Figure 5.3, especially suspended sediment since 2001.

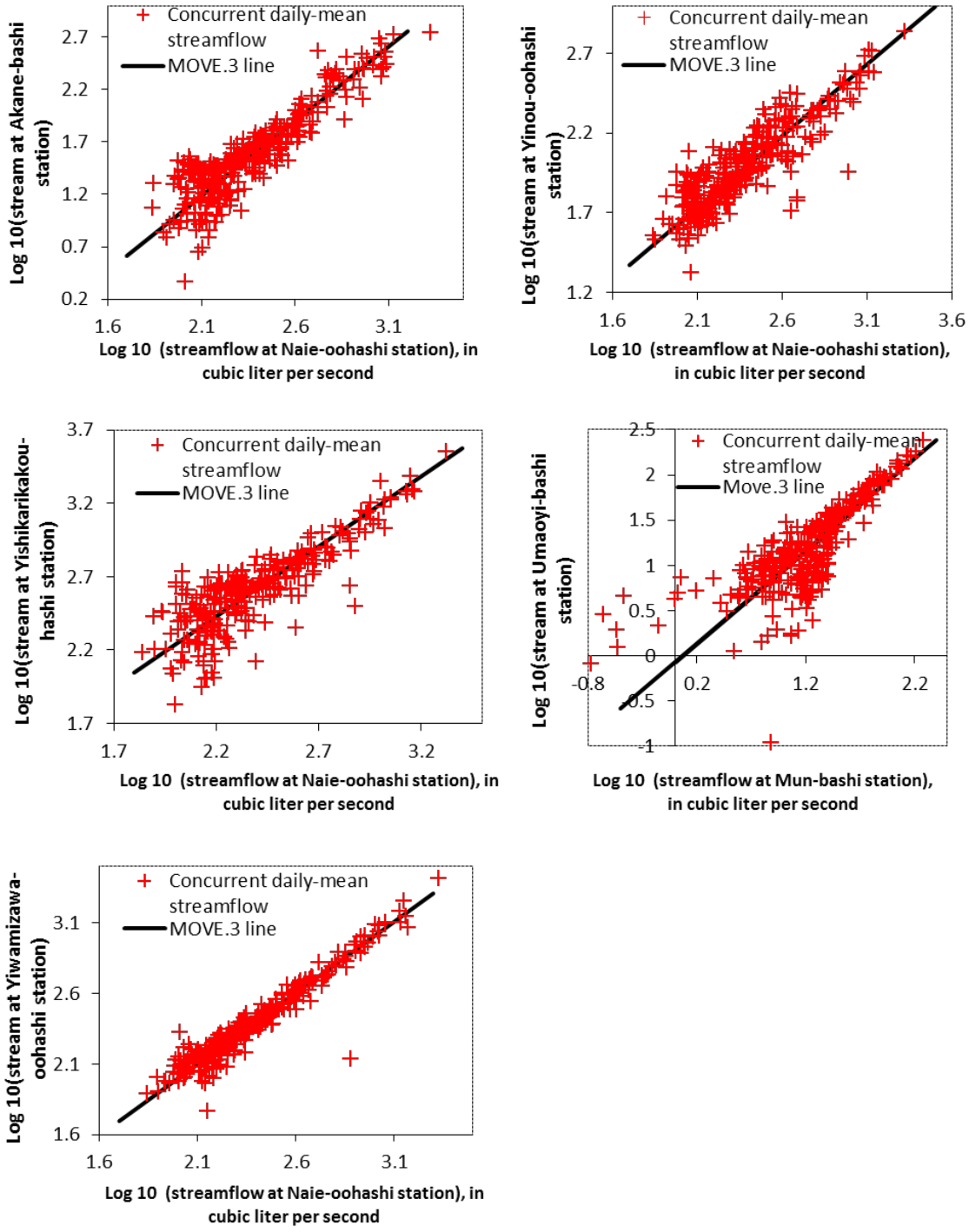

Figure 5.2 Correlation of concurrent daily mean discharge between study stations and nearby index stations

Table 5.3 Regression coefficients, coefficients of determination (R^2) and AIC for load models used to estimate TN, TP, and SS at five sites in the Ishikari River basin, Japan, 1985-2010.

Site name	Regression Coefficient							R^2 (%)	*AIC*
	a	*b*	*c*	*d*	*e*	*f*	*g*		
TN									
Akane-bashi	7.6937	1.0148	-0.0659	0.2336	-0.0402	-0.0166		90.32	0.729
Yinou-oohashi	9.0611	0.9731	0.0170	0.1781	0.1851	-0.0116	0.0006	83.39	0.096
Yiwamizawa-oohashi	10.1437	0.9319	0.1486	0.1252				90.92	-0.405
Yishikarikakou-bashi	10.7179	0.8623	-0.0738	-0.1504	0.1037	-0.0108	0.0013	81.61	0.123
Umaoyi-bashi	6.3542	0.9862	0.0212					89.22	0.928
TP									
Akane-bashi	5.2845	1.0636	-0.0148	0.0437	-0.5664	-0.0241	-0.0019	87.67	1.359
Yinou-oohashi	6.0393	0.9630	0.1034	0.1846	-0.0855	-0.0143		71.86	1.078
Yiwamizawa-oohashi	7.4453	1.2861	0.0946	-0.0039	-0.1948	-0.0142		85.29	0.972
Yishikarikakou-bashi	7.8863	1.1639	0.1012	0.1502	0.0305	-0.0082	0.0007	88.71	0.368
Umaoyi-bashi	3.7506	1.2456	0.0686	0.1754	0.3852	-0.0169	-0.0016	90.94	1.339
SS									
Akane-bashi	11.3048	1.5966	0.0118	-0.0506	-0.3897	-0.0397	-0.0027	84.50	2.247
Yinou-oohashi	11.8067	1.5217	0.3208	0.1214	-0.1172	-0.0114	-0.0026	75.68	1.777
Yiwamizawa-oohashi	13.6406	1.9716	0.1002	-0.124	-0.2088	-0.0289	-0.0022	85.98	1.752
Yishikarikakou-bashi	13.2826	2.0891	0.3045	0.2234	-0.1408	-0.0333		85.58	1.815
Umaoyi-bashi	10.1034	1.5919	0.138	0.3627	0.3484	-0.0262	-0.002	84.21	2.432

Figure 5.4 shows the estimated average loads of TN, TP, and SS by month at all sites, 1985 to 2010, calculated by averaging the monthly averages for each month of the year (for example, the average of all January monthly averages, all February monthly averages, etc.). As can be seen from **Figure 5.4**, the estimated average loads of TN, TP, and SS in April had the largest loads at all sites. For example, at Yishikarikakou-bashi, the values were 122629.31 kg/day, 15630.62 kg/day and 18694484.69kg/day, respectively. After April, the estimated average loads decreased, and then increased again. Usually, there were peaks in TP and SS in September While January, February and March had relatively low loads.

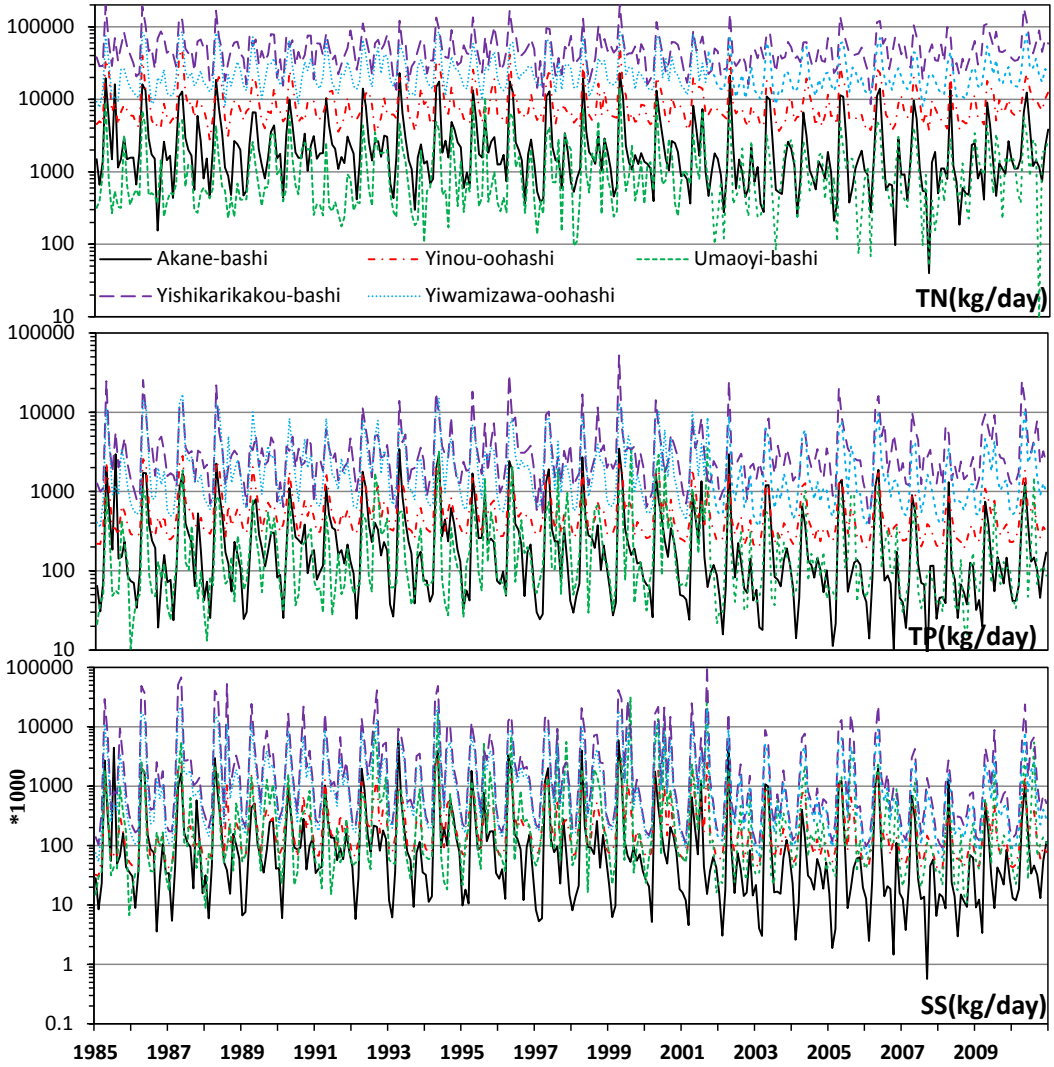

Figure 5.3 Estimated monthly average loads of TN, TP and SS at five sites on the Ishikari River, January 1985 through December 2010

Estimated seasonal loads of TN, TP, and SS at five sites were highly variable between 1985 and 2010 in the Ishikari River and its tributaries, with the greatest loads occurring in the spring and the smallest loads occurring in the winter (**Figure 5.5**), reflecting fluctuations in discharge as a result of the combined effects of seasonal runoff patterns, the exact timing of which vary from year to year. At site Akane-bashi, TN load decreased from 8146.00 kg/day in spring to 1191.00 kg/day in winter, TP load decreased from 907.00 to 60.30 kg/day, and SS decreased from 956854.00 to 26906.00 kg/day. At site Yishikarikakou-bashi, TN load decreased from 78478.00 kg/day in spring to 39091.00 kg/day in winter, TP load decreased from 8110.00 to 1619.00kg/day, and SS decreased

from 11470000.00 to 367458.00 kg/day. Seasonal fluctuations were consistent with monthly fluctuations (**Figure 5.4**). Regardless of season, site Yishikarikakou-bashi had the largest loads of TN, TP, and SS, far more than at other sites, the mean seasonal of which were 46 702 kg/day, 3 560 kg/day and 1 991 033 kg/day (**Table 5.4**).

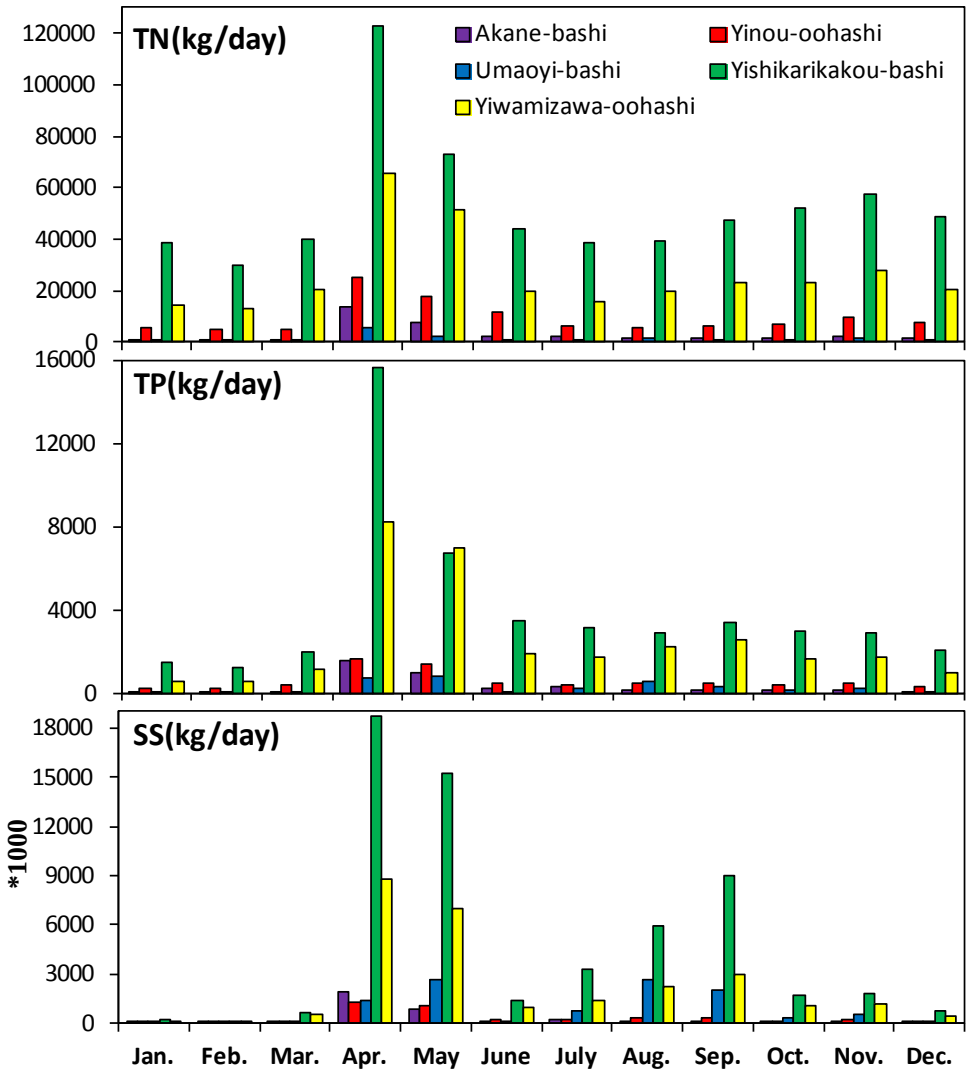

Figure 5.4 Estimated average loads of TN, TP and SS, by month, at five sites on the Ishikari River, January 1985 through December 2010.

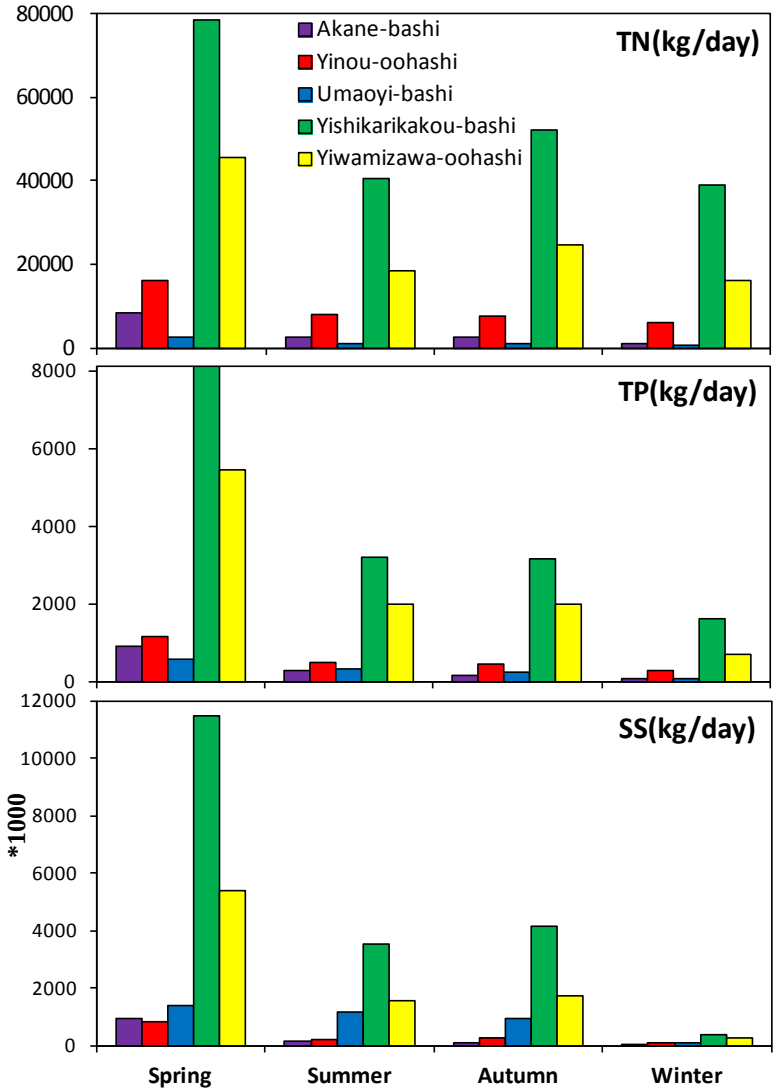

Figure 5.5 Estimated seasonal average loads of TN, TP, and SS at five sites on the Ishikari River, January 1985 through December 2010.

Table 5.4 Estimated mean seasonal loads of TN, TP, and SS at five sites on the Ishikari River (kg/day).

Site name	TN	TP	SS
Akane-bashi	3699.25	350.89	310793.00
Yinou-oohashi	9470.75	600.53	346306.00
Umaoyi-bashi	1444.47	301.07	901897.00
Yishikarikakou-bashi	52634.25	4018.00	4908533.00
Yiwamizawa-oohashi	26233.50	2553.00	2250293.00

5.4 Discussions

Stations with short periods of record or missing flow values were extended using the MOVE.3 method and data from nearby gauges (see **Table 5.2**). On the basis of the lowest *AIC* from different models, the best models were chosen to estimate constituents at each site (**Table 5.3**) to better simulate changes in concentrations and loads. For example, coefficients d and e show seasonal variation directly (i.e. the greater the value of d and e, the greater the seasonal change (Runkel et al., 2004). Meanwhile, calibration data was used to calculate the coefficients using the AMLE method, which can eliminate the influence of censored data as much as possible. Data censoring of values below laboratory detection limit is common in measurements of constituent concentrations, which, in this study, is generally specified using a less-than sign (<) as the first character. The performance of models was measured using R^2. Finally, monthly, seasonal, and annual loads were estimated using these models. Features of estimated seasonal loads are discussed in the following sections.

5.4.1 Large loads of TN, TP and SS at site Yishikarikakou-bashi

Site Yishikarikakou-bashi had the highest loads of TN, TP, and SS, both in monthly and seasonal loads (**Table 5.4**, **Figure 5.3- Figure 5.5**), because this site is located in the lower reaches of the Ishikari River and has the highest average discharge, which is the primary driver of constituent delivery to coastal waters. Constituents from the upper, middle and lower reaches of the mainstream and the Uryū and Yūbari Tributaries move together and are discharged at Site Yishikarikakou-bashi.

5.4.2 Decreasing trends of TN, TP, and SS loads

Decreasing trends in loads of TN, TP, and SS can been seen in **Figure 5.3** (most notably SS decreased after 2001), which support results reported by Luo et al., (2011). Many researchers have shown that land use has a strong impact on water quality, and

significant correlations exist between water quality parameters and land use types (Tu, 2011; Woli et al., 2004). In Hokkaido, urbanization has been increasing, resulting in increasing populations in the Ishikari River basin. **Figure 5.6** shows that the population of the Ishikari River basin has increased from 32.2% of Hokkaido's population in 1920 to 55.5% of Hokkaido's population in 2005. The effects of urbanization include greater frequency and severity of flooding, channel erosion, and destruction of aquatic habitat (Klein, 2007), all of which have increased pressure on the Ishikari River.

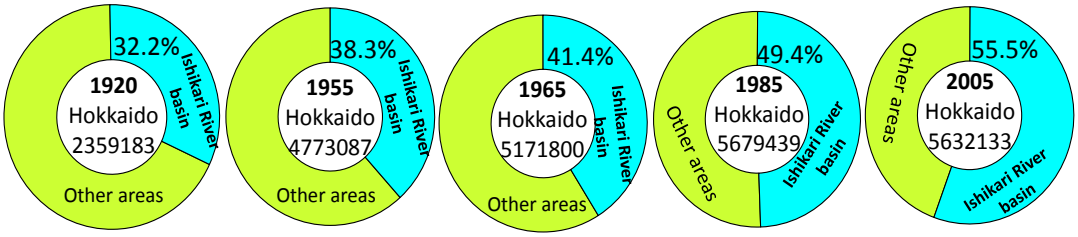

Figure 5.6 Increasing trend of people that live in the Ishikari River basin

Figure 5.7 Changes of coverage rate and length of sewer system in Sapporo (Data from http://www.city.sapporo.jp/kurashi/suido_gesui/index.html).

However, numerous water management measures have been implemented in Japan to prevent deterioration of water quality. First of all, many policies and laws have been enacted to reduce and mitigate pollution, especially since 2000, leading to a comprehensive policy framework concerning water pollution control (Fujikura, 2011). In the 1990s, “Basic Environment Law” was enacted to set environmental quality standards for water quality. “Drinking Water Sources Law”, “Laws Concerning Special Measures for Conservation of Drinking Water Sources” and “Law on Livestock Excreta Management and Recycling” were enacted to keep water sources from being polluted. In the 2000s, “Law Concerning Special Measures against Dioxins” and “Soil Contamination Countermeasures Law” were enacted to prevent pollution caused by hazardous substances (Fujikura, 2011; Kataoka, 2011). Some important international conventions concerning the prevention of water pollution including the “Convention on the Prevention and of Marine Pollution by Dumping of Wastes and other Matter”, “International Convention for the Prevention of Pollution from Ships”, and “International Convention for the Control and Management of Ships' Ballast and Sediments” were also enforced to protect water quality.

In addition, water infrastructures including sewer system have been extended along with urbanization in Japan. As can be seen in **Figure 5.7**, coverage rate (99.97%) and length (8139.7 km) of sewer systems in Sapporo city (the highest population density in the Ishikari River basin) have increased, counteracting pollution associated with increasing wastewater discharge. Improvements in industrial water treatment and distribution of sewage systems and “Joukasou” (a Japanese system for household wastewater treatment) have also contributed to reducing increasing flows of wastewater (Luo et al., 2011). In general, improvements in policies and laws in combination with improvements in water infrastructures have led to decreasing trends in loads of TN, TP, and SS in recent years.

5.4.3 Large loads of TN, TP, and SS in spring

Nitrogen and phosphorus in river systems are derived mainly from atmospheric deposition (mainly nitrogen), erosive runoff, agricultural fertilizer, animal manure from

livestock production, and point sources from domestic and industrial waste-water (Johnes and Heathwaite, 1998; LARRY, 1995; Zhang et al., 2010). Watershed SS sources can be separated into sediment originating in upland regions, sediment from urban areas, and sediment eroded from stream-channels (Langland et al., 2003). Moreover, land use and changes in land use are also important factors influencing erosion and sediment yields. Water quality in rivers constantly changes in response to rainfall in the watershed, and increased sediment and nutrient loads in rivers often occur during periods of high flow (Hubbard et al., 2011).

Hokkaido experiences four distinct seasons. Snowmelt is the main source of river water, with snowmelt generally occurring in April and the Ishikari River experiences large seasonal discharges associated with the spring snowmelt. **Figure 5.8** shows changes in monthly discharge at site Yishikarikakou-bashi, indicating that the highest discharge occurred in April and May. Higher spring stream flows are likely the primary driver of increased springtime loads of TN, TP, and SS in the Ishikari River.

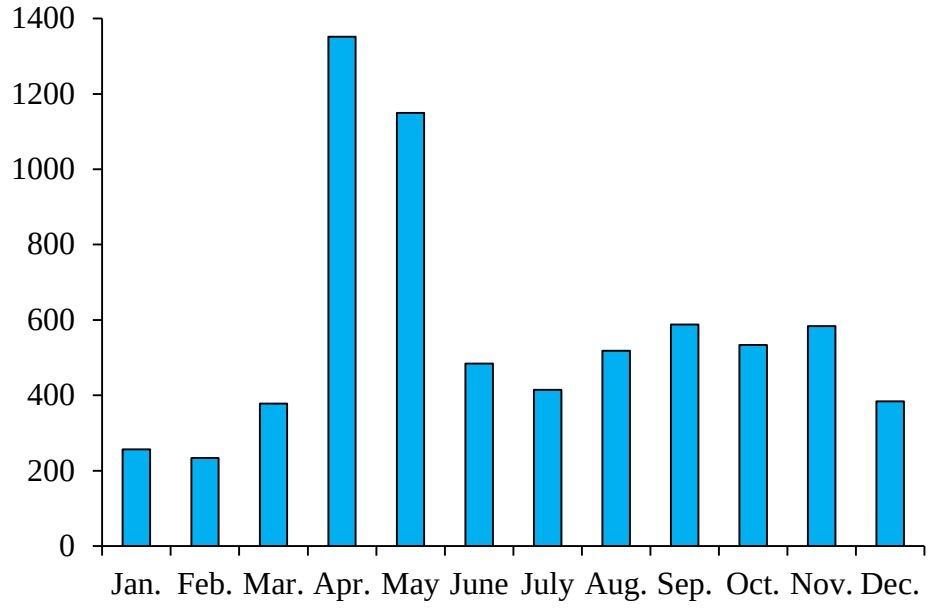

Figure 5.8 Estimated discharge (m^3/s), by month, at site Yishikarikakou-bashi on the Ishikari River, January 1985 through December 2010.

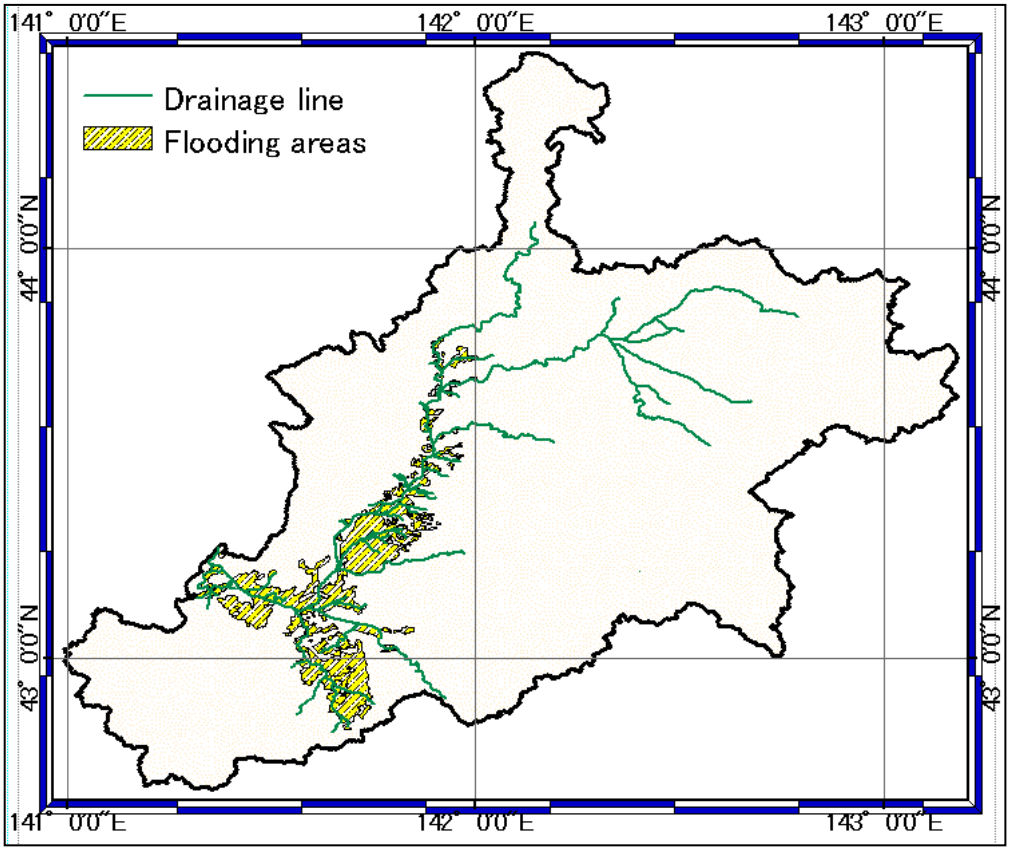

Figure 5.9 Flooding areas in the Ishikari River basin.

5.4.4 Increased loads of TN, TP, and SS post-floods

Besides physical injury, illness and loss of life, floods have significant impacts on the environment, contributing to soil erosion and damage to vegetation as well as impacts on water quality and ecosystem health in general (Buffam et al., 2008; Ko et al., 2010). Through correlation analysis, we found that estimated loads of TN, TP, and SS were relatively high after floods. Floods tend to occur in the middle and lower reaches of the Ishikari River (**Figure 5.9**) meaning that sites such as Yishikarikakou-bashi and Yiwamizawa-oohashi reflect the sudden change in water quality after floods.

A series of unprecedented thunderstorms that began on Aug. 24th, 1988, hit the Ishikari river basin for four days, rapidly sparking devastating flooding of an area of more than 6,500 ha. These floods delivered enormous sediment loads to the Ishikari River (5.27×10^7 kg/day and 1.11×10^7 kg/day at Yishikarikakou-bashi and Yiwamizawa-oohashi,

respectively), eclipsing all daily loads for the rest of the year. From Sep. 8^{th} to 12^{th}, a powerful typhoon (typhoon 15 of 2001) swept close to Japan, bringing strong winds and heavy rain, triggering a large flood in the Ishikari River basin and large SS loads to the Ishikari River. Enhanced loading was captured by measurements at Yishikarikakou-bashi and Yiwamizawa-oohashi in Sep. 2001, with loads of up to 9.25×10^7 kg/day and 1.87×10^7 kg/day, respectively. Also, a series of heavy rains battered Hokkaido in July and August 2010, causing many floods and high estimates of TN, TP, and SS at Yishikarikakou-bashi, the values of which were 4.30×10^3 kg/day, 3.10×10^3 kg/day and 5.49×10^6 kg/day, respectively.

The R^2 and the parameter (*b*) values at Yishikarikakou-bashi and Yiwamizawa-oohashi were relatively high (**Table 5.3**), revealing that the increasing of sediment and nutrient loads commonly driven by increasing water discharge after floods and extreme storms. All of above consequences are in accordance with the R^2 value for the best-fit regression models for loads of TN, TP, and SS, which can be reflected by the parameter (*b*) of water discharge (*Q*), indicating the water discharge is a good predictor of TN, SS, and TP load.

5.5 Conclusions

The Maintenance of Variance-Extension type 3 (MOVE. 3) and the regression model Load Estimator (LOADEST) were used to develop regression equations and to estimate loads of total nitrogen (TN), total phosphorus (TP) and suspended sediment (SS) at five sites on the Ishikari River, Japan, from January 1985 through December 2010, which illustrated how short records of daily waterflow and components concentration can be combined to obtain meaningful estimates of seasonal TN, TP and SS loads. The results show that the best-fit (R^2) regression models for loads of TN, TP, and SS for the five studied sites ranged from 75.36% to 92.37%, suggesting that the model for all three constituents successfully simulated the variability in constituent loads at all sites. The estimated average loads of

TN, TP, and SS, by month, were highly variable at the five sites in the Ishikari River basin, from January 1985 to December 2010. Overall, April had the largest loads, then the estimated average loads decreased, and increased again. The estimated seasonal loads of TN, TP, and SS at the five sites were also highly variable from 1985 to 2010 in the Ishikari River and its tributaries, with the greatest loads occurring in the spring and the smallest loads occurring in the winter, reflecting fluctuations in discharge as a result of the combined effects of seasonal runoff patterns, the exact timing of which vary from year to year. Site Yishikarikakou-bashi is located in the lower reaches of the Ishikari River with the highest average discharge, and therefore had the highest loads of TN, TP, and SS, both in monthly and seasonal loads.

5.6 References

Armour, J.D., Hateley, L.R. and Pitt, G.L., 2009. Catchment modelling of sediment, nitrogen and phosphorus nutrient loads with SedNet/ANNEX in the Tully‐Murray basin. Marine and Freshwater Research, 60(11): 1091-1096.

Brouwer, R. and De Blois, C., 2008. Integrated modelling of risk and uncertainty underlying the cost and effectiveness of water quality measures. Environmental Modelling and Software, 23(7): 922-937.

Bu, H., Meng, W. and Zhang, Y., 2011. Nitrogen pollution and source identification in the Haicheng River basin in Northeast China. Science of the Total Environment, 409(18): 3394-3402.

Buffam, I., Laudon, H., Seibert, J., Mörth, C.M. and Bishop, K., 2008. Spatial heterogeneity of the spring flood acid pulse in a boreal stream network. Science of the Total Environment, 407(1): 708-722.

Carpenter, S.R. et al., 1998. Nonpoint pollution of surface waters with phosphorus and nitrogen. Ecological Applications, 8(3): 559-568.

Chen, D., Dahlgren, R.A., Shen, Y. and Lu, J., 2012. A Bayesian approach for calculating

variable total maximum daily loads and uncertainty assessment. Science of the Total Environment, 430: 59-67.

Christensen, V.G., Jian, X., Ziegler, A.C. and Demonstration, E.B.G.R., 2000. Regression analysis and real-time water-quality monitoring to estimate constituent concentrations, loads, and yields in the Little Arkansas River, south-central Kansas, 1995-99. US Department of the Interior, US Geological Survey.

Conley, D.J., Markager, S., Andersen, J., Ellermann, T. and Svendsen, L.M., 2002. Coastal eutrophication and the Danish national aquatic monitoring and assessment program. Estuaries and Coasts, 25(4): 848-861.

Erturk, A. et al., 2010. Water quality assessment and meta model development in Melen watershed – Turkey. Journal of Environmental Management, 91(7): 1526-1545.

Ferguson, R.I., 1986. River loads underestimated by rating curves. Water Resources Research, 22(1): 74-76.

Ferrer, J., Pérez-Martín, M.A., Jiménez, S., Estrela, T. and Andreu, J., 2012. GIS-based models for water quantity and quality assessment in the Júcar River Basin, Spain, including climate change effects. Science of the Total Environment, 440: 42-59.

Fujikura, M., 2011. Japan's efforts against the illegal dumping of industrial waste. Environmental Policy and Governance, 21(5): 325-337.

Fujikura, R., 2011. Environmental Policy in Japan: Progress and Challenges after the Era of Industrial Pollution. Environmental Policy and Governance, 21(5): 303-308.

Gilbert, R.O., 1987. Statistical methods for environmental pollution monitoring. Wiley.

Gilliom, R.J., Alley, W.M. and Gurtz, M.E., 1995. Design of National Water-Quality Assessment Program. United States Government Print. Office.

Gruber, N. and Galloway, J.N., 2008. An Earth-system perspective of the global nitrogen cycle. Nature, 451(7176): 293-296.

Helsel, D.R. and Hirsch, R.M., 1992. Statistical methods in water resources, 49. Elsevier Science, 510 pp.

Hirsch, R.M., 1982. A comparison of four streamflow record extension techniques. Water

Resources Research, 18(4): 1081-1088.

Hoque, Y.M., Tripathi, S., Hantush, M.M. and Govindaraju, R.S., 2012. Watershed reliability, resilience and vulnerability analysis under uncertainty using water quality data. Journal of Environmental Management, 109: 101-112.

Hubbard, L., Kolpin, D.W., Kalkhoff, S.J. and Robertson, D.M., 2011. Nutrient and sediment concentrations and corresponding loads during the historic June 2008 flooding in eastern Iowa. Journal of Environmental Quality, 40(1): 166-175.

Hurley, M.A., Currie, J.E., Gough, J. and Butterwick, C., 1996. A framework for the analysis of harmonised monitoring scheme data for England and Wales. Environmetrics, 7(4): 379-390.

Johnes, P.J., 2007. Uncertainties in annual riverine phosphorus load estimation: impact of load estimation methodology, sampling frequency, baseflow index and catchment population density. Journal of Hydrology, 332(1): 241-258.

Johnes, P.J. and Heathwaite, A.L., 1998. Modelling the impact of land use change on water quality in agricultural catchments. Hydrological Processes, 11(3): 269-286.

Kataoka, Y., 2011. Water Quality Management in Japan: Recent Developments and Challenges for Integration. Environmental Policy and Governance, 21(5): 338-350.

Klein, R.D., 2007. Urbanization and Stream Quality Impairment. Journal of the American Water Resources Association, 15(4): 948-963.

Ko, C.H. et al., 2010. Impact of flood damage on pollutant removal efficiencies of a subtropical urban constructed wetland. Science of the Total Environment, 408(20): 4328-4333.

Kronvang, B. et al., 2005. Nutrient pressures and ecological responses to nutrient loading reductions in Danish streams, lakes and coastal waters. Journal of Hydrology, 304(1): 274-288.

Kulasova, A., Smith, P.J., Beven, K.J., Blazkova, S.D. and Hlavacek, J., 2012. A method of computing uncertain nitrogen and phosphorus loads in a small stream from an agricultural catchment using continuous monitoring data. Journal of Hydrology, 458-

459: 1-8.

Langland, M.J. et al., 2003. A summary report of sediment processes in Chesapeake Bay and watershed. U.S. Geological Survey, 109 pp.

Larry, J.P., 1995. Identifying the major sources of nutrient water pollution. Environmental Science and Technology, 29(9): 408-414.

Lautz, L.K. and Siegel, D.I., 2006. Modeling surface and ground water mixing in the hyporheic zone using MODFLOW and MT3D. Advances in Water Resources, 29(11): 1618-1633.

Legates, D.R. and McCabe Jr, G.J., 1999. Evaluating the use of "goodness-of-fit" measures in hydrologic and hydroclimatic model validation. Water Resources Research, 35(1): 233-241.

Li, S. et al., 2009. Spatio-temporal dynamics of nutrients in the upper Han River basin, China. Journal of Hazardous Materials, 162(2): 1340-1346.

Li, S., Li, J. and Zhang, Q., 2011. Water quality assessment in the rivers along the water conveyance system of the Middle Route of the South to North Water Transfer Project (China) using multivariate statistical techniques and receptor modeling. Journal of Hazardous Materials, 195: 306–317.

Luo, P. et al., 2011. Spatiotemporal trend analysis of recent river water quality conditions in Japan. Journal of Environmental Monitoring, 13(10): 2819-2829.

Ma, X., Li, Y., Zhang, M., Zheng, F. and Du, S., 2011. Assessment and analysis of non-point source nitrogen and phosphorus loads in the Three Gorges Reservoir Area of Hubei Province, China. Science of the Total Environment, 412-413: 154–161.

Mas-Pla, J. et al., 2012. Development of a stream–aquifer numerical flow model to assess river water management under water scarcity in a Mediterranean basin. Science of the Total Environment, 440: 204–218.

Medellín-Azuara, J., Lund, J.R. and Howitt, R.E., 2007. Water supply analysis for restoring the Colorado River Delta, Mexico. Journal of Water Resources Planning and Management, 133(5): 462-471.

Morvan, X. et al., 2008. Soil monitoring in Europe: a review of existing systems and requirements for harmonisation. Science of The Total Environment, 391(1): 1-12.

Nielsen, J.P., 1999. Record extension and streamflow statistics for the Pleasant River, Maine. U.S. Geological Survey.

Novak, J.M., Szogi, A.A., Stone, K.C., Watts, D.W. and Johnson, M.H., 2007. Dissolved Phosphorus Export from an Animal Waste Impacted In-Stream Wetland. Journal of Environmental Quality, 36(3): 790-800.

Rajagopalan, B. et al., 2009. Water supply risk on the Colorado River: Can management mitigate? Water Resources Research, 45(8): W08201.

Reckhow, K.H., 1994. Water quality simulation modeling and uncertainty analysis for risk assessment and decision making. Ecological Modelling, 72(1): 1-20.

Rosen, M.R. and Lapham, W.W., 2008. Introduction to the US Geological Survey National Water-Quality Assessment (NAWQA) of ground-water quality trends and comparison to other national programs. Journal of Environmental Quality, 37(5_Supplement): S-190.

Runkel, R.L., Crawford, C.G., Cohn, T.A. and US, G.S., 2004. Load Estimator (LOADEST): A FORTRAN program for estimating constituent loads in streams and rivers. U.S. Geological Survey.

Sakamoto, Y., Ishiguro, M. and Kitagawa, G., 1986. Akaike information criterion statistics. Dordrecht, The Netherlands: D. Reidel.

Shrestha, S., Kazama, F. and Newham, L., 2008. A framework for estimating pollutant export coefficients from long-term in-stream water quality monitoring data. Environmental Modelling and Software, 23(2): 182-194.

Shumway, R.H., Azari, R.S. and Kayhanian, M., 2002. Statistical approaches to estimating mean water quality concentrations with detection limits. Environmental Science and Technology, 36(15): 3345-3353.

Smith, V.H., 1982. The nitrogen and phosphorus dependence of algal biomass in lakes: An empirical and theoretical analysis. Limnology and Oceanography, 27(6): 1101-1112.

Sprague, L.A. and Lorenz, D.L., 2009. Regional Nutrient Trends in Streams and Rivers of the United States, 1993− 2003. Environmental Science and Technology, 43(10): 3430-3435.

Terrio, P.J., 2007. Concentrations, Fluxes, and Yields of Nitrogen, Phosphorus, and Suspended Sediment in the Illinois River Basin, 1996-2000..

Tu, J., 2011. Spatial and temporal relationships between water quality and land use in northern Georgia, USA. Journal of Integrative Environmental Sciences, 8(3): 151-170.

Turner, R.E., Baustian, J.J., Swenson, E.M. and Spicer, J.S., 2006. Wetland sedimentation from hurricanes Katrina and Rita. Science, 314(5798): 449-452.

Usutani, T. and Nakatsugawa, M., 2006. Quantitative Analysis of Hydrologic Cycle in Cold Snowy Basin, pp. 45-52.

Vogel, R.M. and Stedinger, J.R., 1985. Minimum variance streamflow record augmentation procedures. Water Resources Research, 21(5): 715-723.

Webb, B.W. et al., 1997. Load estimation methodologies for British rivers and their relevance to the LOIS RACS (R) programme. Science of the Total Environment, 194: 379-389.

Woli, K.P., Nagumo, T., Kuramochi, K. and Hatano, R., 2004. Evaluating river water quality through land use analysis and N budget approaches in livestock farming areas. Science of the Total Environment, 329(1): 61-74.

Zhang, Q.L., Chen, Y.X., Jilani, G., Shamsi, I.H. and Yu, Q.G., 2010. Model AVSWAT apropos of simulating non-point source pollution in Taihu lake basin. Journal of Hazardous Materials, 174(1): 824-830.

Zhang, X., Srinivasan, R., Arnold, J., Izaurralde, R.C. and Bosch, D., 2011. Simultaneous calibration of surface flow and baseflow simulations: a revisit of the SWAT model calibration framework. Hydrological Processes, 25(14): 2313-2320.

Chapter 6 Modeling Suspended Sediment Sources and Transport in the Ishikari River Basin

6.1 Introduction

Suspended sediment (SS) is ubiquitous in aquatic ecosystems and contributes to bottom material composition, water-column turbidity, and chemical constituent transport. However, excessive sedimentation, which can impact material fluxes, aquatic geochemistry, water quality, channel morphology, and aquatic habitats through physical, biological, and chemical processes, is a common and growing problem in rivers, lakes and coastal estuaries (Dedkov and Mozzherin, 1992; Ishida et al., 2010; Meade et al., 1985). In the U.S., for example, approximately 25% of stream length (167,092 miles) has been negatively impacted by excessive sediment loads (U. S. Environmental Protection Agency USEPA, 2006).

Sediment is the largest water pollutant by volume and excessive sediment can have dramatic impacts on both water quality and aquatic biota (Bilotta and Brazier, 2008). High turbidity can significantly reduce or limit light penetration into water with implications for primary production and for populations of fish and aquatic plants. In addition, excessive sedimentation can bring more pollutants containing organic matter, animal or industrial wastes, nutrients, and toxic chemicals because sediment comes mainly from forestlands, agricultural fields, highway runoff, construction sites, and mining operations (Le et al., 2010; Srinivasa et al., 2010), which always cause water quality deterioration and therefore directly or indirectly impair aquatic systems. Eutrophication due to nutrient pollution, for example, is a widespread sediment-related problem recognized at sites world-wide (Conley

* *Part of this chapter has been published in* ***Advanced Materials Research***, 518: 3007-3010, 2012. *Part of this chapter has been submitted into* ***Science of the Total Environment***, 2014.

et al., 2009).

Sediment accumulation can reduce the transport capacity of roadsides ditches, streams, rivers, and navigation channels and the storage capabilities of reservoirs and lakes, which cause more frequent flooding. Dams, including the Three Gorges Project (TGP) on the Yangtze River in China, will gradually lose their water storage capacity as sediment accumulates behind the dam (Fang et al., 2011). Erosion of river banks and increased sedimentation are also impacting the Johnstone River catchment (Hunter and Walton, 2008) and the estuary in the Tuross River catchment of coastal southeast Australia (Drewry et al., 2009) in clogging of land and road drainage systems and river systems. As SS are fundamental to aquatic environments and impairments due to enhanced sediment loads are increasingly damaging water quality and water resources infrastructure, it is extremely important to develop both monitoring systems and technologies to track and to reduce the volume of SS in order to safeguard freshwater systems.

Sediment sources can be separated into sediment originating in upland regions, sediment from urban areas, and sediment eroded from channel corridors (Langland et al., 2003). Land use impacts are commonly seen as resulting in increased sediment loads and therefore as an inadvertent consequence of human activity. Moreover, land use and land use change are also important factors influencing erosion and sediment yields. For example, urbanization may ultimately result in decreased local surface erosion rates when large areas are covered with impervious surfaces such as roadways, rooftops, and parking lots (Wolman, 1967); because of the increased exposure of the soil surface to erosive forces as a result of the removal of the native vegetative cover, agricultural lands can drastically accelerate erosion rates (Lal, 2001). In addition, stream channel erosion can be a major source of sediment yield from urbanizing areas (Trimble, 1997).

Computer based modeling is an essential exercise both for organizing and understanding the complex data associated with water quality conditions and for development of management strategies and decision support tools for water resource managers (Somura et al., 2012). To date, a variety of hydrologic and water-quality models

have been used to describe and explore contaminant sources and transport over various spatial scales (e.g., HSPF (Jeon et al., 2011; Johanson et al., 1980), ANSWERS (Beasley et al., 1978), SWAT (Kirsch et al., 2002; Liew et al., 2012), and ANN (Rajaee et al., 2011)). Recent applications of the GIS-based watershed model SPARROW (SPAtially Referenced Regression On Watershed attributes) (Smith et al., 1997) in the United States have advanced understanding of nutrient sources and transport in large regions such as the Mississippi River Basin (Alexander et al., 2000; 2007) and smaller watersheds such as those draining to the North Carolina coast (McMahon et al., 2003).

In the Japanese context, high suspended sediment loads is increasingly recognized as an important problem for watershed management (Mizugaki et al., 2008; Somura et al., 2012). For example, the Ishikari River basin has long been plagued by high suspended sediment loads, generally causing high turbidity along the river, including in Sapporo, Hokkaido's economic and government center. The pervasiveness of the problem has generated several sediment management studies in the Ishikari River basin. Asahi et al. (2003) found that it is necessary to consider tributary effects directly and that sediment discharged from tributaries contributes to the output sediment discharged from the river's mouth. Wongsa and Shimizu (2004) indicated land-use change has a significant effect on soil eroded from hill slopes, but no significant effect on flooding for Ishikari basin. Ahn et al., (2009) concluded that sedimentation rate increased in the Ishikari River floodplain because of agricultural development on the floodplains. However, detailed accounting of sediment sources (e.g. the type of land-use) and transport in the Ishikari River basin remains poorly understood.

In this study, we therefore use the SPARROW principle and framework to develop a regional-scale sediment transport model for the Ishikari River basin in Hokkaido, Japan. The concrete objectives are (1) to calibrate SS SPARROW for Ishikari River basin on the basis of 31 stations; (2) to use the calibrated model to estimate mean annual SS conditions; and (3) to quantify the relative contribution of different SS sources to instream SS loads. These efforts are undertaken with the ultimate goal of providing information and tools that

will help resource managers identify priority sources of pollution and mitigate this pollution in order to safeguard water resources and protect aquatic ecosystems.

6.2 Materials and methods

6.2.1 Study area

The Ishikari River, the third longest river in Japan (**Figure 6.1**), originates from Mt. Ishikaridake (elevation 1967 m) in the Taisetsu Mountains of central Hokkaido, passes through the west of Hokkaido, and flows into the Sea of Japan, with a total discharge of around 14.8 cubic kilometres per year. The river has the largest river basin with total drainage area of 14,330 km^2, the north-south and east-west distance of which is about 170 and 200 km, respectively. The Ishikari plain occupies most of the basin's area, which is surrounded by rolling hills and is the lowest land in Japan (the highest elevation is less than 50 m) and consequently the best farming region in the country. The Ishikari River basin has cold snowy winters and warm, non-humid summers. The average August temperature ranges from 17 to 22 °C, while the average January temperature ranges from −12 to −4 °C. Mean annual precipitation was 850-1300 mm from 1980 to 2011 (Duan et al., 2014).

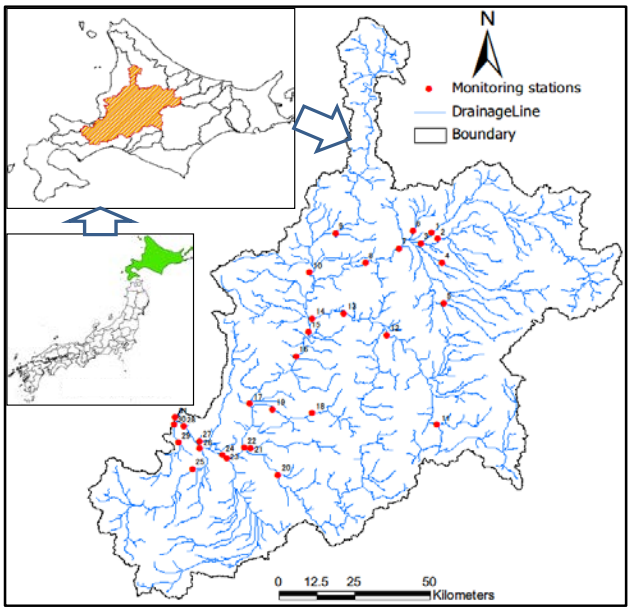

Figure 6.1 Study area, stream networks, and monitoring stations for the Ishikari River basin

6.2.2 Modeling Tools

Based on the mechanistic mass transport components including surface-water flow paths (channel time of travel, reservoirs), non-conservative transport processes (i.e., first-order in-stream and reservoir decay), and mass-balance constraints on model inputs (sources), losses (terrestrial and aquatic losses/storage), and outputs (riverine nutrient export), the SPARROW modeling approach performs a nonlinear least-squares multiple regression to describe the relation between spatially referenced watershed and channel characteristics (predictors) and in-stream load (response) (Schwarz and US, 2006). This allows nutrient supply and attenuation to be tracked during water transport through streams and reservoirs and assesses the natural processes that attenuate constituents as there they are transported from land and upstream (Preston et al., 2009). **Figure 6.2** gives a graphical description of the SPARROW model components. Monitoring station flux estimation refers to the estimates of long-term flux used as the response variable in the model. Flux estimates at monitoring stations are derived from station-specific models that relate contaminant concentrations from individual water-quality samples to continuous records of streamflow time series. To obtain reliable unbiased estimates, the Maintenance of Variance-Extension type 3 (MOVE. 3) and the regression model Load Estimator (LOADEST) were applied to develop regression equations and to estimate monitoring station flux ((for calculation details see Duan et al., (2013)).

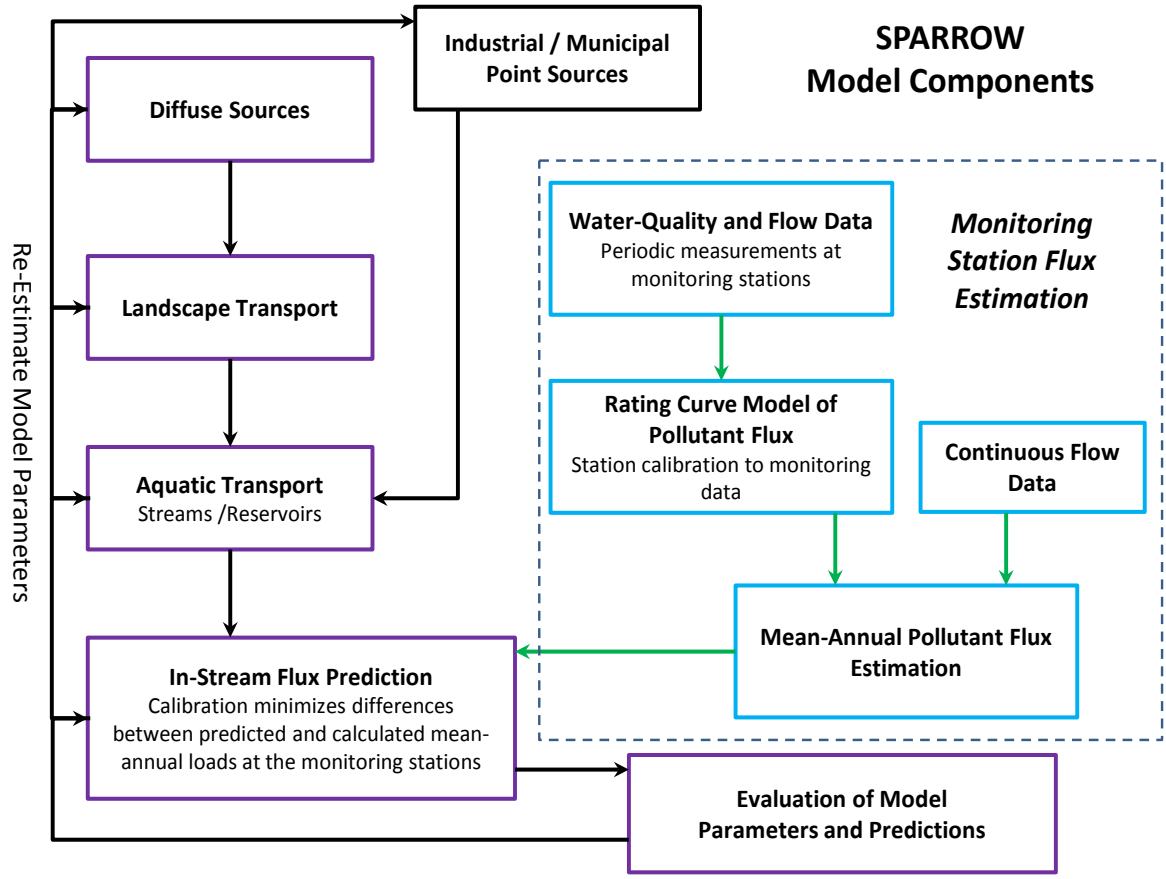

Figure 6.2 Schematic of the major SPARROW model components (from Schwarz and US, 2006)

SPARROW modeling can generally be defined by the following equation (Alexander et al., 2007):

$$F_i^* = \left[\left(\sum_{j\in J(i)} F_j'\right) A\left(Z_i^S, Z_i^R; \theta_S, \theta_R\right) + \left(\sum_{n=1}^{N_S} S_{n,i}\, \alpha_n D_n\left(Z_i^D; \theta_D\right)\right) A'\left(Z_i^S, Z_i^R; \theta_S, \theta_R\right)\right] \varepsilon_i \quad (6.1)$$

where F_i^* is the model-estimated flux for contaminant leaving reach i. The first summation term represents the sediment flux that leaves upstream reaches and is delivered downstream to reach i, where F_j' denotes measured sediment flux (F_j^M) when upstream reach j is monitored and equals the given model-estimated flux (F_j^*) when it is not. $A(\cdot)$ is the stream delivery function representing sediment loss processes acting on flux as it travels along the reach pathway, which defines the fraction of sediment flux entering reach

i at the upstream node that is delivered to the reach's downstream node. Z^S and Z^R represent the function of measured stream and reservoir characteristics, respectively, and θ_S and θ_R are their corresponding coefficient vectors. The second summation term denotes the amount of sediment flux introduced to the stream network at reach i, which is composed of the flux originating from specific sediment sources, indexed by $n = 1,2,\dots,N_S$. Each source has a source variable, denoted S_n, and its corresponding source-specific coefficient, α_n. This coefficient retains the units that convert the source variable units to flux units. The function $D_n(\cdot)$ represents the land-to-water delivery factor. The land-to-water delivery factor is a source-specific function of a vector of delivery variables, denoted by Z_i^θ , and an associated vector of coefficients θ_D. The function $A'(\cdot)$ represents the fraction of flux originating in and delivered to reach i that is transported to the reach's downstream node and is similar in form to the stream delivery factor defined in the first summation term of the equation. If reach i is classified as a stream (as opposed to a reservoir reach), the sediment introduced to the reach from its incremental drainage area receives the square root of the reach's full in-stream delivery. This assumption is consistent with the notion that contaminants are introduced to the reach network at the midpoint of reach i and thus are subjected to only half of the reach's time of travel. Alternatively, for reaches classified as reservoirs, we assume that the sediment mass receives the full attenuation defined for the reach. The multiplicative error term in equation (6.1), ε_i, is applicable in cases where reach i is a monitored reach; the error is assumed to be independent and identically distributed across independent sub-basins in the intervening drainage between stream monitoring stations.

Sediment loss in streams is modeled according to a first-order decay process (Chapra, 1997; Brakebill, et al., 2010) in which the fraction of the sediment mass originating from the upstream node and transported along reach i to its downstream node is estimated as a continuous function of the mean water time of travel (T_i^S; units of time) and mean water depth, D_i, in reach i, such that

$$A\left(Z_i^S, Z_i^R; \theta_S, \theta_R\right) = \exp\left(-\theta_S \frac{T_i^S}{D_i}\right) \quad (6.2)$$

where θ_S is an estimated mass-transfer flux-rate coefficient in units of length time^{-1}. The rate coefficient is independent of the properties of the water volume that are proportional to water volume, such as streamflow and depth (3). The rate can be re-expressed as a reaction rate coefficient (time^{-1}) that is dependent on water-column depth by dividing by the mean water depth.

Sediment loss in lakes and reservoirs is modeled according to a first-order process (Chapra, 1997; Brakebill, et al., 2010) in which the fraction of the sediment mass originating from the upstream reach node and transported through the reservoir segment of reach i to its downstream node is estimated as a function of the reciprocal of the areal hydraulic load $(q_i^R)^{-1}$ (units of time length^{-1}) for the reservoir associated with reach i and an apparent settling velocity coefficient (θ_R; units of length time^{-1}), such that

$$A\left(Z_i^S, Z_i^R; \theta_S, \theta_R\right) = \frac{1}{1+\theta_R\left(q_i^R\right)^{-1}} \quad (6.3)$$

The areal hydraulic load is estimated as the quotient of the outflow discharge to the surface area of the impoundment.

6.2.3 Input data

In this study, input data for building SPARROW models is classified into (**Table 6.1**): 1) stream network data to define stream reaches and catchments of the study area; 2) loading data for many monitoring stations within the model boundaries (dependent variables); 3) sediment sources data describing all of the sources of the sediment being modeled (independent variables); and 4) data describing the environmental setting of the area being modeled that causes statistically significant variability in the land- to- water delivery of sediment (independent variables). Input data types are described in more detail below.

Table 6.1 Summary of input data and calibration parameters. References to data sources are in the main text

Category	Input data	Data source
The stream network	Stream network, stream lengths, sub-catchment boundaries, sub-catchment areas	Automated catchment delineation based on a 50 m DEM, with modification flow diversions
Stream load data	Monitoring station,	Thirty one stations from the National Land with Water Information monitoring network from 1982 to 2010
Sediment source data	Developing land, forest land, agricultural land, and water land	Land use from the Ministry of Land, Infrastructure, Transport and Tourism, Japan, 2006
Environmental Setting Data	Mean annual precipitation	The 20-year (1990-2010) average from Japanese Meteorological Agency
	Catchment slope	Mean value of local slope, obtained from 50 m DEM
	Soil texture, soil permeability	Obtained from the 1:5.000.000-scale FAO/UNESCO Soil Map of the World and the National and Regional Planning Bureau, Japan
	Reservoir (dams) loss	The Japan Dam Foundation (http://damnet.or.jp/)

6.2.3.1 The stream network

The hydrologic network used for the SPARROW model of the Ishikari River basin is derived from a 50 m digital elevation model (DEM) (**Figure 6.1**), which has 900 stream reaches, each with an associated sub-basin. The stream network mainly contains stream reach and sub-basin characteristics such as stream length, direction of water flow, reservoir characteristics like surface area, and local and total drainage area. For example, the areas

of sub-basin range from 0.009 to 117 km^2 with a median of 15.9 km^2. However, mean water flow is not reported for each stream reach, suggesting that we cannot calculate the SS concentration at the stream reach scale but can calculate the total yield SS for each associated sub-basin.

6.2.3.2 Stream load data

Suspended sediment concentration and daily flow data are collected to calculate the long-term (from 1985 to 2010) mean SS flux at every monitoring station. Thirty-one monitoring stations were chosen for model calibration in this study (**Figure 6.1**). SS concentration and daily flow data were collected at each site for the period from 1985 to 2010 by the National Land with Water Information (http://www1.river.go.jp/) monitoring network (**Figure 6.3**). However, some streamflow gaging stations have short periods of record or missing flow values but do not over 10% of the time periods that reflect gaps in long-term monitoring. A streamflow record extension method called the Maintenance of Variance-Extension type 3 (MOVE.3) (Vogel and Stedinger, 1985) is employed to estimate missing flow values or to extend the record at a short-record station on the basis of daily streamflow values recorded at nearby, hydrologically similar index stations. On this basis, the FORTRAN Load Estimator (LOADEST), which uses time-series streamflow data and constituent concentrations to calibrate a regression model that describes constituent loads in terms of various functions of streamflow and time, is applied to estimate SS loads. The output regression model equations take the following general form (Runkel et al., 2004):

$$\ln(L_i) = a + b\ln Q + c\ln Q^2 + d\sin(2\pi dtime) + e\cos(2\pi dtime) + f dtime + g dtime^2 + \varepsilon \quad (6.4)$$

where L_i is the calculated load for sample i; Q is stream discharge; $dtime$ is time, in decimal years from the beginning of the calibration period; ε is error; and a, b, c, d, e, f, g are the fitted parameters in the multiple regression model. The number of parameter maybe

is different at different stations, so the regression model is different at different stations. After determining the model, the SS load can be easy calculated (for details please see Duan et al., 2013).

Then, the mean annual load is normalized to the 2006 base year at the 31 monitoring stations to address the problem of incompatibility in periods of record by using normalizing or detrending methods. The 2006 base year was selected to coincide with the most recently available explanatory geospatial data. The method can be defined by the following equation ((Schwarz et al., 2006) :

$$X^*(t) = X(t) - (h(t) - h(T_0)) \tag{6.5}$$

where $X(t)$ is the original series, the term $h(t) - h(T_0)$ is the adjustment function and the constant $h(T_0)$ is the constant that causes the adjustment to equal zero for the base year, T_0.

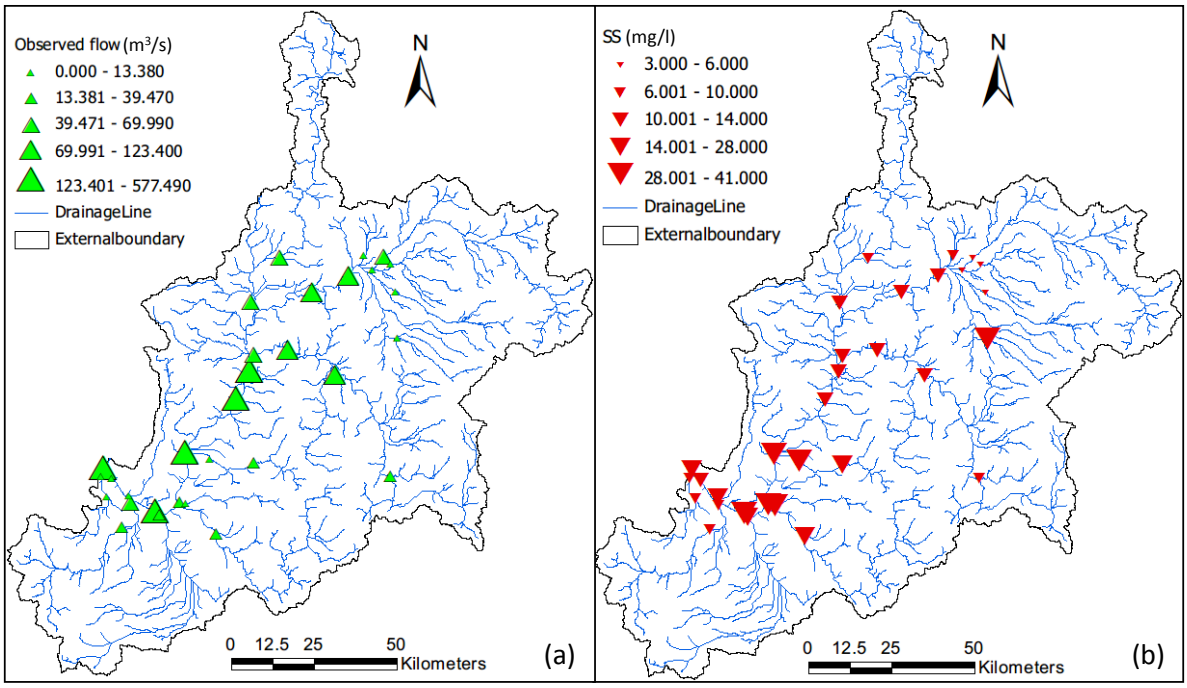

Figure 6.3 Schematic showing (a) the observed water flows (m3/s) and (b) the observed SS concentration (mg/l) at 31 monitoring stations

6.2.3.3 Sediment source data

SS source variables tested in the Ishikari SPARROW model include estimates of developing lands, forest lands, agricultural lands, and stream channels. Estimates of land use were developed using data derived from the Policy Bureau of the Ministry of Land, Infrastructure, Transport and Tourism, Japan, 2006, which mainly contains 11 types of land use (Figure 6.4). It was then merged into 4 types: developing land, forest land, agricultural land, and water land. Finally, different lands are allocated to individual sub-basin using GIS zonal processes. Arc Hydro Tools is employed to get reach length which denotes the streambed source.

6.2.3.4 Environmental Setting Data

Climatic and landscape characteristics considered candidates for SS-transport predictors include climate, topography and soil (Asselman et al., 2003; Dedkov and Mozzherin, 1992). Here, slope, soil permeability, and precipitation are used to evaluate the influences of “land-to-water” delivery terms. Basin slope is obtained using the GIS surface tool (see **Figure 6.5 (a)**). Soil permeability and clay content (see **Figure 6.5 (b)**) are estimated using data derived from the 1:5.000.000-scale FAO/UNESCO Soil Map of the World (FAO, 1988) and the National and Regional Planning Bureau, Japan. Mean annual precipitation data, representing the 20-year (1990-2010) average, were obtained from daily precipitation data at 161 weather stations in Hokkaido from 1990 to 2010; that is, we first calculated the mean annual precipitation over the Hokkaido on the basis of 161 stations, and then clipped the mean annual precipitation distribution for the Ishikari River basin. All these watershed-average values were used to calculate estimates for each sub-basin in the Ishikari model area using the ZONALMEAN and ZONALSTATISTICAL functions of GIS.

Reach-loss and reservoir-loss are used as the mediating factors affecting the mobilization of sediment from the stream network. Reach-loss variable is nonzero only for stream reaches, and is defined for two separate classes, shallow-flowing (small) streams

versus deep-flowing (large) streams. Since stream depth is not known, assume streams with drainage area < 200 km^2 are shallow, small streams. Reservoir-loss is denoted by areal hydraulic load of the reservoir, which is computed as the quotient of mean annual impoundment outflow and surface area (Hoos and McMahon, 2009).

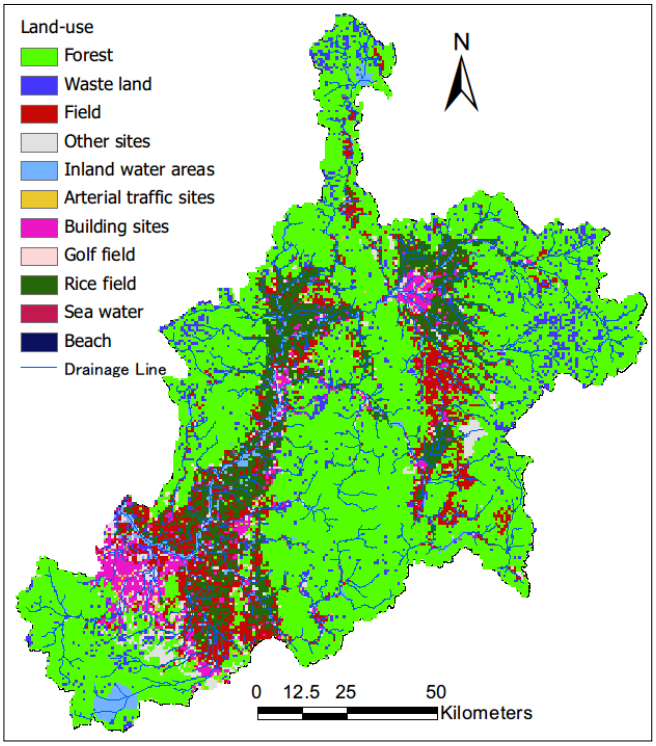

Figure 6.4 Land use of the Ishikari River basin, 2006

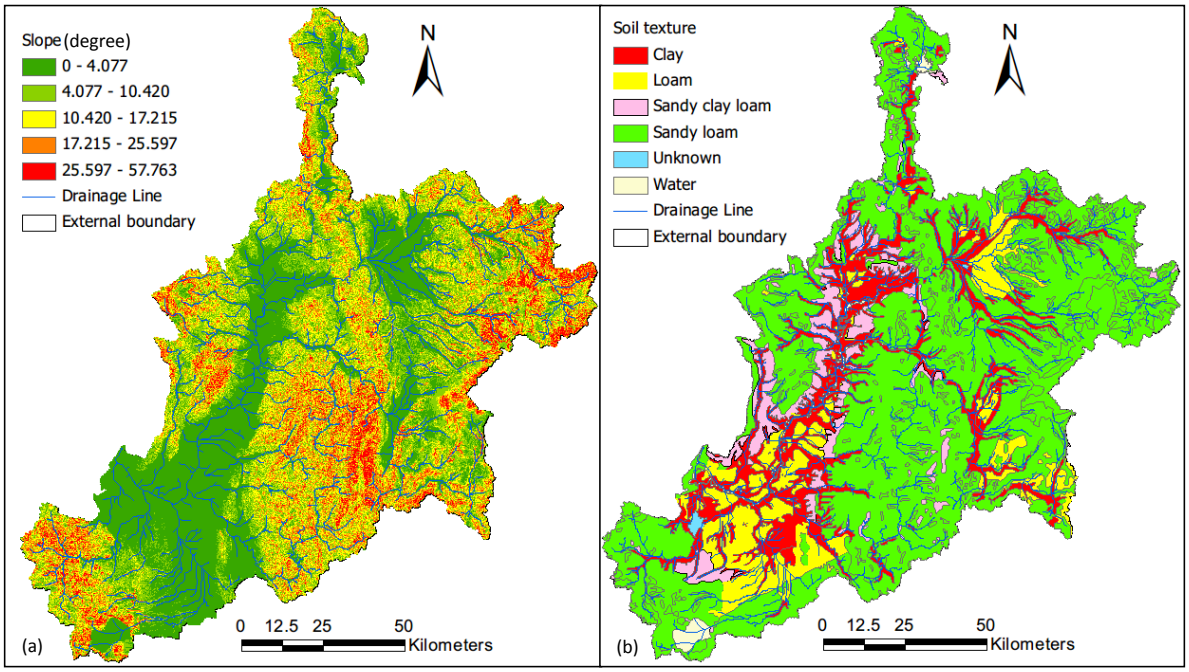

Figure 6.5 Schematic showing the slope (a) and soil texture (b) in Ishikari river basin

6.2.4 Model calibration and application

The final SPARROW model was statistically calibrated using estimates of mean annual SS flux at 31 monitoring stations (see Input data). The explanatory variables represented statistically significant or otherwise important geospatial variables. The statistical significance (alpha=0.05) of the coefficients for each of the SS source terms (which were constrained to be positive) were determined by using a one-sided t-test, and the significance of the coefficients for each of the land- to- water delivery terms (which were allowed to be positive or negative, reflecting either enhanced or attenuated delivery, respectively) and the variables representing SS loss in free-flowing streams and impoundments was determined by using a two-sided t-test (Schwarz et al., 2006). The yield R-squared (R^2), the root mean squared error (RMSE), and the residuals for spatial patterns were the conventional statistical diagnostics used to assess the overall SPARROW model accuracy and performance.

According to the equations of SPARROW, the calibrated model can be used to identify the largest local SS sources; that is, the sediment source contributing the most to the incremental SS yield for each catchment in Ishikari River basin can be calculated. In addition, the models can be used to estimate the contribution from each sediment source to the total SS loads predicted for each reach. Total load was the predicted load contributed from all upstream landscape sediment sources. Finally, the factors that affect mean annual transport in the Ishikari River basin can be identified.

6.3 Results and discussions

6.3.1 Model calibration

Model calibration results for the log transforms of the summed quantities in equation (6.1) and non-linear least-squares estimates are presented in **Table 6.2**, which explains approximately 95.96% (R^2) of the spatial variation in the natural logarithm of mean annual

SS flux (kg/yr), with a mean square error (MSE) of 0.323, suggesting that the SS predicted by the model closely matches the observation load.

The plot of predicted and observed SS flux is shown in **Figure 6.6**, demonstrating model accuracy over a wide range of predicted flux and stream sizes. Generally, for a good SPARROW model, the graphed points should exhibit an even spread about the one-to-one line (the straight line in **Figure 6.6**) with no outliers. However, a common pattern expressed in Figure 6.6 for final SPARROW SS model is the tendency for larger scatter among observations with smaller predicted flux- a pattern of heteroscedasticity. One likely cause for this pattern is greater error in the measurement of flux in small sub-basin due to greater variability in flow or to greater relative inhomogeneity of sediment sources within small sub-basin (Schwarz, 2006). Appropriate assignment of weights reflecting the relative measurement error in each observation (plus an additional common model error) can improve the coefficient estimates and correct the inference of coefficient error if the heteroscedasticity is caused by measurement error. On the other hand, the observations can be weighted to improve the coefficient estimates and correct their estimates of error if the heteroscedasticity is due to structural features of the SPARROW model. **Figure 6.7** shows the standardized residuals at the 31 monitoring sites. Monitoring sites with over-predictions (< 0) mainly exist in the middle area of the Ishikari River basin, and under-predictions (> 0) exist in the upper and lower area. Studentized Residual is quite useful for identifying outliers and it greater than 3.6 are generally considered outliers and warrant further investigation (Schwarz, 2006). Overall, the final model does not show evidence of large prediction biases over the monitoring sites.

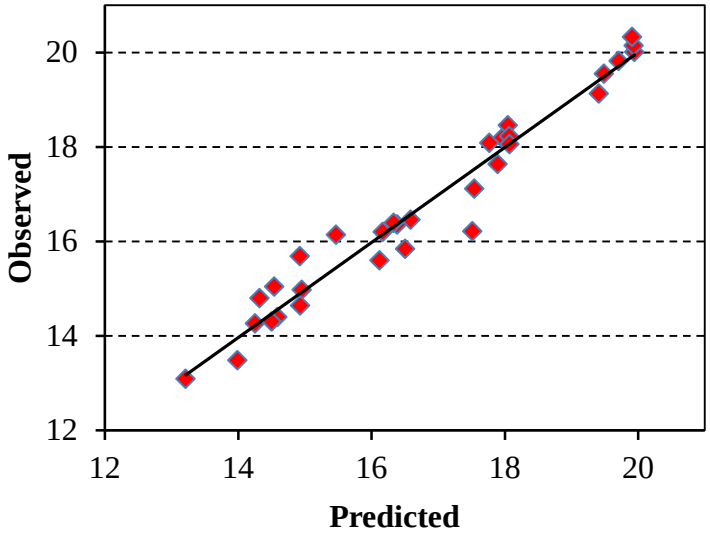

Figure 6.6 Observed and predicted SS flux (kg/yr) at 31 monitoring sites included in the Ishikari SPARROW model (Natural logarithm transformation applied to observed and predicted values)

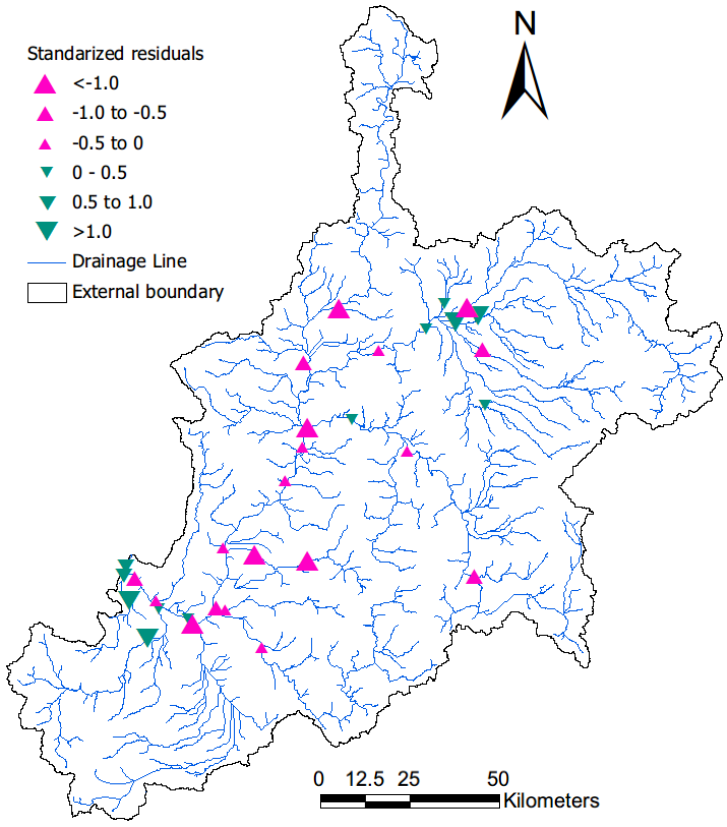

Figure 6.7 Model residuals for 31 monitoring stations used to calibrate the final Ishikari SPARROW model

Table 6.2 SPARROW estimates of model statistics for Ishikari River basin SS

Model parameters	Coefficient units	Estimated coefficient	Standard error	P-value
SS sources				
Developing land	$kg/km^2/yr$	1006.267	586.547	0.021
Forest land	$kg/ km^2/yr$	75.554	123.79	0.011
Agricultural land	$kg/ km^2/yr$	234.211	16.868	0.036
Streambed (stream channels)	kg/km/yr	123.327	89.537	0.148
Land-to-water loss coefficient				
Slope	-	0.349	0.094	0.001
Soil permeability	hr/cm	-9.195	2.431	0.001
Precipitation	mm	0.007	0.001	0.002
In-stream loss rate				
Small stream (drainage area ≤200 km^2)	day^{-1}	-0.044	0.023	<0.001
Big stream (drainage area >200 km^2)	day^{-1}	0.000012	0.0068	0.069
Reservoir-loss	m/yr	26.283	4.364	<0.001
Model diagnostics				
Mean square error	0.323			
Number of observations	31			
R-squared	0.9596			

Notes: SPARROW, SPAtially Referenced Regression on Watershed; Kg, kilograms; km, kilometers; yr, year; <, less than. This table shows overall model calibration results, statistical parameter estimates, standard errors, and probability levels for modeled explanatory variables representing sediment sources, landscape factors affecting the delivery of sediment from uplands to streams (land-to-water), and in-stream and reservoir storage. All sources and storage terms are constrained to nonnegative estimates for more physically realistic simulations of sediment transport. Because of this specification, statistical significance for source and aquatic storage coefficient estimates are reported as a one-sided p statistic. Probability levels for land-to-water parameters are two-sided values (Schwarz et al., 2006).

With the exception of stream channels, all of the source variables modeled are statistically significant (P-value <0.05) and indicate mean levels of sediment supply (**Table 6.2**). The largest intrinsic sediment yield is associated with developing land, the estimated value of which is around 1006.267 kg/km^2/yr. Land developing including removing cover, developing cuts and fills can clearly increase potential erosion and sediment hazards on-site by changing water conveyance routes, soil compaction (both planned and unplanned), longer slopes and more and faster stormwater runoff. With the analysis of factors affecting sediment transport from uplands to streams (mean basin slope, reservoirs, physiography, and soil permeability), developing lands was also the largest sediment source reported in Brakebill et al., (2010) and Schwarz (2008). Agricultural land has the second highest sediment yield with an estimated value of around 234.211 kg/km^2/yr and forest land has the lowest sediment yield with an estimated value of around 75.554 kg/km^2/yr.

Land-to-water delivery for sediment land sources is powerfully mediated by watershed slope, soil permeability, and rainfall, all of which are statistically significant (**Table 6.2**). As expected, **Table 6.1** shows that sediment produced from land transport to rivers is most efficient in areas with greater basin slope, less permeable soils, and greater rainfall, which is consistent with the results calculated by Brakebill et al., (2010). The alteration of these factors can directly and indirectly cause changes in sediment degradation and deposition, and, finally, to the sediment yield (Luce and Black, 1999; Nelson and Booth, 2002). Increased rainfall amounts and intensities can directly increase surface runoff, leading to greater rates of soil erosion (Nearing et al., 2005; Ran et al., 2012) with consequences for productivity of farmland (Julien and Simons, 1985). Watershed slope and soil permeability have a powerful influence on potential surface runoff as they affect the magnitude and rate of eroded sediment that may be transported to streams (Brakebill et al., 2010).

The coefficient for in-stream loss indicates that sediment is removed from large streams (about 0.000012 day^{-1}) and accumulates in small streams (about 0.044 day^{-1}). These results run contrary to several published examples. For example, Schwarz (2008)

argued that greater streamflow causes an increase in the amount of sediment generated from stream channels. The reasons for these results could be the criterion of the two kinds of streams. In this study, streams with drainage area < 200 km^2 are shallow, small streams, which tend to create the sediments; on the contrary, streams with drainage area > 200 km^2 are big streams, which tend to attenuate the sediments. Sediment storage is statistically significant in reservoirs (dams), the estimated value of which is around 26.283 m/yr. This value is much less than a coefficient of 234.92 m/yr reported for the Chesapeake Bay Watershed SPARROW model (Brakebill et al., 2010), one reason of which maybe is the SPARROW estimate is lower than expected for similar particle sizes. And the value is similar to 36 m/yr computed by the conterminous U.S. SPARROW model (Schwarz, 2008).

6.3.2 Model application

Because data from sampling stream networks suffers from sparseness of monitoring stations, spatial bias and basin heterogeneity, describing regional distributions and exploring transport mechanism of sediment is one of the challenges of sediment assessment programs. Through the stream networks, SPARROW can link in-stream water quality to spatially referenced information on contaminant sources and other watershed attributes relevant to contaminant transport (Smith et al., 1997). After calibration, the SPARROW model of total suspended sediment can be applied to evaluate the stream-corridor sediment supply, storage, and transport properties and processes in a regional context, which can inform a variety of decisions relevant to resource managers. Here, we predict and analyze the spatial distribution of total sediment yields and incremental yields. Also, sediment generated from each source is described in each incremental basin in order to further explore and manage sediment sources.

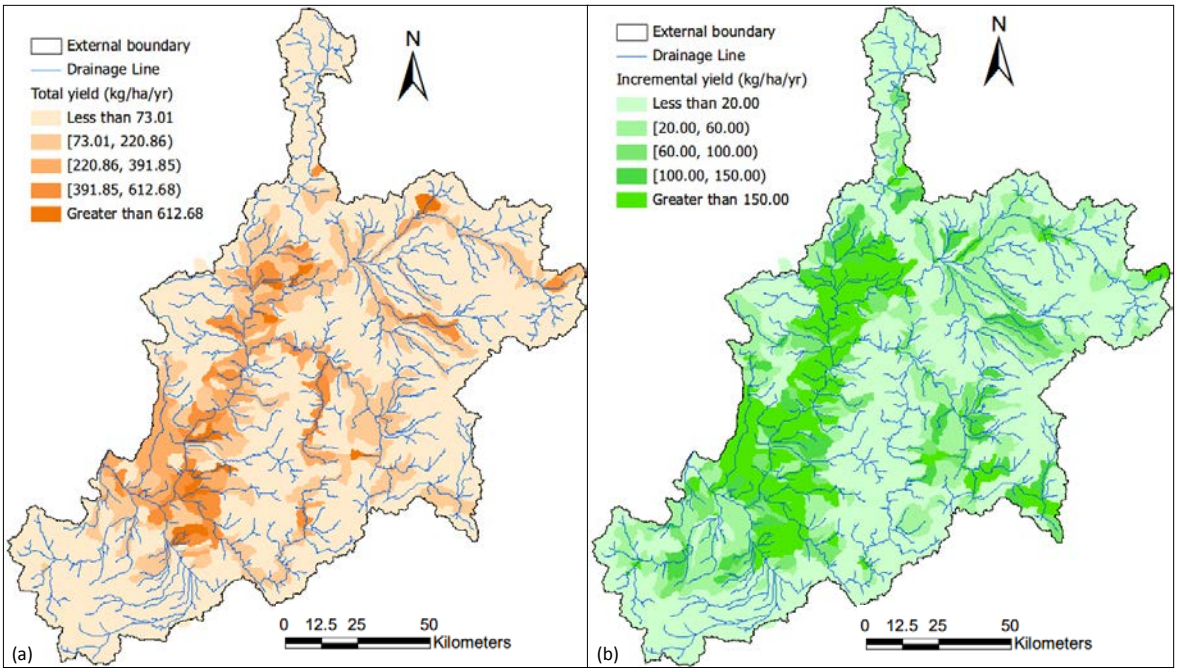

Figure 6.8 Map showing the spatial distribution of total suspended sediment yields (a) and incremental suspended sediment yields (b) estimated by SPARROW.

Total yield (load per area) represents the amount of sediment including upstream load contributed to each stream reach and incremental yields represent the amount of sediment generated locally independent of upstream supply, and contributed to each stream reach, normalized by the local catchment area (Ruddy et al., 2006). **Figure 6.8 (a)** shows the spatial distribution of total yields, describing the sediment mass entering streams per unit area of the incremental drainages of the Ishikari River basin associated with the stream network (**Figure 6.1**). It is mediated by climatic and landscaped characteristics and delivered to the Ishikari gulf of the Sea of Japan after accounting for the cumulative effect of aquatic removal processes. **Figure 6.8 (a)** shows that total yields, ranging from 0.034 to 1190 kg/ha/yr (mean=101 kg/ha/yr), concentrate in the sub-basin along the middle and lower reaches of the Ishikari River. Like total yields, much of the incremental sediment yields are distributed in similar areas (see **Figure 6.8 (b)**), the largest of which is greater than 150 kg/ha/yr. These two kinds of predictions provide localized estimates of sediment that are useful in evaluating local contributions of sediment in addition to identifying

geographic areas of potential water-quality degradation due to excessive sedimentation.

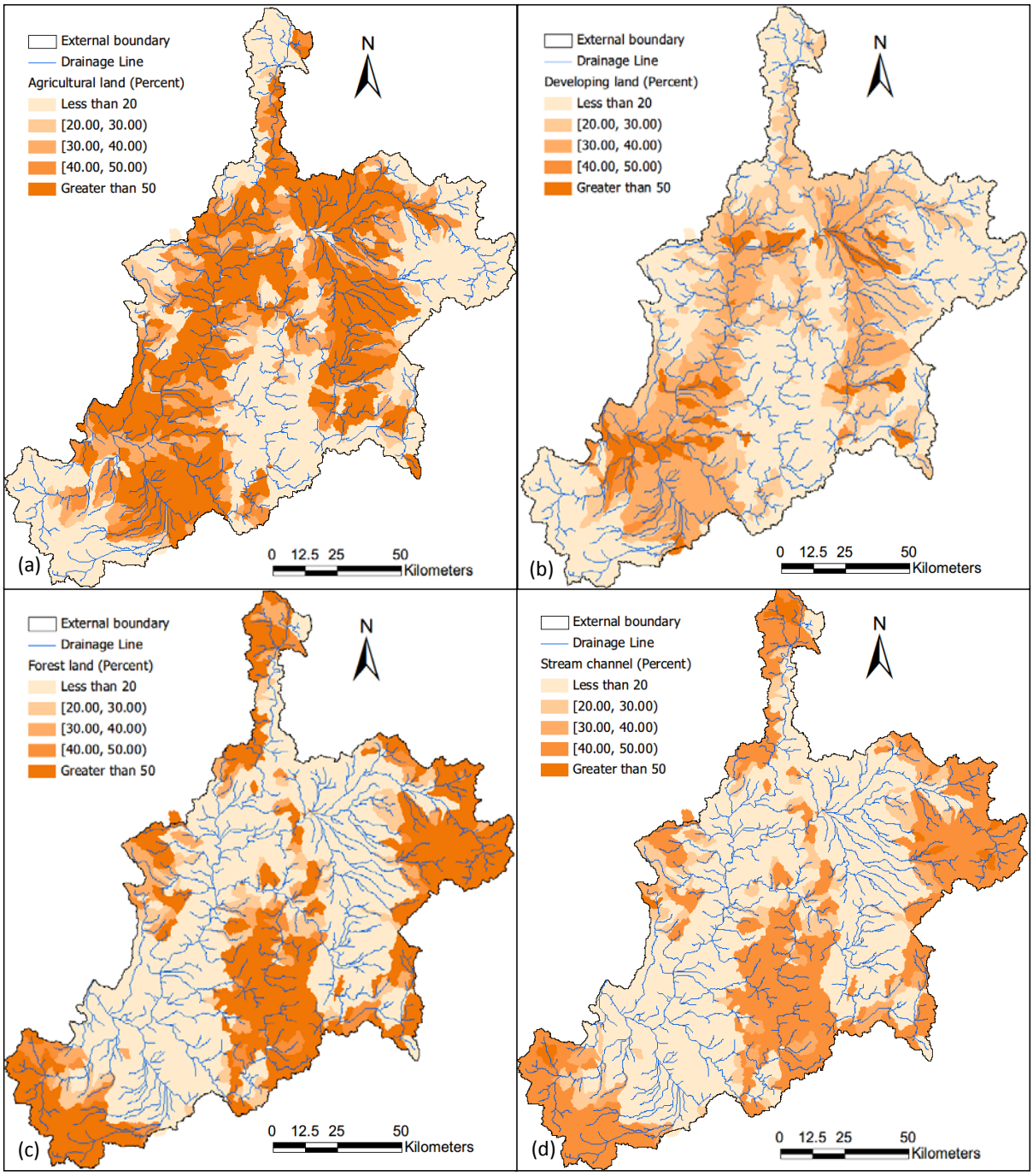

Figure 6.9 Maps showing the spatial distributions of independent sediment sources generated in each incremental catchment for (a) agricultural lands, (b) developing lands, (c) forested lands, and (d) stream channels.

Figure 6.9 shows percent of total incremental flux generated for (a) agricultural lands, (b) developing lands, (c) forested lands, and (d) stream channels, suggesting the relative contributions from the various sources at each sub-basin. The contributions from these sources that go into the sub-basin yield **(Figure 6.8)** are assessed by comparing predicted sub-basin yield with predicted yield from agricultural-land sediment yield (**Figure 6.9 (a)**); predicted developing-land sediment yield (**Figure 6.9(b)**); predicted forest-land sediment yield (**Figure 6.9 (c)**); and predicted steam channels yield (**Figure 6.9(d)**). Generally, the spatial distribution of these contributions from different sources is in accordance with land use (**Figure 6.4**). On average we can see that 35.11% of incremental flux is from agricultural lands (**Figure 6.10**), which is the largest of all sources; the second largest is from forested lands, the value of which is around 23.42%, followed by developing lands (22.91%); the least is from stream channels with a value of 18.56%.

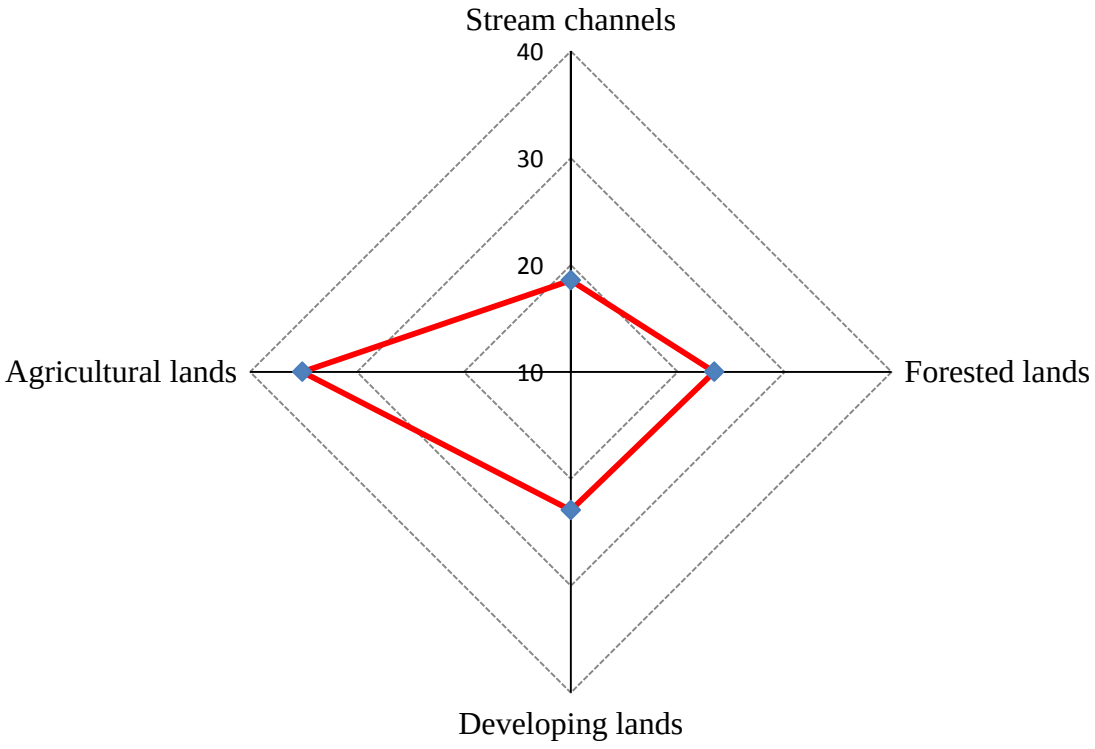

Figure 6.10 The total incremental flux generated for agricultural lands, developing lands, forested lands, and stream channels.

6.4 Conclusions and future work

In this study, we developed a SPARROW-based sediment model for surface waters in the Ishikari River basin, the largest watershed in Hokkaido, Japan. This model is based on stream water-quality monitoring records collected at 31 stations for the period1985 to 2010 and uses four source variables including developing lands, forest lands, agricultural lands, and steam channels, three landscape delivery variables including slope, soil permeability, and precipitation, two in-stream loss coefficients including small stream (drainage area ≤ 200 km^2) and big stream (drainage area > 200 km^2), and reservoir attenuation. Significant conclusions of the calibration procedure and model application are summarized below. Calibration results explain approximately 95.96% of the spatial variation in the natural logarithm of mean annual SS flux (kg/yr) and display relatively small prediction errors on the basis of 31 monitoring stations. Developing-land is associated with the largest intrinsic sediment yield at around 1006.267 kg/km^2/yr, followed by agricultural-land (234.211 kg/km^2/yr). Greater basin slope, less permeable soils, and greater rainfall can directly and indirectly enable sediment transport from land into streams. Reservoir attenuation (26.283 m/yr) is statistically significant, suggesting that reservoirs can play a dramatic role in sediment interception. The percent of total incremental flux generated for agricultural lands, developing lands, forested lands, and stream channels is 35.11%, 23.42%, 22.91% and 18.56%, respectively. Sediment total yields and incremental yields concentrate in the sub-basin along the middle and lower reaches of the Ishikari River, showing which sub-basin is most susceptible to erosion. Combined with land use, management actions should be designed to reduce sedimentation of agricultural lands and developing lands in the sub-basin along the middle and lower reaches of the Ishikari River. Our results suggest several areas for further research, including explicit representation of flow and sediment discharge from each stream and in total to the Sea of Japan, more accurate representation of spatial data in SPARROW, and the design of pollutant reduction strategies for local watersheds.

This study has a number of shortcomings and suggests several areas for future work.

Some important model results lack of statistical significance. For example, statistically insignificant model components and inaccuracies associated with DEM resolution, which contain a source variable (stream channels), and big streams with drainage area >200 km^2. These findings are contrary to the findings of the other researches (Brakebill et al., 2010). In addition, the prediction of the model only indicates mean-annual conditions, not necessarily critical conditions such as low- flow conditions. The reason for these results mainly includes the following points: (1) the hydrologic network was derived from a 50 m digital elevation model (DEM), which is a litter bit different from actual stream network; (2) because of unaware of water discharge in all streams, stream velocity was replaced with drainage area to classify the small stream and big stream; and (3) the calibration data only incorporate monitored-load data from limited number of stations with long-term data.

Excessive sedimentation can have a variety of adverse effects on aquatic ecosystems and water resources infrastructure. Analysis of sediment production and transport mechanisms is therefore necessary to describe and evaluate a basin's water quality conditions in order to provide guidance for development of water quality indicators and pollution prevention measures (Buggy and Tobin, 2008; Meals et al., 2010). As illustrated here, the SPARROW model is a valuable tool that can be used by water-resources managers in water-quality assessment and management activities to support regional management of sediment in large rivers and estuaries.

6.5 References

Alexander, R.B. et al., 2007. Differences in phosphorus and nitrogen delivery to the Gulf of Mexico from the Mississippi River Basin. Environmental Science and Technology, 42(3): 822-830.

Alexander, R.B., Elliott, A.H., Shankar, U. and McBride, G.B., 2002. Estimating the sources and transport of nutrients in the Waikato River Basin, New Zealand. Water Resources Research, 38(12): L1268.

Alexander, R.B., Smith, R.A. and Schwarz, G.E., 2000. Effect of stream channel size on the delivery of nitrogen to the Gulf of Mexico. Nature, 403(6771): 758-761.

Asahi, K., Kato, K. and Shimizu, Y., 2003. Estimation of Sediment Discharge Taking into Account Tributaries to the Ishikari River. Journal of Natural Disaster Science, 25(1): 17-22.

Asselman, N.E.M., Middelkoop, H. and Van Dijk, P.M., 2003. The impact of changes in climate and land use on soil erosion, transport and deposition of suspended sediment in the River Rhine. Hydrological Processes, 17(16): 3225-3244.

Beasley, D.B., Huggins, L.F. and Monke, E.J., 1980. ANSWERS: A model for watershed planning. Transactions of the Asae, 23(4): 938-0944.

Bilotta, G.S. and Brazier, R.E., 2008. Understanding the influence of suspended solids on water quality and aquatic biota. Water Research, 42(12): 2849-2861.

Brakebill, J.W., Ator, S.W. and Schwarz, G.E., 2010. Sources of Suspended‐Sediment Flux in Streams of the Chesapeake Bay Watershed: A Regional Application of the SPARROW Model. Journal of the American Water Resources Association, 46(4): 757-776.

Buggy, C.J. and Tobin, J.M., 2008. Seasonal and spatial distribution of metals in surface sediment of an urban estuary. Environmental Pollution, 155(2): 308-319.

Conley, D.J. et al., 2009. Controlling eutrophication: nitrogen and phosphorus. Science, 323(5917): 1014-1015.

Dedkov, A.P. and Mozzherin, V.I., 1992. Erosion and sediment yield in mountain regions of the world. Erosion, debris flows and environment in mountain regions, 209: 29-36.

Drewry, J.J., Newham, L. and Croke, B., 2009. Suspended sediment, nitrogen and phosphorus concentrations and exports during storm-events to the Tuross estuary, Australia. Journal of Environmental Management, 90(2): 879-887.

Fang, N.F., Shi, Z.H., Li, L. and Jiang, C., 2011. Rainfall, runoff, and suspended sediment delivery relationships in a small agricultural watershed of the Three Gorges area, China. Geomorphology, 135(1-2): 158-166.

FAO-UNESCO-ISRIC, 1988. FAO-UNESCO soil map of the world: revised legend. FAO Rome, Italy.

Hoos, A.B. and McMahon, G., 2009. Spatial analysis of instream nitrogen loads and factors controlling nitrogen delivery to streams in the southeastern United States using spatially referenced regression on watershed attributes (SPARROW) and regional classification frameworks. Hydrological Processes, 23(16): 2275-2294.

Hunter, H.M. and Walton, R.S., 2008. Land-use effects on fluxes of suspended sediment, nitrogen and phosphorus from a river catchment of the Great Barrier Reef, Australia. Journal of Hydrology, 356(1): 131-146.

Ishida, T. et al., 2010. Suspended sediment transport in a river basin estimated by chemical composition analysis. Hydrological Research Letters, 4(0): 55-59.

Jeon, J.H., Lim, K.J., Yoon, C.G. and Engel, B.A., 2011. Multiple segmented reaches per subwatershed modeling approach for improving HSPF-Paddy water quality simulation. Paddy and Water Environment, 9(2): 193-205.

Johanson, R.C., Imhoff, J.C. and Davis, H.H., 1980. Users manual for hydrological simulation program-FORTRAN (HSPF). Environmental Research Laboratory, Office of Research and Development, US Environmental Protection Agency.

Julien, P.Y. and Simons, D.B., 1985. Sediment transport capacity of overland flow. Trans. ASAE, 28(3): 755-762.

Kirsch, K., Kirsch, A. and Arnold, J.G., 2002. Predicting sediment and phosphorus loads in the Rock River basin using SWAT. Transactions of the ASAE, 45(6): 1757-1769.

Lal, R., 2001. Soil degradation by erosion. Land Degradation & Development, 12(6): 519-539.

Langland, M.J. and Cronin, T.M., 2003. A summary report of sediment processes in Chesapeake Bay and watershed. U.S. Geological Survey, 109pp.

Le, C. et al., 2010. Eutrophication of lake waters in China: cost, causes, and control. Environmental Management, 45(4): 662-668.

Liew, M.W.V., Feng, S. and Pathak, T.B., 2012. Climate change impacts on streamflow,

water quality, and best management practices for the Shell and Logan Creek Watersheds in Nebraska, USA. International Journal of Agricultural and Biological Engineering, 5(1): 13-34.

Luce, C.H. and Black, T.A., 1999. Sediment production from forest roads in western Oregon. Water Resources Research, 35(8): 2561-2570.

McMahon, G., Alexander, R.B. and Qian, S., 2003. Support of total maximum daily load programs using spatially referenced regression models. Journal of Water Resources Planning and Management, 129(4): 315-329.

Meade, R.H., Dunne, T., Richey, J.E., Demsantos, U. and Salati, E., 1985. Storage and remobilization of suspended sediment in the lower Amazon River of Brazil. Science, 228(4698): 488.

Meals, D.W., Dressing, S.A. and Davenport, T.E., 2010. Lag time in water quality response to best management practices: A review. Journal of Environmental Quality, 39(1): 85-96.

Mizugaki, S. et al., 2008. Estimation of suspended sediment sources using 137Cs and 210Pbex in unmanaged Japanese cypress plantation watersheds in southern Japan. Hydrological Processes, 22(23): 4519-4531.

Nearing, M.A. et al., 2005. Modeling response of soil erosion and runoff to changes in precipitation and cover. Catena, 61(2): 131-154.

Nelson, E.J. and Booth, D.B., 2002. Sediment sources in an urbanizing, mixed land-use watershed. Journal of Hydrology, 264(1): 51-68.

Preston, S.D. et al., 2009. SPARROW Modeling: Enhancing Understanding of the Nation's Water Quality. U.S. Geological Survey.

Rajaee, T., Nourani, V., Zounemat-Kermani, M. and Kisi, O., 2011. River Suspended Sediment Load Prediction: Application of ANN and Wavelet Conjunction Model. Journal of Hydrologic Engineering, 16(8): 613-627.

Ran, Q., Su, D., Li, P. and He, Z., 2012. Experimental study of the impact of rainfall characteristics on runoff generation and soil erosion. Journal of Hydrology, 424: 99-

111.

Ruddy, B.C., Lorenz, D.L., Mueller, D.K., 2006. County-level estimates of nutrient inputs to the land surface of the conterminous United States, 1982-2001. U.S. Geological Survey.

Runkel, R.L., Crawford, C.G., Cohn, T.A. and US, G.S., 2004. Load Estimator (LOADEST): A FORTRAN program for estimating constituent loads in streams and rivers. USGS Techniques and Methods.

Schwarz, G.E., 2008. A Preliminary SPARROW model of suspended sediment for the conterminous United States, 7 pp.

Schwarz, G.E., et al., 2006. The SPARROW surface water-quality model: Theory, application, and user documentation. USGS Techniques and Methods.

Smith, R.A., Schwarz, G.E. and Alexander, R.B., 1997. Regional interpretation of water-quality monitoring data. Water Resources Research, 33(12): 2781-2798.

Somura, H. et al., 2012. Impact of suspended sediment and nutrient loading from land uses against water quality in the Hii River basin, Japan. Journal of Hydrology, 450-451: 25-35.

Srinivasa G. S., Ramakrishna Reddy, M. and Govil, P.K., 2010. Assessment of heavy metal contamination in soils at Jajmau (Kanpur) and Unnao industrial areas of the Ganga Plain, Uttar Pradesh, India. Journal of Hazardous Materials, 174(1): 113-121.

Trimble, S.W., 1997. Contribution of stream channel erosion to sediment yield from an urbanizing watershed. Science, 278(5342): 1442-1444.

U. S. Environmental Protection Agency (USEPA), 2006. Wadeable streams assessment: a collaborative survey of the nation's streams, 98 pp.

Vogel, R.M. and Stedinger, J.R., 1985. Minimum variance streamflow record augmentation procedures. Water Resources Research, 21(5): 715-723.

Wolman, M.G., 1967. A cycle of sedimentation and erosion in urban river channels. Geografiska Annaler. Series A. Physical Geography: 385-395.

Chapter 7 Impact of Climate Change on the Hydro-climatology of the Upper Ishikari River Basin

7.1 Introduction

The ongoing climate change has significantly affected the spatial and temporal distribution of water resources as well as the intensities and frequencies of extreme hydrological events (Coumou and Rahmstorf, 2012). For example, the distribution of precipitation in space and time is very uneven, leading to tremendous temporal variability in water resources worldwide (Oki and Kanae, 2006). Increases in precipitation in the Northern Hemisphere mid-latitudes, drying in the Northern Hemisphere subtropics and tropics, and moistening in the Southern Hemisphere subtropics and deep tropics were found (Zhang et al., 2007). The rate of evaporation, which depends on factors such as cloudiness, air temperature and wind speed, varies a great deal, significantly affecting the amount of water available to replenish groundwater supplies. The combination of shorter duration but more intense rainfall (meaning more runoff and less infiltration) combined with increased evapotranspiration (the sum of evaporation and plant transpiration from the earth's land surface to atmosphere) and increased irrigation is expected to lead to groundwater depletion (Konikow and Kendy, 2005; Wada et al., 2010). It is therefore necessary to explore and understand the hydrological response of watersheds to climate change for improving the water resource planning and management.

In recent years, outputs (e.g., precipitation, temperature, humidity, and mean sea level pressure) at a global scale from general climate models (GCMs) are popularly downscaled to local-scale hydrologic variables to compute and evaluate hydrological components for

** This chapter is submitted into **Journal of Hydrology**,2014*

water resources variability and risk of hydrologic extremes in the future (Tatsumi et al., 2013; Taye et al., 2011). Meenu et al., (2013) evaluated the impacts of possible future climate change scenarios on the hydrology of the catchment area of the Tunga–Bhadra River, upstream of the Tungabhadra dam using the GCM HadCM3 outputs. Babel et al., (2013) characterized potential hydrological impact of future climate in the Bagmati River Basin, Nepal, and found annual basin precipitation will increase under both A2 and B2 scenarios. Based on outputs from six GCMs (CNRM-CM3, GFDL-CM2.1, INM-CM3.0, IPSL-CM4, MIROC3.2_M and NCAR-PCM) under three emission scenarios (A1B, A2, B1), Li et al., (2012) indicated extreme precipitation events will tend to occur in the southeast and northwest region while extreme temperature events happen in the north and southeast region on the Loess Plateau of China during the 21st century.

Evidence for climate change impacts on the hydro-climatology of Japan is plentiful (Solomon, 2007). The Japan Meteorological Agency (JMA) show that annual average air temperatures nationwide rose by a rate equivalent to 1.15°C per century between 1898 and 2010, which is considerably higher than the global average temperature rise of 0.74°C over the last century (according to the Intergovernmental Panel on Climate Change's "Climate Change 2007: Synthesis Report Summary for Policymakers"); moreover, although no clear trends have been observed, the annual precipitation in Japan varies largely from year to year. All these changes in precipitation and temperature have greatly influenced water supply in Japan. For instance, concerning precipitation, years of low rainfall have become frequent since around 1970, and the amount of precipitation was much below average in 1973, 1978, 1984, 1994, and 1996, when water shortages caused damage. It tremendously affected drinking water supply because approximately 78% of it (actual record in the fiscal year 2004) is taken from rivers, lakes, marshes and so forth. The possibility of frequent occurrence of extremely low rainfall, decrease in snowfall, and earlier thaw will tend to increase the vulnerability of water resources. Meanwhile, extreme rainfall and temperature induced many hydrological disasters including floods, water quality incidents, and so on (Duan et al., 2013; Duan et al., 2014). Therefore, to predict and evaluate the temperature,

precipitation and surface water in japan is also necessary and important in the future.

Based on the GCMs output, lots of efforts at evaluation of hydro-climatology of Japan under climate change have been made. For example, Sato et al., (2013) investigated the impact of climate change on river discharge in several major river basins in Japan through a distributed hydrological simulation using the MRI-AGCM and found winter river discharge is projected to increase more than 200% in February, but decrease approximately 50-60% in May in the Tohoku and Hokuriku regions. In the Agano River basin, the monthly mean discharge for the 2070s was projected to increase by approximately 43% in January and 55% in February, but to decrease by approximately 38% in April and 32% in May (Ma et al., 2010). However, there is less done on small river basins in Hokkaido about the hydro-climatology variations under climate change.

The objective of this study is to investigate the possible effects of climate change on water resources in the Upper Ishikari River basin, Hokkaido, Japan, on the basis of outputs from GCM HadCM3. The paper is organized as follows: The study area, GCM outputs data and methodology including SWAT model and downscaling techniques are briefly described in the next section. The comparison results of temperature, precipitation and waterflow in Section 3, followed by discussions (Section 7.4) and conclusions (Section 7.5). The results of this study offer insights into hydrological response under climate change and provide tools for forecasting future climate conditions.

7.2 Study area, datasets and Methods

7.2.1 Study area

The Upper Ishikari River Basin (UIRB) is a headwater basin of the Ishikari River, which originates from Mt. Ishikaridake (elev. 1967 m) in the Taisetsu Mountains of central Hokkaido and flows southward into the broad Ishikari Plain and finally into the Sea of Japan, and is the third longest river in Japan (**Figure 7.1**).

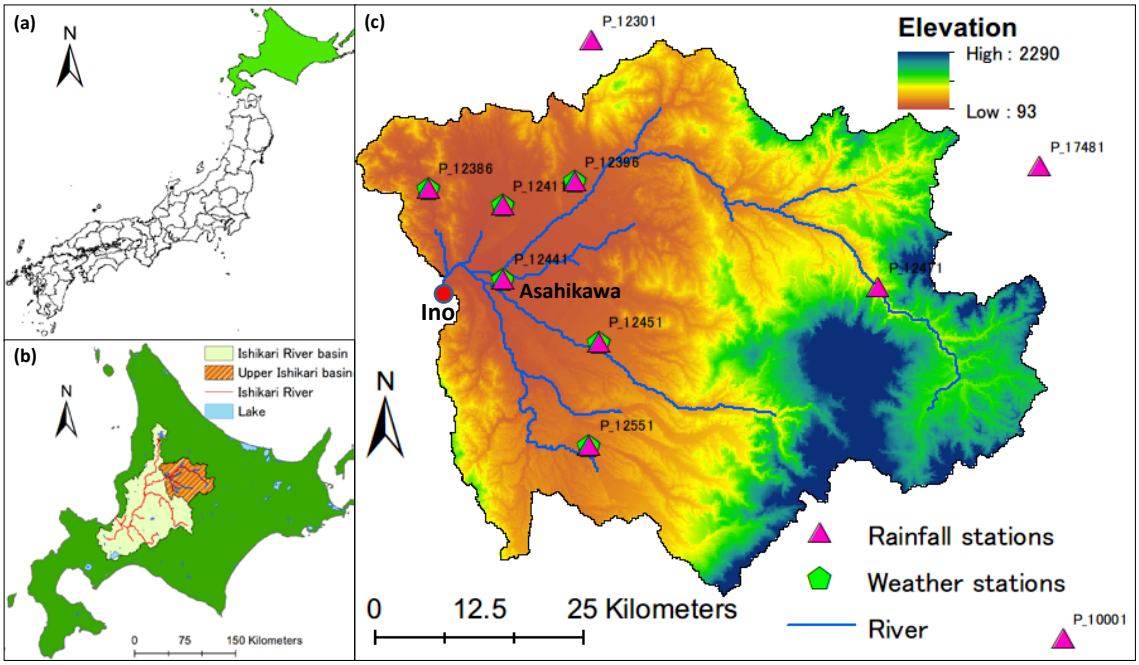

Figure 7.1 The Upper Ishikari River basin with rainfall and weather stations

The UIRB extends from the source of the Ishikari River in the Taisetsu Mountains and to an area of Asahikawa city. This study focused on the watershed area above Ino discharge monitoring station (by the side of the Ishikari River), which is about 3, 450 km^2, approximately a quarter of the Ishikari River Basin. At the Asahikawa weather station (elev. 120 m) from 1981 to 2010, the mean annual, monthly air temperature in the warmest month (August) and the coldest month (January) are 6.9°C, 21.3 °C and -7.5 °C, respectively; the mean annual precipitation is 1042.0 mm.

7.2.2 SWAT model

The Soil and Water Assessment Tool (SWAT) model is a semi-distributed model that can be applied at the river basin scale to simulate the quality and quantity of surface and ground water and predict the environmental impact of land use, land management practices, and climate change (Arnold et al. 1998, Narsimlu et al. 2013). SWAT model uses hydrological response units (HRUs) to describe spatial heterogeneity in terms of land cover, soil type and slope of land surface within a watershed. For each HRUs unit, the

model can estimate relevant hydrological components such as evapotranspiration, surface runoff and peak rate of runoff, groundwater flow and sediments yield. Currently, SWAT is embedded in an ArcGIS interface called ArcSWAT. The SWAT model simulates the hydrological cycle based on the water balance equation

$$SW_t = SW_0 + \sum_{i=1}^{t}(R_{day} - Q_{surf} - E_a - w_{seep} - Q_{gw}) \quad (7.1)$$

in which SW_t is the final soil water content (mm water), SW_0 is the initial soil water content in day i (mm water), t is the time (days), R_{day} is the amount of precipitation in day i (mm water), Q_{surf} is the amount of surface runoff in day i (mm water), E_a is the amount of evapotranspiration in day i (mm water), w_{seep} is the amount of water entering the vadose zone from the soil profile in day i (mm water), and Q_{gw} is the amount of return flow in day i (mm water). More detailed descriptions of the SWAT model principles are given by (Neitsch et al., 2005).

72.2.1 SWAT model Input datasets

Generally, the SWAT model requires the resolution digital elevation model (DEM) data, land use data, soil data, and climate data for calibrating the model. A 100m by 100 m resolution (DEM) data downloaded from the National and Regional Policy Bureau, Japan, was used to delineate the UIRB and to analyze the drainage patterns of the land surface terrain in the ArcSWAT 2012 interface. The stream network characteristics such as channel slope, length, and width and the associated subbasin parameters such as slope gradient and slope length of the terrain were derived from the DEM. Land use is very important factor that affect runoff, evapotranspiration, and surface erosion in a watershed. Soil type is one of the most important factors that significantly affect water transport in the soil because different soil types have different soil textural and physicochemical properties such as soil texture, available water content, hydraulic conductivity, bulk density, and organic carbon content. The land use and soil data were used for the definition of the HRUs. Land use data

were developed using data derived from the Policy Bureau of the Ministry of Land, Infrastructure, Transport and Tourism, Japan, 2006, which mainly contains 11 types of land use. Here, the UIRB has 9 types of land use (**Figure 7.2**). Soil data were extracted from a 1:50,000 soil map of the Fundamental Land Classification Survey developed by the Hokkaido Regional Development Bureau (www.agri.hro.or.jp/chuo/kankyou/soilmap/html/map_index.htm). The daily weather data for precipitation, maximum and minimum temperature, wind speed, solar radiation, and relative humidity were obtained from the records of the rainfall and weather stations (**Figure 7.1**) from 1981 to 2005. The daily river discharge data from 1995 to 2005 at the Inou station were downloaded from the website of the Japanese Ministry of Land, Infrastructure, and Transport (www1.river.go.jp), which were used for model calibration and validation.

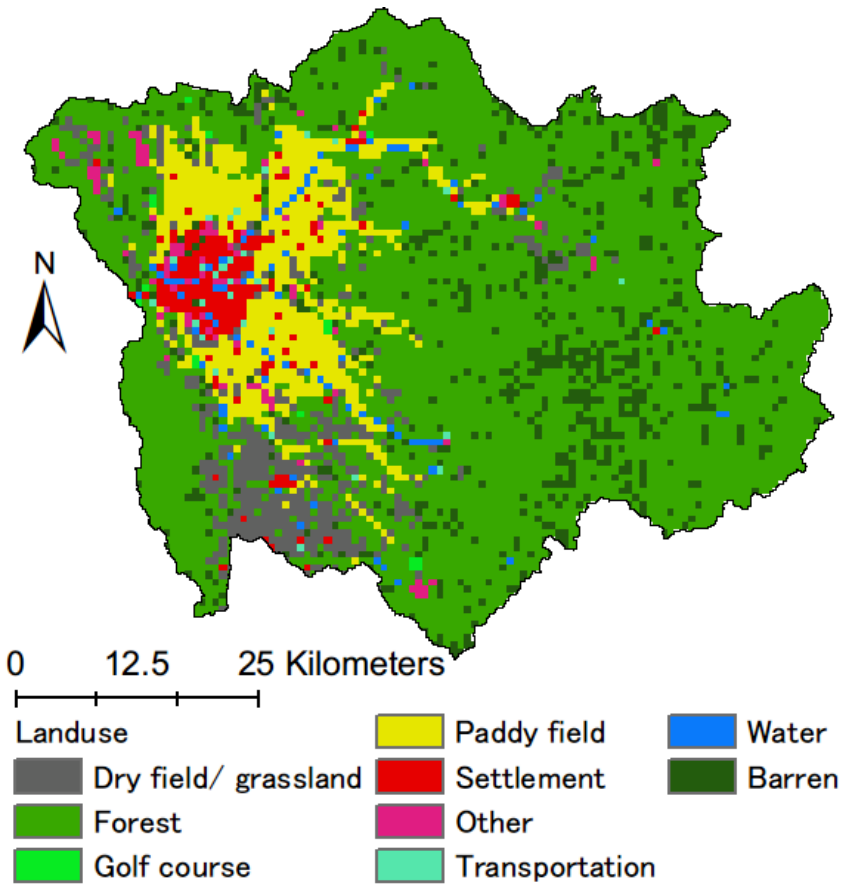

Figure 7.2 Land use data

7.2.2.2 Model setup, calibration

The model application involved six steps: (1) data preparation, (2) watershed and sub-basins discretization, (3) HRU definition, (4) parameter sensitivity analysis, (5) calibration and validation, and (6) uncertainty analysis. The steps for the delineation of watershed and sub-basins include DEM setup, stream definition, outlet and inlet definition, watershed outlets selection, and definition and calculation of sub-basin parameters. Here, the Ino river discharge monitoring station was chose to be the outlet of the UIRB. Then, the resulting sub-basins were divided into HRUs based on the land use, soil and slope combinations.

Sensitivity analysis was performed to delimit the number of parameters which affected the fit between simulated and observed data in the study area. The data for the period 1996-2000 were used for calibration, and data for the period 2001–2005 were used for validation of the model. Five years (1991-1995) were chosen as a warm-up period in which the model was allowed to initialize and then approach reasonable starting values for model state variables. The calibration and uncertainty analysis were done using the sequential uncertainty fitting algorithm (SUFI-2) in SWAT-CUP (Abbaspour et al. 2007).

To assess the performance of model calibration, the coefficient of the determination (R^2) and Nash-Sutcliffe efficiency (NSE) between the observations and the final best simulations are calculated. The former is usually used to evaluate how accurately the model tracks the variation of the observed values. The latter measures the goodness of fit and would approach unity if the simulation is satisfactorily representing the observed data, which describes the explained variance for the observed data over time that is accounted for by the SWAT model (Green and Van 2008). Both of them can be expressed using the following equations respectively.

$$R^2 = \frac{\left[\sum_{i=1}^{n}\left(Q_{i,obs}-\overline{Q_{obs}}\right)*\left(Q_{i,sim}-\overline{Q_{sim}}\right)\right]^2}{\sum_{i=1}^{n}\left(Q_{i,obs}-\overline{Q_{obs}}\right)^2*\sum_{i=1}^{n}\left(Q_{i,sim}-\overline{Q_{sim}}\right)^2} \quad (7.2)$$

$$NSE = 1 - \frac{\sum_{i=1}^{n}(Q_{i,obs} - Q_{i,sim})^2}{\sum_{i=1}^{n}(Q_{i,obs} - \overline{Q_{obs}})^2} \quad (7.3)$$

where $Q_{i,obs}$ is the observed data value at time unit n, $Q_{i,sim}$ is the simulated data value at time unit n, and $n = 1, 2, 3, \ldots\ldots, t$, $\overline{Q_{obs}}$ is the mean observed data for the entire evaluation time period, $\overline{Q_{sim}}$ is the mean model simulated data for the entire evaluation time period. R^2 ranges between 0.0 and 1.0 and higher values mean better performance. NSE indicates how well the plot of observed values versus simulated values fits the 1:1 line and ranges from $-\infty$ to 1 (Nash and Sutcliffe, 1970). Larger NSE values are equivalent with better model performance. Therefore, a few standards were adopted currently for evaluating model performance. For example, Santhi et al., (2001) used the standards of $R^2 > 0.6$ and $NSE > 0.5$ to determine how well the model performed. Chung et al., (2002) used the criteria of $R^2 > 0.5$ and $NSE > 0.3$ to determine if the model result is satifactory. In this study, $R^2 > 0.5$ and $NSE > 0.5$ are chosen as criteria for acceptable SWAT simulation.

7.2.3 GCM data and NCEP predicators

GCMs are the most advanced tools currently available for simulating the response of the global climate system to increasing greenhouse gas concentrations, which can provide global climatic variables under different emission scenarios. Because some researches (He et al., 2011, Tatsumi et al., 2014) indicated that the HadCM3 (Hadley Centre Coupled Model, version 3) GCM was chosen as representative for Japan area, the HadCM3 GCM output was considered suitable for the study watershed.

Large-scale predictor variables information including the National Centers for Environmental Prediction (NCEP_1961-2001) reanalysis data for the calibration and validation, and HadCM3 (Hadley Centre Coupled Model, version 3) GCM (H3A2a_1961-2099 and H3B2a_1961-2099) data for the baseline and climate scenario periods, were downloaded from the Canadian Climate Change Scenarios Network (http://www.cccsn.ec.

gc.ca/). The NCEP reanalysis predictor contains 41 years of daily observed predictor data, derived from the NCEP reanalyses, normalised over the complete 1961-1990 period. These data were interpolated to the same grid as HadCM3 (2.5 latitude x 3.75 longitude) before the normalisation was implemented. The HadCM3 GCM predictor contains 139 years of daily GCM predictor data, derived from the HadCM3 A2 (a) and B2 (a) experiments, normalised over the 1961-1990 period. The predictors of the NCEP and HadCM3 GCM experiments with descriptions are presented in **Table 7.1**.

7.2.4 Downscaling techniques

Because the GCM output data are too coarse in resolution to apply directly for impact assessment in a certain area, so it is necessary to downscale the GCM output data for bridging the spatial and temporal resolution gaps. Generally, downscaling techniques are divided into two main forms. One form is statistical downscaling, where a statistical relationship is established from observations between large scale variables, like atmospheric surface pressure, and a local variable, like the wind speed at a particular site. Then the relationship is subsequently used on the GCM data to obtain the local variables from the GCM output. The other form is dynamical downscaling, which can simulate local conditions in greater detail because the GCM output is used to drive a regional, numerical model in higher spatial resolution. Here, the statistical downscaling method was applied because of its simplicity and less computational time compared to dynamically downscaling (Wilby et al., 2000).

The statistical downscaling contains many methods such as regression methods, weather pattern-based approaches, stochastic weather generators. The Statistical downscaling model (SDSM), which is a hybrid of a stochastic weather generator and a multivariate regression method for generating local meteorological variables at a location of interest (Wilby et al., 2002), was applied to assess the impacts of climate change under future climate scenarios in this study. Based on a combination of multi-linear regressions and a weather generator, the SDSM simulates daily climate data for current and future time

periods by calculating the statistical relationships between predictand and predictor data series.

Table 7.1 Daily predictor variable held in the grid box data archive

Variable	**Description**
temp	Mean temperature at 2 m
mslp	Mean sea level pressure
p500	500 hPa geopotential height
p850	850 hPa geopotentail height
rhum	Near surface relative humidity
r500	Reative humidity at 500 hPa height
r850	Relative humidity at 850 hPa height
shum	Near surface specific humidity
s500	Specific humidity at 500 hPa height
s850	Specific humidity at 850 hPa height
Derived variable	**The following variables have been derived using the geostrophic approximation**
**_f	Geostrophic air flow velocity
**_z	Vorticity
**_u	Zonal velocity component
**_v	Meridional velocity component
**zh	Divergence
**th	Wind direction

Notice: The derived variables have been derived using the geostrophic approximation.

** refers to different atmospheric levels: the surface (p_), 850 hPa height (p8) and 500 hPa height (p5)

As shown in **Figure 7.2**, the procedures of the SDSM downscaling mainly contain six steps. The quality control was used to identify gross data errors, specify missing data codes and outliers prior to model calibration. The main purpose of the screen variable option is to choose the appropriate downscaling predictor variables. The calibrate model operation constructs downscaling models based on multiple regression equations, given daily weather data (the predictand) and regional–scale, atmospheric (predictor) variables. In this study, the ordinary least squares optimization was selected to evaluate the SDSM optimizes. The calibrated model was used to generate synthetic daily weather series using the observed (or NCEP re-analysis) atmospheric predictor variables and regression model weights. Then, the generated weather series was compared with observed station data to validate the model.

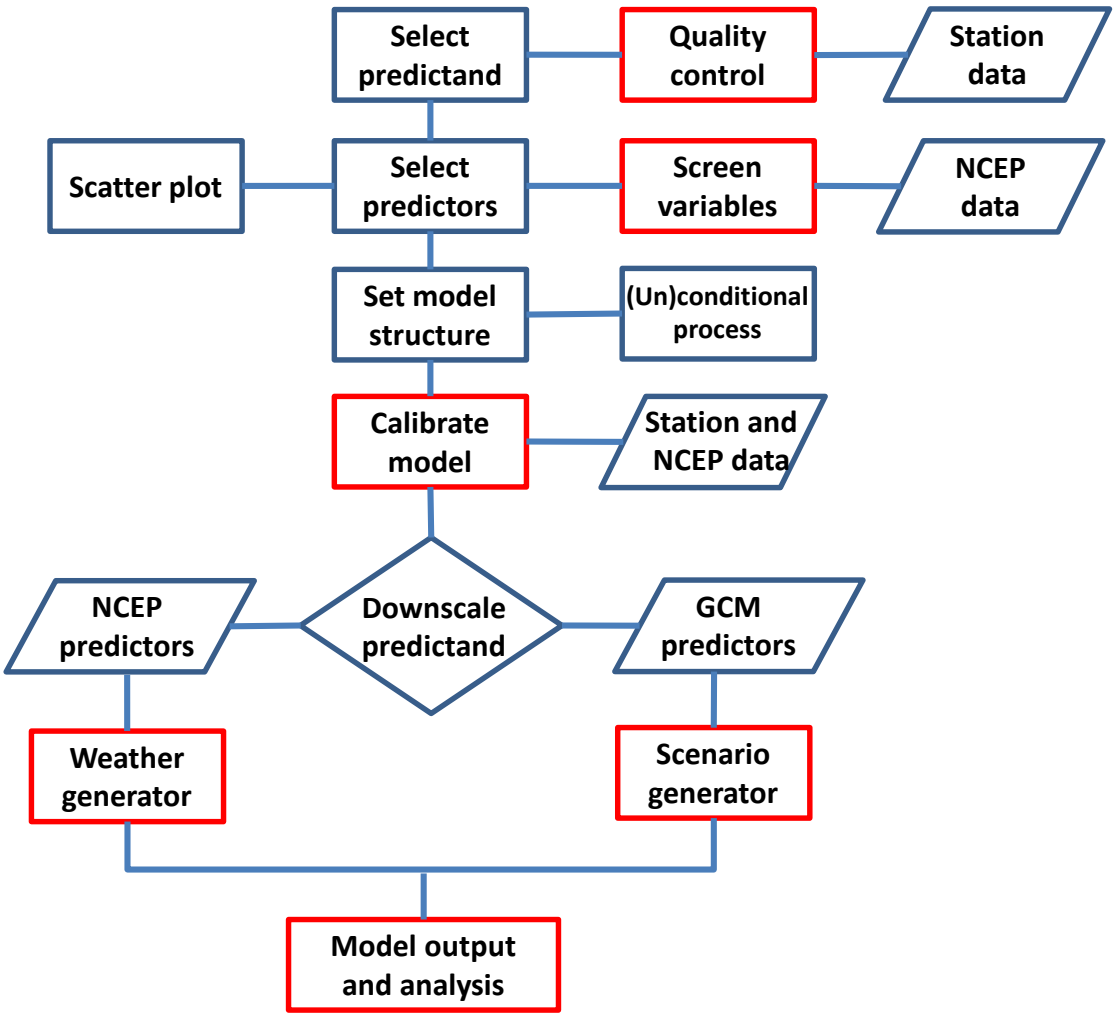

Figure 7.3 SDSM downscaling procedures (modified from (Wilby & Dawson 2007))

The SDSM bias correction was applied to compensate for any tendency to over- or under-estimate the mean of conditional processes by the downscaling model (e.g., mean daily rainfall totals). The variance inflation scheme was also used to increase the variance of precipitation and temperatures to agree better with observations. When using bias correction and variance inflation, SDSM essentially becomes a weather generator, where a stochastic component is superimposed on top of the downscaled variable. This is especially true for precipitation, where the explained variance is generally less than 30% (Wilby et al., 1999).

7.3 Results and discussions

7.3.1 SWAT Calibration and Validation

In the discretization procedure, each available waterflow gauging station was imposed as a sub-basin outlet, and a threshold area of 10,000 ha (minimum area drained through a cell for the latter to be defined as a stream cell) was selected to discretize the watershed into sub-catchments of homogeneous size. In this study, the Inou station was the only waterflow gauging station that was used to calibrate the model. The UIRB was divided into 22 sub-basins with a total watershed area of 3, 335 km^2, and the minimum, maximum, and mean elevation in the watershed were 91, 2290, and 608.2 m amsl, respectively. The overlay of land-use and soil grid maps resulted into 100 HRUs. The discretization was done trying to respect the original distribution of land use and soil, while keeping the number of HRUs down to a reasonable number.

The parameters responsible for stream-flow assessment for the Tungabhadra catchment, viz. r_CN2.mgt (curve number), v__ALPHA_BF.gw (base flow alfa factor), v__GW_DELAY.gw (groundwater delay time), v__GWQMN.gw (threshold depth of water in shallow aquifer required for return flow), v__GW_REVAP.gw (groundwater ‘revap’ coefficient), r__SOL_AWC.sol (soil available water capacity), r__SOL_K.sol (soil hydraulic conductivity) v__ESCO.hru (soil evaporation compensation factor),

v__CH_N2.rte (manning roughness for main channel), V__SFTMP.bsn (Snowfall temperature), V__SMFMX.bsn (Maximum melt rate for snow during years), and V__SMFMN.bsn (Minimum melt rate for snow during years) have been considered for model parameterization and calibration process. **Table 7.3** shows the ranking, description, minimum and maximum ranges of the 12 parameters fitted for the monthly calibration in the SUFI-2.

Based on the sensitive SWAT-input parameters of **Table 7.3**, the SWAT-model was calibrated on the observed monthly streamflow at the Inou gauging station. **Figure 7.4** shows the simulated and observed monthly streamflows for both the calibration- and validation periods. A more quantitive picture of the performance of the calibrated model for the calibration and validation period is gained from the two regression line plots of the simulated versus observed monthly streamflow of **Figure 7.5**. For both periods the regression lines have a slope close to 1, indicting a good agreement between the monthly observed and simulated streamflow. The values of the statistical parameters NSE for both the calibration and validation periods were 0.87 and 0.86, respectively, exhibiting calibration results was in a reasonable agreement between monthly observed and simulated streamflow.

From the calibration and validation results, it may be deduced that the model represents the hydrological characteristics of the watershed and can be used for further analysis.

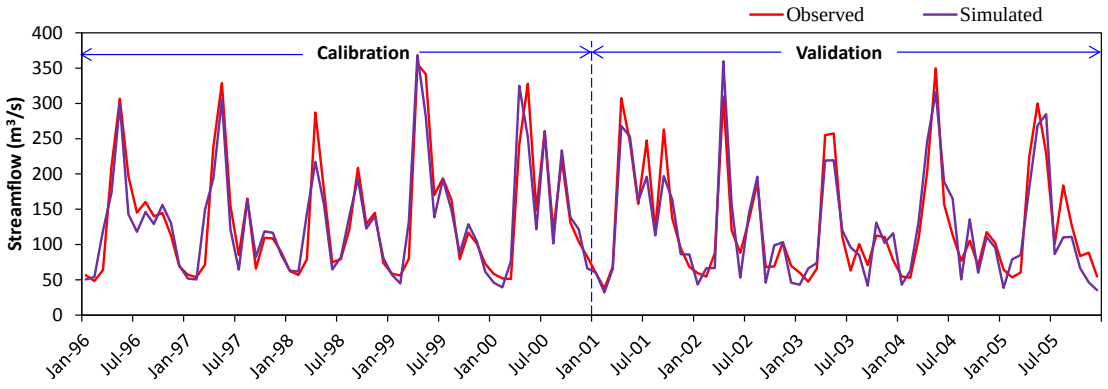

Figure 7.4 Simulated and observed monthly streamflow for calibration- and validation periods.

Table 7.2 Parameter global sensitivity ranking and final auto-calibration results

Rank	Parameter	Description	Optimal value	Lower bound	Upper bound
1	SFTMP	Snowfall temperature (°C)	4.358	-5	5
2	ESCO	Soil evaporation compensation factor	0.307	0	1
3	GW_REVAP	Groundwater "revap" coefficient	0.694	0	1
4	SOL_K	Saturated hydraulic conductivity	-0.666	-0.8	0.8
5	SOL_AWC	Available water capacity of the soil layer (mm H_2O mm^{-1} soil)	0.184	-0.5	1
6	GWQMN	Shallow aquifer required for the return flow to occur (mm)	0.112	0	2
7	GW_DELAY	Groundwater delay (days)	68.25	0	1000
8	ALPHA_BF	Baseflow alpha factor (days)	0.059	0	1
9	CH_N2	Manning's "n" value for the tributary channels	0.164	0	0.3
10	SMFMN	Minimum melt rate for snow during years (mm $°C^{-1}d^{-1}$)	4.03	0	8
11	SMFMX	Maximum melt rate for snow during years (mm $°C^{-1}d^{-1}$)	4.402	0	8
12	CN2	Initial SCS runoff curve number for moisture condition II	-0.163	-0.2	0.8

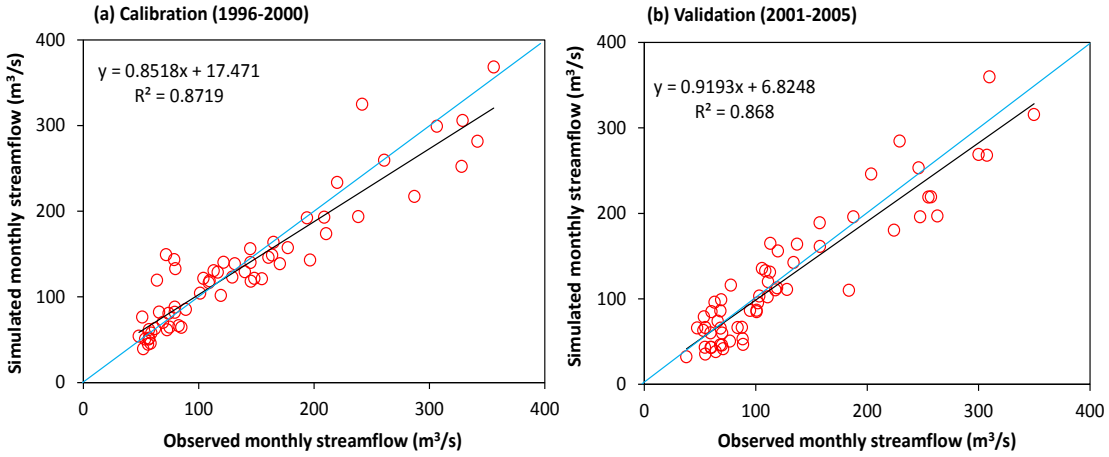

Figure 7.5 Scatter-plot of simulated versus observed monthly streamflow during calibration (a) and validation (b).

7.3.2 Climate Projects

7.3.2.1 SDSM validation

Changes in precipitation, maximum temperature and minimum temperature at the Asahikawa station were downscaled using the SDSM 4.2. The Asahikawa station can be taken to be representative of all stations in the UIRB area since the UIRB area is relatively small compared with the GCM's resolution. The calibration was carried out from 1961 to 1981 for 21 years and the withheld data from 1982 to 2001 were used to validate the model. **Figure 7.6-7.8** show the performance of the simulated versus observed daily maximum temperature, minimum temperature, and precipitation during calibration and validation periods, respectively, which indicate good agreement between the simulated and observed values of daily maximum and minimum temperature, but bad in daily precipitation. Maybe it because rainfall predictions have a larger degree of uncertainty than those for temperature since precipitation is highly variable in space and the relatively coarse GCM models cannot adequately capture this variability (Wilby and Dawson, 2007; Bader et al., 2008). As shown in **Figure 7.9**, however, the comparison between observed average long term mean monthly precipitation, and maximum and minimum temperature with corresponding simulations indicated that the results of the SDSM model generally

replicated the basic pattern of observations.

The climate scenario for the future periods in the UIRB area was developed from statistical downscaling using the HadCM GCM predictor variables for the two SERS emission scenarios (A2 and B2) based on the 20 ensembles and the analysis was done based on 20-year periods centered on the 2030s (2020-2039), 2060s (2050-2069) and 2090s (2080-2099).

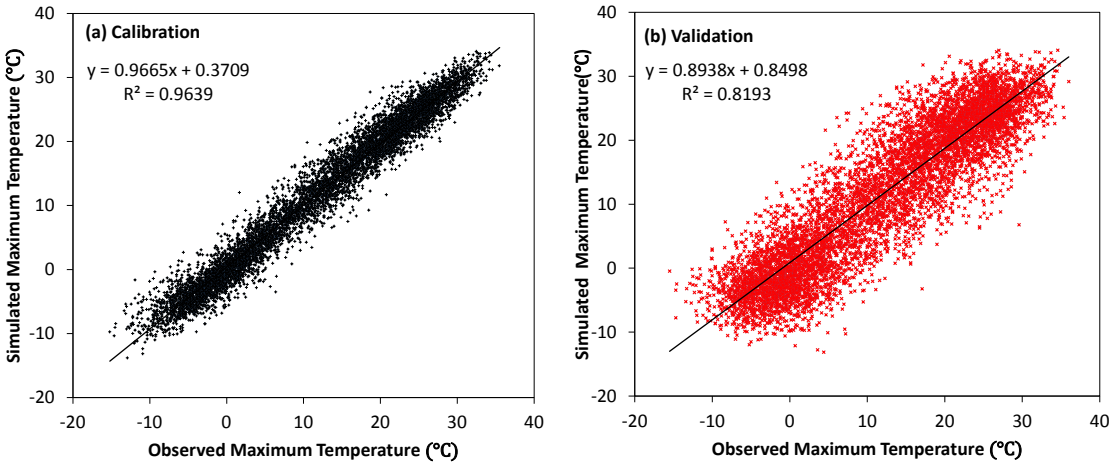

Figure 7.6 Scatter-plot of simulated versus observed daily maximum temperature during calibration (a) and validation (b).

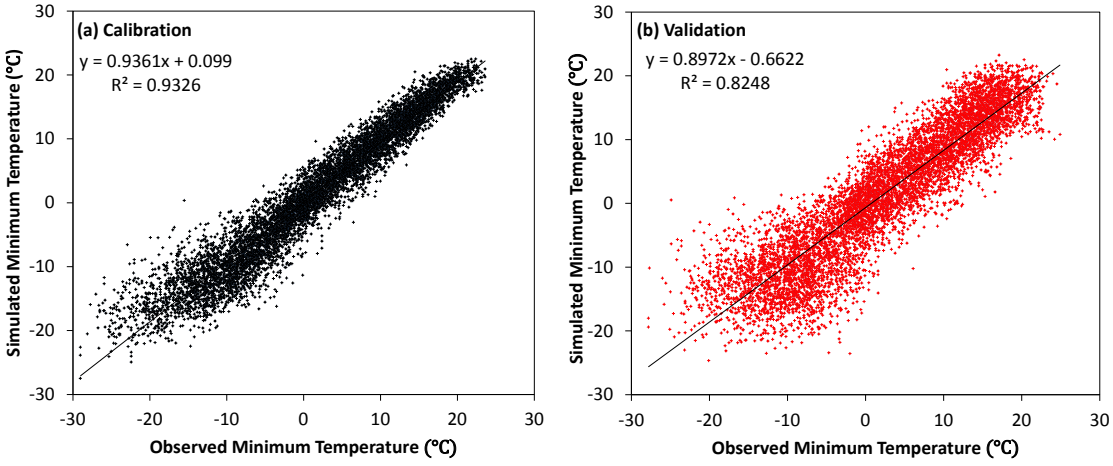

Figure 7.7 Scatter-plot of simulated versus observed daily minimum temperature during calibration (a) and validation (b).

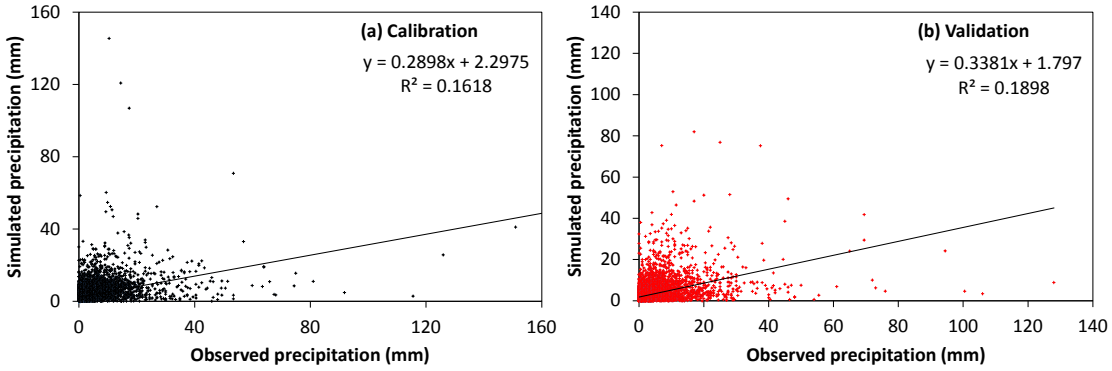

Figure 7.8 Scatter-plot of simulated versus observed daily precipitation during calibration (a) and validation (b).

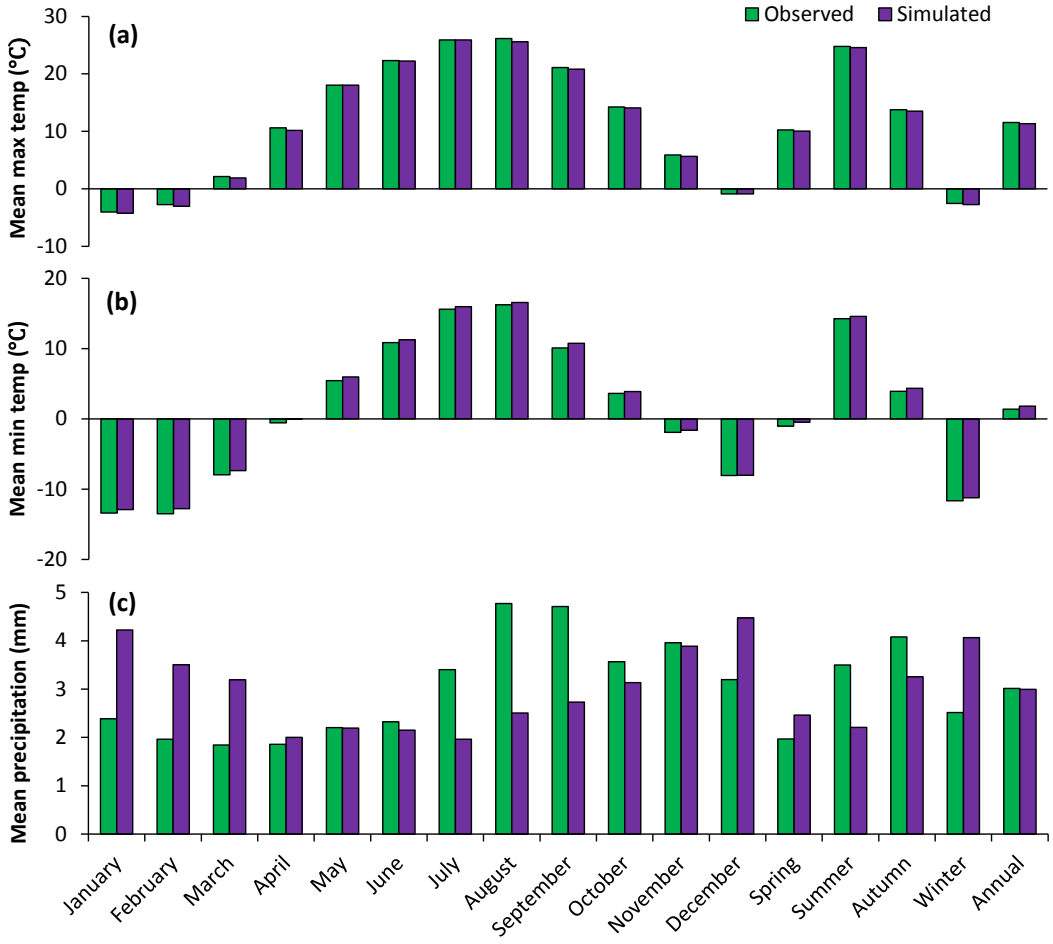

Figure 7.9 Comparison between observed and generated mean daily precipitation and maximum and minimum temperature in the time step for the Inou station. (a) maximum temperature (°C), (b) minimum temperature (°C), and (c) precipitation (mm).

7.3.2.2 Future temperature

As shown in **Figure 7.10** and **Figure 7.11**, the mean monthly, seasonal, and annual changes in daily temperature from the baseline period data exhibited an increasing trend for both scenarios (A2a and B2a) in 2030s, 2060s and 2090s, and increases in the A2a scenario are much bigger than the B2a scenario.

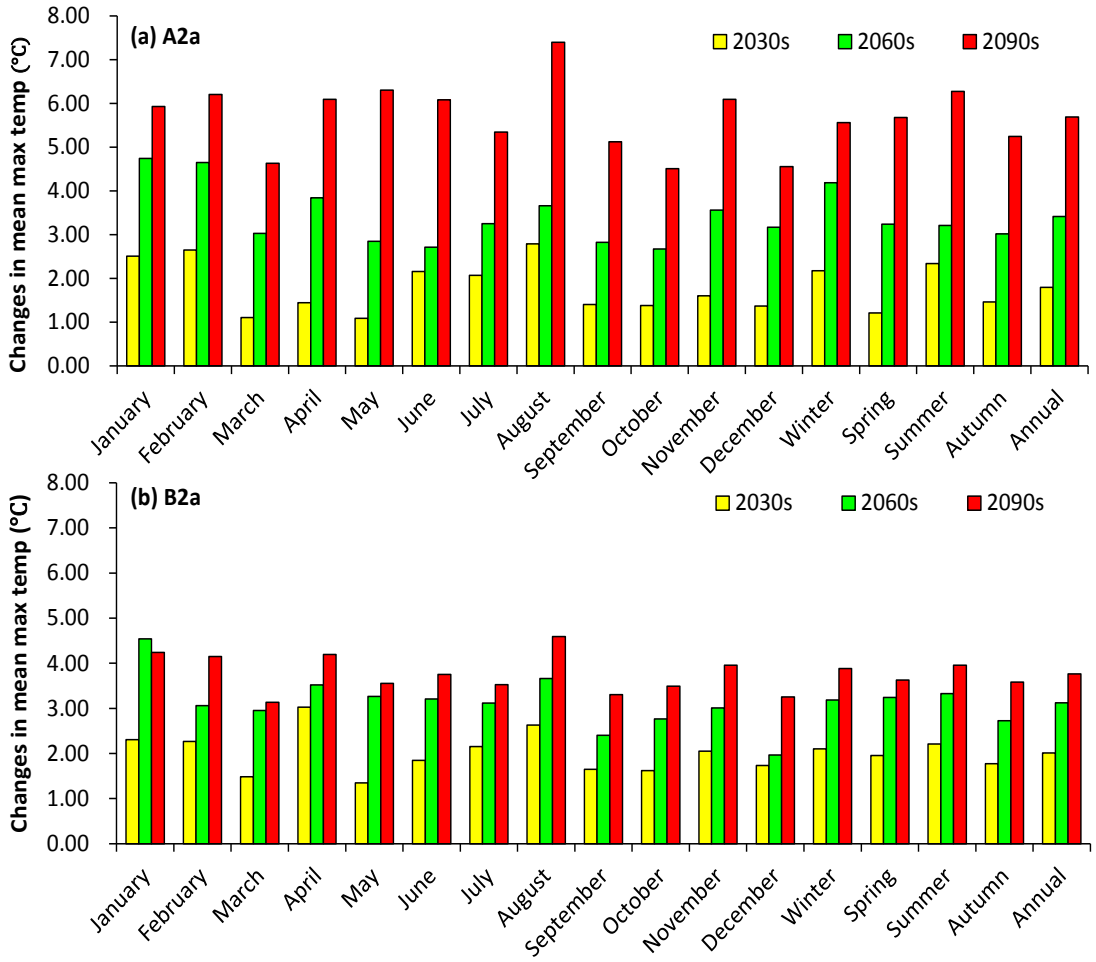

Figure 7.10 Changes in monthly, seasonal and annual mean maximum temperature for the future periods 2030s, 2060s and 2090s as compared to the baseline period (1981-2000) at the Inou station. (a) A2a scenario and (b) B2a scenario.

The average annual maximum temperature might increase by 1.80°C and 2.01°C, 3.41°C and 3.12°C, and 5.69°C and 3.76°C in 2030s, 2060s and 2090s for A2a and B2a emission scenarios respectively. Results from the seasonal scale reveal that summer has the highest increases under both A2a and B2a emission scenarios in 2090s, up to 6.27 °C and 3.96°C respectively, while autumn has the lowest increases with approximately 5.24 °C and 3.59 °C respectively. Monthly, the largest increase in mean maximum temperature is indicated during the august for both A2a (approximately 7.40 °C) and B2a (approximately 4.59 °C) emission scenarios in 2090s.

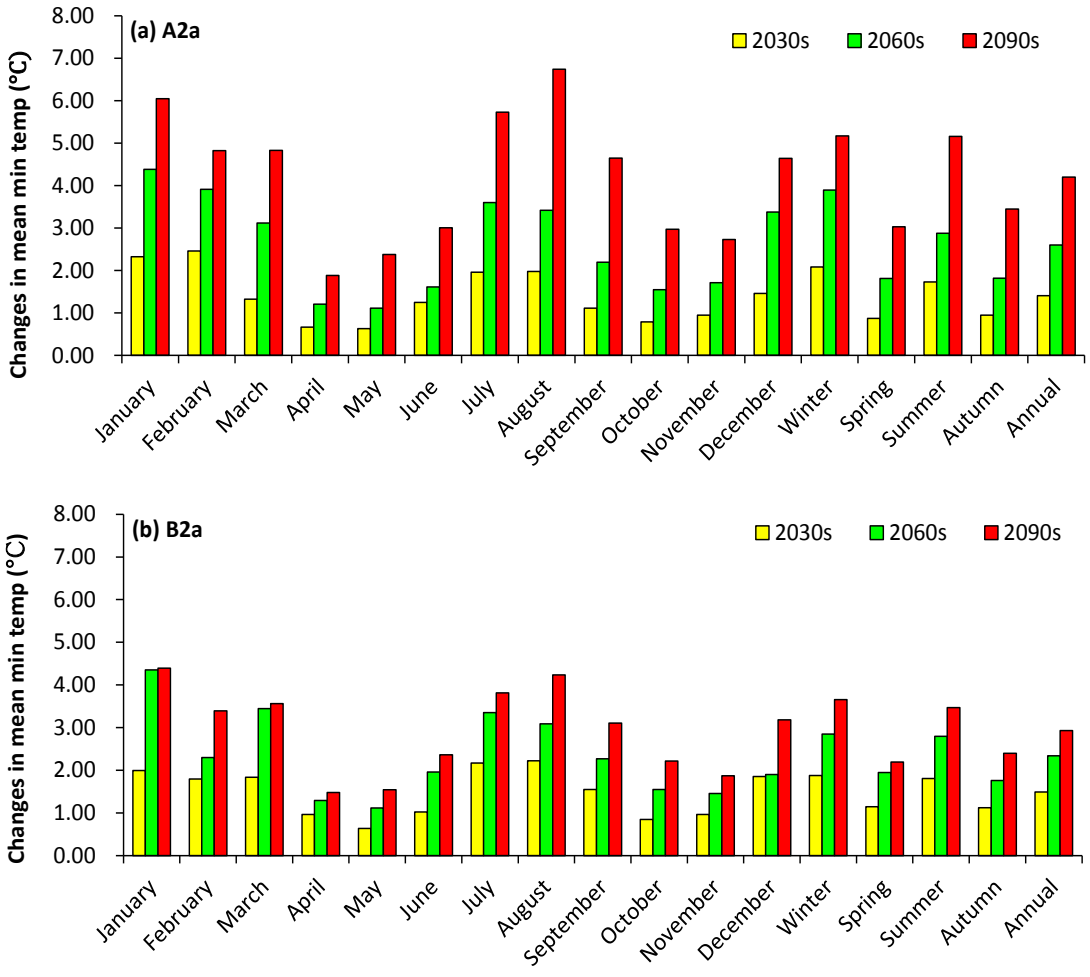

Figure 7.11 Changes in monthly, seasonal and annual mean minimum temperature for the future 2030s, 2060s and 2090s periods as compared to the baseline period (1981-2000) at the Inou station. (a) A2a scenario and (b) B2a scenario.

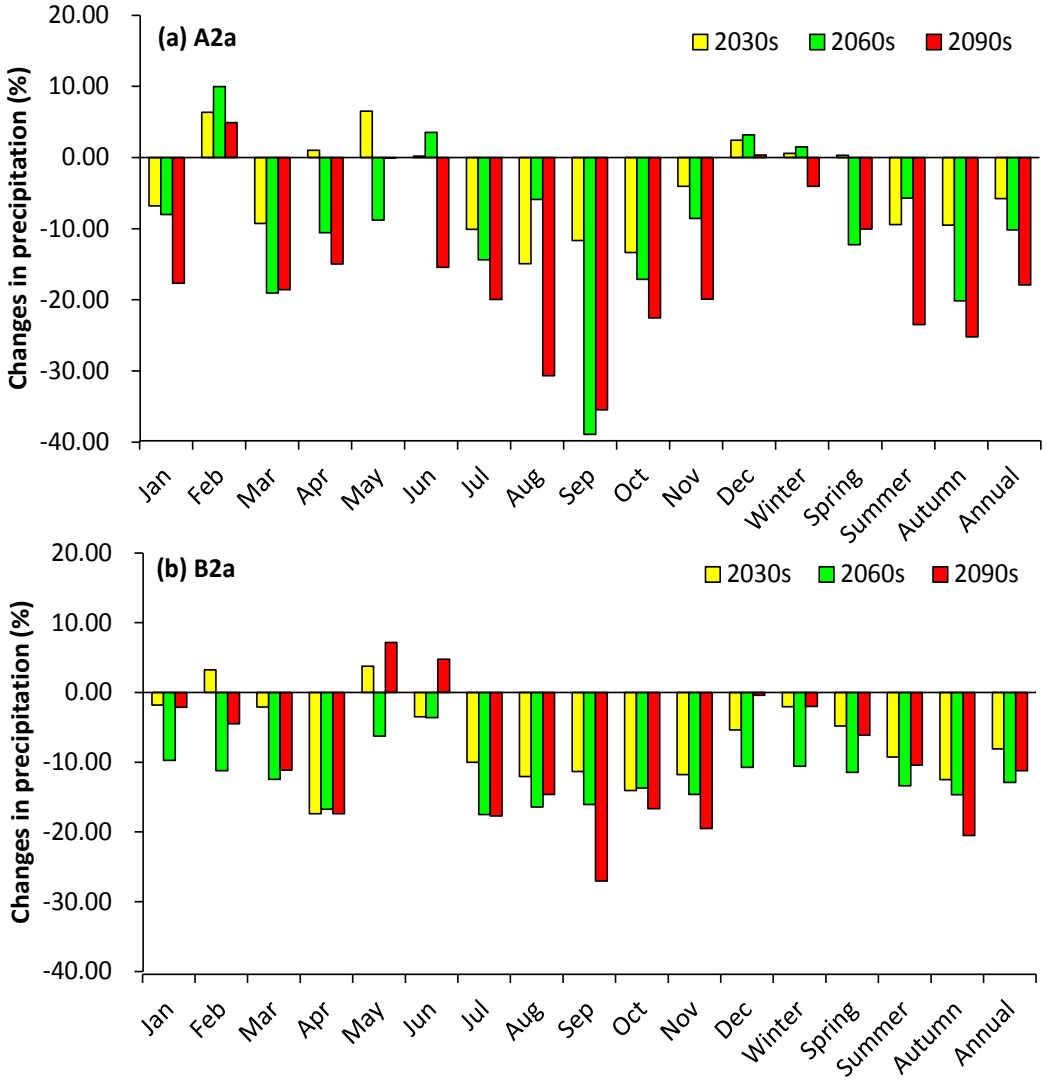

Figure 7.12 Changes in monthly, seasonal and annual mean precipitation for the future 2030s, 2060s and 2090s periods as compared to the baseline period (1981-2000) at the Inou station. (a) A2a scenario and (b) B2a scenario.

Results for minimum temperature indicated that the average annual minimum temperature might increase by 1.41°C and 1.49°C, 2.60°C and 2.34°C, and 4.20°C and 2.93 in 2030s, 2060s and 2090s for the A2a and B2a emission scenarios respectively. Seasonally, winter had the largest increase for both scenarios in each period, followed by summer, autumn and spring. For the 2090s, the average minimum temperature in winter possibly increase by 5.17°C and 2.66°C for A2a and B2a scenarios, respectively. As in the

case of monthly simulation, the minimum temperature tends to increase during all twelve months for both scenarios in all future periods (**Figure 7.11**). August has the largest increase (around 6.74°C) under the A2a scenario in 2090s, followed by January (around 6.05°C) and July (around 5.73°C); January has the largest increase (around 4.40°C) under the B2a scenario in 2090s, followed by August (around 4.24°C) and July (around 3.82°C).

7.3.2.3 Future precipitation

Figure 7.12 shows that the average annual precipitation might decrease by 5.78% and 8.08%, 10.18% and 12.89%, and 17.92% and 11.23% in the future 2030s, 2060s and 2090s for A2a and B2a emission scenarios respectively, suggesting that a remarkable decreasing trend in precipitation will be likely to appear in the UIRB area in future. On a seasonal timescale, there may be a decrease in mean precipitation for all seasons under both scenarios except for winter in 2030s and 2060s and spring in 2030s under A2a scenario. Among them, autumn has the largest decrease, up to 9.52%, 20.12% and 25.22 for the 2030s, 2060s and 2090s respectively for A2a scenario, and 12.49%, 14.66% and 20.49% for B2a scenario, followed by summer, spring and winter. Simulation results for the average monthly precipitation indicate that there may be a mixed trend. As shown in **Figure 7.12**, in the 2030s there may be a decrease in mean monthly precipitation for all months except for February, April, May, and December under A2a scenario, and February and May under B2a scenario. In addition, there is an increasing trend in both February and December for all three future periods for A2a scenario as compared to the base period. More decreases are possibly observed in September for the 2090s for both A2a (approximately 35.47%) and B2a (approximately 27.05%) scenarios compared to other months and the largest decrease is also found in September for the 2060s for the A2a scenario, up to 38.90%.

7.3.3 Climate change impact

The impact of climate change on water flow was predicted and analyzed taking the

water flow from 1981 to 2000 as the baseline flow against which the future flows for the 2030s, 2060s, and 2090s compared. Precipitation, maximum and minimum temperature were the climate change drivers, which were inputted into the calibrated SWAT model to fulfill the climate impact assessment. **Figure 7.13** shows the percentage changes in mean monthly, seasonal, and annual flow volume for the future 2030s, 2060s and 2090s periods compared with the baseline period (1981-2000) at the Inou gauging station, suggesting that there are all basically the same trend in A2a and B2a emission scenarios. Results indicate an increase in annual mean streamflow for the all three future periods except the 2090s under the A2a scenario. Among them, the largest increase is observed in the 2030s for A2a scenario, up to approximately 7.56%.

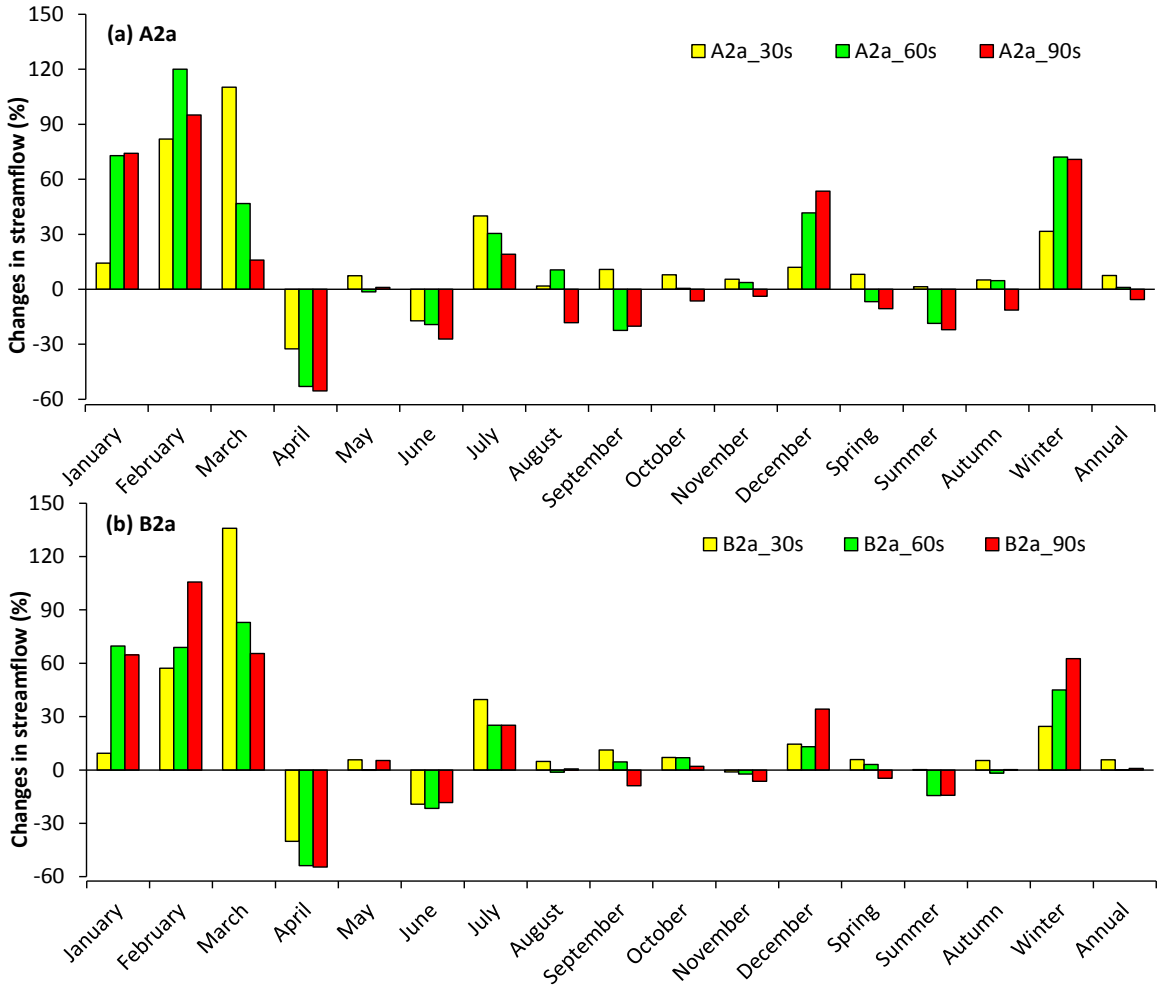

Figure 7.13 Percentage change in mean monthly, seasonal, and annual flow volume for the future 2030s, 2060s and 2090s periods as compared to the baseline period (1981-2000) at the Inou gauging station. (a) A2a scenario and (b) B2a scenario.

As in the case of seasonal prediction, a pronounced increase is exhibited in winter for the all future periods for both scenarios, while a decrease is found in summer except the 2030s for A2a scenario. The highest increase is up to 72.17% in the 2060s under A2a scenario, followed by 70.89% in the 2090s under A2a scenario and 62.61 % in the 2090s under A2a scenario, and the largest decrease is about 22.09%, which is predicted in the 2090s under A2a scenario. Spring and autumn have a mixed and slight trend for future periods for both scenarios.

On a monthly scale, an increasing trend is found in January, February, March, July and December for all future periods for both scenarios, while a decrease happens in April and June. For the 2030s, the mean monthly flow shows an increase for all months except April and June in both scenarios. In this period, the highest increase is up to 135.86% for the B2a scenario, followed by 110.19% and 81.99% for the A2a scenario; on the other hand, the largest decrease is up to 40.07% for the B2a scenario, followed by 32.46% for the A2a scenario and 19.21% for the B2a scenario. There are more months in which mean precipitation has a decreasing trend in the 2060s and 2090s compared to the 2030s.

7.4 Discussions

Using the outputs from HadCM3 GCM A2a and B2a climatic scenarios, the changes in temperature, precipitation, as well as the waterflow were evaluated on the Upper Ishikari River Basin for the 2030s, 2060s and 2090s periods. The SDSM statistical downscaling tool was applied to compute the future temperature and precipitation. All these data were inputted into the calibrated SWAT model for calculating the waterflow for all three periods under both scenarios. All the results obtained from this study are representative for a majority of GCM output and that therefore our results are plausible estimates of future effects of climate change in the UIRB area. These findings also generate several interesting questions despite clearly indicating significant changes in hydro-climatology in the UIRB area in the future.

First, the performance of the downscaling results in daily maximum temperature and minimum temperature are very good, but relative bad in daily precipitation. Some other researches got the similar results in the downscaled daily precipitation (Dile et al., 2013). Bader et al., (2008) pointed out the prediction of rainfall by GCMs is often poor as the variables that force rainfall patterns are dominated by topography and to a lesser extent vegetation. Prudhomme et al., (2002) also indicated that the current generation of GCMs still does not provide reliable estimates of rainfall variance, and it is currently difficult to develop appropriate downscaling methodologies. For example, the rainfall patterns predicted by ensembles of GCMs for India completely miss the higher rainfall areas of the sub-Himalaya and the Western Ghats, although they slightly over-estimate current average rainfall, while modelled peak daily rainfall intensity was only two-thirds of that recorded. All these may be the reasons for getting the relative bad performance for the daily rainfall prediction.

In addition, the annual precipitation exhibits a decreasing trend in the future, but the waterflow shows no trends or even increasing trend. Also, this situation appears in the some months (e.g., January, March, and so on). The waterflow is expected to change according to temperature and precipitation changes. Obviously, remarkable decreasing trend (i.e., the average annual precipitation might decrease by 5.78% and 8.08%, 10.18% and 12.89%, and 17.92% and 11.23% in the future 2030s, 2060s and 2090s for A2a and B2a emission scenarios respectively) in precipitation will be likely to reduce the runoff in the UIRB area. Temperature, however, will tend to increase, which contributes to the snow melting. The UIRB area is located in Hokkaido, which is covered in snow for as long as 4 months a year. From the results of calibrated SWAT model, the temperature was a very sensitive to streamflow in the UIRB area; that is, snowfall temperature (STFMP), minimum melt rate for snow during years (SMFMN) and maximum melt rate for snow during years (SMFMX) will significantly affected the river flow. The average annual maximum temperature might increase by 1.80°C and 2.01°C, 3.41°C and 3.12°C, and 5.69°C and 3.76°C in 2030s, 2060s and 2090s for A2a and B2a emission scenarios

respectively, which will extremely increase snowmelt. These variations are also in line with the results of Sato et al., (2013).

Finally, although the results from the cascade of models in this study indicated a satisfactory and acceptable performance, there is much uncertainty due to in all used models. It is a combination of uncertainties in the hydrological parameter university (Maurer and Duffy, 2005), GCM outputs as a result of the downscaling (Chen et al., 2011), and neglect of land use changes or potential changes in soil properties (Setegn et al., 2011). As shown in **Table 7.3**, not all the SWAT parameters were discussed except for some main parameters that greatly affect the water balance. Moreover, HaDCM3 GCM outputs have kind of uncertainty, which cannot perfectly simulate the future (Buytaert et al., 2009). So, each GCM output will give different results. In this study, we focused on the UIRB area by downscaling HaDCM3 outputs, and there are probably some different results if some other GCMs would be used. Downscaling techniques also bring some uncertainties (Fowler et al., 2007; Khan et al., 2006). For example, Prudhomme and Davies (2009) found some times bias is not visible with SDSM-downscaled scenarios although there is a tendency towards underestimation, but this is within natural variability. Thirdly, we neglected land use changes or potential changes in soil properties; however, land cover will change due to natural and anthropogenic influences and corresponding features should be changed in the model.

7.5 Conclusions

SWAT model was successfully applied to simulate the possible effects of climate change on water resources in the UIRB area on the basis of n projected climate conditions by using GCM out puts of HadCM3 SRES A2a and B2a emissions scenarios with Statistical Downscaling (SDSM) modeling approach. Major conclusions can be summarized as follows: (1) The values of the statistical parameters NSE for both the calibration and validation periods were 0.87 and 0.86, respectively, exhibiting calibration

results was in a reasonable agreement between monthly observed and simulated streamflow, and therefore it could be used to evaluate the hydrological response under climate change in the UIRB area; (2) The downscaling results indicated that the average annual maximum temperature might increase by 1.80°C and 2.01°C, 3.41°C and 3.12°C, and 5.69°C and 3.76°C, the average annual minimum temperature might increase by 1.41°C and 1.49°C, 2.60°C and 2.34°C, and 4.20°C and 2.93°C, and the average annual precipitation might decrease by 5.78% and 8.08%, 10.18% and 12.89%, and 17.92% and 11.23% in 2030s, 2060s and 2090s for A2a and B2a emission scenarios respectively; (3) The annual mean streamflow will be likely to increase for the all three future periods except the 2090s under the A2a scenario. Among them, the largest increase is observed in the 2030s for A2a scenario, up to approximately 7.56%. Also, a pronounced increase is exhibited in winter for the all future periods for both scenarios, while a decrease is found in summer except the 2030s for A2a scenario.

7.6 Reference

Abbaspour, K.C. et al., 2007. Modelling hydrology and water quality in the pre-alpine/alpine Thur watershed using SWAT. Journal of Hydrology, 333(2): 413-430.

Arnold, J.G., Srinivasan, R., Muttiah, R.S. and Williams, J.R., 1998. Large area hydrologic modeling and assessment part I: Model development1. Journal of the American Water Resources Association, 34(1): 73-89.

Babel, M.S., Bhusal, S.P., Wahid, S.M. and Agarwal, A., 2013. Climate change and water resources in the Bagmati River Basin, Nepal. Theoretical and Applied Climatology, 115: 639-654.

Bader, D. et al., 2008. Climate models: an assessment of strengths and limitations. A report by the US Climate Change Science Program and the Subcommittee on Global Change Research, Office of Biological and Environmental Research, Department of Energy, Washington, DC, USA: 124 pp.

Buytaert, W., Célleri, R. and Timbe, L., 2009. Predicting climate change impacts on water resources in the tropical Andes: Effects of GCM uncertainty. Geophysical Research Letters, 36(7): L07406.

Chen, J., Brissette, F.P. and Leconte, R., 2011. Uncertainty of downscaling method in quantifying the impact of climate change on hydrology. Journal of Hydrology, 401(3): 190-202.

Chung, S.W., Gassman, P.W., Gu, R. and Kanwar, R.S., 2002. Evaluation of EPIC for assessing tile flow and nitrogen losses for alternative agricultural management systems. Transactions of The ASAE, 45(4): 1135-1146.

Coumou, D. and Rahmstorf, S., 2012. A decade of weather extremes. Nature Climate Change, 2(7): 491-496.

Dile, Y.T., Berndtsson, R. and Setegn, S.G., 2013. Hydrological Response to Climate Change for Gilgel Abay River, in the Lake Tana Basin-Upper Blue Nile Basin of Ethiopia. PloS one, 8(10): e79296.

Duan, W. et al., 2013. Spatial and temporal trends in estimates of nutrient and suspended sediment loads in the Ishikari River, Japan, 1985 to 2010. Science of the Total Environment, 461: 499-508.

Duan, W. et al., 2014. Anomalous atmospheric events leading to Kyushu’s flash floods, July 11–14, 2012. Natural Hazards: 1-13.

Fowler, H.J., Blenkinsop, S. and Tebaldi, C., 2007. Linking climate change modelling to impacts studies: recent advances in downscaling techniques for hydrological modelling. International Journal of Climatology, 27(12): 1547-1578.

Green, C.H. and Van Griensven, A., 2008. Autocalibration in hydrologic modeling: Using SWAT2005 in small-scale watersheds. Environmental Modelling and Software, 23(4): 422-434.

He, B., Takara, K., Yamashiki, Y., Kobayashi, K. and Luo, P., 2011. Statistical Analysis of Present and Future River Water Temperature in Cold Regions Using Downscaled GCMs Data. Disaster Prevention Research Institute Annuals. B, 54(B): 103-111.

Khan, M.S., Coulibaly, P. and Dibike, Y., 2006. Uncertainty analysis of statistical downscaling methods. Journal of Hydrology, 319(1): 357-382.

Konikow, L.F. and Kendy, E., 2005. Groundwater depletion: A global problem. Hydrogeology Journal, 13(1): 317-320.

Li, Z., Zheng, F., Liu, W. and Jiang, D., 2012. Spatially downscaling GCMs outputs to project changes in extreme precipitation and temperature events on the Loess Plateau of China during the 21st Century. Global and Planetary Change, 82: 65-73.

Ma, X. et al., 2010. Hydrological response to future climate change in the Agano River basin, Japan. Hydrological Research Letters, 4: 25-29.

Maurer, E.P. and Duffy, P.B., 2005. Uncertainty in projections of streamflow changes due to climate change in California. Geophysical Research Letters, 32(3): L03704.

Meenu, R., Rehana, S. and Mujumdar, P.P., 2013. Assessment of hydrologic impacts of climate change in Tunga–Bhadra river basin, India with HEC–HMS and SDSM. Hydrological Processes, 27(11): 1572-1589.

Narsimlu, B., Gosain, A.K. and Chahar, B.R., 2013. Assessment of Future Climate Change Impacts on Water Resources of Upper Sind River Basin, India Using SWAT Model. Water Resources Management, 27(10): 3647-3662.

Nash, J. and Sutcliffe, J.V., 1970. River flow forecasting through conceptual models part I–A discussion of principles. Journal of Hydrology, 10(3): 282-290.

Neitsch, S.L., Arnold, J.G., Kiniry, J.R., Williams, J.R. and King, K.W., 2005. SWAT theoretical documentation version 2005. Blackland Research Center, Temple, TX.

Oki, T. and Kanae, S., 2006. Global hydrological cycles and world water resources. Science, 313(5790): 1068-1072.

Prudhomme, C. and Davies, H., 2009. Assessing uncertainties in climate change impact analyses on the river flow regimes in the UK. Part 1: baseline climate. Climatic Change, 93(1-2): 177-195.

Prudhomme, C., Reynard, N. and Crooks, S., 2002. Downscaling of global climate models for flood frequency analysis: where are we now? Hydrological Processes, 16(6): 1137-

1150.

Santhi, C. et al., 2001. Validation of the SWAT model on a large river basin with point and non-point source. Journal of the American Water Resources Association, 37(5): 1169–1188.

Sato, Y., Kojiri, T., Michihiro, Y., Suzuki, Y. and Nakakita, E., 2013. Assessment of climate change impacts on river discharge in Japan using the super– high– resolution MRI- AGCM. Hydrological Processes, 27(23): 3264-3279.

Setegn, S.G., Rayner, D., Melesse, A.M., Dargahi, B. and Srinivasan, R., 2011. Impact of climate change on the hydroclimatology of Lake Tana Basin, Ethiopia. Water Resources Research, 47(4): W04511.

Solomon, S., 2007. Climate change 2007-the physical science basis: Working group I contribution to the fourth assessment report of the IPCC, 4. Cambridge University Press, 1056 pp.

Tatsumi, K., Oizumi, T. and Yamashiki, Y., 2013. Introduction of daily minimum and maximum temperature change signals in the Shikoku region using the statistical downscaling method by GCMs. Hydrological Research Letters, 7(3): 48-53.

Tatsumi, K., Oizumi, T. and Yamashiki, Y., 2014. Effects of climate change on daily minimum and maximum temperatures and cloudiness in the Shikoku region: a statistical downscaling model approach. Theoretical and Applied Climatology, DOI: 10.1007/s00704-014-1152-9.

Taye, M.T., Ntegeka, V., Ogiramoi, N.P. and Willems, P., 2011. Assessment of climate change impact on hydrological extremes in two source regions of the Nile River Basin. Hydrology and Earth System Sciences, 15(1): 209–222.

Wada, Y. et al., 2010. Global depletion of groundwater resources. Geophysical Research Letters, 37(20): L20402.

Wilby, R.L. et al., 2000. Hydrological responses to dynamically and statistically downscaled climate model output. Geophysical Research Letters, 27(8): 1199-1202.

Wilby, R.L. and Dawson, C.W., 2007. SDSM 4.2- A decision support tool for the

assessment of regional climate change impacts, Version 4.2 User Manual. Lancaster University: Lancaster/Environment Agency of England and Wales.

Wilby, R.L., Dawson, C.W. and Barrow, E.M., 2002. SDSM– a decision support tool for the assessment of regional climate change impacts. Environmental Modelling and Software, 17(2): 145-157.

Wilby, R.L., Hay, L.E. and Leavesley, G.H., 1999. A comparison of downscaled and raw GCM output: implications for climate change scenarios in the San Juan River basin, Colorado. Journal of Hydrology, 225(1): 67-91.

Zhang, X. et al., 2007. Detection of human influence on twentieth-century precipitation trends. Nature, 448(7152): 461-465.

Chapter 8 Conclusions and Future Research

Global environmental change including all the future changes due to anthropogenic activities and natural climate variations, has significantly affected water resources availability and quality, extreme events, surface and ground water, marine and continental water, and, consequently, the accomplishment of different water policies related to river basin management, marine environment, water quantity (floods, droughts, water scarcity), water and health (drinking and bathing water) and water pollution (water treatment). Evidence for climate change impacts on the hydro-climatology of Japan is plentiful; for example, the annual average air temperatures nationwide rose by a rate equivalent to 1.15°C per century between 1898 and 2010 and annual precipitation in Japan varies largely from year to year. All these changes in precipitation and temperature have greatly influenced water supply. Meanwhile, extreme rainfall and temperature induced lots of hydrological disasters including floods, water quality incidents, and so on. So this thesis this thesis mainly focused on the climate and human impacts on water quality and water resources in Japan. After investigating spatiotemporal trends and causes of the water quality incidents, changes of precipitation extreme events were analyzed in whole Japan, which indicated Hokkaido was a special area under climate change compared to other places. So over the subsequent Chapters the thesis just focused on the climate and human impacts on water quality and water resources in Hokkaido. Major conclusions can be summarized as follows:

1) Fast growth of water quality incidents was the most prominent recent trend observed. The nationwide trend for Japan and that the total number of water quality incidents fluctuated between 400 and 1600/year, and the average from 1996-2007, from

1996 to 1999, from 2000 to 2003 and from 2004 to 2007 are 962, 499, 902 and 1487, separately. The average from 2004 to 2007 reflects a three-fold increase over the average from 1996 to 1999. “Natural” causes will likely remain important for water pollution.

2) Precipitation extremes varied substantially in spatial-temporal. Variations in R10mm, R20mm, CWD and PRCPTOT indicated a decreasing trend for a whole Japan, with while an increasing trend for R95p, R99p, CDD, RX1day, RX5day, and SDII. The spatial differences of these indices were obvious. Negative trends dominated for PRCPTOT, R10mm and R20mm, with the exception of the Hokkaido, and stations with statistical significant trends for R95p, R99p and SDII mainly scattered in the southwest area of Japan.

3) Precipitation tended to increase across Hokkaido during 1980-2011 at both the annual and seasonal scales, and varied substantially in spatial-temporal. The changes of the water vapor transport and budget in whole layers under 300hpa for the period 1980-2011 possibly explain the spatiotemporal distribution of precipitation trends in Hokkaido. Water vapor flux decreased gradually from the south to the north in all seasons, possibly explaining the annual and seasonal mean precipitation. Seasonal distributions of water vapor flux may reflect precipitation was mainly concentrated in summer and autumn, while precipitation was reduced in winter and spring.

4) The combination of the MOVE. 3 and the LOADEST successfully estimated loads of TN, TP and SS at five sites on the Ishikari River, from January 1985 through December 2010, illustrating how short records of daily waterflow and components concentration can be combined to obtain meaningful estimates of seasonal TN, TP and SS loads. The estimated seasonal loads of TN, TP, and SS at the five sites were highly variable from 1985 to 2010 in the Ishikari River and its tributaries, with the greatest loads occurring in the spring and the smallest loads occurring in the winter especially after floods, reflecting fluctuations in discharge as a result of the combined effects of seasonal runoff patterns, the exact timing of which vary from year to year.

5) For SS in Ishikari River basin, the percent of total incremental flux generated for agricultural lands, developing lands, forested lands, and stream channels is 35.11%, 23.42%, 22.91% and 18.56%, respectively. Sediment total yields and incremental yields concentrate in the sub-basin along the middle and lower reaches of the Ishikari River, showing which sub-basin is most susceptible to erosion. Combined with land use, management actions should be designed to reduce sedimentation of agricultural lands and developing lands in the sub-basin along the middle and lower reaches of the Ishikari River. Results can improve our understanding of SS dynamics and watershed processes in general, which will benefit both the scientific and the management community in safeguarding water resources.

6) In the Upper Ishikari River basin, the downscaling results indicated that the average annual maximum temperature might increase by 1.80°C and 2.01°C, 3.41°C and 3.12°C, and 5.69°C and 3.76°C, the average annual minimum temperature might increase by 1.41°C and 1.49°C, 2.60°C and 2.34°C, and 4.20°C and 2.93°C, and the average annual precipitation might decrease by 5.78% and 8.08%, 10.18% and 12.89%, and 17.92% and 11.23% in 2030s, 2060s and 2090s for A2a and B2a emission scenarios respectively. The annual mean streamflow will be likely to increase for the all three future periods except the 2090s under the A2a scenario. Among them, the largest increase is observed in the 2030s for A2a scenario, up to approximately 7.56%. Also, a pronounced increase is exhibited in winter for the all future periods for both scenarios, while a decrease is found in summer except the 2030s for A2a scenario.

Overall, the results obtained in this thesis substantially enhance the knowledge of climate change impacts on the water quality and water resources in Japan, which may provide a means to reduce water quality incidents and mitigate future impacts by adapting water management. Furthermore, the improved methods for water quality modeling in data scarce regions are transferable to other study areas and applicable in future research.

Also, this study has a number of shortcomings and suggests several areas for future work. First, in the part of modeling suspended sediment sources and transport in the

Ishikari River basin, some important model results lack of statistical significance. For example, statistically insignificant model components and inaccuracies associated with DEM resolution, which contain a source variable (stream channels), and big streams with drainage area >200 km^2. The prediction of the model only indicates mean-annual conditions, not necessarily critical conditions such as low- flow conditions. The reason for these results mainly includes the following points: (1) the hydrologic network was derived from a 50 m digital elevation model (DEM), which is a litter bit different from actual stream network; (2) because of unaware of water discharge in all streams, stream velocity was replaced with drainage area to classify the small stream and big stream; and (3) the calibration data only incorporate monitored-load data from limited number of stations with long-term data. So, in the future work, the more detailed conditions should be considered in evaluating the SS. In addition, although the results from the cascade of models in this thesis indicated a satisfactory and acceptable performance, there is much uncertainty due to in all used models. It is a combination of uncertainties in the hydrological parameter, GCM outputs as a result of the downscaling, and neglect of land use changes or potential changes in soil properties. All these shortcomings will be considered and solved in the future work.

List of Publications

Peer-reviewed Journal Publications:

- **Weili Duan**, Bin He, Kaoru Takara, Pingping Luo, Daniel Nover, Yosuke Yamashiki and Wenrui Huang, Anomalous atmospheric events leading to Kyushu's flash floods, 11-14 July 2012, ***Natural Hazards***, 73(3): 1255-1267, 2014.
- **Weili Duan**, Bin He, Kaoru Takara, Pingping Luo, Maochuan Hu, Nor Eliza Alias, Masahito Ishihara and Yi Wang. Climate Change Impacts on Wave Characteristics along the Coast of Japan from 1986 to 2012, ***Journal of Coastal Research***, 2014, in press.
- Maochuan Hu, Kaoru Takara, Pingping Luo, Bin He, **Weili Duan**, Climate change and land use change impact analysis in a data sparse watershed using a hydrological model, ***Journal of Japan Society of Civil Engineers, Ser.B1 (Hydraulic Engineering),*** 70(4): I_109-I_114, 2014.
- Netrananda Sahu, Swadhin K. Behera, J. V. Ratnam, Roberto Valmir Da Silva, Pradipta Parhi, **Weili Duan**, Kaoru Takara, R. B. Singh, Toshio Yamagata. El Nin˜o Modoki connection to extremely-low streamflow of the Paranaı´ba River in Brazil, ***Climate Dynamics***, 12: 1509-1516, 2014.
- Pingping Luo, Kaoru Takara, Bin He, **Weili Duan**, Apip, Daniel Nover, Watanabe Tsugihiro, Maochuan Hu, Kenichi Nakagami and Izumi Takamiya, Assessment of paleo-hydrology and paleo-inundation conditions: the process, ***Procedia Environmental Science***, DOI 10.1016/j.proenv.2014.03.089, 2014.
- **Weili Duan**, Kaoru Takara, Bin He, Pingping Luo, Daniel Nover, Yosuke Yamashiki, Spatial and temporal trends in estimates of nutrient and suspended sediment loads in the Ishikari River, Japan, 1985 to 2010, ***Science of the Total Environment***, 461: 499-508, 2013.
- **Weili Duan**, Bin He, Kaoru Takara, Pingping Luo, Daniel Nover, Netrananda Sahu, Yosuke Yamashiki, Spatiotemporal evaluation of water quality incidents in Japan between 1996 and 2007. ***Chemosphere***, 93(6): 946–953. 2013.
- **Weili Duan**, Kaoru Takara, Bin He, Pingping Luo, Daniel Nover, Yosuke Yamashiki. Nutrients and Suspended Sediment Load Estimates for the Ishikari River Basin, Japan,

Over a Decade. ***Kyoto University Disaster Prevention Research Institute Annuals***, No56 B: 59-64, 2013.

- ✧ **Weili Duan**, Bin He, Kaoru Takara, Pingping Luo, Yosuke Yamashiki. Estimating the Sources and Transport of Nitrogen Pollution in the Ishikari River Basin, Japan. ***Advanced Materials Research***, 518: 3007-3010, 2012.
- ✧ Bin He, **Weili Duan**, Pingping Luo, Kaoru Takara, Yosuke Yamashiki, Cause mechanism and GIS based spatial-temporal analysis of anthropogenic environmental disasters in EastAisa. ***Journal of Disaster Research***, 8(1): 171-172, 2012.
- ✧ **Weili Duan**, Guohua Chen, Qing Ye, Qingguang Chen. The situation of hazardous chemical accidents in China between 2000 and 2006, ***Journal of Hazardous Materials***, 186 (2-3): 1489-1494, 2011.

Book chapter:

- ✧ Pingping Luo, Apip, Kaoru Takara, Bin He, **Weili Duan** and Maochuan Hu, Numerical Assessment of shallow landslide using the distributed hydrological-geotechnical model in a large scale, ***Chapter on Landslide Science for a Safer Geo-Environment, 2014 World Landslides Forum***, Springer Press, DOI 10.1007/978-3-319-04999-1_62. 2014.

Papers in submission:

- ✧ **Weili Duan**, Bin He, Kaoru Takara, Pingping Luo, Daniel Nover and Yosuke Yamashiki, Spatiotemporal variability of Hokkaido's seasonal precipitation in recent decades and connection to water vapor flux, ***Journal of Hydrology***, under review, 2014.
- ✧ **Weili Duan**, Kaoru Takara, Bin He, Pingping Luo, Daniel Nover, and Maochuan Hu. Modeling suspended sediment sources and transport in the Ishikari River basin, Japan using SPARROW, ***Science of the Total Environment***, under review, 2014.
- ✧ **Weili Duan**, Kaoru Takara, Bin He, Pingping Luo, Maochuan Hu, Nor Eliza Alias, Masahito Ishihara and Yosuke Yamashiki. Changes of precipitation amounts and precipitation extremes in Japan, 1901-2012, ***Climate Dynamics***, submitted, 2014.

- ✧ **Weili Duan**, Bin He, Kaoru Takara, Pingping Luo, Daniel Nover, Maochuan Hu and Netrananda Sahu, Impact of climate change on the hydro-climatology of the upper Ishikari River Basin, Japan, ***Journal of Hydrology***, under review, 2014.
- ✧ Nor Eliza Aliasa, Kaoru Takara, Masahito Ishihara, Pingping Luo, **Weili Duan**. Considering regional frequency analysis to improve the fitting of extreme outliers within long historical rainfall observations: a study case in Japan, ***Journal of Hydrology***, submitted, 2014.